ON THE USE OF MODELLING, OBSERVATIONS AND REMOTE SENSING TO BETTER UNDERSTAND THE CANADIAN PRAIRIE SOIL-CROP-ATMOSPHERE SYSTEM

by

Julian Charles Brimelow

A thesis submitted to the Faculty of Graduate Studies of the University of Manitoba
in partial fulfilment of the requirements of the degree of

DOCTOR OF PHILOSOPHY

Department of Environment and Geography
University of Manitoba
Winnipeg, Manitoba
CANADA

April 2011

Thesis advisor:

Dr. John M. Hanesiak,

Department of Environment and Geography, University of Manitoba

Examining Committee:

Dr. Richard Raddatz,

Department of Soil Science, University of Manitoba

Dr. Tim Papakyriakou,

Department of Environment and Geography, University of Manitoba

Dr. Peter Taylor,

Department of Earth and Space Science and Engineering, York University (External)

ABSTRACT

Thunderstorms have been identified as an important component of the hydrological cycle on the Canadian Prairies, a region that is postulated to have the potential to exert a detectable influence on convective precipitation in the summer. However, very little work has been undertaken exploring and elucidating those aspects of biophysical forcing on the Canadian Prairies that affect lightning activity during the summer months, the constraints under which any linkages operate, and the mechanisms by which surface anomalies modify the structure and moisture content of the convective boundary layer (CBL) so as to modulate lightning activity.

Evapotranspiration (ET) from the soil and vegetation canopy is known to be important for modulating the moisture content in the CBL, and this in turn has important implications for the initiation and intensity of deep, moist convection. The Second Generation Prairie Agrometeorological Model (PAMII) of Raddatz (1993) has been used extensively for the purpose of quantifying the evolution of soil moisture and ET in response to atmospheric drivers on the Canadian Prairies. However, the ability of PAMII to simulate the evolution of root-zone soil moisture and ET during the growing season has yet to be verified against a comprehensive set of in-situ observations.

In this thesis, we address the above knowledge gaps using unique datasets comprising observed lightning flash data, satellite-derived Normalized Difference Vegetation Index (NDVI) data, observed atmospheric soundings, in-situ soil moisture observations and estimates of daily ET from eddy-covariance systems.

A thorough quantitative validation of simulations of root-zone soil moisture and ET from PAMII was undertaken against in-situ soil moisture measurements and ET from eddy-covariance systems at sites on the Canadian Prairies. Our analysis demonstrates that PAMII shows skill in simulating the evolution of bulk root-zone soil moisture content and ET during the growing season, and for contrasting summer conditions (i.e., wet versus dry). As part of the soil moisture validation, a novel multi-model pedotransfer function ensemble technique was developed to quantify the uncertainty in soil moisture

simulations arising from errors in the specified soil texture and associated soil hydraulic properties.

An innovative approach was used to explore linkages between the terrestrial surface and deep, moist convection on the Canadian Prairies, using datasets which avoid many of the problems encountered when studying linkages between soil moisture and thunderstorm activity. This was achieved using lightning flash data in unison with remotely sensed NDVI data. Specifically, statistical analysis of the data over 38 Census Agricultural Regions (CARs) on the Canadian Prairies for 10 summers from 1999 to 2008 provided evidence for a surface-convection feedback on the Canadian Prairies, in which drought tends to perpetuate drought with respect to deep, moist convection. The constraints in which such a feedback operates (e.g., areal extent and magnitude of the NDVI anomalies) were also identified. For example, our data suggest that NDVI anomalies and lightning duration are asymmetric, with the relationship between NDVI and lightning duration strengthening as the area and amplitude of the negative NDVI anomaly (less vegetation vigour) increases.

Finally, we focused on how surface anomalies over the Canadian Prairies can condition the CBL so as to inhibit or facilitate thunderstorm activity, while also considering the role of synoptic-scale forcing on modulating summer thunderstorm activity. We focused on a CAR located over central Alberta for which observed lightning flash data, NDVI data, and in-situ sounding data were available for 11 summers from 1999 to 2009. Our analysis suggests that storms over this region are more likely to develop and are longer-lived or more widespread when they develop in an environment in which the surface and upper-air synoptic-scale forcings are synchronized. On days when a surface or upper-air feature is present, storms are more likely to be triggered when NDVI is much above average, compared to when NDVI is much below average. We propose a conceptual model, based almost entirely on observations, which integrates our findings to describe how a reduction in vegetation vigour modulates the partitioning of available energy into sensible and latent heat fluxes at the surface, thereby modulating the lifting condensation level heights, which in turn affect lightning duration.

TABLE OF CONTENTS

LIST OF FIGURES

LIST OF TABLES

ACKNOWLEDGEMENTS

Undertaking the research contained in this thesis has been a tremendous learning experience, and a memorable journey to boot. A journey that was made possible because of the generosity, kindness and support of many individuals. Without the help of all concerned, I would not have been able to accomplish this daunting task. I am greatly indebted to the Drought Research Initiative (DRI), a Canadian Foundation for Climate and Atmospheric Sciences (CFCAS) Network for financing this research.

I sincerely wish to thank my supervisor, Dr. John Hanesiak, for his guidance, encouragement, support and invaluable insight. I was very fortunate to be in his capable hands and I could not have wished for a better supervisor. Thanks also to my committee members for their feedback and support, especially in the early days of this endeavour when I was unsure and in need of guidance. I am also indebted to my co-authors for their valuable contributions to the papers contained within this thesis.

I am very grateful to Mr. Ralph Wright from Alberta Agriculture and Rural Development for sharing the DroughtNet station data, and to the Fluxnet-Canada Research Network for providing the eddy covariance data for Lethbridge. I also wish to thank Larry Woolliams for the access to the WNC site; Jaclyn Schmidt, Rebecca Haspel, and John Jackson for data collection and analysis at the WNC site; Alberta Environment Climate Change Research User Group, Canada-Alberta Water Supply Expansion Program, Alberta Ingenuity Centre for Water Research, Natural Sciences and Engineering Research Council, and Environment Canada Science Horizons Program for funding support for the WNC site. I am very grateful to Dr. Larry Flanagan from the

University of Lethbridge for providing the eddy covariance data and background insight into these data for the FLUXNET site at Lethbridge.

Mr. Ron Goodson and Mr. Brian Wiens from the Meteorological Service of Canada very kindly provided archived surface, upper-air and other data that were essential for my research. I am indebted to Mr. Neil Taylor for his support and his insightful discussions about my research. Mr. Patrice Constanza and Dr. George Liu were invaluable in preparing and processing the North American Regional Reanalysis data used in this research. I am very grateful to Dr. Geoff Strong for all of his support and encouragement over the years.

On a personal note, I wish to thank my mom for always being there for me and for her unwavering support, love and encouragement, and for having faith in me. You have somehow managed to do so even when on the other side of the planet, and your support has been instrumental in getting me to where I am today. Of course, I will never forget the tremendous support and encouragement over the years from my dear sisters (Stella and Suzanne). I cannot find the words to thank you both — you are the best.

My thanks and love to my loving wife Nyree, who has been an unwavering rock of support throughout this challenge. I remember the trepidation and anxiety we both felt on that frigid day in January when we set out in our car to cross the Prairies as we embarked on this journey together. [And let us not forget poor Jennifer, not even one year old, squished between boxes in the back seat as we trekked across the Prairies]. Nyree, I could never possibly thank you enough for all those hours proof-reading and editing. Not to mention you indulging me venting about problems, letting me bounce ideas of you, and having to deal with a distracted husband all these years. You have not complained

once. You are a star. My heartfelt thanks also go to my beautiful daughters Jennifer and Amy for dealing with a very preoccupied and distracted dad for the first five years or so of your lives. You kept my spirits up with your giggles and hugs. I am so incredibly happy that I got to spend time at home with you both and watch you grow — those have been amongst the fondest memories of my life.

DEDICATION

This thesis is dedicated to my mom who has supported me ever since I first showed an interest in clouds and weather as a boy. I really could not have gotten to where I am today without your love, support and encouragement Muttie. It is also dedicated to my sisters (Stella and Suzanne) — no matter how far apart we are, we will always be together in spirit and you have shared in this journey too. And last but not least, this thesis is dedicated to my family (Nyree, Jennifer and Amy) — you mean everything to me, thank you for being there for me.

CHAPTER 1

1. INTRODUCTION

1.1 Motivation

Linkages and feedbacks between the terrestrial ecosystem (i.e., vegetation and soil) and precipitation play a critical role in regulating regional weather and climate (Jones and Brunsell 2009) and have been the focus of much research. The coupling between the terrestrial surface and overlying atmosphere is strongest during the warm season because it is then that soil moisture and vegetation have the greatest affect on the energy and moisture exchange between the ground and atmosphere (Betts et al. 1996; Koster et al. 2004; Seneviratne et al. 2006). During the growing season, vegetation and soil states are known to regulate the structure and moisture content of the boundary layer by influencing the partitioning of incoming solar radiation, and by modulating fluxes of mass and momentum (Kaufmann et al. 2003; Dominguez and Kumar 2008).

The importance of the terrestrial ecosystem in determining weather and climate has been illustrated by observations that land-atmosphere interactions and feedbacks affect regional climate, and the hydrological cycle (e.g., Shukla and Mintz 1982; Chahine 1992; Dirmeyer 2000; Koster and Suarez 2000; Zeng and Neelin 2000). Because soil moisture and vegetation states change much more slowly than the rapidly evolving atmospheric flow, the "memory" of soil moisture anomalies have been found to be an important factor in explaining intra-seasonal variability of the climate system (e.g., Schlosser and Milly 2002; Guo et al. 2006; Dong et al. 2007). Also, modelling studies have suggested that

positive feedbacks can be important for perpetuating soil moisture anomalies and drought (e.g., Atlas et al. 1993; Dirmeyer 1994; Sud et al. 2003).

The inherent memory of soil moisture, for example, suggests that seasonal forecasts can benefit by having accurate initial soil moisture conditions (e.g., Dirmeyer 2000; Koster and Suarez 2001). Dirmeyer (2000) and Douville (2003) showed the positive impact of using more realistic initial land surface state estimates when making seasonal forecasts. Koster et al. (2003) and Koster et al. (2004) found the quality and consistency of the initial state of the land surface could affect model forecast skill for months. Jiang et al. (2009) note that understanding the complex interactions between the land surface and atmosphere is key to improving precipitation forecasts. An important aspect to consider when studying land-atmosphere interactions and feedbacks is the size and duration of the soil moisture anomalies in space and time — that is, the anomalies must be sufficiently long-lived and cover a sufficiently large area before they can begin to significantly influence the overlying atmosphere (e.g., Raupach and Finnigan 1995; Mahrt 2000; Desai et al. 2006).

The strength of the coupling between the land-surface and atmosphere is regional in nature. Modelling studies (e.g., Koster et al. 2004) have identified certain terrestrial "hot spots" around the globe where linkages between the land-surface and atmosphere are especially strong. As we will show in Chapter 2, the Great Plains in the USA and Canadian Prairies have been identified as "hot spots". One possible contributing factor to this is the presence of the Rocky Mountains. For example, van der Ent et al. (2010) found that mountain barriers act to increase the precipitation recycling in regions downwind of the barrier by impeding the transport of oceanic moisture into that region.

An important process to consider when exploring linkages between the land surface and atmosphere is deep, moist convection. Guo et al. (2006) postulated that because moist convection is very sensitive to variations in near surface air temperature and humidity, one would expect moist convection to be a key component of the pathway linking soil moisture variations and precipitation. The linkages between the surface and vegetation and the overlying atmosphere can sometimes result in positive or negative feedback loops, which, for example, may either favour or inhibit the triggering (and intensity) of deep, moist convection (e.g., Findell and Eltahir 2003a,b). On the Canadian Prairies, early research has found tentative support for positive feedback between soil moisture and deep convection. For example, Hanesiak et al. (2004) used satellite imagery to investigate the impact of soil moisture on the timing of formation of deep convective clouds on the Canadian Prairies. They found that, under weak synoptic forcing, the initiation time of clouds was delayed as the root-zone soil moisture decreased. In addition, Hanesiak et al. (2009) determined that knowledge of the root-zone soil moisture at the beginning of the summer could provide some indication as to the potential severity of the upcoming thunderstorm season on the Canadian Prairies.

However, as noted by Siqueira et al. (2009) and Seneviratne et al. (2010), while the coupling between soil moisture, vegetation and convection has received much attention in recent years the results remain inconclusive (e.g., Koster and Suarez 2004; Kim and Wang 2007). This is partly attributable to the fact that interactions between the terrestrial components and the overlying atmosphere are extremely complex, and consequently, are still not completely understood (e.g., Seneviratne et al. 2010). Additionally, trying to extract a signal or assign causality between anomalies in the terrestrial surface on deep,

moist convection is especially difficult because there are both thermodynamic and hydrometeorologic processes taking place simultaneously in a highly non-linear system (e.g., Bosilovich and Schubert 2001). One of the primary objectives of this thesis is to elucidate the connection between the land surface state and deep, moist convection on the Canadian Prairies.

In the absence of a high spatial resolution in-situ soil moisture monitoring network on the Canadian Prairies, one has to rely on alternative methods for obtaining observed conditions. The second-generation Prairie Agrometeorological Model (PAMII) of Raddatz (1993) has been used extensively by researchers in Canada (e.g., Hochheim et al. 2002; Hanesiak et al. 2004; Raddatz 2005; Gervais et al. 2010; Mkhabela et al. 2010), to map the continually evolving spatial distribution of soil moisture and ET in response to atmospheric drivers. However, the ability of PAMII to simulate the evolution of both root-zone soil moisture and ET during the growing season has yet to be verified against a comprehensive set of in-situ observations.

Understanding land-atmosphere interactions has become especially important since the introduction of numerical weather prediction and climate models equipped with sophisticated land-surface schemes. Additionally, knowledge of how the terrestrial ecosystem components interact with the atmosphere is valuable for both validating and improving the numerical prediction models. Thus, the accurate simulation of root-zone soil moisture and ET by the surface-vegetation-atmosphere-transfer (SVAT) models is a necessary condition for the host numerical weather prediction model to accurately forecast the timing and location of convection. To achieve this goal requires that the SVAT models are capable of realistically modelling both soil and vegetation

characteristics and processes (De Lannoy et al. 2006). Realistic modelling of soil moisture content in turn requires accurate specification of the soil hydraulic parameters (Shao and Irannejad 1999; Zhu and Mohanty 2002). In this thesis we expand on these findings as they pertain to the PAMII model.

Thunderstorms form an important part of the Canadian Prairie hydrological cycle. Statistics from Environment Canada indicate that up to 50% of the annual precipitation on the Canadian Prairies falls during the summer months. Also, an analysis of sounding data from central Alberta by Reuter and Aktary (1995) found that 95% of the summer precipitation occurred on days when the potential for convective instability was present. Raddatz and Hanesiak (2008) investigated over 1000 significant summertime rain events on the Canadian Prairies between 2000 and 2004. They found that almost 80% of the significant rain events were solely or partially convective.

Most studies investigating feedbacks between the land surface, atmosphere and precipitation have had to rely on modelled data. This is because precipitation and soil moisture are typically not adequately resolved at the spatial and temporal scales of summertime precipitation events. One dataset which has received virtually no attention in terms of exploring land-atmosphere influences on convection is lightning flash data. These data are available at a higher spatial and temporal resolution than are the processes driving thunderstorms. Further, by combining lightning flash data with high spatial resolution measurements of Normalized Difference Vegetation Index (NDVI), one could, for the first time, explore land-atmosphere linkages without having to rely on output data from numerical models.

Above, we have identified some major gaps in our knowledge. Despite its wide use, the PAMII model has yet to undergo comprehensive and objective validation. Thunderstorms have been identified as an important component of the hydrological cycle on the Canadian Prairies, a region that has been identified as having the potential to exert a detectable influence on convective precipitation in the summer. However, very little work has been undertaken exploring and elucidating those aspects of biophysical forcing on the Canadian Prairies that affect lightning activity during the summer months, the constraints under which any linkages operate (e.g., size and magnitude of soil moisture anomalies), and the mechanisms by which surface anomalies modify the structure and moisture content of the CBL so as to modulate lightning activity. In this thesis, we address these knowledge gaps using unique datasets comprising observed lightning, satellite-drived NDVI, observed atmospheric soundings, in-situ soil moisture observations and estimates of daily ET from eddy-covariance systems.

1.2 Objectives of Research

The primary objectives of the research conducted in this thesis are as follows:

1) To use in-situ observations of root-zone soil moisture to assess the ability of the second-generation Prairie Agrometeorological Model (PAMII) to simulate the evolution of root-zone soil moisture for various soil types during the growing season.

2) To assess the ability of PAMII to simulate the daily evapotranspiration (ET) during the growing season. The ability of PAMII to simulate daily and seasonal ET for contrasting growing seasons (i.e., drought versus pluvial) will also be investigated.

3) To determine whether a link exists between vegetation vigour (i.e., Normalized Difference Vegetation Index; NDVI) and lightning activity on the Canadian Prairies, and to identify the thresholds for both the areal extent and the magnitude of the NDVI anomaly required to affect lightning activity.

4) To investigate the relationship between NDVI and root-zone soil moisture on the Canadian Prairies.

5) To explore the relative importance between synoptic-scale forcing and NDVI anomalies in modulating lightning flash activity over central Alberta, and to ascertain whether or not lightning activity is influenced by significant NDVI anomalies on days with similar synoptic-scale forcing.

6) To identify mechanisms by which anomalies in vegetation vigour (i.e., NDVI) affect the observed structure and characteristics of the convective boundary layer (CBL) so as to modulate lightning activity.

The first objective — of validating simulations of root-zone soil moisture from PAMII during the growing season — will be achieved by quantitatively comparing the model output against in-situ soil moisture measurements at three DroughtNet sites in Alberta. The selected sites have contrasting, but uniform, soil texture in the root zone. The sensitivity of the model simulations to errors in the specified soil hydraulic properties will be investigated using 20 different pedotransfer functions. Additionally, guidelines for the minimum accuracy required to produce accurate simulations of root-zone soil moisture content are provided.

The ability of PAMII to simulate evapotranspiration over the course of the growing season will be investigated by comparing simulated daily ET against estimates of daily ET derived from eddy-covariance systems. The model will be validated at a barley crop site northwest of Calgary and a native short-grass Prairie site at Lethbridge. To establish the ability of PAMII to discern between different growth conditions, the model will be validated for three contrasting growing seasons at the grassland site. The sensitivity of the simulated ET over the two vegetation types to changes in the minimum reference stomatal resistance will also be investigated.

The third objective will be achieved using NDVI and lightning flash data for 38 Census Agricultural Regions (CARs) on the Prairies for 10 summers (1999–2008). Specifically, correlations between pairs of standardized anomalies of NDVI and lightning duration (for June through August) are calculated. The impacts of both the areal extent and magnitude of the NDVI anomalies on the correlations between NDVI and lightning duration are explored by grouping the data by the size of the CAR and/or by the magnitude of the NDVI anomalies.

The fourth objective investigates an important premise of our research, namely that NDVI is responding to changes in root-zone soil moisture (i.e., antecedent precipitation). The relationship between root-zone soil and NDVI is addressed by comparing in-situ observations of root-zone soil moisture with concomitant NDVI at three sites in Alberta during a dry-down period in the summer of 2003. Additionally, the relationship between area-averaged plant available soil moisture (over CARs) and NDVI for those CARs experiencing contrasting vegetation vigour is investigated. The purpose is to determine whether or not the simulated root-zone plant available water (RZPAW) is consistent with

the observed NDVI and to identify below which level of RZPAW significant anomalies in NDVI are observed.

The fifth objective is achieved by first identifying a subset of 22 summer months for which daily information about synoptic-scale forcing (both at the surface and upper-air) is available over a CAR in central Alberta. The synoptic-scale upper-air forcing is quantified by calculating the mean daily 500-mb vertical motion from the North American Regional Reanalysis. Synoptic-scale surface feautures are identified by visual inspection of 3-hrly surface weather maps over the study area. Each day for the 22 summer months is then assigned one of six classifications according to the surface and upper-air information; lightning statistics are then calculated for each class. A series of statistical tests are performed to quantify the response (if any) of lightning duration on days with similar synoptic forcing, but occurring during weeks with contrasting NDVI conditions. In this way, the impact of synoptic forcing is removed (or at least minimized), thereby allowing us to focus on the response, if any, of the lightning to changes in antecedent vegetation vigour.

Finally, objective six is addressed by exploring the impact of NDVI on the structure and characteristics of the CBL over central Alberta for 33 summer months from 1999 to 2009. For this purpose, quality-controlled daily 00 UTC soundings released from Stony Plain are processed to calculate monthly averages and standardized monthly anomalies of sounding parameters. Key sounding-derived parameters (e.g., those variables describing low-level moisture, lapse rates, CBL structure and cloud-base heights) are identified and then correlated with both NDVI and lightning duration. A conceptual model is then proposed which integrates all of the above findings to describe how changes in the CBL

in response to changes in vegetation vigour can modulate lightning activity over the study region.

1.3 Structure of Thesis

The above objectives were addressed within four research papers, three of which have appeared (or are in press) in peer-reviewed journals at the time of submission. The papers form the core of this sandwich thesis, which is structured as follows. In Chapter two, a detailed background is provided on relationships between the terrestrial surface and the convective boundary layer, including a review on how anomalies in soil moisture and vegetation vigour can affect precipitation (especially convective precipitation) occurrence and intensity. Chapter three addresses objective one above by validating root-zone soil moisture simulations from PAMII at key sites in Alberta, and also presents the multi-model pedotransfer function ensemble technique. Chapter four addresses objective 2 above by validating daily ET estimates from PAMII against estimates of ET from eddy-covariance data located over a barley site and a short-grass prairie site. In Chapter five we briefly explore the potential of using PAMII as a drought tracking tool on the Canadian Prairies. Chapter six addresses objectives three and four by investigating linkages between NDVI and lightning activity for 38 census agriculture regions across the Canadian Prairies for 10 summers from 1999 to 2008. Chapter seven addresses objectives five and six by focussing on how land-atmosphere processes (e.g., NDVI anomalies) over the Canadian Prairies can condition the convective boundary layer so as to inhibit or facilitate thunderstorm activity during the summer months for 11 summers from 1999 to 2009, while also considering the role of synoptic-scale forcing on

modulating thunderstorm activity. The thesis concludes in Chapter eight with a review of the research conducted as well as suggestions for future research.

1.4 Contributions to Science

In the course of undertaking this research, several novel and original scientific concepts were advanced. Specifically:

1) A thorough quantitative validation of simulations of both root-zone soil moisture and ET from PAMII was undertaken using in-situ measurements and observations from the Canadian Prairies. This validation identified several areas where the model could be improved. Most notably, the manner in which the infiltration of precipitation into the soil column is dealt with, and the water-stress function in the canopy resistance module.
2) A novel multi-model pedotransfer function ensemble technique was developed to quantify the uncertainty in simulating soil moisture and to quantify impacts of errors in the specified soil texture (and associated soil hydraulic properties) on root-zone soil moisture simulations.
3) A novel approach was used to explore linkages between the terrestrial surface and deep, moist convection on the Prairies, using datasets which avoid many of the problems encountered when studying linkages between soil moisture and thunderstorm activity — both of which are known to exhibit significant spatial and temporal variability. This was achieved using lightning flash data in unison with remotely sensed NDVI data.

4) These unique observed data, as opposed to numerical model simulations, found evidence for a surface-convection feedback on the Canadian Prairies, in which drought tends to perpetuate drought with respect to convective storms and associated rainfall. The constraints in which such a feedback operates (e.g., extent and magnitude of the NDVI anomalies) were also identified.

5) A conceptual mode was proposed, based almost entirely on observations, which describes how reduction of vegetation vigour — in response to soil moisture deficits — modulates the partitioning of available energy into sensible and latent heat fluxes at the surface. This in turn modulates the structure and characteristics of the convective boundary layer, which affects lightning duration. This is believed to be the first time such a conceptual model has been developed based almost exclusively on observations.

CHAPTER 2

2. BACKGROUND

2.1 The Land-Atmosphere Energy Budget

Pielke (2001) quantifies the surface energy budget during the warm season as follows:

$$R_n = Q_G + H + LE + LT_r \quad (2.1)$$

where R_n represents the net radiative flux, which is equivalent to $Q_S(1-\alpha) + Q_{DLW} - Q_{ULW}$ where Q_s is solar insolation, α is albedo, Q_{ULW} is upwelling longwave radiation given by $(1-\varepsilon)\, Q_{DLW} + \varepsilon\sigma T^4$, Q_{DLW} is the downward longwave radiation, ε is the surface emissivity, σ is the Stefan-Boltzmann constant and T is the surface temperature; Q_G is the soil heat flux; H is the turbulent sensible heat flux; L is the latent heat of vaporization; E is evaporation from the soil; T_r is transpiration from vegetation.

Over bare soil there is no transpiration or evaporation of intercepted precipitation from vegetation canopy. Consequently, the latent heat flux will be determined primarily by the near-surface soil moisture content. For soils having a dry near-surface layer the evaporation is practically zero. The albedo for surfaces that are covered by vegetation is typically 0.1 to 0.3, and the albedo for bare soil typically varies between 0.1 and 0.4 (Segal et al. 1988). Generally the albedo decreases as the near-surface moisture increases.

The Bowen ratio (BR) is a very useful parameter for quantifying the partitioning of

heat between the sensible and latent heat fluxes. It is defined as the ratio of the sensible heat flux to latent heat flux. Typical values for BR range from 0.1 over the ocean to 10 over deserts. Over vegetated surfaces, BR is typically between 0.2 and 1.5.

2.2 The Influence of Vegetated Surfaces on Climate

Vegetation coverage and type are mainly controlled by temperature, water availability, solar radiation and landscape (e.g., Budyko 1974; Bonan et al. 2002). Notaro et al. (2006) outline the complex feedbacks between the vegetation and climate and vice versa. Siqueira et al. (2009) noted that the dynamics of surface fluxes and the soil-plant-atmosphere variables are central to the growth of the convective boundary layer (CBL).

Critical properties of vegetation are: leaf area, stomatal resistance and root depth. All of these factors are dynamic — they are a function of vegetation type and vary on intra- and inter-annual time scales (Raddatz 2007). Observations and modelling studies have found that vegetation is a primary pathway for coupling the surface and the atmosphere (e.g., Tsvetsinskaya et al. 2001). Thus it is critical to take into consideration the impacts of the dynamic nature of vegetation when modelling boundary layer processes and land-atmosphere feedbacks.

Segal et al. (1988) summarised the primary factors governing transpiration:

i) *Ambient atmospheric conditions:* The conductance tends to decrease (i.e., stomata close) as the vapour pressure deficit increases, when the leaf temperature is either above or below an optimal value, and when the plant-available moisture in the root-

zone moisture decreases. ET will be higher (lower) under warm (cool), dry (humid) and windy (calm) conditions.

ii) *Vegetation properties:* The transpiration rate is governed by a) leaf area, b) shielding factor and c) leaf age. Both a) and b) are low for crops early in the growing season, reducing transpiration. Transpiration decreases as leaves age, and is negligible after the onset of senescence. The albedo of vegetation determines the energy available for photosynthesis (through R_n). In addition, the shape of leaves and height of the canopy influence the aerodynamic coupling with the overlying atmosphere, and this can ultimately affect the turbulent momentum, heat and moisture fluxes from the canopy.

iii) *Root zone moisture:* The moisture in the root zone can limit transpiration if the plant-available moisture is not high enough to allow plants to meet the atmospheric demand. As the root-zone moisture decreases, plants begin to experience water stress, the stomata contract to preserve water, and transpiration is reduced. However, a plant can still transpire when the surface layer of the soil column is dry, provided that there is sufficient water in the root zone.

The above findings are in agreement with Collins and Avissar (1994), who used the Fourier amplitude sensitivity test in conjunction with a land-surface scheme to identify those land surface properties that affect the partitioning of the turbulent latent and sensible heat fluxes. They found that the most important characteristics were the plant stomatal conductance, leaf area index, surface roughness and albedo. Of these, stomatal resistance was found to have a predominant role during daytime hours and under clear

sky conditions. The stomatal resistance is strongly modulated by soil moisture in the root zone. When no vegetation was present, their analysis indicated that land-surface wetness (water available for evaporation) was important.

According to Segal et al. (1988), about 70% of the estimated net radiation over vegetated areas is converted to latent heat flux, leaving only 30% to be converted to the sensible heat flux. Alfieri et al. (2007) investigated which environmental drivers (net radiation, water vapour pressure deficit, wind speed, soil moisture and greenness fraction) were responsible for modulating the latent heat flux during drought conditions over a rangeland site with sparse C4 grass in Oklahoma. They found that soil moisture content (at 5-cm depth) was critical in modulating the latent heat flux, and that this was achieved through changes in the surface resistance to water vapour transfer.

2.3 Conditions Required for Deep, Moist Convection

Thunderstorms require three criteria to develop: instability, moisture in the (CBL) and a trigger mechanism to initiate convection. All three have to be satisfied to initiate surface-based convection. Reuter and Aktary (1995) showed that the atmosphere is conditionally unstable on the majority of summer days on the Canadian Prairies. That is, the atmosphere is primed for deep convection and needs only a trigger. Here we will limit our discussion to surface-based convection, because elevated convection is not as tightly linked to boundary-layer processes.

A common method for assessing the instability is to calculate the lapse rate of the potential temperature or of the equivalent potential temperature (θ_e). It can be shown that if $d\theta_e/dz < 0$ the atmosphere is unstable (e.g., Pielke 1984). On a micrometeorological

scale, this instability facilitates the vertical (upward) transport of sensible and latent heat fluxes, and also affects the wind profile in the CBL (Oke 1987). There are a number of ways of increasing the instability. One process is by cooling the free atmosphere while adding heat to the CBL, which results in an increase in the lapse rate of θ_e. Alternatively, it follows from the definition of θ_e that if moist air in the CBL is overlain with dry air, the atmosphere tends to be convectively unstable. Therefore, adding moisture to the CBL also increases the instability.

The amount of instability is typically quantified in terms of the convective available potential energy (CAPE; units J kg^{-1}). The maximum updraft velocity is proportional to the square root of CAPE; so increasing CAPE increases the potential for stronger thunderstorms. The convective inhibition (CIN) is the negative buoyancy that must be overcome by a parcel lifted from the surface to its level of free convection (LFC). If the CIN is too large (> -50 J kg^{-1}), then deep convection is unlikely to be initiated except in the presence of strong lift from synoptic or mesoscale features (Mueller et al. 1993).

Crook (1996) investigated the relative sensitivity of CAPE and the CIN to small changes in the near-surface temperature and moisture. Through a scaling analysis of the equation for moist static energy he found that an increase in mixing ratio of only 1 g kg^{-1} has approximately 2.5 times the effect on CAPE as increasing the surface temperature by 1 °C. Additionally, Crook demonstrated that convective initiation is very sensitive to changes in temperature and mixing ratio of ~1 °C and ~1 g kg^{-1}, respectively. Further, once convection is initiated, small increases in the moisture content of air feeding the updraft can have significant impact on the thunderstorm's intensity.

2.4 The Prairie Landscape

The grassland eco-climate region of the Canadian Prairies (Fig. 2.1) covers an estimated 500 000 km^2. Annual field crops (wheat, canola and barley) cover about 60% of this area, with spring wheat alone accounting for about 50% of the cropped area (Hanesiak et al. 2009). By comparison, 30% is native perennial grasses or pasture, 10% fallow, and 5% is not used for agriculture (Raddatz 2005).

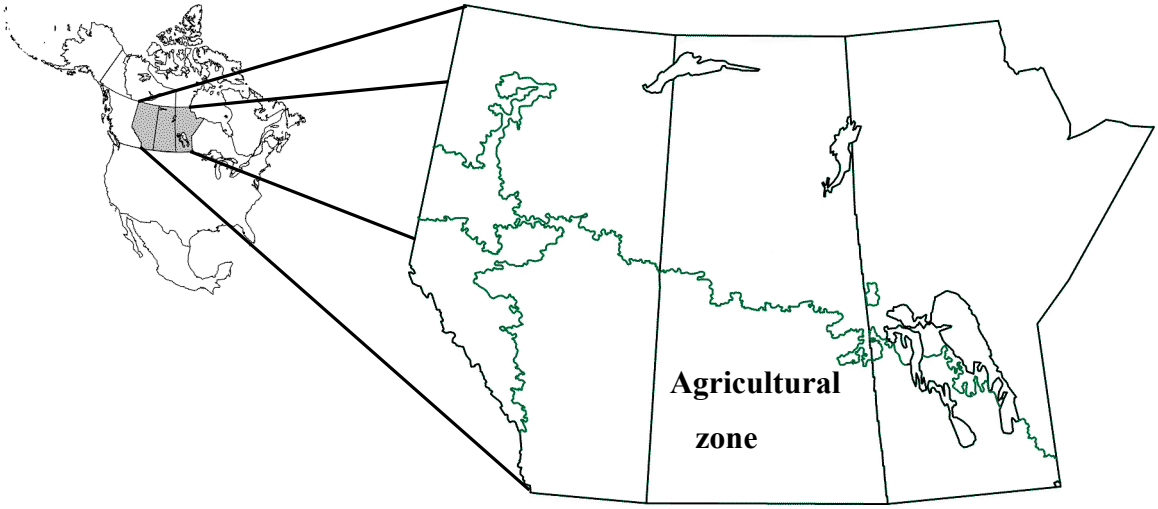

Figure 2.1: The Canadian Prairie provinces. The agricultural zone lies within the green border.

An analysis of sounding data from central Alberta by Reuter and Aktary (1995) found that 95% of the summer precipitation occurred on days when the potential for convective instability was present. Raddatz and Hanesiak (2008) showed that almost 80% of significant rainfall events (≥ 10 mm) on the Canadian Prairies between 2000 and 2004 were solely or partially convective. Hence, it is clear that thunderstorms form an integral part of the hydrological cycle on the Canadian Prairies during the warm season, and warm season rainfall can account for 50% or more of the annual precipitation.

The Feekes (e.g., Large 1954) and Zadoks scales (Zadoks et al. 1974) are commonly

used to describe the seasonal phenology of wheat. Robertson's biometeorological time (BMT; Robertson 1968) index is also often used and it takes into account the impacts of both the minimum and maximum air temperatures, as well as photoperiod, on a crop's development. BMT varies from 0 at planting to 6 at post-harvest.

Spring wheat undergoes six phases during a season: planting, emergence, jointing, heading, soft dough and maturity. Planting dates vary from year to year, and can range from the end of April to the end of May depending on soil moisture and temperature conditions. Juskiw et al. (2001) studied the phenological development of barley at three sites in southern Alberta between 1993 and 1996. They calculated the growing degree days (GDD) as the sum of daily mean temperatures above 0º C. According to Juskiw et al. (2001), emergence usually occurs 10-15 days after planting at 135 GDD, jointing at 680 GDD, heading at 915 GDD, soft dough at 1240 GDD, and harvest at 1455 GDD. Raddatz (1993) describes the phenology of wheat in the second-generation prairie agrometeorological model (PAMII; see section 2.15) using BMT as follows: emergence at 1.0, jointing at 2.0, heading at 3.0, soft dough at 4.0 and ripe at 5.0. Using BMT data from PAMII for Swift Current (approximate geographical centre of the Prairies) between 1998 and 2005, the mean date for emergence is 22 May (about two weeks after seeding), jointing near 12 June, heading near 8 July, soft dough near 30 July and ripe near 11 August. Juskiw et al. (2001) found the maximum leaf-area index (LAI_{max}) for a barley crop to occur near GDD 1040 (just prior to the soft dough stage). The LAI_{max} in their study was near 5.0 m^2 m^{-2}, but varied depending on the location and year. The phenologies of barley and wheat are very similar, so these values should also pertain to wheat. Wheat and barley crops are typically between 60 and 80 cm high at maturity.

The phenology of a short-grass Prairie site near Lethbridge differs significantly from that of the cereal crops. Field data (courtesy of Dr. L. Flannigan, University of Lethbridge) from 1998 to 2006 show that green-up typically occurs in late April, with LAI_{max} occurring in mid-to late June — a full month earlier than the cereal crops. Moreover, the LAI_{max} values were typically only ~1.0 m^2 m^{-2}, with maximum canopy heights near 30 cm. One would expect the peak latent heat fluxes from the grassland site to precede those of the cereal crops by about one month.

The contrasting LE fluxes (and phenology) between different vegetation types is highlighted by the eddy-covariance measurements analysed by Fischer et al. (2007) for different vegetation types near the border between Oklahoma and Texas. Specifically, they showed that the maximum latent heat fluxes above winter wheat were observed near day-of-year (DOY) 110 (early April), compared to DOY 175 (late June) for sorghum and pasture. Crop phenology thus plays an important role in modulating the flux of moisture into the boundary layer.

The Prairies are a source of boundary-layer moisture during the summer, with the majority of this terrestrially sourced moisture originating from agricultural crops, perennial grasses, and aspen groves (e.g., Raddatz 2000). Moisture recycling is potentially important in this region, with up to 30% of the summer precipitation sourced to regional ET (Raddatz 2000). Also, using PAM, Raddatz (1998) showed that crop phenology on the Prairies exerts an important control on the seasonal pattern and inter-annual variability of regional moisture fluxes. So while the base moisture level in the CBL is determined by advection, this moisture level can be enhanced by ET, resulting in a marked increase in CAPE. Raddatz and Cummine (2003) investigated whether there

was a link between crop phenology on the Canadian Prairies and the seasonal pattern of tornadoes. They concluded that there was a correlation between the amount of boundary layer moisture (from ET), which affected the amount of CAPE and the seasonal pattern of tornado days. Specifically, the timing of the peak number of tornado days was found to change in step with the time of the maximum of specific humidity and phenology of spring wheat.

Raddatz (1998) noted that different phenological properties of crops and native grassland have a significant impact on the surface energy balance and ET during the warm season,

i) Transitional-grassland: The Bowen ratio is less than 1 near the end of April. Bowen ratios remain between 0.3 and 0.7 between early May and mid September. These numbers indicate that regional ET adds moisture to the boundary layer for most of the growing season. Therefore, the potential for convection is increased throughout the season.

ii) Arid Grassland: Bowen ratios drop below 1 in the middle of May, and remain between 0.6 and 1 until September. This indicates that less moisture is added to the boundary layer due to the lower soil moisture, thereby reducing the potential for storms.

iii) Spring wheat: Bowen ratios remain below 1 until early June, with typical Bowen ratios varying between 0.15 and 0.3 between mid June and the end of July. These very low values indicate that transpiration from the crops add significant amounts of moisture to the boundary layer, thereby increasing the potential for convection. The

Bowen ratios are higher in spring and autumn (1.0–1.5), and do not favour the formation of storms.

2.5 The Role of Land Breeze Dynamics

The partitioning of the surface heat fluxes adjoining areas of forest and prairie grassland, for example, can lead to thermal gradients, which can in turn lead to the formation of thermally direct circulations. These so-called land breezes enhance convergence when they collide with other boundaries or stationary air, which may be strong enough to provide the lift required to trigger convection. According to Holton (1979), the thermally forced circulation (or land breezes for areas distant from the coast) may be represented mathematically as follows:

$$\frac{dv}{dt} = \left[\frac{R \ln\left(\frac{p_o}{p_1}\right)}{2(h+L)} \right] (\overline{T}_2 - \overline{T}_1) \qquad (2.2)$$

where v is the wind speed tangential to the temperature gradient, R the gas constant, p_o the pressure at the surface, p_1 the pressure at the top of the boundary layer, h the height of the boundary layer, L the horizontal scale of the circulation, $\overline{T}_2$ the mean boundary-layer temperature over the warmer surface, and $\overline{T}_1$ the mean boundary-layer temperature over the cooler surface.

Equation 2.2 is very simple, yet it demonstrates that the larger the temperature difference and the shorter the circuit length the greater the acceleration. It does not take into account friction, or the fact that the increase in wind speed would act to reduce the thermal contrast. Ookouchi et al. (1984), Pielke and Segal (1986) and Segal et al. (1988)

present more complicated mathematical formulae for describing mesoscale circulations arising from thermal contrasts.

2.6 Rossby Radius of Deformation

Modelling studies by Avissar and Chen (1993) and Lynn et al. (1995, 1998) demonstrated that the strongest mesoscale circulations and rainfall are generated over patches that are similar in size to the local Rossby radius of deformation (R_o). That is, there exists an optimum horizontal dimension of variations that maximizes the strength of mesoscale circulations. According to Lynn et al. (1998), this occurs when the scale of forcing by the land surface corresponds to the typical scale of the circulation producing the precipitation. R_o is calculated as follows:

$$R_o = \left(\frac{z_i N}{(f^2 + \lambda^2)} \right) \tag{2.3}$$

where N is the Brunt-Vaisala frequency = $[(g/\theta)(d\theta/dz)]^{0.5}$, f is the Coriolis parameter, z_i is the depth of the planetary boundary layer, and λ is a long wavelength damping coefficient. For typical values of $d\theta/dz$ (~1 °C 100 m^{-1}), z_i (~1 km), f (10^{-4} s^{-1}) and λ (10^{-4} s^{-1}), R_o is about 100 km. This estimate is in agreement with the results of 2D model simulations made by Yan and Anthes (1987) and Lynn et al. (1998). Their results indicate that heterogeneities in land surface moisture on scales of 100-200 km can initiate convective rainfall due to the lift resulting from the collision of the associated land breezes. Thus, the magnitude of the Rossby radius of deformation has important implications when considering whether or not a particular heterogeneity or surface anomaly is large enough to induce mesoscale circulations.

2.7 Quantifying the Strength of Coupling Between the Land Surface and Atmosphere

McNaughton and Jarvis (1983) calculated the rate of change of the stomatal conductance with respect to relative change in latent heat to derive the "decoupling coefficient (Ψ),

$$\Psi = \frac{\Delta + \gamma}{\Delta + \gamma(1 + G_a / G_c)} \tag{2.4}$$

where Δ is the slope of the saturation vapour pressure curve (kPa K^{-1}), γ is the slope of the psychometric constant (kPa K^{-1}), G_a is the aerodynamic resistance (m s^{-1}), and G_c is the canopy conductance (m s^{-1}). The decoupling coefficient represents the sensitivity of transpiration to a change in canopy conductance (Magnani et al. 1998). Specifically, when Ψ approaches 0 then the canopy and atmosphere are aerodynamically coupled and ET is limited by the vapour pressure deficit and G_c; when Ψ approaches 1 the vegetation canopy is decoupled from the atmosphere and ET is controlled by the available energy (Hao et al. 2007). Thus, Ψ is the extent to which canopy transpiration is controlled by stomatal aperture.

While coniferous forests tend to be well coupled with the atmosphere, short vegetation and temperate broad-leaf forests are partly decoupled from the atmosphere (Magnani et al. 1998). Alfieri et al. (2007) found that the latent heat flux went from being primarily water limited to being energy limited as soil moisture increased. This is consistent with the fact that Ψ tends to be very low under water-stressed conditions (i.e., latent heat flux is modulated by stomatal conductance), and closer to 1 when soil moisture is abundant (i.e. latent heat flux limited by available energy). Therefore, the decoupling coefficient is suitable for identifying those areas where the vegetation canopy

and atmosphere are strongly coupled and sensitive to soil moisture.

2.8 Precipitation Recycling

Within a given region, moisture that falls as precipitation comes from a combination of two sources: 1) convergence of moisture advected over the basin from remote regions (e.g., Liu et al. 2004; Brimelow and Reuter 2005), and 2) moisture from ET (Brubaker et al. 1993; Trenberth 1999). One metric that has been derived to quantify the amount of precipitation recycling is the precipitation recycling ratio (ρ). The recycling ratio is the fraction of total precipitation, which originates from local ET. Anderson et al. (2008) stated that ρ can also be used to obtain information about the impacts of land surface-precipitation feedback interactions on recycled moisture. Anderson et al. (2008) noted that while the concept of ρ is easy to define in theory, calculating it is problematic on account of the assumptions that need to be made. Szeto (2002) stated that the magnitude of ρ over a region is a measure of the importance of land-surface interactions, and that the memory of soil moisture, and its impact on regional climate, may be enhanced over regions with active recycling.

Several methods have been developed to calculate ρ. However, the majority are based on the seminal work of Budyko (1974), who developed a 1D model to quantify the relative contributions of local ET and advected moisture to regional precipitation. Consider a domain of length L aligned along the trajectory of air with a flux of F^+, with total precipitation of P and evapotranspiration E along L. Then,

$$\rho = \frac{EL}{(EL + 2F^+)} \tag{2.5}$$

where F^+ is the *magnitude* of the vertically integrated moisture flux vector ($\mathbf{F}^+ = F_x\mathbf{i}$

$+F_y\mathbf{j}$, where $F_x = \omega u$, with ω the precipitable water in the air column and u the mixing-ratio weighted mean zonal wind component through the column). F_y is calculated in a similar manner. The magnitude of the recycling ratio (ρ) is dependent on the scale length (L) and varies between 0 for a point source to 1 for the entire globe (e.g., Trenberth 1999). Typical values of L applied in the literature are 500 km (~$2x10^5$ km^2) or 1000 km ($8x10^5$ km^2). The fraction of water vapour which participates in the hydrological cycle is the intensity (I = PL/F), which reflects how often conditions are favourable for rainfall formation. The moistening efficiency (M= EL/F) is the contribution of ET to moisture advection along L. An assumption is that the moisture in the atmospheric column is well mixed, and water vapour molecules from local and remote sources have equal chances of precipitating out. It is also assumed that precipitation and ET are spatially and temporally homogeneous.

Other methods that have been adopted to quantify regional precipitation recycling include passive tracers in climate models (e.g., Koster et al. 1986; Numaguti 1999; Bosilovich and Shubert 2002), sophisticated quasi-isentropic back trajectory analysis modelling (Dirmeyer and Brubaker 1999) and isotopes (e.g., Kurita and Yamada 2008). Eltahir and Bras (1996) proposed a two-dimensional recycling model that uses area-averaged fluxes. Dominguez et al. (2006) developed a dynamic bulk recycling model that can be applied at timescales from days to months. Anderson et al. (2008) proposed a new metric for quantifying precipitation recycling, based on the atmospheric moisture tendency equation, called the local convergence ratio.

2.9 Global Variability in Regional Precipitation Recycling

Due to its importance in regional water budgets, precipitation recycling has been the subject of many studies (Brubaker et al. 1993; Eltahir and Bras 1994; Trenberth 1999; Bosilovitch and Schubert 2001; Brubaker et al. 2001; Szeto 2002; Zangvil et al. 2004; Raddatz 2005; Dirmeyer and Brubaker 2007; Dominguez and Kumar 2008; Anderson et al. 2008, 2009; van der Ent et al. 2010).

Precipitation recycling studies typically rely on reanalysis data to describe the atmospheric flow and ET, while merged observed data sets are often used for precipitation. While absolute values vary between studies for a given region or river basin, after taking into effect the scale dependence, there is generally good agreement between the values. Dirmeyer and Brubaker (2007) note that recycling is relatively high over much of South America south of the Amazon River, much of subtropical southern Africa, interior China, southern Europe, western North America, and the high latitudes of the Northern Hemisphere (see Fig. 5 in Dirmeyer and Brubaker (2007)).

Szeto (2002) estimated mean annual recycling ratio for the Mackenzie River Basin (MRB) to be 25% (L ~ 1500 km). In comparison, Stohl and James (2005) estimated the annual ρ over the MRB to be 28–31%, while Dirmeyer and Brubaker (2007) estimated ρ to be 35.6% in JJA. Dirmeyer et al. (2009) found that the JJA value of ρ over the Canadian Prairies to be about 15%, but up to 25% over the MRB. Typical values for annual recycling ratios for the Amazon basin are ~0.25–0.35 (L ~ 2500 km; Eltahir and Bras (1994), ~0.24 for the Mississippi basin (L ~ 1400 km; Brubaker et al. (1993), and ~0.35 for the Sahel (L ~ 1500 km; Brubaker et al. 1993).

Raddatz (2000) estimated the summertime recycling ratio over census agricultural

regions (CARs) on the Canadian Prairies to be 28% based on data between 1997 and 1999 (Table 2.1).

Table 2.1: Aggregated recycling ratios (ρ), moistening efficiency (M) and precipitation intensity (I) values calculated by Raddatz (2005) for CARs experiencing pluvial, near-normal and drought conditions on the Canadian Prairies between 1997 and 2003.

	ρ	M	I
Pluvial	24.0 (22.1–24.9)	66.2 (60.6–68.5)	73.1 (66.9–78.3)
Near-normal	20.8 (19.6–24.2)	51.8 (48.7–63.1)	45.8 (38.8–57.7)
Drought	16.7 (9.5–22.4)	39.0 (20.7–55.5)	29.2 (16.3–45.3)

Raddatz (2005) concluded that an intra-summer feedback between ET and precipitation, with moisture recycling influencing whether or not a CAR had a dry, normal or wet summer. Between 1997 and 2003, dry and wet conditions were perpetuated over CARs through moisture and energy feedbacks between the surface and atmosphere. This is corroborated by the finding that the moistening efficiency was positively correlated with the recycling ratio — that is, higher precipitable water contents were typically associated with increased ET from the vegetation. Raddatz (2005) also noted that there was generally sufficient moisture advected over the area to produce the observed rainfall amounts, so other processes were responsible for either muting or enhancing the convective activity. He suggested that the critical ingredients required for the realization of convection (such as lift and CAPE) were less prevalent over drought areas than pluvial areas. This is corroborated by the finding that the precipitation efficiency was much higher during pluvials than under drought or normal conditions

(Table 2.1). That is, during pluvials mechanisms were in place to initiate convection and allow the storms to tap into the available moisture.

Stohl and James (2005) used a Lagrangian particle dispersion model, driven with ECMWF analyses, to calculate the trajectories of "particles" for 39 major river basins across the globe. One basin of interest was the Nelson basin, which encompasses most of the Canadian Prairies. They calculated an annual ρ of ~20% for the Nelson River Basin. Brubaker et al. (2001) used a back-trajectory technique to calculate a recycling ratio of 32% for the Mississippi river basin between 1963 and 1998. They also calculated ρ for the Missouri Basin, which lies immediately to the south of the Canadian Prairies. Brubaker et al. (2001) calculated the JJA recycling ratio for the Missouri basin to be 22%. They estimated that about 9% of the moisture in JJA in the Missouri basin typically originates over the Gulf of Mexico and Caribbean, 8% over the N. Pacific and 8% over the Baja Peninsula. About 29% of all the moisture came from oceanic sources, compared to 49% from adjacent continental regions.

Bosilovich and Chern (2006) found that the recycling ratio over the Mississippi basin is positively correlated with P (0.73) and E (0.79), and negatively correlated with moisture transport (-0.41). Dominguez and Kumar (2008) suggested that this strong correlation indicates that moisture storage in the Mississippi can affect ET enough to change the recycling ratio, and that the recycling ratio increases as the CBL height and Bowen ratio decrease. They found that years with high recycling in the Mississippi basin were dominated by lower 1000–500 mb thicknesses, higher ET, reduced meridional moisture transport and below average temperatures. Bosilovich and Schubert (2001) investigated the recycling ratio over the central US and noted that the recycling ratio for

the Mississippi basin is high when moisture transport is weak and when ET and, to a lesser extent, convergence are high.

Zangvil et al. (2004) calculated the recycling ratio over the U.S. corn belt for four contrasting growing seasons. The found that ET was weakly related to P on monthly and seasonal time scales, and that ρ varied between 0.19 and 0.24. On daily timescales, ρ decreased rapidly as precipitation intensity increased. So the absolute amount of recycled precipitation on days with high recycling ratio is extremely small. Zangvil et al. (2004) conclude that land-atmosphere interactions are a critical component of climate system in this region, but that the interactions are complex and span a wide range of scales.

Liu et al. (2004) studied the moisture transport and upper-air circulation patterns for the 2000-2001 drought over the Canadian Prairies and placed the observed patterns relative to the 1948-2001 means. They noted that during the drought, moisture transport from the N. Pacific was reduced in the winter and summer, with no compensatory increase in moisture from the Gulf of Mexico. Large-scale subsidence on account of a persistent high led to lower precipitation and above-average temperatures. They noted that, in the summer, precipitation is positively correlated with meridional moisture transport (0.33), suggesting that the N. Pacific is not a dominant source of moisture over the MRB in the summer.

The results of Stohl and James (2005) suggest that the N. Pacific is not a major source of moisture for the Mississippi, Nelson or Mackenzie basins. This conflicts with the work of Dirmeyer and Brubaker (1999) and Brubaker et al. (2001), who found the N. Pacific to contribute about 9% of the precipitation during the spring and summer over the Missouri basin, which is in close proximity to the Nelson and Mackenzie river basins.

Their calculations were, however, made using much coarser NCEP reanalysis data (1.9ºx1.9º grid and 28 vertical levels) while Stohl and James (2005) used ECMWF reanalysis on a 1ºx1º grid with 60 vertical levels. The mountain ranges over western N. America would pose more of a barrier to moisture from the Pacific in the ECMWF model, with more moisture precipitating out on the western slopes.

2.10 Global "hot spots" in Land-Atmosphere Coupling

Koster et al. (2002) postulated that the strength of the coupling between the land and the atmosphere controls the degree to which precipitation-induced soil moisture anomalies affect the overlying atmosphere and thereby the subsequent generation of precipitation. They conducted controlled numerical experiments using four atmospheric general circulation models (AGCMs). They found that the strength of land–atmosphere coupling on short (weekly) timescales varied significantly between the AGCMs. Here "coupling" is not the same as the decoupling coefficient of McNaughton and Jarvis (1983), which was introduced in section 2.7. Rather it represents the degree by which changes in a surface variable (such as soil moisture) are reflected in the overlying atmosphere. Alternatively, according to Koster et al. (2004), the coupling coefficient (Ω) represents the fraction of the total variance of a variable (e.g., precipitation) that is explained by changes in a surface variable (e.g., soil moisture).

Since the seminal work of Koster et al. (2002), there has been a consolidated effort to try to quantify the coupling between the land surface and atmosphere using climate models. One such international effort was the Global Land-Atmosphere Coupling Experiment (GLACE; Koster et al. 2006). To quantitatively measure the strength of the

land-atmosphere coupling, Koster et al. (2004) measured the coherence of a seasonal time series of a model variable (e.g., ET) across a range of ensemble members using the coupling coefficient.

Koster et al. (2004, 2006) ran 12 independent climate models in ensemble mode (16 members) for the boreal summer (June, July, August) to identify those locations in the world where the multi-model ensembles predicted that precipitation is most sensitive to soil moisture anomalies. Their research identified several hot spots including: the central Great Plains of North America (including the southern portions of the Canadian Prairies, northern India, the Sahel, and equatorial Africa.

Koster et al. (2004) suggested that in order for soil moisture to affect evaporation, the standard deviation of the model-predicted ET must be large, and that the coupling between the surface fluxes and precipitation occurs through the convective precipitation in the models. They conclude that hot spots (see Fig. 1 in Koster et al. 2004) of land–atmosphere coupling stem from the coexistence of a high sensitivity of ET to soil moisture and a high temporal variability of ET. In wet climates, where soil moisture is plentiful, ET is controlled not by soil moisture but rather by the available energy. Thus, the soil moisture state in wet climates has little impact on ET and rainfall generation. In arid climates, ET rates are sensitive to soil moisture, but the typical variations are generally too small to affect rainfall generation. Only in the transition zone between wet and dry climates, where ET variations are suitably high but are still sensitive to soil moisture, do the land states tend to have strong impacts on precipitation. Moreover, in these zones the atmosphere is often convectively unstable.

Dirmeyer et al. (2009) presented an integrated analysis for quantifying land-

atmosphere interactions, which was not based on model runs from climate models. Specifically, they used observations of precipitation, re-analysis data (NCEP–DOE) of atmospheric variables, and soil moisture from the Global Soil Wetness Project. They found that the soil memory in JJA over the Canadian Prairies is about 15–20 days. Dirmeyer et al. (2009) found a positive correlation between daily soil moisture and ET in JJA (significant at 95% level of confidence) over the Canadian Prairies and the Great Plains of the US. They argued that such high positive correlations are likely to occur where moisture is more limited than is net radiation. Dirmeyer et al. (2009) found positive correlations between soil moisture and the recycling ratio. This hints that soil moisture anomalies reinforce local precipitation anomalies through a positive feedback, but a positive correlation between soil moisture and ET is a necessary but not sufficient condition for a land-atmosphere feedback.

Dirmeyer et al. (2009) identified areas where soil moisture controls ET, the precipitation regime favours the persistence of anomalies in soil moisture, and the circulation is conducive to reinforcing soil moisture anomalies through recycling. Allowing for all of these criteria, Dirmeyer et al. (2009) identified the Great Plains and southern Canadian Prairies as hot spots for feedbacks in JJA, along with portions of China and the Soviet Union. The Great Plains are shown to be especially "vigorous in their land-atmosphere interactions. Their results corroborate the findings of land-atmosphere interactions in model-only studies. They note that they have not included the impacts of vegetation, and that while the data were constrained by observations, there are still uncertainties in the soil moisture-ET-atmosphere relationships.

Using a coupled land-atmosphere model (COLA), Del Sole et al. (2009) found that

corrections to the land variables resulted in higher root-zone soil moisture contents over the US Midwest and portions of the Canadian Prairies. The increase in soil moisture was associated with positive increases in the near-surface mixing ratio over the same areas, especially over the southern Great Plains where increases were >3 g kg^{-1}. Over the Canadian Prairies, increases were only ~1 g kg^{-1}. Nudging the land component only resulted in statistically significant increases in precipitation over those areas where the soil moisture added was sufficient to increase the mixing ratio by 3 g kg^{-1} or more. Del Sole et al. (2009) concluded that, in the mid-latitudes, moisture introduced into the soil is transferred to the atmosphere through ET, and is then advected downstream where positive precipitation anomalies are observed. Dirmeyer et al. (2006) assessed whether or not global models used in GLACE properly represent the land-atmosphere feedbacks. Their results show that most of the models do not capture the relationship between surface and atmospheric variables and fluxes. That is, the models likely do not simulate the coupling accurately. They noted that systematic biases in some of the modelled near-surface humidity and temperature might result in incorrect responses of the surface fluxes.

2.11 Soil Moisture

Soil moisture has been shown to have a persistence timescale on the order of months, which is longer than any other land-surface parameter (Robock et al. 2000). Soil moisture plays a critical role in governing the amount of moisture that is available for ET. It also affects the partitioning between latent and sensible heat fluxes, which in turn affect the low-level temperature, moisture and depth of the boundary layer, which can

ultimately influence convection. Research has suggested that improved initialization of soil moisture in climate models can improve warm season precipitation forecasts (e.g., Viterbo and Betts 1999). On shorter time scales (< 48 hrs), soil moisture has been shown to be important for improving the skill of precipitation forecasts (e.g., Nachamkin and Cotton 2000).

2.11.1 Soil moisture and vegetation

Adegoke and Carleton (2002) conducted an innovative study on the impact of soil moisture on subsequent vegetation state. They did this by examining relationships between in-situ soil moisture anomalies (from observations) and concomitant NDVI anomalies for two sites in Illinois over five growing seasons. They noted that the highest positive correlations were obtained when they (1) aggregated the high-resolution NDVI data into a 7 km by 7 km square centred on the soil moisture monitoring site, and (2) calculated lagged correlations. Specifically, they found that at the agricultural site, the highest correlations (up to 0.40) between soil moisture departures (in the top 1 m) and subsequent NDVI anomalies were obtained when NDVI lagged soil moisture by 2-4 weeks. That is, it took 2-4 weeks for the vegetation canopy to respond fully to the antecedent soil moisture anomalies. Another important finding is that the correlations increased if they calculated the soil moisture anomalies in the top 1 m of the soil column compared to those in the 10-30 cm layer. Their findings suggest that other factors (such as air temperature) are also responsible for modulating the health and density of vegetation. Nevertheless, their results do demonstrate that soil moisture has a marked impact on crop health, and that the vegetation acts to extend the soil moisture memory.

2.11.2 Soil moisture and the CBL

Entekhabi et al. (1996) provide an excellent overview of how soil moisture affects the overlying atmosphere. They state that the surface heat is dissipated by thermal radiation and turbulent flux, both of which are affected by soil moisture. Additionally, the partitioning between the two is a function of the surface temperature and static stability. The turbulent heat flux is partitioned into sensible and latent heat fluxes, and the relative partitioning of the two fluxes is controlled by soil moisture. Betts et al. (1996) note that the moist static energy (MSE) is equal to the sum of the latent and sensible heat fluxes, so that the portioning of the available energy does not affect the total MSE. On the other hand, the diurnal range of the MSE is controlled by the partitioning of the surface fluxes, with greater sensible heat fluxes leading to a deeper boundary layer with more entrainment, which reduces the diurnal rise of the MSE.

Basara and Crawford (2000) used near-surface meteorological measurements and soil moisture measurements (at varying depths) from the Oklahoma mesonet to investigate the links between soil moisture and atmospheric processes in the CBL on summer days with weak synoptic forcing. They found that soil water content in the root zone (30–40 cm below the surface in this case) was linearly correlated with evaporation and the maximum observed values of sensible and latent heat fluxes. In contrast, the daily ET was not strongly correlated with the soil moisture in the surface layer (top 5 cm). Furthermore, Basara and Crawford (2002) found a strong correlation between the root-zone moisture content and the 1.5 m temperature and mixing ratio.

Betts and Ball (1995) showed that soil moisture plays an important role in controlling the diurnal ranges of θ_e and specific humidity. Wai and Smith (1998) found

that, following intense precipitation, strong ET reduced the depth of the planetary boundary layer. Santanello et al. (2007) used sounding data and model output for a test site in northern Oklahoma to investigate interactions of the CBL with the land surface, and identified soil moisture and atmospheric stability as being key controls of CBL growth. Chang and Wetzel (1991) conducted a modelling study over central US and concluded that the reduced heating associated with surface evaporation alone is not sufficient to affect surface temperatures, but that the same is not true when vegetation is present to tap into root-zone moisture.

2.11.3 Impact of soil moisture on convection initiation and intensity

An appropriate representation of the land surface and its interaction with the overlying atmosphere becomes a necessary component for the proper simulation of convective precipitation. This point was highlighted by Georgescu et al. (2003), who noted that changes in local thermodynamics could translate into changes in CAPE and lifting condensation level (LCL) height, which can ultimately influence the timing and location of convection initiation. Also, Colby (1984) modelled boundary layer processes using a 1D model and found that soil moisture had a marked impact on the amount of convective inhibition and the partitioning of surface heat fluxes.

Research has shown that the amount and depth of moisture in the boundary layer is critical in determining the amount of convective instability, as well as the intensity of storms. For example, Lakhtakia and Warner (1987) found that high surface soil moisture (and higher low-level mixing ratio) is conducive to deep convection in the presence of sufficient lift.

Modelling results of deep convection over a homogeneous surface by Segal et al.

(1995) suggest that lowering the Bowen ratio increases the potential for deep convection. The reason for this is that an increase in latent heat flux (through increased transpiration) acts to increase the specific humidity in the CBL from vegetation and decreased entrainment of dry air from the free atmosphere (from reduced turbulent mixing). However, Segal et al. (1995) note that sensible heating of the boundary layer can be important for assisting in the erosion of capping lids (e.g., Crook 1996).

Numerical model simulations by McCaul and Cohen (2002) demonstrated that a deep layer of boundary layer moisture creates an environment that is more suitable for severe storms than an environment (having the same amount of CAPE and shear) that has only a shallow layer of moisture. They noted that increases in the sensible heat flux deepen the boundary layer, which can lead to the entrainment of drier air from the free atmosphere, which in turn reduces the depth of the low-level moisture. Consequently, despite the higher temperatures, the increase in CAPE is quite small (Segal et al. 1995) and the potential for storms is reduced.

Clark and Arritt (1995) expanded upon the work of Segal et al. (1995) and modelled the effect of soil moisture and vegetation on the potential for deep convection in the absence of large-scale forcing in Topeka, Texas. They found that while higher values of soil moisture delayed the onset of convection, the precipitation amounts associated with storms were higher. Also, values of the surface-based CAPE were sensitive to the influence of soil moisture.

Likewise, Wetzel et al. (1996) found that over an Oklahoma study area (where soil moisture was low), cumulus clouds first formed over dry, sparsely vegetated areas. Clouds formed one to two hours later over forested areas due to the suppression of

vertical mixing caused by an increase in the latent heat flux. In contrast, over a Kansas study area (where soil moisture was higher), clouds first developed above vegetated areas. Wetzel et al. (1996) concluded that the reason for this discrepancy was a very shallow nocturnal inversion in Oklahoma that was easily eroded by daytime heating. For the Kansas case, the CBL was characterized by a pre-existing deep stable layer, which suppressed rising thermals. Consequently, latent heat was allowed to build up and this led to clouds forming over areas that had the largest latent heat flux.

Modelling studies conducted by Pan et al. (1996) showed that increasing the soil moisture increased domain rainfall, but could decrease or increase rainfall at the local scale, depending on the thermal and moisture structure of the CBL. For example, increased ET reduced rainfall over areas that were already humid and lacked sufficient thermal forcing to initiate deep convection. However, if the atmosphere was unstable and the CBL was relatively dry, then increased ET tended to increase the local rainfall. Pan et al. (1996) proposed that sensible heating is more important in initiating convection, while ET is more important in amplifying convection.

Hanesiak et al. (2004) studied the impact of soil moisture on convective initiation over the Canadian Prairie provinces using satellite imagery and the crop phenology and water use model of Raddatz (1993). They found that the onset of deep convection was delayed significantly as the root-zone soil moisture content declined. In contrast, the correlation between soil moisture in the upper layers and initiation time was poor. Their findings are consistent with those of Rabin et al. (1990), who found that deep convection typically forms earlier over areas with a lower Bowen ratio — that is, areas where the latent heat flux is greater than the sensible heat flux.

Hanesiak et al. (2009) investigated whether the modelled root-zone plant available soil moisture (RZPAW) of the cropped grassland of the Canadian Prairies had predictive value in determining the occurrences and event days of severe summer convective weather. Dry areas with RZPAW ≤50% and wet areas with RZPAW >50% were identified at post-snowmelt, 15 June, and 5 July. Statistical analysis of the data showed that the relative number of occurrences and the relative number of severe event days were greater in the wet areas than in the dry areas.

Findell and Eltahir (2003a) developed a framework based on the low-level temperature and humidity structure of the early morning atmosphere for the purpose of quantifying feedbacks between soil moisture and convective rainfall potential. They organized atmospheric soundings into three groups: (1) convection favoured over dry soil, (2) convection favoured over wet soil, and (3) atmospherically controlled convection. For the atmospherically controlled profiles, the partitioning of fluxes at the land surface was not the critical factor determining the convective potential of the system. For example, the air was too dry and/or stable for deep convection. Findell and Eltahir (2003b) applied their classification system to 12 UTC soundings across the US for summers between 1957 and 1998. Over the northern US plains (south of the Canadian Prairies), 15% of the summers between 1957 and 1998 were predicted to experience a positive soil moisture-rainfall feedback, while only 1% were predicted to experience a negative feedback using their classification. About 80% of soundings in this region were classified as being atmospherically controlled, with 8% favouring wet soil and 7% favouring dry soil. Thus, the work of Findell and Eltahir underscores the importance of considering the early-morning temperature and humidity structure when predicting how

the CBL will respond to fluxes from the land surface, and how this will affect convection.

Siqueira et al. (2009) explored links between soil moisture dynamics and convection triggers over a pine plantation in the southeastern US. They coupled a soil-plant hydrodynamics model with a boundary layer budget model, and then modelled the response of the boundary layer over a 30-day dry-down period. They found that, as expected, the boundary layer grew more quickly under water-stressed conditions than when soil moisture was plentiful. However, the rapid growth of the CBL did not translate into triggering of convection because the height of the LCL also increased rapidly under water-stressed conditions, thereby preventing parcels from reaching the LCL. Siqueira et al. (2009) investigated the possibility that rapid boundary layer growth could tap into moisture immediately above the boundary layer and trigger convection. Their simulations showed that large amounts of moisture had to be added to the free atmosphere for this to occur. Thus, moisture from external sources had to be present to initiate convection above dry soils.

2.11.4 Soil moisture-precipitation feedback at seasonal timescales

Wang et al. (2006) noted that, while the impact of precipitation anomalies on soil moisture is obvious, the impact of those soil moisture anomalies on subsequent precipitation is much more difficult to quantify, because of the numerous mechanisms involved. Alfieri et al. (2008) noted that a primary restriction on assessing the impact of soil moisture on precipitation is the circularity of the problem. That is, precipitation is auto correlated because of the persistence associated with large-scale events. Alfieri et al. (2008) noted that studies using observed data are rare, and that the conclusions are often contrary. For example, a positive feedback between soil moisture anomalies and

future precipitation has been suggested by many studies (e.g., Eltahir and Bras 1996; Findell and Eltahir 1997; D'Odorico and Porporato 2004), a negative feedback is supported by Giorgi et al. (1996), Findell and Eltahir (2003b) and Cook et al. (2006), and no feedback was found by Salvucci et al. (2002).

Numerical studies have demonstrated that soil moisture has a marked impact on precipitation and surface temperature (Hong and Kalnay 2000; Beljaars et al. 1996). Specifically, it has been found that the atmosphere responds to moisture anomalies in such a way as to perpetuate the initial soil moisture anomaly (Rowntree and Bolton 1983). Also, Beljaars et al. (1996) found that dry soil moisture anomalies contribute to the maintenance of local drought conditions. Thus, it is postulated that if the root-zone soil layer is wet in the spring, the summer may either have a large or a small amount of convective rainfall and associated severe weather, depending on the attendant atmospheric circulation (Shukla and Mintz 1982). However, if the soil is dry, there is little transpiration to provide energy and water vapour to the convective boundary layer and the summer will likely be dry. An anomalously high soil moisture content in the root zone, coupled with growing vegetation, is a necessary though not sufficient condition for active convection. More recent studies (e.g., Oglesby et al. 2001; Schubert et al. 2004) have also found a positive feedback between below average precipitation anomalies and soil moisture by way of a reduction in ET.

Kochendorfer and Ramirez (2005) used a numerical model to investigate the effect of land-atmosphere interactions on the temporal variability of soil moisture over Illinois. Their results suggest that a positive correlation exists between soil moisture and precipitation efficiency.

Namais (1991) suggested that lower soil moisture values in the late winter and/or spring over the central US could potentially induce and amplify large-scale circulation anomalies. He postulated that this mechanism could help extend droughts. Oglesby (1991) found that early reduction of soil moisture had very little impact on the subsequent rainfall and soil moisture, but that a reduction of late spring moisture had a significant impact. Raddatz (2005) compared the June-August rainfall within census agricultural regions on the Canadian Prairies with the area-average moisture in the top 1.2 m of soil on 1 June, and found that there was a very poor positive correlation. These data suggest that the soil moisture level at the start of the season has a very limited effect on the subsequent summer rainfall in this region.

Feedback mechanisms can operate on timescales ranging from hours to years (Lawrence and Slingo 2005). While the exact strength of the coupling is unknown, there also exists observational evidence that supports the soil moisture-precipitation feedback hypothesis. Taylor and Lebel (1998) purport that in order for the convective feedback process to work, storms must pass over an area regularly. If the time interval between large-scale events is less than the characteristic timescale required to dry the topsoil (10 cm; 1-2 days), then the pre-storm evaporation rates will be uniformly high, and persistence is not favoured. If the event timescale is 3-4 days, heterogeneity in the deeper soil moisture may affect the CBL through transpiration rates. At scales of a few kilometres, advection and turbulence mix out surface-induced variability in the CBL (Raupach and Finnigan 1995). Oglesby et al. (2002) conducted modelling studies over Mississippi basin using idealized soil moisture anomalies and found that the magnitude of the anomaly is critical.

Fennessy and Shukla (1999) conducted modelling studies (using a GCM) to investigate the impact of soil moisture on precipitation. They found that the strength of the linkage was also governed by factors such as the magnitude of the soil moisture anomaly, soil wetness persistence, solar forcing, accessibility to other moisture sources and large-scale dynamics.

The case for the soil moisture-precipitation feedback mechanism is not clear-cut. For example, Findell and Eltahir (1997) found only a small feedback between soil moisture and subsequent rainfall over Illinois. They noted, however, that the strength of the feedback between soil moisture and future rainfall was strongest in the summer, when they found statistically significant lag correlations between observed soil moisture anomalies and subsequent observed rainfall. If soil moisture values differ significantly, the likelihood of persistence over a period of a few weeks is increased. In contrast, Findell and Eltahir (1999) found that the feedback was not transmitted by way of a positive feedback between soil moisture and MSE, nor was there a positive correlation between the MSE and rainfall. There was, however, a significant negative correlation between the soil moisture and the LCL, and between the LCL and the rainfall. Also, Huang et al. (1996) argued that increased evaporation from anomalously wet soil has little impact on future precipitation. Georgescu et al. (2003) simulated precipitation in July over the Mississippi river basin between 1995 and 1997 using six different soil moisture patterns. Their results suggest that it could be the distribution of soil moisture that is more important than the actual soil moisture amount.

Schär et al. (1999) conducted modelling experiments over continental Europe using homogeneous positive soil moisture anomalies. They concluded that higher levels of soil

moisture (and ET) led to more precipitation, but that moisture recycling alone does not explain the enhanced precipitation over anomalously moist soil. Rather, they suggest that the enhanced precipitation over moist soils is also largely derived from horizontal moisture advection, while moisture advection over dry soils does not initiate precipitation events as frequently.

Taylor et al. (2005) analyzed cloud-free brightness temperatures from satellite over the semi-arid Sahel region of Africa. They noted that rainfall produced noteworthy differences in the spatial distribution of soil moisture and surface temperatures. Moreover, they found that soil moisture variations on the order of several hundred kilometres could generate low-level circulations, which in turn modulated the presence of deep convective clouds in their vicinity.

While climate models do reflect an increase in precipitation above anomalously wet areas (Dirmeyer 2000), it is not clear whether this is a real difference or simply an artefact. To address this question, Koster et al. (2003) made a 50-yr simulation (1948–1997) using the average of four parallel runs made by an atmospheric general circulation model. They then correlated forecast precipitation fields with a five-day time lag for the month of July. For example, the rainfall total between 1 and 5 July was correlated with rainfall observed between 11 and 15 July. They found a high correlation in a broad band extending from the Canadian Prairies southwards to the Gulf coast. High correlations were also evident over Florida and in the Pacific Northwest. In their no-feedback run, ET was permitted to continue along mean seasonal cycles, but wetter than normal soil conditions were not allowed to enhance ET. In this run, only very weak correlations were found. They conclude that the swath of high correlations is unique and attributable

to the land-atmosphere feedback and not a result of SST anomalies.

Kim and Wang (2007) investigated the impact of the soil moisture-precipitation feedbacks using a coupled land-surface and climate model. They found statistically significant correlations between soil moisture and subsequent precipitation at lead times of two to four weeks over the Great Plains. They also found statistically significant positive correlations between ET and future precipitation over the same area for lag times of up to four weeks.

Alfieri et al. (2008) investigated the relationship between warm season soil moisture and subsequent precipitation for 16 locations in the US Midwest between 1971 and 2003. They first identified convective precipitation days using calculations of CAPE from observed soundings. Next, they correlated convective rainfall occurrence against antecedent soil moisture (in the top 50 cm) from model runs using a lag time of one day (i.e., precipitation lagged soil moisture by one day). A critical finding is that the positive correlation between soil moisture and precipitation is due to the autocorrelation of long stratiform precipitation events, which dominate the data. When only convective events were investigated, they found that the correlations were both positive and negative. They conclude that their analysis indicates that the possibility of a positive feedback between antecedent soil moisture and convective precipitation exists, but that soil moisture alone is not capable of unambiguously isolating the signal.

2.11.5 Soil heterogeneity and land-atmosphere modelling

Soil structure and associated hydraulic parameters are notoriously heterogeneous in both the horizontal and vertical planes (Islam et al. 2005). McBratney and DeGruijter (1992) stated, *"it is well accepted that we can neither measure all the properties of the*

soil at a particular location in space and time nor even one property at all points in space (and time)".

Numerous studies have been conducted which quantify the spatial variability of soil structure (e.g., Wösten et al. 1987) and demonstrate that the spatial variability of soil hydraulic parameters exists on scales ranging from the microscale to the macroscale (Mengelkamp et al. 2006). Accurately modelling the evolution of moisture in the root zone and the exchange of moisture between the land surface and atmosphere requires simulating several complex processes in addition to using appropriate input data. The inherent variability in soil hydraulic parameters is of particular concern for land surface models (Gutmann and Small 2005), whose grid scale is often larger than the autocorrelation length of many soil texture and hydraulic parameters. Lenhardt (1984) identified three primary sources of error when modelling soil moisture content: (1) error in the estimation of rainfall, (2) error due to the spatial variability of soil hydraulic properties, and (3) error due to the parameterization of certain processes.

Shao and Irannnejad (1999) concluded that uncertainties in soil hydraulic parameters could overwhelm the uncertainties in the theory of hydraulic models. Given that the impact of soil hydraulic models on the performance of land surface schemes can be significant, the use of an appropriate hydraulic model and an accurate set of soil hydraulic parameters is critical for land-surface modelling. According to Gijsman et al. (2003), *"an incorrect estimate may make the difference between a purely academic simulation or one that tries to mimic reality"*.

Brimelow et al. (2010a) validated PAM against in-situ soil moisture observations from three sites on the Canadian Prairies. They found that correct modelling of soil

moisture and attendant ET was contingent on accurately specifying the site-specific soil hydraulic properties.

2.12 Vegetation

Zhang et al. (2007) stated that the interactions between vegetation and the atmosphere in arid and semi-arid regions, and the mechanisms by which they interact, are a critical component in ecohydrology. Jiang et al. (2009) noted that neglecting the response of vegetation to precipitation and temperature anomalies could lead to either an over- or underestimation of latent heat fluxes by land-surface schemes in models. Many studies have shown that changes in vegetation phenology can have a marked impact on the partitioning of available energy (e.g., Liu et al. 2006; Notaro et al. 2006; Xue et al. 2006). Jiang et al. (2009) included a dynamic vegetation growth model — that is the vegetation was allowed to respond in terms of leaf area, and ET to environmental drivers such as soil moisture and temperature — in a coupled land-atmosphere model over the central US. They found that including dynamic vegetation played a significant role in enhancing the persistence of intra-seasonal precipitation in the model. Specifically, they noted that the model was better able to simulate the diurnal cycle of surface fluxes, temperature and precipitation. In addition, the inclusion of dynamic vegetation resulted in stronger land-atmosphere feedback in the summer.

Land-vegetative processes have an important impact on the structure of the CBL. Vegetation plays a crucial role in transporting moisture from the root zone to the CBL. As I will show below, transpiration can greatly increase the moisture content of the boundary layer. Of course, vegetation also alters the surface albedo and roughness of the

surface, and these in turn can have significant effects on the energy budget and low-level wind profiles, respectively.

After completing numerical simulations using the Coupled Ocean/Atmosphere Mesoscale Prediction System to investigate the impact of land–vegetation processes on the prediction of mesoscale convection over Oklahoma, Holt et al. (2006) found that adding a sophisticated transpiration model allowed the atmospheric model to respond to the more detailed representation of soil moisture and temperature.

Evapotranspiration from a very moist surface in summer can reach 8 mm day^{-1}, which for a 1000-m deep CBL (and ignoring entrainment) equates to increasing the specific humidity by approximately 8 g kg^{-1} (Segal et al. 1995). Similarly, modelling results for the Canadian Prairies suggest that ET can increase the specific humidity by 4–8 g kg^{-1} per day (Raddatz 1993). During drought, reduced vegetation cover and plant stress reduce the amount of water vapour transpired by the plants.

As was stated earlier, the soil moisture content in the root zone has a longer memory than the weather pattern that may have originally produced the wet or dry anomaly. Therefore, the moisture and energy fluxes into the CBL from the vegetation associated with these soil moisture anomalies can have a profound effect on the structure of the boundary layer and contribute to the persistence of wet or dry conditions long after the precipitation anomaly that created them has passed (Schubert et al. 2004). Sellers and Hall (1992) used a GCM to simulate the response of the atmosphere to such a scenario by initializing the model with a low soil moisture content on 1 April and dormant prairie vegetation that would be observed during a drought. They found that including dormant vegetation in the spring and early summer in their model greatly reduced the ET by

eliminating transpiration. The effect of reduced ET on the local climate increased as the summer progressed, and ultimately led to a severe drought. However, because the dormant vegetation was prevented from accessing root-zone soil moisture, the soil moisture there began to rebound toward the middle of summer.

Rabin et al. (1990) used satellite imagery and detailed landscape information to study spatial variations of cumulus clouds over flat terrain during relatively dry conditions. They found that convective clouds first developed over a large area (100 km by 300 km) of harvested spring wheat in Oklahoma where the ground temperature was warmer than that of the surrounding areas with active vegetation growth. They also noted that convection was suppressed downwind from small lakes and forested areas.

McPherson et al. (2004) used Oklahoma mesonet data between 1994 and 2001 and noted that in March, prior to harvest, surface dewpoints over the cropland were higher (by 2–10°C) than over the surrounding (dormant) grassland. McPherson and Stensrud (2005) undertook a numerical modelling study to investigate the effect of replacing tallgrass prairie with winter wheat. The cropland was non-irrigated and about 150 km wide. McPherson and Stensrud concluded that the presence of the spring wheat increased values of latent heat flux and lowered sensible heat flux. This resulted in higher mixing ratios above and downstream of wheat, as well as a shallower CBL above and downstream of the cultivated area.

2.12.1 Vegetation and convective clouds

As discussed previously, the amount of moisture in the CBL has important consequences concerning the initiation and intensity of convective clouds and thunderstorms (Segal et al. 1995). Raddatz (1998) found that the occurrence of

thunderstorms has likely increased in the middle of the growing season, while the average onset of convection was delayed because of changes in ET associated with the landscape changing from grass to wheat. Johns et al. (2000) concluded that ET played a significant role in conditioning the pre-storm boundary layer structure for violent tornadoes over the north-central US. Segal et al. (1995) demonstrated the greater sensitivity of CAPE to the latent heat flux than to the sensible heat flux. Also, while higher rates of ET can increase CAPE, the associated reduction in sensible heat could preclude the triggering of thunderstorms on account of lower temperatures.

Rabin (1977) used a surface energy budget model to investigate the impact of vegetation and soil moisture on the timing of convection. He found that there was a coupling between the two, especially when the synoptic forcing was weak. Moreover, the strength of the coupling depended on the profile of temperature and moisture, as well as on the nature of the surface. When the CBL was moist, convective clouds formed downwind of moist areas. When the lower atmosphere was relatively dry, development first occurred over drier, warmer areas. The amount of heat required to modify a sounding to allow for convection varies with the Bowen ratio. Less energy is required to form convective clouds when the Bowen ratio is low (i.e., during moist conditions). Therefore, on days when the Bowen ratio is low, clouds should first form over forested areas, or areas with high surface wetness. Conversely, on dry days convection is expected over areas where the Bowen ratio is high.

Carleton et al. (1994) observed a higher incidence of cumulus cloud cover over forested areas in the American Midwest. Similarly, O'Neal (1996) noted that over North America, forested areas have a higher incidence of convective cloud cover than do crop

areas, especially under quiescent atmospheric conditions.

2.12.2 The vegetation-precipitation feedback on seasonal timescales

Dirmeyer (2006) suggested that soil moisture is strongly modulated by antecedent precipitation, that soil moisture in turn exerts a "moderate" influence on ET, but that the impact of ET on precipitation is "tenuous". Liu et al. (2006) noted that most research on global vegetation-atmosphere feedbacks has been conducted using paired sensitivity experiments with or without certain key vegetation variables (e.g., Bounoua et al. 2000).

Kim and Wang (2007) examined the impact of dynamic vegetation on the evolution of soil moisture anomalies and subsequent precipitation. To do this they ran a coupled regional climate model with a predictive/dynamic vegetation phenology scheme over the Mississippi river basin for 10 summers. They found that positive soil anomalies increase the LAI, which is associated with a concomitant increase in precipitation on account of additional moisture in the CBL from increased ET, and surface heating (lower albedo and higher net radiation). They found that dry soil moisture anomalies do not show a marked impact on subsequent vegetation growth or precipitation. They attribute this to the model's dry bias, which results in a reduction of LAI in the control run, leaving little room for further depletion in LAI and transpiration. Also, wet soil moisture anomalies in the spring were expected to delay the growth of vegetation, and the precipitation feedback was negative. During the summer the negative vegetation feedback muted the positive feedback of soil moisture on precipitation. This is because the increased evaporation in April, and increased ET once the vegetation emerges, results in a rapid draw down of the soil moisture, and even dry anomalies in the soil moisture in June and July.

Matsui et al. (2005) incorporated a satellite-derived vegetation greenness fraction in a regional climate model and found a strong link between greenness and evaporative fraction and near-surface temperature and relative humidity in the CBL.

Notaro et al. (2006) used the photosynthetically active radiation (PAR) derived from satellite data to examine the interaction between vegetation and precipitation over the US between 1982 and 2000. They found that much of the prairie has a statistically significant correlation between JJA PAR anomalies and precipitation anomalies from the previous month. This is consistent with the delays found by Adegoke and Carleton (2002) in the response of NDVI to precipitation. Notaro et al. (2006) also noted that increases in PAR generally led to higher temperatures because the effects of the lower albedo outweighed the reduced warming from increased ET. Regarding the impacts of PAR on precipitation, they noted that the feedback was weaker than for temperature and was complex, with the result that the feedback for precipitation was often not statistically significant. However, correlations of PAR leading precipitation are positive in JJA over tornado alley. In contrast, the correlations are negative over the northern Great Plains in JJA, but positive in fall and spring. Averaged over the entire year, the feedback was found to be positive for the Great Plains. Notaro et al. (2006) concluded that a longer time series could yield larger areas of statistically significant vegetation forcing on precipitation, but they suspected that the response would probably be weak.

Liu et al. (2006) conducted a similar study to that of Notaro et al. (2006), but for all ice-free landmasses in the world. Specifically, they investigated feedbacks between PAR, observed surface temperature and precipitation on a 2.5º grid. They then calculated lead and lag correlations to infer feedbacks. They found that over northern Asia and

northern North America there is a positive feedback between PAR and temperature, on account of the surface albedo feedback. As was noted by Notaro et al. (2006), Liu et al. (2006) found that on an annual time scale, positive correlations existed when temperature led PAR by one month over most of the conterminous US on an annual time scale. They also found positive annual correlations when precipitation led PAR over the Canadian Prairies. Seasonally, there were positive correlations between precipitation leading PAR over the grasslands of western N. America, including the Canadian Prairies. However, they were unable to identify a significant correlation over N. America when PAR led precipitation. In fact, in JJA over the Canadian Prairies, they identified a negative correlation when PAR led precipitation by one month. This suggests a negative feedback between precipitation and preceding PAR. Liu et al. (2006) noted that, while the vegetation feedback increased the precipitable water, the moisture might not precipitate locally, resulting in low or no correlations between vegetation cover and local precipitation.

2.13 Land Heterogeneity

Lynn et al. (1998) noted that satellite observations show significant landscape discontinuities of soil type, soil wetness, vegetation cover, waterbodies, and topography across land areas (Matthews 1983; Rabin et al. 1990; Calvet et al. 1997). This natural heterogeneity often produces horizontal pressure and thermal gradients of sufficient strength to generate and sustain organized thermal circulations. Observational studies have found that landscape-generated mesoscale circulations are associated with landscape patches defined by these discontinuities (Rabin et al. 1990; Bougeault et al. 1991; Mahrt

et al. 1994; Cutrim et al. 1995; Doran et al. 1995). Fischer et al. (2007) noted large differences in water, carbon and energy fluxes between different vegetation types in the southern Great Plains over distances < 5 km.

Conventional meteorology observation networks are too coarse to resolve mesoscale differences or identify circulations arising on account of surface heterogeneity. Consequently, extensive research has been undertaken in the last 25 years to study the physical mechanisms responsible for the formation of land breezes, as well as their impact on the boundary layer and antecedent precipitation (Anthes 1984; Mahfouf et al. 1987; Segal et al. 1988; Rabin et al. 1990; Dalu and Pielke 1993; Avissar and Chen 1993; Mahrt et al. 1994; Chen and Avissar 1994; Wang et al. 1996; Vidale et al. 1997; Lynn et al. 1998). Field observations have found that mesoscale circulations arising from strong thermal contrasts are often weak and/or shallow because they are damped by the large-scale circulation (Mahrt et al. 1994; Doran et al. 1995). Satellite observations, however, provide evidence of mesoscale circulations producing convective clouds (Rabin et al. 1990; Cutrim et al. 1995; Weaver and Avissar 2001).

Adjacent areas having different land vegetation types affects the partitioning of sensible and latent heat fluxes, which in turn can form sharp gradients in the low-level surface temperature and moisture fields. Moreover, surface heterogeneity can lead to horizontal pressure gradients that are strong enough to generate organized circulations in the CBL (Segal and Arritt 1992). Observational evidence exists of surface heterogeneity inducing mesoscale land breezes (e.g., Mahrt et al. 1994; Shaw and Doran 2001).

Weaver and Avissar (2001) showed that strong synoptic-scale winds do not necessarily inhibit mesoscale circulations. In contrast, Avissar and Schmidt (1998) found

that synoptic winds nearly eliminated mesoscale circulations. Baidya Roy and Avissar (2002) used the RAMS model to simulate mesoscale flow over heterogeneous area of the Brazilian forest. Their model simulations showed that coherent mesoscale circulations did develop in response to the surface heterogeneity, and that the synoptic flow did not disrupt them, but rather advected them downwind. Weaver (2004a,b) used RAMS to investigate land-atmosphere interactions during the warm season over the southern Great Plains and noted that the large-scale flow affected the orientation of coherent roll structures in the CBL, but not so much their intensity.

Weaver and Avissar (2001) used a mesoscale model and surface observations over Oklahoma and southern Kansas, and found that surface heterogeneity forced strong lower-tropospheric circulations, causing significantly enhanced vertical heat and moisture fluxes. Pielke (1984) calculated the magnitude of horizontal gradients of the sensible heat flux from observational and modelling studies. He suggested that gradients less than 10 W m^{-2} per 30 km have a limited influence on wind patterns. For gradients of 100 W m^{-2} per 30 km up to 1000 W m^{-2} per 30 km, significant effects are observed.

One of the difficulties in forecasting summer season rainfall amounts and location is attributable to interactions between the surface and the CBL (Robock et al. 2000). Under the right conditions, these surface heterogeneities can have important consequences for surface energy budgets and ultimately enhance convective clouds and convective precipitation (e.g., Rabin et al. 1990; Segal et al. 1995; Avissar and Liu 1996; Basara and Crawford 2000; Negri et al. 2004). Mahfouf et al. (1987) used a 2D model to examine the impact of surface heterogeneity (in terms of soil and vegetation) in forcing mesoscale circulations. They concluded that the transition zone between bare soil and vegetation is

a preferred region for the initiation of convection. Wang et al. (2000) found that surface-driven mesoscale circulations can trigger moist convection and precipitation under quiescent conditions.

Lynn et al. (1998) used a high-resolution 2D model to investigate the impact of soil moisture and boundary layer conditions on landscape-generated deep moist convection for a region dominated by tall broadleaf and coniferous trees. In their modelling experiments, the soil moisture was forced to alternate between broad wet and dry patches ranging from 1 km to 256 km in width. They found that land breeze fronts initially developed on the boundary between a moist and a dry region and then propagated towards the centre of the dry region. Shortly after the breeze fronts formed, thunderstorms were predicted to develop along the breeze fronts. The highest rainfall amounts were predicted in domains between 100 km and 200 km in width, which corresponds closely to the Rossby radius of deformation. The heaviest rainfall was not forecast to occur where the CAPE was largest (i.e., in areas with high soil moisture), but rather along the land breeze fronts located between the patches where the CAPE was of intermediate values.

Hanesiak et al. (2004) studied the effect of soil moisture and evapotranspiration on the initiation of convective clouds over the Canadian Prairies using satellite imagery and the crop phenology and water-use model of Raddatz (1993). Their research showed that under quiescent atmospheric conditions, *"transient evapotranspiration gradients influenced the location of deep convection initiation"*.

Cheng and Cotton (2004) examined the sensitivity of varying horizontal heterogeneities of soil moisture anomalies on simulations of a mid-latitude mesoscale

convective system using a cloud-resolving model. Their results are very similar to those of Lynn et al. (1998). Specifically, Cotton and Chen found that deep, moist convection was suppressed over areas having high moisture content, while enhanced development was predicted to occur on the edge of wet soil anomalies.

Blyth et al. (1994) included the role of vegetation in their modelling study investigating the influence of surface features on pre-storm conditions. They found that forest stands produced enhanced mass, heat and momentum transfer where rough elements of forest stands covered the surface. Consequently, forecast precipitation over the forests was 30% greater than over bare soil. James et al. (2009) incorporated near-real time values of vegetation fraction into the land-surface scheme of a high-resolution mesoscale model to investigate the impact on forecasts for eight severe thunderstorm events over the Great Plains. They found that including the actual vegetation state improved the forecasts of near-surface temperature and moisture, as well as the CAPE and CIN. However, these improvements did not translate into a marked improvement in the forecasts of convection initiation and intensity. They argue that this could be because they did not update the soil moisture to be consistent with the observed vegetation fraction data.

2.14 Conceptual Models of Feedback Mechanisms and Processes

Various authors argue that one should refer to the "indirect soil moisture-precipitation feedback" mechanism (e.g., Schär et al. 1999). According to Lawrence and Slingo (2005), the reason for this is that the *"influence of wet soil on precipitation is not simply via recycling of the extra water vapour associated with enhanced surface*

evaporation into rainfall. Instead, the indirect feedback considers how soil moisture affects the precipitation through its influence on boundary layer characteristics and atmospheric instability".

Wei et al. (2008) noted that climate processes include complex interactions, and that unambiguously identifying the presence of a particular feedback mechanism depends on whether it is discernable from the background noise (i.e., other processes and feedbacks). They also noted that not only does the precipitation time series include both random and low-frequency components, but it can also include low-frequency components arising from both its own intrinsic variability (i.e., autocorrelation) and land memory. Consequently, a lagged soil moisture–precipitation correlation may be influenced by the autocorrelation of precipitation and may not always be an indicator of a causal relationship. Santanello et al. (2007) noted that the degree to which the land affects the atmosphere (and vice versa) is difficult to quantify given the disparate resolutions and complexities of land surface and atmospheric models and the lack of comprehensive observations at the process level (Entekhabi et al. 1999; Gu et al. 2006).

Kim and Wang (2007) stated that the net impact of wet soils on vegetation and subsequent precipitation is uncertain. They reason that this is because wet soils allow for a positive feedback because denser vegetation lowers the albedo and Bowen ratio which in turn creates an environment which favours more precipitation (e.g., Bounoua et al. 2000). In contrast, denser vegetation depletes the soil moisture faster through transpiration than does less dense vegetation, and if good rains do not persist, the soil moisture will decrease to the point where transpiration is reduced, lowering moisture in the boundary layer and resulting in a negative precipitation feedback (Wang et al. 2006).

Past modelling studies have determined that, in general, wet soils favour positive precipitation feedbacks, and vice versa. Recently, satellite-derived vegetation indices have been used to initialize models to ascertain the effects of changing the vegetation. The results have not been conclusive. For example, Bounoua et al. (2000) found that as vegetation increased so did modelled global precipitation, although the increases were less than those in ET. On the other hand, Guillevic et al. (2002) found that allowing for inter-annual variability in vegetation affected ET, but that there was no discernible effect on model precipitation.

The key is to understand under which conditions a particular feedback will be favoured, and this requires a detailed understanding of the processes involved. Koster et al. (2009) identified climate regimes suited to supporting land-atmosphere interactions. Specifically, they generated maps of the US showing where ET is governed by soil moisture, energy availability or both.

Koster et al. (2009) showed that over most of the Great Plains (including the Canadian Prairies) JJA-averaged evaporation typically lies in the soil moisture-controlled regime, and rarely lies in the energy-controlled regime. That is, the climate in this particular region favours strong land-atmosphere coupling. These findings are corroborated by calculations of the decoupling coefficient made by Wever et al. (2002), using eddy covariance and solar radiation data at a short-grass Prairie site in southern Alberta between 1998 and 2000. They found that the decoupling coefficient ranged between 0.1 and 0.3 (mean 0.27), indicating that ET was strongly controlled by surface conductance (which is in turn a function of soil moisture) and the vapour pressure deficit.

Pal and Eltahir (2001) give a detailed discussion of the major processes at work in

the indirect rainfall feedback, namely:

i) *Radiation feedbacks*—wet soils are typically associated with denser vegetation, which lowers the albedo. The lower albedo increases the absorption of the solar radiation, thereby increasing the surface temperatures. The increase in ET also increases the amount of moisture in the boundary layer, and results in an increase in the downward long-wave radiation. This process cools the surface, which then reduces the outgoing terrestrial radiation. If higher soil moisture increases the cloud coverage, then cloud cover can offset or even outweigh the albedo effect.

ii) *Instability feedbacks*—an increase in soil moisture tends to increase the MSE through an increase in ET. Dry soils increase the sensible heat flux, which increases the turbulent mixing and the depth of the CBL. The opposite is true over moist soils. The increase in MSE and shallower CBL depth over moist soils result in higher MSE per unit depth. Also, the slower growing CBL above moist soils is less likely to entrain dry air above the CBL.

iii) *Moist deep convection*—an increase in soil moisture increases the MSE. Also, adding latent energy into the boundary layer increases the instability. It follows intuitively that an increase in the number of days with positive CAPE will increase the potential for thunderstorms. Moreover, increasing the boundary layer moisture and lowering surface temperatures lowers the cloud-base height of the convective clouds. This not only increases the depth of the cloud, but also increases the liquid water content in the cloud, thereby enhancing the precipitation efficiency. This process leads to a positive feedback, with moist soil conditions leading to an increased potential for heavy convective rainfall events.

Pal and Eltahir (2001) noted that a negative feedback could occur under the right conditions. That is, lower soil moisture can increase deep, moist convection. This is because the increase in sensible heat allows the CBL to grow quickly, and parcels can reach the LFC when they otherwise would not have been able to. They suspect that this mechanism may be most effective in areas when instability is the limiting factor (Bernadet et al. 2000).

Trier et al. (2004) modelled convective initiation using a mesoscale model and high-resolution land surface conditions. They concluded that the land surface-atmosphere interactions were important for convective initiation and originated from several processes:

i) the partitioning of sensible and latent heat fluxes, which controls the depth of CBL and instability
ii) horizontal gradients of virtual potential temperature in the CBL due to differential heating over heterogeneous land surfaces lead to horizontal pressure gradients capable of generating mesoscale solenoidal circulations (e.g., Segal and Arritt 1992)
iii) the strength of the mesoscale circulation is proportional to the magnitude of the potential temperature gradient and depth through which it extends, which can reduce CIN and lead to convective initiation.
iv) fine-scale CBL circulations within a region of enhanced CBL depth are responsible for convective initiation.

Like Pal and Eltahir (2001), Trier et al. (2004) noted that their model simulations were sensitive to the location and magnitude of soil moisture anomalies. They also noted a greater likelihood of convective initiation over relatively dry soil, where more net

radiation is partitioned into sensible heat flux. Schär et al. (1999) proposed that the soil-precipitation feedback relies on the mechanisms that increase the efficiency of the convective process, namely:

i) lower Bowen ratio, shallower CBL, greater MSE per unit depth

ii) lower LCL, deep clouds (and higher LWC in clouds)

iii) Net shortwave radiation at the surface is decreased (increases cloud cover), but this effect is overpowered by the decrease in net longwave emission. The net result is an increase in the convective instability.

Lawrence and Slingo (2005) also provided a conceptual model outlining the indirect rainfall feedback mechanism:

i) Wet soil generated by heavy rains induces a strong ET response.

ii) As a result of enhanced ET, portioning of the latent and sensible heats fluxes is changed, with more of the available energy going into latent heat rather than sensible heat. This reduces the Bowen ratio and also results in a relatively shallow CBL.

iii) Increased moisture also increases downward longwave radiation. There is also a net increase in the longwave radiation at the surface.

iv) The increase in low-level moisture increases the convective instability.

v) The wet soil and denser plant growth lower the albedo, which in turn enhances the net radiation (reduces outgoing longwave radiation) and increases the heat flux into the CBL.

vi) These factors act to increase the MSE, which increases the potential for convection.

Dominguez and Kumar (2008) proposed a mechanism whereby soil moisture and precipitation are negatively correlated. They based this conceptual model on their

observations from the Ohio valley, and also on the integrated findings from several other studies. Their conceptual model also allows for a positive feedback when there is insufficient moisture in the root zone to sustain ET or when the MSE in the CBL is not large enough to support convection. They noted that in water-limited ecosystems, or droughts, the positive feedback dominates, but that in the eastern US the negative feedback typically dominates on account of the predominance there of ample root-zone soil moisture. Consequently, Dominguez and Kumar (2008) concluded that over the Ohio valley, ET variability is not one of the primary drivers of precipitation recycling. They argued that precipitation recycling only becomes important when the moisture advection decreases and when the total precipitation also decreases.

2.15 The Second-generation Prairie Agrometeorological Model

The second-generation Prairie agrometeorological model (PAMII; Raddatz 1993) simulates the evolution of soil moisture content and vegetation using a daily time step. Two versions of the model were used in this thesis, a cereal crop version and a pasture/grassland version. Unless otherwise specified the following discussion pertains to the crop version.

Input data for the model consist of observed daily observations of minimum and maximum temperature and rainfall. In addition to observed precipitation and minimum and maximum temperatures, PAMII also requires the vapour deficit and a profile of temperature, humidity and wind in the PBL. To this end, 0- hour soundings from the daily 1200 UTC and 0000 UTC model runs from the regional version of the Canadian Global Environmental Multi-scale (GEM; Côté et al. 1998) model were used. The

surface characteristics are described in terms of the terrain height, roughness length, soil class, crop stage, root- and top-zone moisture levels.

For crops, the phenological stage is determined by the planting date, accumulated heat and photoperiod. Specifically, the model uses bio-meteorological time (BMT; Robertson 1968) to estimate the crop stage, rooting depth and the fractional leaf area (L_A; fraction of the surface area that is shaded by vegetation), which is zero at planting and increases to 100% at the heading stage, followed by a decline (Raddatz 1993). The root depth (R_z) increases with time from 10 cm at time of sowing to a maximum of 120 cm,

$$R_z = 5 + 115.0/[(1+ \exp\{5.0 – (8(BMT*3.5))\}) \quad (2.6)$$

Green up for pasture/grasses is assumed to occur at the first occurrence of five consecutive days having a mean temperature greater than 5 °C, while dormancy occurs following the first day with a minimum temperature of -5 °C (Raddatz 2005). For pasture/grasses, the maximum rooting depth is held constant at 110 cm, and the fractional leaf area is also set to 1.0 during the active growth period.

2.15.1 Evapotranspiration

Evapotranspiration is the sum of evaporation from the soil and transpiration from the canopy,

$$ET = (1 - L_A)[h\rho(T_o) - \rho(Td_o)]/(r_a + r_g) + L_A[\rho(T_o) - \rho(Td_o)]/(r_a + r_c) \quad (2.7)$$

Equation 2.7 shows that transpiration is governed by the difference between the saturated vapour density of the air ($\rho(T_o)$) and actual vapour density ($\rho(Td_o)$), fractional leaf area, aerodynamic resistance (r_a) and canopy resistance (r_c). Here T_o and Td_o represent the air temperature and the dew-point temperature, respectively. The stability adjusted aerodynamic resistance term quantifies the atmosphere's ability to transport

water vapour in the vertical (e.g., Raddatz 1993; Gervais et al. 2010). The humidity of the skin layer immediately above the soil surface is denoted by h. The magnitude of r_c is inversely proportional to the relative plant available moisture present in the root zone (PAW), and L_A. The total canopy resistance is given by,

$$r_c = (r_{cmin})/L_A[(W - W_x)/(W_f - W_x)]^{-1.0} \quad (2.8)$$

where r_{cmin} is the minimum stomatal resistance (set to 80 s m^{-1} for both pasture and cereal crops), W is the root-zone soil moisture content (in mm), W_x the soil moisture content at the permanent wilting point and W_f the content at field capacity.

The resistance of the top-zone soil moisture (w) to the capillary action of water in equation 2.7 (r_g) is calculated using,

$$r_g = (r_g(soil)[(w - w_x)/(w_f - w_x)]^{-2.5} \quad (2.9)$$

where r_g (soil) is a reference value set to 100 s m^{-1}. Minimum and maximum ET values are calculated at sunrise and for the daily maximum temperature (assumed to occur two thirds of the way through the daylight period). A sinusoidal curve is then fitted to the minimum and maximum ET values to derive hourly values for ET. The sum of the hourly values is then used to calculate the daytime ET.

2.15.2 Soil moisture

Eleven soil types from the USDA soil triangle can are discerned; values of wilting point, field capacity, saturation level and available water content are specified for each soil class in look-up tables. The same soil type is specified for both the top zone (top 10 cm) and root plus sub zones (120 cm), and the soil's texture is assumed to be homogeneous throughout the soil column. The subzone shrinks as the as the root zone grows. The bulk soil moisture in the root/subzone and top zone are tracked separately.

Moisture in the top zone is depleted by both transpiration and by evaporation; in the root-zone by transpiration and by deep drainage from the subzone. The root-zone moisture is adjusted daily using the following formula:

$$W(JD) = W(JD-1)-(ET-P_i) + \theta\,(Z_R(JD)- Z_R\,(JD-1) \qquad (2.10)$$

Where W is the root-zone soil moisture content (equivalent depth in mm), JD is the Julian Day, ET is the evapotranspiration, P_i is the infiltration of precipitation, θ is the volumetric soil moisture in the sub zone. The top-zone soil moisture (w; equivalent depth in mm), varies according to the following formulation,

$$w(JD) = w(JD-1) - (C_1ET - P_i) - \tau C_2(\theta_{tz} - \theta_{rz}) \qquad (2.11)$$

In the model, the amount of daily ET from the top-zone is modulated by the coefficient C_1, which is a function of L_A, and varies between 0.4 (L_A = 1) and 1 (L_A = 0). The last term in (2.11) restores the top zone moisture towards the root-zone moisture when the moisture content in the root zone (θ_{rz}) is greater than that of the top zone (θ_{tz}), τ is the portion of night-time hours in each day. The coefficient C_2 controls the rate at which the soil moisture content is restored to equilibrium. Rainfall less than 25.4 mm infiltrates into the soil until field capacity is achieved. To allow for run-off during heavy rainfall events (> 25.4 mm), rainfall on such days is partitioned between infiltration and run-off depending on the soil moisture in the top 10 cm, even when there is available capacity. Infiltration into the root zone is not permitted when the top zone is saturated.

2.15.3 Comparison of PAMII with other land-surface schemes

Here we briefly discuss two prominent land-surface schemes used in numerical models in Canada and compare them with PAMII. The Canadian GEM numerical weather prediction model currently uses the Interactions Soil-Biosphere-Atmosphere

(ISBA) soil-vegetation-atmosphere-transfer model to simulate processes occurring at the interface between the soil, vegetation and the boundary layer (Bélair et al. 2003). ISBA treats the land surface as a composite of three main elements: vegetation, soil and snow. ET is calculated using a bulk transfer scheme similar to that used in PAMII. A Jarvis-type scheme models the canopy resistance to respond to environmental stresses such as global solar radiation, vapour pressure deficit, soil moisture potential (i.e., moisture stress) and canopy temperature. Current operational version of ISBA has two soil layers. The fraction of vegetation, minimal stomatal resistance (r_{smin}), Leaf Area Index (LAI), and root depth are assigned using climatological mean values from lookup tables.

The Canadian Land Surface Scheme (CLASS) was created for the Canadian climate model (Verseghy 1991, Verseghy et al. 1993) and provides a one-dimensional parametrization of surface-atmosphere interactions. In CLASS, the land surface is a composite of vegetation, soil and snow. The vegetation has its own temperature, heat capacity, roughness, and can hold water. The model has three soil layers and infiltration of precipitation into the soil depends on the rainfall rate, the amount of water on the ground and the soil moisture profile. CLASS uses a bulk-transfer scheme to model ET, with canopy resistance being modulated using a Jarvis-type scheme. Daily values are assigned to the vegetation physiological parameters (e.g., fractional coverage, LAI, and rooting depth) using climatological look-up tables. The primary differences between PAMII and ISBA and CLASS for crops are as follows:

1) In PAMII the observed precipitation and temperature data are used to drive the model. In contrast, ISBA and CLASS use the predicted precipitation and temperatures. All three schemes use the predicted atmospheric moisture content.

2) In PAMII, the planting dates for crops are specified, whereas in CLASS the initiation of growth is assumed to be a function of latitude, with crops taking two months to reach maturity and one month between the onset of senescence and harvest.

3) In PAMII, the vegetation fraction and rooting-depth respond to the photoperiod and observed accumulated heat. In contrast, ISBA and CLASS use climatological values.

4) Unlike for PAMII, ISBA and CLASS both model the interception and subsequent re-evaporation of precipitation.

5) PAMII is only run at locations with observed temperature and precipitation data, and where GEM prognostic soundings are available during the growing season. In contrast, ISBA and CLASS are run at all model grid points year round.

6) ISBA and CLASS use more sophisticated canopy resistance schemes than does PAMII, which allow for impacts of environmental stressors on canopy resistance.

CHAPTER 3

3. VALIDATION OF SOIL MOISTURE SIMULATIONS FROM THE PAMII MODEL, AND AN ASSESSMENT OF THEIR SENSITIVITY TO UNCERTAINTIES IN SOIL HYDRAULIC PARAMETERS

[1]Abstract

Soil moisture simulations by the Canadian Prairie agrometeorological model (PAMII) were validated against in situ observations from three sites on the Canadian Prairies. Skill scores indicate that PAMII shows significant skill in simulating the evolution of bulk root-zone soil moisture content during the growing season, and that PAMII also captures the salient features of the soil moisture at each site. Specifically, correlation coefficients between simulated and observed bulk root-zone soil moisture content varied between 0.65 and 0.90, while the relative mean absolute errors were typically less than 10%.

We adopted an ensemble approach to quantify the uncertainty in simulating soil moisture that results from errors in the soil hydraulic properties. The ensemble was assembled by running PAMII using soil hydraulic properties from 20 pedotransfer functions (PTFs). Our results suggests that the uncertainty in soil moisture estimates is typically less than 10% of the bulk root-zone soil moisture content, and that there appears to be merit in using a PTF ensemble to improve estimates of the soil's hydraulic

[1] This chapter is a copy of a paper by Brimelow et al. (2010a) that appeared in the journal of Agricultural and Forest Meteorology. Reproduced here with permission.

properties. In addition, the simulated soil moisture was quite sensitive to the reference stomatal resistance term. For the grassland sites, a reference value of 100 s m^{-1} yielded the best results. The accuracy of the soil moisture simulations was insensitive to errors <5% in the initial plant-available soil moisture content.

The skill of PAMII is strongly modulated by errors in the estimated permanent wilting point and field capacity, with the skill of model simulations typically increasing as the errors decrease. Consequently, the correct modelling of soil moisture is contingent on accurately specifying the site-specific soil hydraulic properties.

3.1 Introduction

Soil moisture content and vegetation are two critical and closely related components of the land surface and are heterogeneous in both space and time (Kim and Wang 2005). During the growing season, precipitation and evaporative demand modulate soil moisture content and vegetation health, which in turn affect the surface moisture flux into the atmospheric boundary layer, and the regional hydrologic cycle. Additionally, next to precipitation, the heterogeneity of soil structure is one of the primary causes for the spatial variability of infiltration and evapotranspiration (Gutmann and Small 2005; Zhu and Mohanty 2002).

The Canadian Prairies contribute to boundary layer moisture during the summer (e.g., Raddatz 2000), with the majority of this terrestrially sourced moisture originating from agricultural crops, perennial grasses and aspen groves (Raddatz et al. 1994). This moisture fuels thunderstorms which form an integral part of the hydrological cycle on the Canadian Prairies. Specifically, thunderstorms can account for 50% or more of the annual

precipitation in this region. Additionally, Raddatz and Hanesiak (2008) showed that almost 80% of heavy rainfall events (≥10 mm) on the Canadian Prairies between 2000 and 2004 were solely or partially convective.

In this paper, we are concerned with modelling soil moisture on the Canadian Prairies. Because precipitation tends to be highly variable in both space and time, it is expected that the root-zone soil moisture fields will be heterogeneous at any given time across the agriculture zone of the Prairies. In the absence of a high spatial resolution in situ soil moisture monitoring network on the Canadian Prairies, one has to rely on alternative methods for tracking soil moisture and evapotranspiration. Surface-vegetation-atmosphere-transfer (SVAT) models are often used to map the continually evolving spatial distribution of soil moisture and evapotranspiration (ET) in response to atmospheric drivers. Here, we use the second-generation prairie agrometeorological model (PAMII) of Raddatz (1993). PAMII is similar to other models such as the Variable Infiltration Capacity model (VIC; Liang et al. 1994) and the Decision Support System for Agrotechnology Transfer (DSSAT; Ritchie and Otter 1985) that are routinely used to simulate soil moisture and evapotranspiration.

It is known that the partitioning of sensible and latent heat fluxes is an important factor in determining the growth and evolution of the boundary layer (e.g., Betts et al. 1996). For example, Findell and Eltahir (2003a) and Findell and Eltahir (2003b) demonstrated that soil extremes in moisture can have a significant impact on the evolution of the planetary boundary layer, which in turn plays a large role in determining whether or not convection develops. Further, Findell and Eltahir (2003a) demonstrated that there is a strong connection between the underlying soil moisture content and amount

of moist static energy in the boundary layer. Consequently, factors which determine the partitioning of terrestrial fluxes (such as soil moisture) can affect the potential for convection. Hanesiak et al. (2004) and Pielke (2001) also found that discontinuities in evapotranspiration (ET) can lead to inherent spatial patterns of deep convection, as the result of enhanced mesoscale circulations (Clark and Arritt 1995; Chang and Wetzel 1991) developing between areas having contrasting soil moisture. This connection between the land surface and the initiation of deep convection on the mesoscale is supported by the finding of Raddatz and Hanesiak (2008) that approximately 30% of convective events on the Canadian Prairies are attributable to mesoscale processes. Given the high frequency of convection over the Prairie agriculture zone, and the fact that the amount and distribution of moisture in the boundary layer can have a significant impact on the initiation and intensity of thunderstorms (e.g., Crook 1996), it is important to accurately and adequately map soil moisture and evapotranspiration there.

While PAMII has been used extensively by the agriculture and research community in Canada (e.g., Hanesiak et al. 2004; Hochheim et al. 2002), its ability to simulate the evolution of the root-zone soil moisture has yet to be verified against a comprehensive set of in situ observations. Further, it is clear that the accurate simulation of root-zone soil moisture content and ET by a SVAT model is a necessary condition for the host numerical weather prediction model to accurately forecast the timing and location of convection. To achieve this goal requires that the SVAT model is capable of realistically modelling both soil and vegetation characteristics and processes (De Lannoy et al. 2006). Realistic modelling of soil moisture content in turn requires accurate specification of the soil hydraulic parameters (Zhu and Mohanty 2002; Shao and Irannejad 1999; Xue et al.

1996). Doing so is not trivial, but one promising method for dealing with this uncertainty in soil hydraulic parameters is to employ ensembles.

The objectives of this paper are threefold. First, to establish the ability of PAMII to reproduce the root-zone soil moisture content below native grasses at three sites in Alberta, Canada. Second, to test the utility of using model ensembles for the purpose of mitigating the impact of uncertainties in the soil hydraulic properties on the soil moisture content simulations. Third, to quantify the uncertainty in modelled root-zone soil moisture content predictions arising from uncertainties in the soil hydraulic properties.

3.2 Background

3.2.1 Soil heterogeneity and land surface modelling

Soil structure and associated hydraulic parameters are notoriously heterogeneous in both the horizontal and vertical planes (Islam et al. 2005; Nielsen et al. 1973; McBratney and DeGruijter 1992).

Numerous studies have been conducted which quantify the spatial variability of soil structure (e.g., Wösten et al. 1987; Nielsen et al. 1973) and have demonstrated that the spatial variability of soil hydraulic parameters exists on scales ranging from the microscale to the macroscale (Mengelkamp et al. 2006; Blöschl and Sivapalan 1995). Recently, van der Keur and Iversen (2006) provided a thorough review of the spatial variability of soil structure and hydraulic parameters across all scales. Making detailed assessments of soil hydraulic parameters is a costly and time-consuming task (Cresswell et al. 2006), and this precludes acquiring these parameters over large regions. This makes specifying soil hydraulic properties over a model domain complicated, because one

typically only has data at sampled points and the land-surface model requires data at all the intervening grid points where soils have not been sampled.

Accurately modelling the evolution of moisture in the root zone and the exchange of moisture between the land surface and atmosphere requires simulating several complex processes in addition to using appropriate input data. The inherent variability in soil hydraulic parameters is of particular concern for land surface models (Gutmann and Small 2005) whose grid scale is often larger than the autocorrelation length of many soil texture and hydraulic parameters. Leenhardt et al. (1984) identified three primary sources of error when modelling soil moisture content: (1) error in the estimation of rainfall; (2) error due to the spatial variability of soil hydraulic properties; (3) error due to the parameterization of certain processes.

Shao and Irannejad (1999) concluded that uncertainties in soil hydraulic parameters can overwhelm the uncertainties in the theory of hydraulic models. Given that the impact of soil hydraulic models on performance of land surface schemes can be significant, the use of an appropriate hydraulic model and accurate set of soil hydraulic parameters is critical for land-surface modelling (e.g., Gijsman et al. 2003). Mohanty and Zhu (2007) note that the use of look-up tables to specify the soil hydraulic parameters represents one of the weakest links in our efforts to model land surface processes. Prior to this study, PAMII used look-up tables to specify the soil hydraulic parameters and is unable to take into account the impact of soil heterogeneity on the soil simulations.

3.2.2 Pedotransfer functions

Soil hydraulic behaviour can be explained by the soil water retention curve that relates the volumetric water content to the soil water pressure head, and by the hydraulic

conductivity curve that relates hydraulic conductivity to the water content or pressure head. On the field scale, it is possible to obtain numerous soil samples that adequately characterize the field conditions, and to then derive a water retention curve by making laboratory measurements of the soil moisture content at several matric potentials. This approach is, however, both time consuming and expensive, and consequently does not lend itself to determining the water retention characteristics of soils at basin or regional scales.

A more cost effective approach is to derive soil hydraulic parameters from more widely available basic soil physical properties (such as soil texture) using empirical relationships in the form of pedotransfer functions (PTFs). To create a PTF one requires a dataset that contains the observed soil hydraulic parameters and potential predictors for a large range of soil types (Reynolds et al. 2000). Linear (or nonlinear) regression analysis is then performed, seeking out statistically significant linkages between the soil hydraulic properties and the soil characteristics (e.g., bulk density, percent clay, organic matter content). Bouma and van Lanen (1987) coined the term pedotransfer function, and since then a myriad of PTFs has been developed. For example, Timlin et al. (1996) listed 49 PTFs and estimated that this sample represented only 30% of all PTFs available at that time. For more information on PTFs the reader is referred to the review of Wösten et al. (2001).

Over the years several soil hydraulic equations have been developed which relate the soil water potential (h) as a function of the volumetric soil moisture content (θ). The most widely cited hydraulic equations are those of Brooks and Corey (1964), Campbell (1974) and van Genuchten (1980). Before the volumetric water content at key reference levels

can be estimated, several soil-specific fitting parameters must be specified which determine the shape of the water retention equation curves predicted by the hydraulic functions. These parameters are oftentimes estimated using so-called parameter PTFs (Tomasella and Hodnett 1998). PAMII uses the hydraulic equation of Cosby et al. (1984) to specify the volumetric water content at permanent wilting point, field capacity and saturation point for 11 soil texture classes. In the original version of PAMII, the wilting point and field capacity were estimated for each soil class corresponding to a matric potential of −2 MPa, and a hydraulic conductivity of 0.1 mm d^{-1}, respectively. PAMII uses a water balance approach to track water in the top and root zone (see Section 3.3.1) and does not require soil hydraulic conductivity. Consequently, those PTFs used to estimate this parameter will not be discussed.

3.2.3 The ensemble technique

The variation of the soil system is so complex that no description of it can be complete. Consequently, modelling the soil moisture content and other land–atmosphere processes is inevitably uncertain (Heuvelink and Webster 2001). Additionally, soil hydraulic functions and PTFs used to estimate the soil hydraulic properties introduce uncertainty into the accuracy of model simulations. The uncertainty surrounding PTFs stems from the fact that they should ideally not be used outside of the geomorphic region for which they were developed because the applicability of a particular PTF outside of its development dataset is often unknown (Nemes et al. 2006). Thus PTFs should not be used in new regions until their skill there has been established (McBratney et al. 2002; Minasny et al. 1999).

How then does one go about reducing this uncertainty while also quantifying the degree of uncertainty arising from using imperfect soil hydraulic parameters? One approach that has been successfully adopted recently to address the problem of forecast uncertainty is the use of model ensembles. Producing a forecast based on the ensemble approach essentially means averaging the outcomes predicted by a number of individual model forecasts. Ensembles can be generated in a number of ways: (1) running the same model but perturbing the initial or boundary conditions (e.g., Margulis et al. 2006); (2) running several independent models (e.g., Guo et al. 2007); (3) running the same model but with different parameterization schemes used to simulate certain critical processes (e.g., Challinor and Wheeler 2008; Guber et al. 2006). When using ensemble averages, those features that are consistent between the ensemble members are preserved, while the impact of outliers is reduced. The output from each model ensemble can be viewed as a sample from the possible real-world outcomes and can therefore be used to calculate the uncertainty associated with the forecasts (Hamill et al. 2004).

Another rationale behind using model ensembles is that the choice of a superior model or model configuration is not obvious a priori. In the context of land-surface schemes, independent studies often identify different PTFs or soil hydraulic functions as being superior at simulating the soil water content at given matric potentials. For example, Schaap et al. (2004) evaluated 11 PTFs against a database in the USA containing over 47,000 records, and found that no given PTF was superior. Shao and Irannejad (1999) applied four different soil hydraulic functions in an atmosphere and land-interaction scheme and verified the resulting model output against in situ measurements from HAPEX. They found that the van Genuchten hydraulic functions

produced the best results. On the other hand, Kern (1995) evaluated six water retention models using almost 24,000 samples from almost 6000 pedons, and recommended the Rawls model (Rawls et al. 1982) for representing the relationship between water content and matric potential. Schädler (2007) compared the performance of the Campbell and van Genuchten soil hydraulic functions when using different parameter sets. Specifically, the hydraulic functions were paired with the parameter sets of Clapp and Hornberger (1978), Cosby et al. (1984) and Rawls and Brakensiek (1982) to create six different combinations. Schädler concluded that (for a sandy loam site in Germany) the best overall results were produced using the van Genuchten–Clapp–Hornberger, and van Genuchten–Rawls Brakensiek combinations.

Recently Guber et al. (2006) tested the performance of an ensemble of 22 PTFs to estimate soil water retention curves and then used those data to model soil moisture flow. Their findings demonstrated that there is merit in applying the ensemble technique when predicting soil hydraulic properties for use in soil moisture models. Additionally, Braun and Schädler (2005) employed a multi-model technique to determine which combination of some commonly used soil hydraulic functions within a SVAT scheme (VEG3D; Braun and Schädler et al. 2005) gave superior results when used in a mesoscale model. They verified the different versions of the model against in situ observations of soil moisture content at three sites in Germany. Specifically, they used the water retention functions of Campbell, Brooks and Corey and van Genuchten. Parameters used in each of the hydraulic functions were then specified using the soil parameter datasets of Clapp and Hornberger, Rawls and Brakensiek, Carsel and Parrish, and Rawls. This resulted in seven

combinations of water retention functions and soil parameter datasets that were used in VEG3D.

In this study we identified a total of 20 point and parameter PTFs from the literature for the purpose of generating an ensemble. Specifically, an ensemble was generated by running PAMII using 20 PTFs to specify the soil hydraulic properties which are used by PAMII to simulate evolution of the soil moisture content. Details of each PTF are summarized in Table 3.1. The water retention functions of Brooks and Corey, van Genuchten and Campbell are included, and input parameters for the water retention functions are based on large soil datasets from four continents.

3.3 Methods

3.3.1 The prairie agrometeorological model

The prairie agrometeorological model (PAMII; Raddatz 1993) simulates the evolution of the bulk soil moisture content and vegetation (pasture in this particular version) using a daily time step. Evapotranspiration is governed by photoperiod (time between sunrise and sunset), vapour pressure deficit, vegetation ground cover fraction (set to 1.0 during the period of active growth for perennial grasses), aerodynamic resistance and canopy resistance (r_s). Specifically, the magnitude of r_s is modulated by the relative plant-available water in the root-zone (PAW) and the leaf fraction. For perennial grasses, the rooting depth is constant at 110 cm.

The model does not allow for the interception of precipitation by the canopy, or the re-evaporation of intercepted moisture. The surface temperature of the leaves is assumed to be the same as that of the ambient air. Transpiration is proportional to the difference

Table 3.1: Details of the pedotransfer functions used in this study. %Cl = Percent clay, %Sa = Percent sand, %Si = Percent Silt, ρ_b = Bulk density, OM = Organic matter content.

Pedotransfer Function	Code	Source Soil Textural Properties	Input variables	Location of soil samples for training
Cosby et al. (1984)	CON	Midpoint USDA textural triangle	See Table 3 in Cosby et al. (1984)	23 States, USA
Bruand et al. (1994)	BR	Carsel and Parrish (1988)	%Cl	France
Campbell and Norman (1988)	CN	Not required	See Table 2 in Chen et al. (2007)	Rawls (1992)
Clapp and Hornberger (1978)	CH	Not required	See Table 2 in Clapp and Hornberger (1978)	23 States, USA
Federer et al. (2003)	FED	Not required	See Table 3 in Federer et al. (2003)	23 States, USA
Hall et al. (1977)	HAL	Carsel and Parrish (1988)	%Si, %Cl, ρ_b (SAR 2006)	UK
Peterson et al. (1968)	PET	Carsel and Parrish (1988)	%Cl	Pennsylvania, USA
Rawls et al. (1982)	RAW	Rawls et al. (1982)	See Table 2 in Rawls et al. (1982)	32 States, USA
Saxton et al. (1986)	SAX	Cosby et al. (1984)	%Sa, %Cl	32 States, USA
Tomasalla and Hodnett (1998)	TOM	Carsel and Parrish (1988)	%Si, %Cl	Amazonia, Brazil
Van Genuchten (1980)	VAN	Not required	See Table 4 in Schaap and Leij (1998)	International

Table 3.1 cont'd

Zacharias and Wessolek (2007)	ZAC	Carsel and Parrish (1988)	%Sa, %Cl, ρ_b (from SAR 2006)	International
Cosby II	COS	Cosby et al. (1984)	%Sa, %Cl	23 States, USA
Da Silva and Kay (1997)	DAS	Carsel and Parrish (1988)	%Cl, OM, ρ_b (SAR 2006; OM = 1.5%)	Ontario, Canada
Mayr and Jarvis (1999)	MAJ	Dunne and Willmott (1996)	%Sa, %Si, %Cl, OM, ρ_b (SAR 2006; OM = 1%)	Scandinavia
Saxton and Rawls (2006)	SAR	Saxton and Rawls (2006)	%Sa, %Cl, OM	USA
Batjes (1996)	BAT	Carsel and Parrish (1988)	%Sa, %Si, OM (2% all classes)	International
Boone et al. (1999)	NOL	Cosby et al. (1984)	%Sa, %Cl	N/A
Williams et al. (1992)	WIL	Carsel and Parrish (1988)	%Sa, %Cl, ρ_b (SAR 2006)	Australia
Oosterveld and Chang (1980)	OOS	Carsel and Parrish (1988)	%Sa, %Cl, ρ_b (SAR 2006, OM = 1%)	Canada

between the vapour density of the air and the saturation vapour density in the leaves' stomata. A reference value for the canopy stomatal resistance (rs_min) is specified.

The surface characteristics are described in terms of the terrain height, roughness length, soil class, crop stage, root- and top-zone moisture levels. Green up is assumed to occur at the first occurrence of five consecutive days having a mean temperature greater than 5 °C, while foliage die-off occurs following the first day with a minimum temperature of −5 °C (Raddatz 2005).

Eleven soil types from the USDA soil triangle are discerned; values of wilting point, field capacity, saturation level and available water capacity are specified for each soil class in look-up tables. However, the same soil type is specified throughout the root zone.

Two water balances track the bulk soil moisture in the root/sub zone (0–120 cm) and a separate top zone (0–10 cm). The water balances are interconnected via a force-restore term which attempts to equalize their moisture content per unit depth, and the top zone's moisture level influences infiltration into the root zone. The equations are provided in Raddatz (1993). In the perennial forage/pasture version of the model which is used here, the root zone extends from the surface to 110 cm and the sub zone from 110 cm to 120 cm. A "bucket-type" approach is employed to model the root-zone soil moisture, and the moisture is assumed to be uniformly distributed through this layer. The water content of the root zone (W, in mm) is adjusted daily using $W(JD) = W(JD - 1) - (ET - P_i)$, where JD is the Julian day, ET is evapotranspiration, and P_i is the infiltrating precipitation. If W(JD) exceeds field capacity, the excess water is dumped from the root zone "bucket" to the sub zone "bucket". When the moisture in the sub zone exceeds its field capacity, the excess moisture is dumped to deep percolation and no longer tracked. Rainfall in excess

of 25 mm is partitioned between recharging the top-zone moisture and run-off as determined by the soil moisture in the top 10 cm. Infiltration of rainfall into the root zone is not permitted when the top 10 cm is saturated.

3.3.2 Validation sites

Starting in the fall of 2002, a drought monitoring network (DroughtNet) has been established over cropped land throughout Alberta, Canada. In the spring of 2008, DroughtNet comprised 37 stations, with volumetric soil moisture content being measured at 31 sites. Data are archived hourly. All weather stations have been built to World Meteorological Organization (WMO) standards and data from the following sensors were used in this study:

• Volumetric soil moisture content (ThetaProbe™ type ML2X).

• Air temperature at 1.2 m (Vaisala HMP45).

• A Geonor T-200B weighing rain gauge with an Alter shield.

3.3.2.1 Soil moisture sensor calibration

The ML2X measures the volumetric soil moisture content (cm^3 [H_2O] cm^{-3} [soil]) by responding to changes in the soil's dielectric constant. Specifically, a standing wave measurement is used to determine the impedance of a sensing rod array, which is then related to the volumetric soil moisture content. Two calibration coefficients are required to convert the signal (in mV) to the volumetric soil moisture content. The manufacturer claims that with soil-specific calibration the probes can achieve an accuracy of ±0.02 m^3 m^{-3}.

Consequently, soil-specific calibration coefficients were calculated for soil samples retrieved from pits at seven DroughtNet monitoring sites to encompass a range of soil

types having different textures, dry bulk density and salinity properties. Six samples were retrieved from each of the four depths (5 cm, 20 cm, 50 cm and 100 cm), to yield a total of 24 cores per site.

The calibration report (available upon request) states that constant weights, probe output and volume at 0.33 MPa and after drying at 65 °C were used to compute sample-specific calibration coefficients. These sample-specific results were then stratified according to soil characteristics (e.g., texture), and coefficient and conversion factor means were then calculated for each group. R^2 values between computed volumetric soil moisture content (from soil-group calibration coefficients) and gravimetric core soil moisture content for samples collected in the field were 0.85, which suggests that the coefficients derived for each soil group would work well under most field conditions.

3.3.2.2 Study sites

In addition to observed precipitation and temperature, PAMII also requires the vapour deficit and a profile of temperature, humidity and winds in the PBL. To this end, prognostic soundings from the regional version of the Canadian Global Environmental Multiscale (GEM; Côté et al. 1998) model were used. Specifically, soundings from the daily 1200 UTC and 0000 UTC analysis fields from the GEM model were used as input for PAMII. These data were only archived at selected locations across the Canadian Prairies. An archived sounding had to be within 30 km of a DroughtNet site to be considered representative of conditions there. Also, for the purposes of verifying PAMII soil moisture estimates we excluded sites having a complex vertical soil profile. Finally, we wished to run the model at sites located in different eco-regions, and sites having different soil textures. Using these criteria only three suitable sites (Mundare, Two Hills

and Barnwell) were identified which are listed in Table 3.2. The soil classes represented in this study are present at 53% of the sites on the Canadian Prairies. Thus, the soil classes considered here are representative for the majority of localities within this zone.

The Mundare site (53.561 N; 112.296 W, 690 m) is located in the Aspen Parkland eco-region of Alberta, Canada. The station is located on an elongated knoll, and surrounded by hummocky terrain. Slope at the site is 1%. Approximately 80% of the plot is covered by tame grasses (meadow brome and alfalfa) with only 10% bare soil. Rooting depth was estimated at 90 cm, with abundant fine roots present above 50 cm. The soil order is Chernozemic, and classified as loam according to textural data from the soil pit. Coarse fragments were typically less than 3%. Layer-weighted soil composition in the top 60 cm is 46% Sand, 37% Silt and 17% Clay.

The Two Hills site (53.625°N; 111.678°W, 678 m) is also located in the Aspen Parkland eco-region about 40 km east-northeast of Mundare. The terrain is hummocky, with the station located on a knoll. Slope at the site is 1%. Approximately 45% of the plot is covered by grasses (brome and creeping red fescue), 45% residue and 10% bare soil. Maximum rooting depth was estimated at 100 cm, with a plentiful number of roots present above 80 cm. The soil order is Luvisolic, and classified as sandy clay loam according to soil textural data from the soil pit. Coarse fragments are typically less than 5% in the top 20 cm, increasing to 5–10% below 20 cm. Layer-weighted soil composition at this site is 44% Sand, 31% Silt and 25% Clay.

The Barnwell site (49.802 N; 112.302 W, 824 m) is located in the mixed grassland eco-region. The terrain is undulating, with the station located mid-slope. The slope at the site is 2%. Approximately 70% of the plot is covered by tame grasses (June grass and

Table 3.2: Details of stations used to validate the PAMII model.

Station	Lat	Lon	Elevation (m)	Ecoregion	Vegetation Type	Soil sensor depth (cm)	Soil Class	% Sand	% Silt	% Clay
Barnwell	49.80	-112.30	824	Mixed Grassland	Native Grasses	5, 20, 50, and 100 cm	Sandy Loam	73	15	12
Mundare	53.56	-112.30	690	Aspen Parkland	Pasture	5, 20, 50, and 100 cm	Loam	46	37	17
Two Hills	53.63	-111.68	678	Aspen Parkland	Native Grasses	5, 20, 50, and 100 cm	Sandy Clay Loam	44	31	25

wheat grass), and 30% is bare soil. Maximum rooting depth was estimated at 100 cm, with plentiful numbers of very fine roots present above 60 cm. The soil order is Chernozemic, and classified as sandy loam according to soil textural data from a soil pit dug at the site. Coarse fragments are typically less than 1%. Layer-weighted soil composition at this site is 73% Sand, 15% Silt and 12% Clay.

3.3.3 Selection of wilting point and field capacity

There is still much debate as to which matric potential values are appropriate for estimating the permanent wilting point (PWP) and field capacity (FC). Historically, water potentials of −0.33 MPa and −1.5 MPa have been used for the FC and PWP, respectively. However, these values represent only arbitrary points on a continuum. Also FC and PWP in the field are dependent on the proximity of roots to the water table, gravel content and plant characteristics.

In this study, the PWP at each site was approximated by selecting the lowest daily mean volumetric water content observed at 20-cm depth between 15 May and 30 September for the entire record at each site; this typically spanned a 4–6-year period. The FC at each site was approximated by identifying the volumetric soil moisture content at 20 cm, 72 h following the time of maximum soil moisture content associated with a heavy precipitation event (>10 mm). None of the sites experienced drought conditions during the period of observation, so the estimates of PWP shown in Table 3.3 may be too high, especially at Mundare and Two Hills. The impact of the possibility of the PWP being too high on the model validation is discussed further in Section 3.5.

Table 3.3: Summary of water retention characteristics at each validation site derived from in-situ soil moisture measurements (ACT) and the 20 PTFs. AWC is the available water content in the top 110 cm in mm.

	Two Hills				Mundare				Barnwell			
	θwp	θfc	θsat	AWC	θwp	θfc	θsat	AWC	θwp	θfc	θsat	AWC
ACT	0.180	0.300	0.427	144	0.125	0.295	0.452	204	0.100	0.235	0.431	162
AVG	0.164	0.271	0.427	128	0.136	0.264	0.452	154	0.097	0.209	0.431	134
CON	0.111	0.241	0.404	156	0.089	0.236	0.439	176	0.068	0.218	0.434	180
COSII	0.205	0.323	0.460	142	0.135	0.258	0.444	148	0.087	0.197	0.423	132
BRU	0.186	0.262	0.420	91	0.145	0.221	0.451	91	0.094	0.169	0.435	90
CH	0.175	0.255	0.420	96	0.155	0.240	0.451	102	0.114	0.195	0.435	97
CN	0.150	0.260	0.398	132	0.120	0.270	0.463	180	0.100	0.210	0.453	132
FED	0.141	0.317	0.420	211	0.118	0.324	0.451	247	0.086	0.266	0.435	216
HAL	0.230	0.320	0.476	108	0.159	0.266	0.451	128	0.101	0.204	0.435	124
PET	0.188	0.321	0.472	160	0.148	0.276	0.461	154	0.096	0.215	0.417	143
RAW	0.124	0.257	0.398	160	0.125	0.282	0.463	188	0.080	0.206	0.453	151
SAX	0.160	0.264	0.472	125	0.124	0.262	0.461	166	0.094	0.202	0.417	130
TOM	0.195	0.332	0.540	164	0.148	0.292	0.525	173	0.091	0.194	0.491	124
VAN	0.179	0.252	0.384	88	0.142	0.225	0.399	100	0.125	0.205	0.387	96
ZAC	0.177	0.289	0.424	134	0.161	0.293	0.442	158	0.094	0.229	0.415	162
DAS	0.192	0.307	0.424	138	0.150	0.279	0.442	155	0.098	0.237	0.415	167
WIL	0.149	0.282	0.424	160	0.164	0.292	0.442	154	0.084	0.221	0.415	164
BAT	0.153	0.223	0.398	84	0.151	0.255	0.463	125	0.102	0.170	0.453	82
SAR	0.171	0.283	0.463	134	0.133	0.277	0.474	173	0.083	0.184	0.451	121
MAJ	0.176	0.262	0.398	103	0.200	0.298	0.414	118	0.129	0.249	0.407	144
OOS	0.148	0.305	0.472	188	0.142	0.292	0.461	180	0.100	0.206	0.417	127
NOL	0.193	0.282	0.432	107	0.158	0.245	0.448	104	0.117	0.199	0.432	98

3.3.4 Model runs

We used PAMII to simulate the evolution of the root-zone soil moisture content and PAW during the growing season (1 May through 30 September) at three DroughtNet sites in Alberta, Canada. The model was driven using *observed* rainfall, minimum and maximum temperatures from each site, and prognostic profiles of temperature, moisture and winds from the GEM regional model. The surface dew-point depression from the GEM model was used to calculate the near-surface vapour density required for the calculation of transpiration from the canopy. The soil moisture content was initialized on 1 May using the observed volumetric soil moisture content data from each site. The model was validated for the 2004 growing season at Barnwell and the 2005 growing season at Two Hills and Mundare.

The model was run 24 times for each site using the same input data, but using different methods for calculating the soil hydraulic parameters. Specifically:

(1) A control version of the model (CON) was run using the soil hydraulic parameters from the scheme of Cosby et al. (1984) for the designated soil class, and a reference stomatal resistance (rs_min) of 100 s m^{-1}.

(2) The model was then run once for each of the 20 PTFs for the observed soil class at each site (see Table 3.1 for details). A rs_min of 100 s m^{-1} was used.

(3) The model was then run using the mean hydraulic properties (derived from all 20 PTFs) for the designated soil textural class at each site, and a rs_min of 100 s m^{-1} (AVG_1.0).

(4) The model was then run once using the hydraulic properties derived using the in situ soil moisture observations (see Section 3.3.3) and a rs_min of 100 s m^{-1} (ACT_1.0).

(5) Two final runs were made using the same specifications in experiments 3 and 4, except with a rs_min of 80 s m^{-1} (AVG_0.8 and ACT_0.8).

Keeping in mind the limitations of using pre-determined matric potentials to calculate FC and PWP, we opted to use soil water contents at matric potential of −0.33 MPa and −1.5 MPa to calculate FC and PWP, respectively. The following methods (see Table 3.1 for more information) were exceptions: (a) In CON and FED, the PWP was calculated using a matric potential of −2.0 MPa (Wetzel and Chang 1987), (b) In CON the FC was calculated assuming a hydraulic conductivity of 0.1 mm d^{-1} (Wetzel and Chang 1987), and in FED the FC was calculated as the water volume fraction at 30-cm depth after 48 h of drainage from an initially saturated, homogeneous profile of the material with a fixed gravity potential gradient at 2-m depth (Federer et al. 2003). Fig. 3.1 shows the pairs of FC and PWP derived using the different PTF schemes for the three soil classes used in this study. While there is some clustering, a range of values is evident. The specific values of FC, PWP and saturation point for each simulation are shown in Table 3.3.

3.3.5 Verification

The DroughtNet sites record the volumetric soil moisture content (θ; in %) at four discrete levels every hour, whereas output from PAMII is the bulk soil moisture water content (in mm) in the root zone on a daily time step. Thus, the discrete observations of volumetric soil moisture content were converted into a measure of soil moisture that is comparable with the model output. To do so we assumed that θ varied linearly between the discrete observation levels. Hourly θ data at each level were used to calculate daily means, which were then used to calculate the daily bulk root-zone soil moisture content.

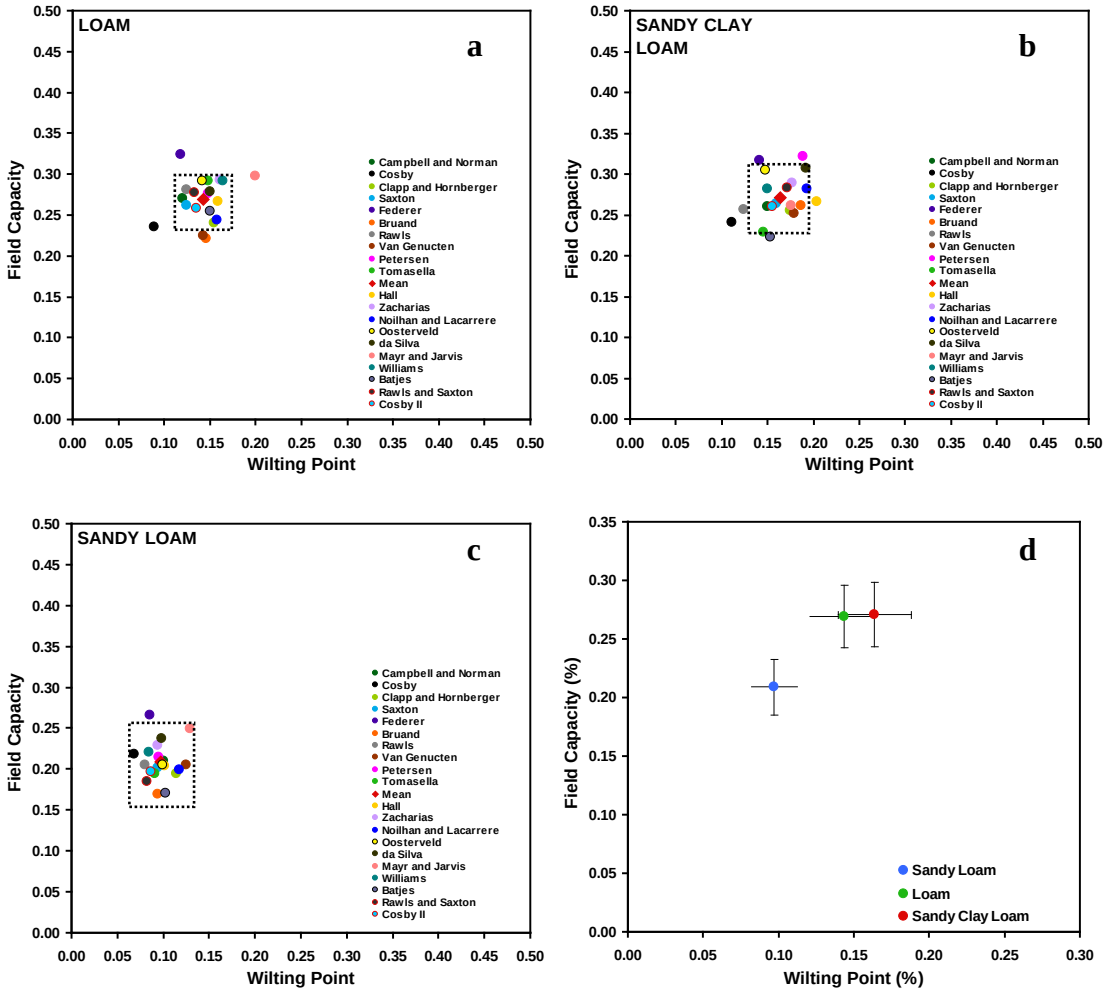

Figure 3.1: Range of predicted field capacities and permanent wilting points for the three soil texture categories derived using 20 PTFs. Panel (a) shows the values for Mundare, (b) Two Hills and (c) Barnwell. The error bars in (d) represent ± standard deviation from the mean value calculated from the 20 pedotransfer functions. The large red diamond represents the average values.

Specifically, we divided the soil column between the surface and 100 cm into discrete layers. The equivalent soil moisture contents (in mm) for all the layers in the root zone were then integrated to obtain a bulk soil moisture amount. The observed θ between 100 cm and 110 cm was assumed to be constant.

While the bulk soil moisture content in the root zone (top 110 cm) is suitable for verifying the accuracy of the model simulations, it provides little insight concerning whether or not the plants' moisture requirements are being adequately satisfied. For this purpose, it is convenient to quantify the moisture in the root zone in terms of the relative plant available water content (e.g., Anderson et al. 2000). The relative plant available water content (or PAW) is equal to $[(\theta - \theta_{pwp})/(\theta_{fc} - \theta_{pwp})]$ where θ is the observed volumetric water content in the root zone, θ_{pwp} is the permanent wilting point and θ_{fc} the field capacity. PAW is an important variable in PAMII because it is used to modulate the amount of transpiration through the canopy stomatal resistance term and the amount of transpiration affects the rate of depletion of moisture from the root zone. A recently completed validation of ET estimates from PAMII (against ET estimates from eddy covariance data) suggests that the soil moisture stress function in PAMII may limit ET too strongly, especially at higher soil moisture contents. Future work will focus on improving this aspect of the model.

The following statistical measures were used to quantify the performance of the model's root-zone soil moisture predictions: mean error (ME), mean absolute error (MAE), root-mean square error (RMSE), square of the Pearson product-moment correlation coefficient (R^2), and the Index of agreement (IA). The IA is calculated as follows:

$$IA = 1.0 - \left[\frac{\sum_{i=1}^{N} \left(O_i - M_i \right)^2}{\sum_{i=1}^{N} \left[\left| O_i - \overline{O} \right| + \left| M_i - \overline{O} \right| \right]^2} \right] \qquad (3.1)$$

where M and O are the modelled and observed data points, and $\overline{O}$ is the mean of the observed series. R^2 represents the percentage of the total variation in the observations that is explained by the forecast. Legates and McCabe (1999) suggested that the IA statistic is superior to the correlation coefficient for the purpose of evaluating forecasted soil moisture data series. IA ranges from 0 to 1, with 1 indicating perfect skill.

3.4 Results

3.4.1 Bulk soil moisture content

Fig. 3.2 shows the evolution of the observed and modelled bulk soil moisture content in the root zone (top 110 cm) at the three test sites. At Mundare (Fig. 3.2a) the observed root-zone soil moisture content varied between 225 mm and 275 mm. A cyclical pattern was evident, with the bulk moisture content increasing following wet events, declining and then increasing again following the next rainfall event. Evident from Fig. 3.2a is that the control model run (CON) systematically underestimated the soil moisture, and was almost exclusively outside the one standard deviation envelope surrounding the ensemble mean. In contrast, the observed soil moisture content trace was within the uncertainty envelope for the entire simulation. The envelope of uncertainty was generated by calculating the standard deviation of the predicted soil moisture (using the 20 PTFs) on each day; this value was then added and subtracted from the ensemble mean.

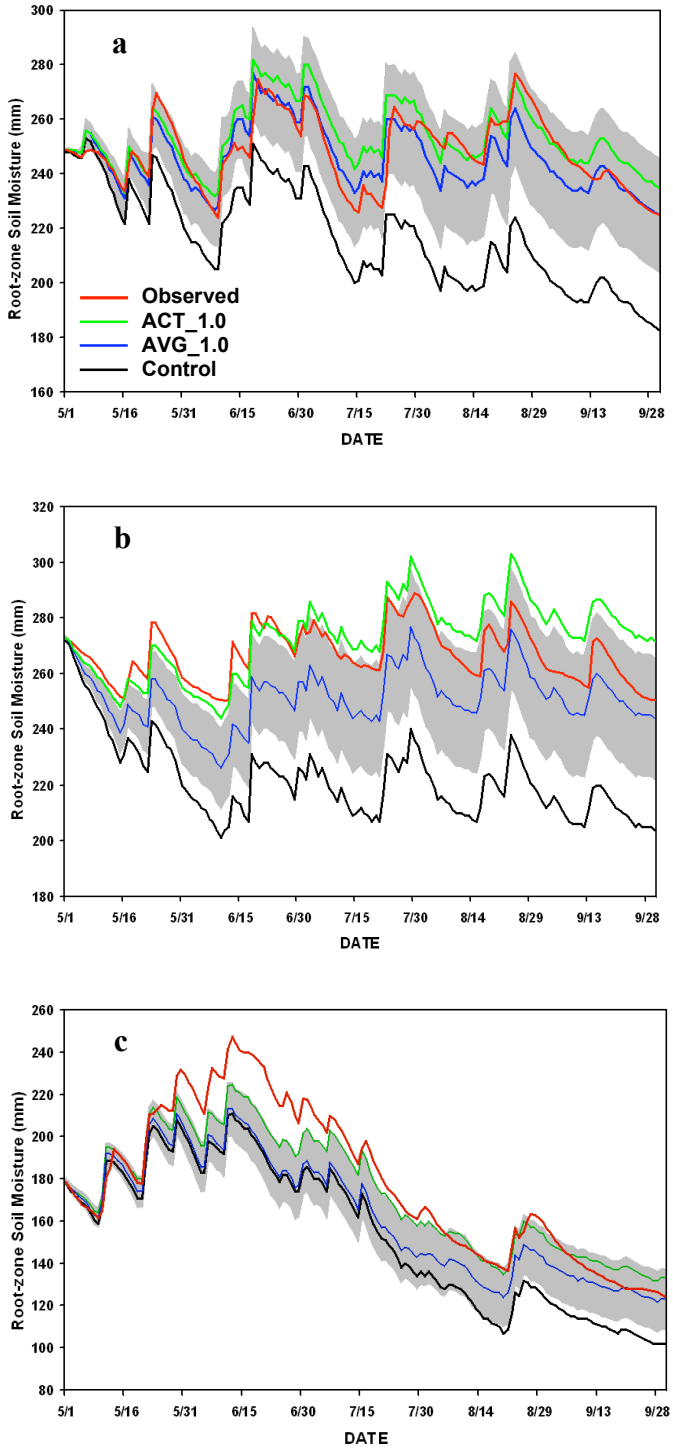

Figure 3.2: Time series of root-zone moisture between 1 May and 30 September for Mundare (a), Two Hills (b), and Barnwell (c). Red trace represents the observed soil moisture, green trace modelled soil moisture using estimated soil hydraulic properties from in-situ observations (ACT_1.0), blue trace the modelled soil moisture using the average soil hydraulic properties from all 20 PTFs (AVG_1.0), and the black trace modelled soil moisture form the control run. The grey shaded area represents ± standard deviation from the mean.

The ensemble mean simulation (AVG_1.0) was in very close agreement with the observed soil moisture content until early July, after which the modelled values started to deviate from the observations. The simulation that was made using the in situ estimates of the actual soil hydraulic properties (ACT_1.0) also performed very well.

Considering the individual model runs, it is evident from Table 3.4 that there is a wide range of skill, with IA values ranging between 0.43 and 0.90. If one ranks the different simulations' performances in terms of the RMSE and IA then the model run using HAL ranks the best, followed by RAW, PET, AVG_1.0, and AVG_0.8 in 5th place. The performance of the control simulation (CON) was the worst of all the simulations. Simulations using a rs_min of 80 s m^{-1} and 100 s m^{-1} for the ACT model runs showed very similar skill; however, the skill of the AVG and other model simulations improved when using 100 s m^{-1}.

There was an almost even split between those PTFs displaying a systematic negative bias and those displaying a positive bias. The mean absolute error (MAE) for the AVG_1.0 run was 6.1 mm (relative error of 2.5%). This equates to a mean error in volumetric soil moisture content of 1.0%, which is less than the expected error of the soil moisture sensors.

Fig. 3.2b indicates that the observed soil moisture content in the root zone at Two Hills was higher than at Mundare and varied between 250 mm and 290 mm. As was the case at Mundare, a cyclical pattern was evident. The control model displayed a significant and systematic negative bias at the Two Hills site. The ensemble mean also displayed a negative bias, while the ACT_1.0 run displayed a slight positive bias.

Table 3.4: Verification statistics of soil moisture forecasts for Mundare between 1 May and 30 September 2005.

	Root-zone soil moisture					Plant available moisture (%)		Evapotranspiration (mm)		
	ME	**MAE**	**R^2**	**IA**	**RMSE**	**ME**	**MAE**	**Total ET**	**P-E**	**P/E**
ACT_1.0	4.9	6.9	0.69	0.87	8.8	2.6	3.7	328	-7	0.98
ACT_0.8	-10.7	11.5	0.55	0.74	14.2	-5.7	6.1	350	-29	0.92
AVG_1.0	-2.4	6.1	0.67	0.89	7.9	4.5	5.4	337	-16	0.95
AVG_0.8	-15.7	16.1	0.50	0.65	18.6	-5.0	6.9	354	-33	0.91
BAT	-8.1	9.2	0.61	0.80	11.6	6.1	7.3	343	-22	0.93
BR	-32.5	32.5	0.38	0.44	34.5	8.5	11.5	352	-30	0.91
CH	-15.6	15.9	0.52	0.65	18.3	7.4	9.6	350	-30	0.91
CN	-7.8	9.1	0.61	0.81	11.5	6.5	6.9	345	-24	0.93
CON	-31.6	31.7	0.28	0.43	35.3	14.2	14.2	379	-58	0.85
COSII	-10.1	10.2	0.57	0.76	13.5	7.1	7.6	347	-26	0.93
DAS	4.3	6.7	0.69	0.88	8.5	2.6	4.1	328	-7	0.98
FED	14.8	15.0	0.57	0.68	17.4	-0.4	3.8	313	8	1.03
HAL	0.5	6.0	0.68	0.90	7.4	3.4	5.0	333	-11	0.97
MAJ	28.8	28.8	0.41	0.49	31.2	-6.3	8.5	290	32	1.11
NOL	-12.0	12.6	0.56	0.72	15.0	6.7	8.7	347	-26	0.93
OOS	8.1	8.7	0.66	0.81	11.1	1.5	3.8	323	-2	0.99
PET	2.3	6.2	0.69	0.90	7.7	3.1	4.3	331	-10	0.97
RAW	-1.2	6.0	0.68	0.90	7.5	4.5	5.0	336	-15	0.95
SAR	-1.3	7.0	0.51	0.84	9.5	4.4	5.0	336	-15	0.95
SAX	-10.9	11.5	0.56	0.74	14.2	7.4	7.7	349	-28	0.92
TOM	10.5	11.2	0.64	0.77	13.2	1.6	4.0	322	-1	1.00
VAN	-29.2	29.2	0.39	0.47	31.4	9.3	11.6	357	-36	0.90
WIL	14.5	14.6	0.59	0.69	16.9	-0.6	5.5	314	7	1.02
ZAC	14.1	14.2	0.60	0.70	16.6	-0.4	4.8	315	6	1.02

Nevertheless, the observed soil moisture content trace was mostly within the bounds of the uncertainty envelope. The performance statistics for the individual model runs are shown in Table 3.5. The model simulations showed a wide range of skill, with IA values ranging between 0.28 and 0.92. HAL ranks the highest followed by NOL, ZAC, FED and OOS. The ACT_1.0 run ranked 7th, and that of AVG_1.0 ranked 10th. Those model runs made using a rs_min of 100 s m^{-1} were superior to those made using 80 s m^{-1}.

With the exception of the ACT, PET and DAS simulations, the model runs displayed a systematic negative bias when modelling the soil moisture content at this site. HAL, NOL, and ZAC scored the lowest MAEs (<7 mm). The ACT_1.0 and ACT_0.8 simulations scored a higher MAE of 7.9 mm. MAE values less than 8 mm translate into a relative MAE of less than 3%. This is equivalent to a mean volumetric soil moisture content error in the top 110 cm of less than 1%.

The different models' performance statistics for simulating the bulk soil moisture content at the Barnwell site are shown in Fig. 3.2c. As expected for a coarse-textured soil, the mean soil moisture content in the top 110 cm was lower (178 mm) than at the two northern sites (250 mm). The trace of soil moisture content was more variable than at the other two sites, with the soil moisture ranging between 125 mm and 250 mm. Soil moisture content at this site was not cyclical, rather it increased steadily from late May to reach a peak in early June, after which it declined. The marked increase in soil moisture content between mid May and mid June was associated with two heavy rainfall events (>25 mm).

Table 3.5: Verification statistics of soil moisture forecasts for Two Hills between 1 May and 30 September 2005.

	Root-zone soil Moisture					Plant available moisture (%)		Evapotranspiration (mm)		
	ME	**MAE**	**R^2**	**IA**	**RMSE**	**ME**	**MAE**	**Total ET**	**P-E**	**P/E**
ACT_1.0	4.1	7.9	0.53	0.81	9.8	3.1	6.1	289	-5	0.98
ACT_0.8	-7.8	7.9	0.70	0.81	9.3	-5.5	6.0	304	-20	0.93
AVG_1.0	-15.4	15.4	0.68	0.61	16.4	8.4	8.6	315	-30	0.90
AVG_0.8	-26.6	26.7	0.55	0.43	27.6	-1.2	4.6	330	-46	0.86
BAT	-44.9	44.9	0.13	0.29	46.6	16.4	16.4	352	-68	0.81
BR	-12.5	12.5	0.76	0.69	13.4	7.7	8.5	311	-27	0.90
CH	-20.2	20.2	0.68	0.52	21.0	9.5	9.8	321	-37	0.89
CN	-25.3	25.3	0.56	0.45	26.3	11.1	11.1	327	-43	0.87
CON	-45.3	45.3	0.21	0.28	47.1	17.3	17.3	354	-70	0.80
COSII	-23.8	23.8	0.59	0.47	24.8	10.7	10.7	325	-41	0.87
DAS	11.7	12.8	0.45	0.67	15.8	1.0	7.6	278	6	1.02
FED	-2.0	7.7	0.50	0.82	9.0	4.5	5.6	295	-11	0.96
HAL	-3.2	4.7	0.80	0.92	5.6	5.3	8.3	301	-17	0.94
MAJ	-16.1	16.1	0.72	0.60	17.0	8.2	8.6	314	-30	0.90
NOL	0.7	5.3	0.67	0.90	6.4	4.5	6.9	296	-12	0.96
OOS	-4.7	7.6	0.55	0.81	9.1	5.3	6.0	300	-12	0.96
PET	15.9	16.5	0.37	0.57	20.5	-0.4	7.7	272	12	1.05
RAW	-34.1	34.1	0.39	0.36	35.3	13.7	13.7	338	-54	0.84
SAR	-6.9	7.7	0.66	0.81	9.4	6.1	6.5	304	-20	0.93
SAX	-20.4	20.4	0.65	0.52	21.3	9.5	9.5	320	-35	0.89
TOM	-43.5	43.5	0.25	0.29	45.2	16.3	16.3	351	-67	0.81
VAN	-20.5	20.5	0.70	0.52	21.2	9.4	9.9	321	-36	0.89
WIL	-14.2	14.3	0.64	0.63	15.6	8.1	8.2	313	-29	0.91
ZAC	-2.1	6.3	0.62	0.87	7.4	4.7	6.0	297	-13	0.96

The systematic negative bias in predicted soil moisture content from the CON run at Barnwell was not as marked as it was at the other sites. The uncertainty (standard deviation) of the simulations increased steadily with time, followed by a plateau (11% or 14 mm) late in the season. These data suggest that the uncertainty associated with the modelled soil moisture content at this site was less than 12% for the duration of the simulations.

All versions of the model struggled to predict the rapid and sustained increase in root-zone soil moisture amounts between mid May and mid June at Barnwell. However, the model did capture the timing of the peaks, and also reflected the steady decrease in soil moisture content from mid June onwards. By the end of September soil moisture amounts predicted by ACT_1.0 and AVG_1.0 were very close to the observed values. The observed soil moisture content trace was only located within the uncertainty envelope from early August onwards. Table 3.6 summarizes the performance statistics for the Barnwell site. With the exception of MAJ and FED, all the model runs displayed negative biases. Although the IA scores for the Barnwell simulation were higher than those attained at Two Hills and Mundare, there was still a relatively wide range of skill as quantified by the IA (0.71–0.99). The FED simulation ranked highest, followed by ACT_1.0, DAS, ZAC, and PET; AVG_1.0 ranked 10th. Mean absolute errors were higher for the Barnwell site, although the highest-ranking PTFs scored MAEs less than 10 mm. The relative MAEs of the top 10 ranked PTFs were less than 10%. This is equivalent to a mean volumetric soil moisture content error in the top 110 cm of less than 1.5%.

Table 3.6: Verification statistics of soil moisture forecasts for Barnwell between 1 May and 30 September 2005.

	Root-zone soil moisture					Plant available moisture (%)		Evapotranspiration (mm)		
	ME	**MAE**	**R^2**	**IA**	**RMSE**	**ME**	**MAE**	**Total ET**	**P-E**	**P/E**
ACT_1.0	-4.8	7.9	0.97	0.97	10.6	-3.2	5.3	316	-53	0.83
ACT_0.8	-14.7	15.2	0.92	0.91	19.0	-9.9	10.3	325	-62	0.81
AVG_1.0	-15.6	16.1	0.92	0.91	19.5	-0.6	5.6	327	-64	0.80
AVG_0.8	-24.8	25.0	0.84	0.82	29.1	-8.0	10.7	333	-70	0.79
BAT	-31.2	31.3	0.75	0.72	36.9	0.5	11.0	321	-58	0.82
BR	-35.3	35.3	0.75	0.71	39.9	1.7	10.4	329	-66	0.80
CH	-13.4	15.9	0.88	0.88	20.7	-1.6	7.2	315	-52	0.84
CN	-13.7	14.5	0.92	0.92	18.1	-0.8	5.6	325	-62	0.81
CON	-24.4	24.6	0.91	0.87	26.5	2.0	5.8	346	-83	0.76
COSII	-25.0	25.2	0.88	0.84	28.1	1.6	6.2	338	-75	0.78
DAS	-5.3	8.2	0.96	0.97	11.0	-3.3	5.7	315	-52	0.84
FED	0.4	6.2	0.97	0.99	7.5	-3.5	7.5	317	-54	0.83
HAL	-15.6	16.1	0.91	0.90	20.1	-0.7	5.9	325	-62	0.81
MAJ	13.6	16.4	0.96	0.89	19.4	-8.1	9.1	285	-22	0.92
NOL	-9.9	14.2	0.90	0.90	18.6	-2.3	6.8	311	-48	0.84
OOS	-15.6	16.1	0.91	0.91	19.9	-0.5	5.8	326	-63	0.81
PET	-14.0	14.5	0.93	0.93	17.7	-0.9	5.3	326	-63	0.81
RAW	-24.7	24.9	0.90	0.86	27.2	1.5	5.6	340	-77	0.77
SAR	-32.0	32.1	0.83	0.79	35.2	3.5	7.7	346	-83	0.76
SAX	-19.7	20.1	0.89	0.88	23.3	0.4	6.0	331	-68	0.79
TOM	-24.7	24.8	0.87	0.84	28.0	1.1	6.6	334	-71	0.79
VAN	-4.0	14.1	0.91	0.91	17.0	-4.0	6.6	302	-39	0.87
WIL	-16.3	16.8	0.93	0.92	19.0	0.0	5.2	334	-71	0.79
ZAC	-10.1	10.9	0.95	0.95	14.2	-2.4	5.6	320	-57	0.82

3.4.2 Relative plant available water

The model estimates of PAW were also verified. It must be noted that we do not know for certain that our estimates of the soil water retention characteristics at the sites were representative of the in situ field values, and this in turn will affect the PAW values used to validate the model.

The evolution of the observed and modelled PAW at Mundare is shown in Fig. 3.3a. The PAW varied between 50% and 75% during the growing season, suggesting that the vegetation did not experience moisture stress. When dealing with model ensembles, the spread of modelled values (from individual ensemble members) typically increases with time. However, here the variability of modelled soil moisture amongst the different model simulations was greatest in early May, and then decreased steadily as the season progressed. The reason for this apparent paradox (decreasing spread with time) is that all the model runs were initialized with the same amount of moisture in the root-zone. So those model versions having an available water capacity (FC minus PWP) that is much lower/higher than that determined from the in situ soil moisture observations, initially have a much higher/lower PAW. Those models starting with a higher PAW then have a lower canopy resistance and are able to transpire more freely than those model versions having a relatively low PAW. This in turn results in those model versions having a high initial PAW losing soil moisture (through transpiration) relatively quickly, while those with low initial PAW losing soil moisture at a slower rate. Ultimately this leads to the PAW values from the model ensembles converging with time which results in a decrease in standard deviation with time.

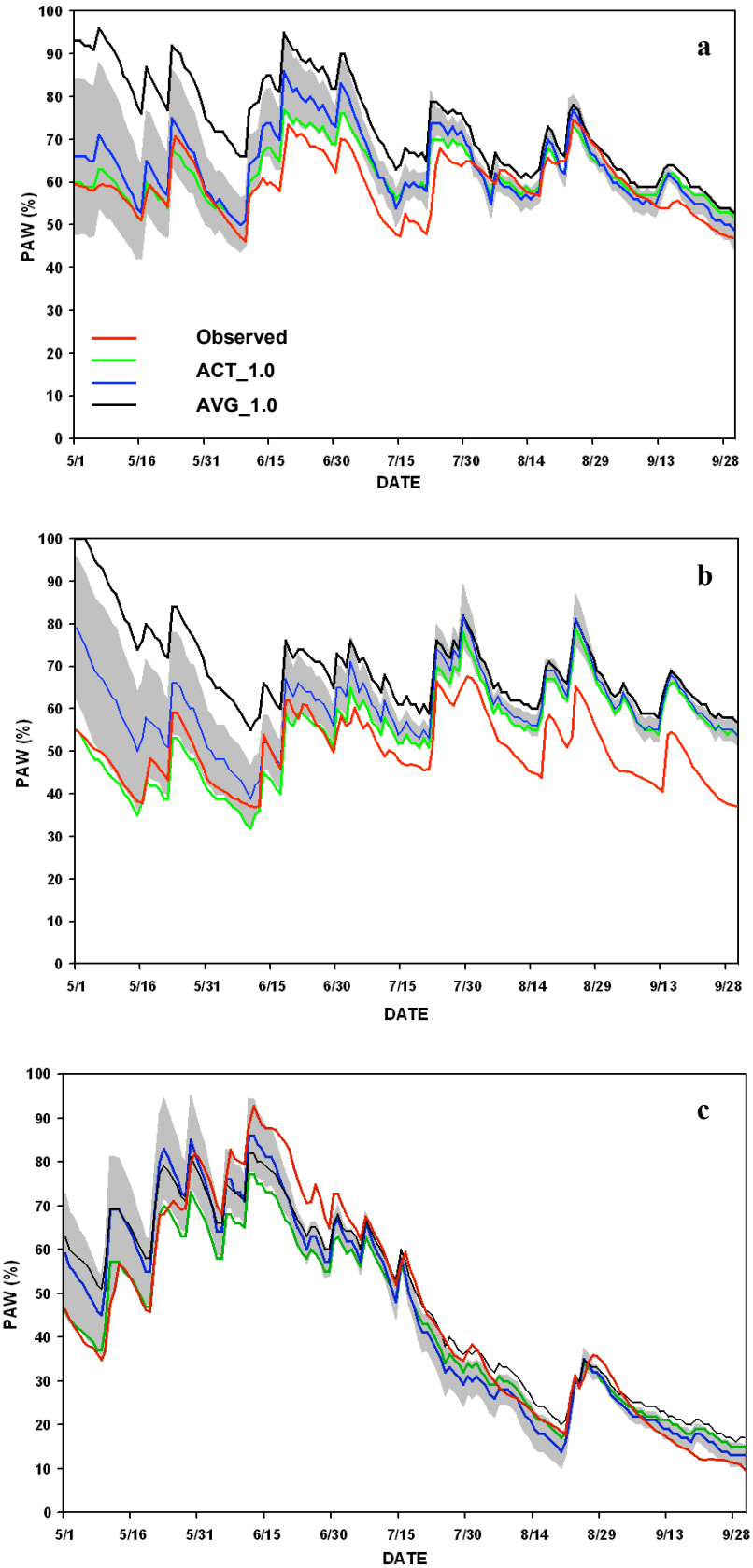

Figure 3.3: Same as Fig. 3.2 except for the relative plant available moisture.

While PAW from simulations made using the different PTFs converge with time, the projections only converge late in the season. Consequently, differences in the modelled PAW and ET can be significant at those times in the growing season when the vegetation is most active. The AVG and ACT simulations agreed very well with the estimated PAW observations, although the AVG_1.0 simulation was noticeably higher than the observations between mid June and the end of July. The PAW from the CON run was much too high early in the season, but came into closer agreement with the observations from early August onwards.

Table 3.4 shows that most of the model simulations had mean MAE less than 8% when predicting the PAW at Mundare. The lowest MAE in PAW (3.7%) was obtained for the simulation using the best estimates of the water holding characteristics as defined in Section 3.3, followed closely by the simulations of FED, DAS and TOM. In contrast, the simulations using PTFs of CON, BR and VAN had MAEs in excess of 11%. The AVG_1.0 simulation scored a MAE of 5.4%. Most of the simulations tended to have a positive bias when predicting the PAW, the notable exception is the simulation using the PTF of MAJ which had a negative bias of −6.3%.

The observed PAW at Two Hills was very similar to that observed at Mundare (Fig. 3.3b). The most noticeable difference was that the mean PAW values at Two Hills were generally about 7% lower than those observed at Mundare. The reason for this being that the available water content (AWC) of the sandy clay loam soil at Two Hills (130 mm) was lower than that of the loam soil at Mundare (205 mm), but the stations both received a similar amount of rain (270 mm).

Unlike at Mundare, the PAW values at Two Hills regularly dipped below the 50% threshold, with values ranging between 35% and 65%. As was the case at Mundare, the CON and AVG simulations tended to overestimate the PAW, whereas the ACT simulation started to overestimate the PAW from early July onwards. All the simulations significantly overestimated the PAW from mid August onwards, with PAW values 10–15% too high.

The performance statistics for the Two Hills site are shown in Table 3.5. Most of the simulations of PAW had a positive bias. This was especially true for simulations made using the PTFs of CON, TOM and RAW. The simulations made using AVG_0.8, FED, ZAC, OOS and ACT0.8/1.0 scored the lowest MAEs. Most of the simulations had MAEs less than 10%.

At Barnwell, there was better agreement amongst the PAW values predicted by the different model simulations (Fig. 3.3c). As was the case for the northern sites, the PAW values estimated by AVG and CON were initially noticeably higher than the estimates of PAW based on the in situ measurements. However, the modelled PAW time series quickly converged, and from late June onwards there was little to choose amongst the different model simulations. The two peaks of PAW in late May and mid June were detected by the model simulations, although they were lower than the observed values. The steady decline in the PAW from mid June onwards, interrupted for a short time by a peak in late August, was well captured by the simulations. Specifically, the PAW was modelled and observed to decline below 50% in the third week of July, and even to drop below 30% in August and September. These data suggest that the vegetation likely experienced some moisture stress later in the season.

Referring to Table 3.6 we see that the majority of model simulations displayed a negative bias. This was especially true for the simulations of MAJ and VAN. There was not much variability amongst the different model simulations in terms of the MAE, with most of the simulations calculated to have errors of PAW between 5% and 8%. Only the simulations of BAT and BR had MAE errors for predicted PAW greater than 10%.

3.4.3 Evapotranspiration

The integrated evapotranspiration (ET) between 1 May and 30 September for each site is shown in Fig. 3.4. The envelope of uncertainty was generated by calculating the standard deviation of the ET from all model runs on each day and then adding/subtracting it from the ET calculated using the ensemble mean. At all three sites the uncertainty in accumulated ET increased with time. The greatest uncertainty in accumulated ET was predicted at Mundare, with a range of accumulated ET of ±47 mm (±14%) by 30 September. By comparison, the range of accumulated ET at Barnwell and Two Hills was ±25 mm (±9%). The ratio of precipitation (P) to ET was just below 1.0 at Two Hills and Mundare, reflecting the moist conditions observed there. In contrast, at Barnwell the ratio of P to ET was near 0.80, reflecting the drier conditions and greater evaporative demand there.

Another observation evident in Fig. 3.4 is that the ET calculated using CON was significantly higher than the AVG and ACT runs. At Mundare and Two Hills the ET was almost exclusively located outside the envelope of uncertainty. Another theme of all three graphs is that the ET predicted by the ACT_1.0 run was the lowest; this was especially true at Two Hills.

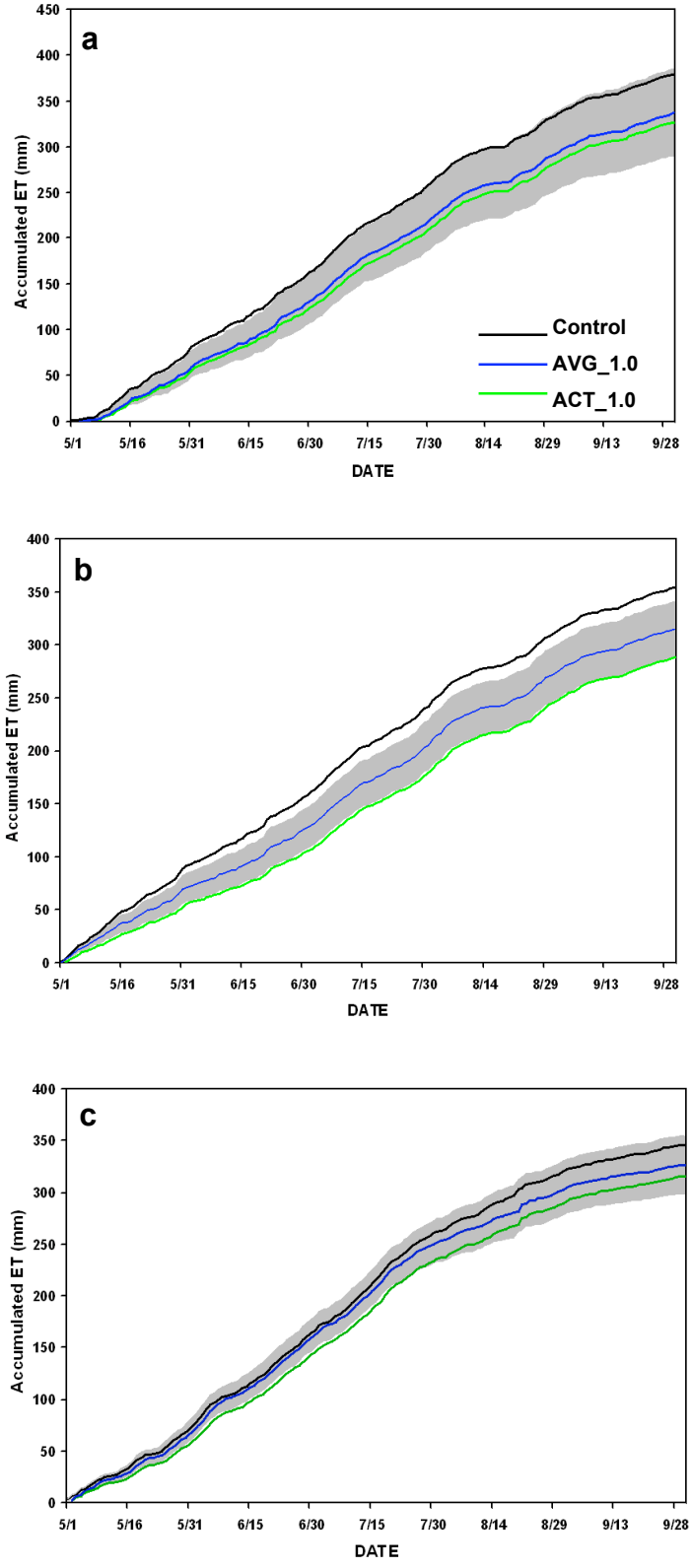

Figure 3.4: Same as Fig. 3.2 except for accumulated evapotranspiration.

The highest integrated ET was predicted at Mundare, with 340 mm. Interestingly, the predicted ET at Two Hills and Barnwell were similar at 315 mm. The distribution of the ET was different though, with the greatest accumulation of ET at Barnwell occurring before mid July, whereas at Two Hills the rate of increase was almost constant throughout the period. This reflects the PAW values dropping below 50% at Barnwell late in the season.

In the absence of in situ estimates of ET from eddy covariance (EC) systems, it is not possible to determine which of the model simulations of accumulated ET was most realistic. We do have access to EC data from an AmeriFlux site located 45 km west-southwest of Barnwell. The reader is referred to Wever et al. (2002) for a full description of the site and EC data. The AmeriFlux site is also located over native grassland, and both sites experienced very similar weather conditions during the summer of 2004. Specifically, between 1 May and 31 August 2004 the AmeriFlux site received 231 mm precipitation compared to 258 mm at Barnwell. Given the similar meteorological forcing and vegetation type observed at the two sites, it is reasonable to deduce that the accumulated ET at the AmeriFlux site should provide a good approximation of the expected ET at Barnwell. The accumulated ET between 1 May and 31 August at the AmeriFlux site was 268 mm versus 292 mm at Barnwell. The ratio of P to ET was 0.86 at AmeriFlux, compared to the estimate of 0.88 at Barnwell (for the ACT_1.0 simulation). It is therefore reasonable to deduce that the estimated accumulated ET from the ACT_1.0 simulation was probably very close to the actual ET. In a follow-on paper we will validate the modelled ET from PAMII against ET estimates from the AmeriFlux site for three contrasting summers.

3.5 Discussion

Table 3.7 compares the performance of PAMII with the skill of 14 similar models from around the world.

Table 3.7: Performance statistics for various agrometeorological models cited in the literature.

Study	R^2	RMSE	IA	Comments
PAMII	0.53-0.96	9-17 mm	0.81-0.93	Alberta, Canada. Grasses and pasture.
Xia and Shao (2008)	0.60-0.85	—	—	China. SWCCV model. Pea shrub.
Crawford et al. (2000)	0.52-0.80	9-13% VWC	—	Oklahoma mesonet. Soil Hydrology Model.
Kersebaum et al. (2008)	0.80	24 mm	0.94	Saskatchewan, Canada. HERMES model. Wheat.
Robinson and Hubbard (1990)	0.40-0.99	13-49 mm	0.78-1.0	Nebraska, USA. Only 5-14 days data.
Meng and Quiring (2008)	0.59-0.94	5-12% VWC	—	Midwestern USA. VIC and DSSAT models
Mirschel et al. (1995)	0.77	—	—	Germany. BOWET model. Cereals crops.
Wegehenkel and Mirschel (2006)	—	3.6-10.4 VWC	0.23-0.75	OPUS. Cereals crops. Germany.
Casanova and Judge (2008)	—	1.5-8.5% VWC	—	Florida, USA. DSSAT. Corn.
Sridhar et al. (2008)	—	3-15% VWC	—	Nebraska, USA. Model of Robinson and Hubbard (1990).
Kunkel (1990)	—	35 mm	—	CERES-maize model. Midwestern USA.
Wang et al. (2003a)	—	3.5% VWC	—	DSSAT-CROPGRO., USA. Soybean and corn.
Garrison et al. (1999)	—	~4.5% VWC	—	CERES-Maize. Iowa, USA.
Ma et al. (2005)	—	4.0% VWC	—	DSSAT-CROPGRO. Soybean. USA
		2.6% VWC		RZQM-CROPGRO. Soybean.
Wen et al. (2007)	—	—	0.84	CLASS. Bean. China

It shows that the performance statistic can span a wide range, not only between different models, but also for the same model under different conditions and/or vegetation types. This complicates trying to specify a benchmark for an accurate soil moisture content forecast. A closer analysis of the data suggests that R^2 typically varies between 0.50 and 0.95, compared to 0.53 and 0.96 in this study. The best expected RMSE for θ varies between 2% and 5% (although errors in θ in excess of 10% have been reported), compared to less than 2% in this study. Finally, the IA typically varies between 0.75 and 0.95, compared to 0.81 and 0.93 for PAMII. Thus the data in Table 3.7 clearly indicate that the skill of PAMII is comparable and even superior to a wide range of models of varying complexity.

To illustrate the importance of accurately specifying the soil water retention characteristics we plotted the mean seasonal RMSE (mm) against the Euclidean distance (E) calculated for PWP and FC specified by each of the 20 PTFs. The Euclidean distance is defined as follows: $E = [(\theta_{ppwp} - \theta_{opwp})^2 + (\theta_{pfc} - \theta_{ofc})^2]^{0.5}$, where θ_{ppwp} and θ_{opwp} are the predicted and observed PWP, respectively. Similarly, θ_{pfc} and θ_{ofc} are the predicted and observed FC, respectively. We also plotted the mean RMSE against the absolute error of the available water content (AWC). That is, AWC predicted by PTFs minus the estimated AWC based on in situ data.

The scatter plot shown in Fig. 3.5 indicates that 48% of the variability of the RMSE can be explained by the accuracy of the soil hydraulic properties (as quantified by E). Given all the factors that regulate the observed soil moisture, we feel that this is significant. There are two outliers present in the plot (both from Two Hills). If one removes these outliers, the R^2 of the scatter plot in Fig. 3.5 increases to almost 60%. A

scatter plot between RMSE and the absolute error of the predicted AWC (not shown) shows virtually no correlation between these parameters. Thus, at least for the data considered, the model skill is not a function of the accuracy of the predicted AWC.

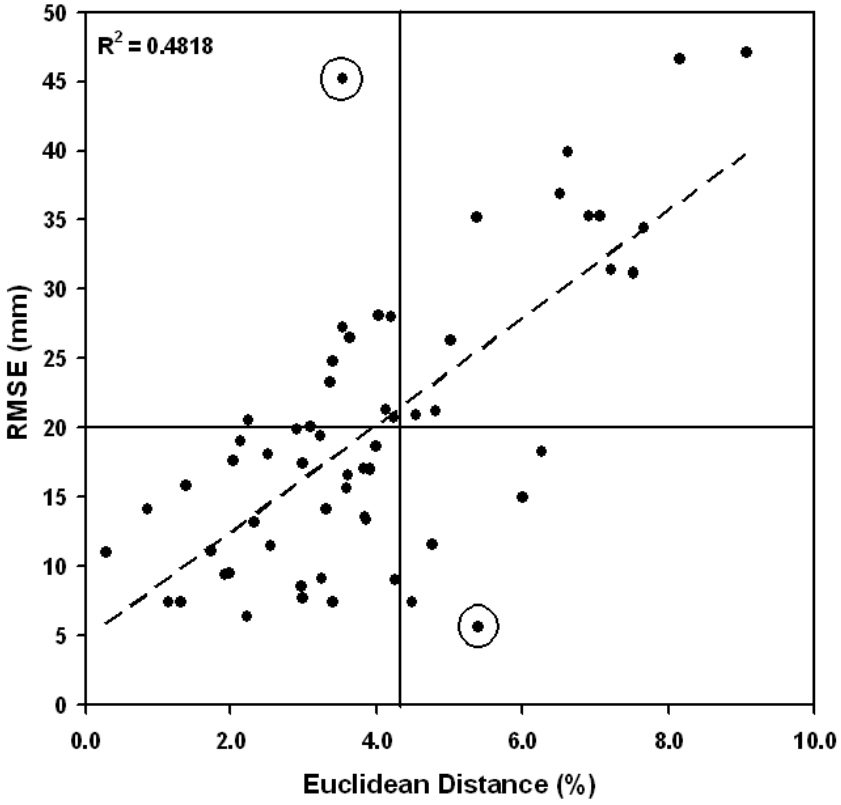

Figure 3.5: Scatter plot of RMSE (mm) versus the Euclidean distance (%) calculated for estimates of PWP and FC from the 20 PTFs for Mundare, Two Hills and Barnwell. The vertical line represents a Euclidean distance of 4.5%, the horizontal line represents a RMSE of 20 mm, and the dashed line represents the best-fit line. N = 60. Outliers are circled.

In view of the data shown in Fig. 3.5, we purport that accurately specifying the AWC alone is not sufficient to produce an accurate simulation, but that accurately specifying the soil water retention characteristics (in this case PWP and FC) does appear to greatly

improve the likelihood of an accurate simulation. We note that the Euclidean distance calculated here did not include the saturation point. The saturation point does obviously play a role in regulating the soil moisture content, but because we had no means of accurately inferring its value we could not take its influence into account here.

More insight can be gained by separating Fig. 3.5 into four quadrants delineated by a RMSE of 20 mm and an E of 4.5%. The RMSE threshold represents about 10% of the root-zone soil moisture at the three sites, while an E of 4.5% is equivalent to an error of 3% in both the FC and PWP. Using these thresholds, it is evident from Fig. 3.5 that if E is less than 4.5%, then there was a high likelihood that the RMSE will be less than 20 mm. Specifically, almost 75% of the model projections made with an E of less than 4.5% had a RMSE of less than 20 mm. In contrast, if E was greater than 4.5%, then 72% of the model simulations had a RMSE greater than 20 mm. These data underscore the importance of using accurate soil hydraulic parameters, and also suggest that there is little leeway when specifying FC and PWP in order to accurately simulate the soil moisture content.

To quantify the accuracy of the different model simulations in predicting soil moisture content, it is also useful to rank the different simulations in terms of the IA and RMSE (Table 3.8). Before looking at the rankings, it is important to recall that all the soil water retention properties used in the different simulations used the mean soil texture data for each class, or mean values from field surveys. At Mundare the observed soil texture was relatively close to the median values for loam (as determined by the Euclidean distance). In contrast, at Two Hills the observed soil texture was located near the triple point of the loam, sandy clay loam and clay loam classes. Consequently, the soil

texture data at this site are atypical of all three classes, making it difficult to accurately simulate the soil moisture using values of FC and PWP that were determined using representative of the class mean texture. Consequently, those PTFs which happened to accurately predict the hydraulic properties for a site (even if they were atypical for a given soil textural class) tended to produce lower errors.

Table 3.8: Comparison between ranked performance of soil moisture content forecasts (RVS; shown in Tables 3.4 to 3.6) versus the corresponding ranks of the predicted permanent wilting point and field capacity estimates (RHP, as determined by the Euclidean error) for each PTF.

	Two Hills		**Mundare**		**Barnwell**	
	RVS	**RHP**	**RVS**	**RHP**	**RVS**	**RHP**
ACT	7	-	5	-	2	-
AVG	10	6	4	7	10	6
BAT	20	18	9	13	20	17
BR	8	10	13	19	21	18
CH	13	13	16	15	13	15
CN	17	15	8	5	7	5
CONT	21	19	19	16	15	12
COSII	16	7	12	10	18	14
DAS	9	2	5	6	3	1
FED	4	12	15	6	**1**	**10**
HAL	**1**	**16**	**1**	**12**	12	8
MAJ	11	10	17	18	11	9
NOL	2	4	12	14	9	14
OOS	5	5	7	2	11	7
PET	12	4	3	6	5	3
RAW	18	17	2	1	16	11
SAR	6	3	6	3	19	16
SAX	15	11	11	8	14	10
TOM	19	8	10	4	17	15
VAN	14	14	18	17	6	13
WIL	9	9	14	11	8	4
ZAC	3	1	13	9	4	2

An intriguing observation when looking at the rankings in Table 3.8 is that those model runs made using the best estimate of the in situ soil water retention characteristics did not necessarily have the lowest RMSE. Specifically, after ranking all the model runs by RMSE and IA, we found that the ACT_1.0 runs ranked 7th, 5th and 2nd at Two Hills, Mundare and Barnwell, respectively. There are several possible explanations for this: (a) the method for estimating the FC and PWP was not accurate; (b) the soil moisture sensors had biases; (c) variability in soil moisture is not explained by soil water retention characteristics alone; (d) parameterization of certain processes, and physical limitations of the PAMII model (e.g., only two layers and one soil type) would lead to inaccuracies even if the input data were perfect. Reducing the PWP would affect the observed PAW, as well as the output from the ACT model runs. In terms of the observations at Two Hills in 2005, using a lower PWP (16% versus 18%) resulted in higher observed PAW values of between 5% and 9%. The resultant higher PAW values would then affect the modelled ET through the soil moisture stress function. However, the impact on the modelled ET stemming from lowering the PAW by 2% was not significant. Specifically, the accumulated ET between 1 May and 30 September was only slightly higher (9 mm or +3.0%) using the lower PWP for both the ACT_0.8 and ACT_1.0 runs. So while differences arising from errors in the actual PWP are not large, they would affect the validation statistics to a small degree. This is especially true for the validation of PAW. If the PWP at Two Hills was indeed 2% too high, the new ACT_1.0 run would be ranked 5th for soil moisture content instead of 7th.

Despite the uncertainties in PWP, the ACT_1.0 runs were ranked in the top five at two of the sites. It is instructive to assess how the ensemble average simulations

performed overall. The AVG_1.0 simulations ranked 4th at Mundare, and 10th at Barnwell and at Two Hills. Considering the overall performance at Mundare and Barnwell (i.e., those sites with soil textures which are relatively close to the class mean), simulations made using ACT_1.0 ranked highest, followed by DAS, PET, HAL and AVG_1.0. Of note is that none of the simulations (using soil hydraulic properties derived from individual PTFs) were ranked higher than AVG_1.0 at *all* three sites.

3.6 Summary and conclusions

We validated the prairie agrometeorological model (PAMII) against in situ soil moisture observations made in 2004 and 2005 at three Canadian Prairie sites having contrasting soil texture. Quantitative skill scores indicate that the model does well in simulating the evolution of root-zone soil moisture content and relative plant available water content (PAW) during the growing season, and that PAMII also captures the salient features of the soil moisture content and PAW at each site.

Specifying the soil hydraulic properties for the purpose of modelling soil moisture content and ET is particularly challenging because of the high spatial variability of soil structure. One method that is widely used to address forecast uncertainty is that of model ensembles. In this study, we tested the utility of using an ensemble technique to quantify the uncertainty associated with simulating the root-zone soil moisture using PAMII. The ensemble was assembled by running PAMII using soil hydraulic properties derived from 20 pedotransfer functions (PTFs) cited in the literature. The major findings may be summarized as follows:

- The skill of PAMII in simulating root-zone soil moisture content is comparable and even superior to similar agrometeorological models.
- For the sites considered here, model runs using the mean soil hydraulic properties for the relevant soil textural class were ranked in the top 10 at all three sites.
- None of the runs using soil hydraulic properties from the PTFs ranked higher than those simulations run using the mean soil hydraulic properties (derived from the 20 PTFs) at *all* three sites.
- Relative mean absolute errors for bulk root-zone soil moisture content at the three sites varied between 3% and 9% for runs using the mean soil hydraulic properties.
- Simulated relative plant-available soil moisture values were typically within 10% of the observations.
- Ensemble runs suggest that the model uncertainty is typically less than 10% of the bulk root-zone soil moisture content.
- For the sites considered here, the skill of model runs using a particular PTF appears to be strongly modulated by the Euclidean error of the PWP and FC estimated by that PTF.
- To improve the likelihood of an accurate soil moisture content simulation, the FC and PWP should be within 3% of the observed values.
- The accumulated ET is sensitive to the values of PWP and FC specified for a particular soil textural class.
- Model runs made using a reference stomatal resistance of 100 s m^{-1} typically yielded superior results than using a value of 80 s m^{-1}.

In view of the above results, we are confident that PAMII can be used successfully as a diagnostic tool to track the evolution of root-zone soil moisture content. However, the correct modelling of soil moisture content is contingent on accurately specifying the site-specific soil hydraulic properties. Simply using mean percentages of sand and clay for an entire soil textural class to estimate the soil hydraulic properties can lead to inaccurate results should the in situ soil texture depart significantly from the class average values. This is relevant because combinations of FC and WP in nature are probably randomly distributed across the FC/WP parameter space, and cannot be pigeon holed into a particular class. Even in the absence of site-specific soil texture data, one can still quantify the associated uncertainty/error arising from soil heterogeneity and mitigate the uncertainty to some extent by using an ensemble technique.

CHAPTER 4

4. VALIDATION OF ET ESTIMATES FROM THE CANADIAN PRAIRIE AGROMETEOROLOGICAL MODEL FOR CONTRASTING VEGETATION TYPES AND GROWING SEASONS

[2]Abstract

The objective of this study was to establish the ability of the prairie agrometeorological model (PAMII) to simulate daily ET. Specifically, modelled ET estimates from PAMII were validated using daily ET estimates from eddy-covariance systems at West Nose Creek (barley field located northwest of Calgary) and a FluxNet site (short-grass prairie located west of Lethbridge). Additionally, we wished to establish the ability of PAMII to discern between different growth conditions. To this end, PAMII was validated for three contrasting growing seasons at the grassland site.

PAMII performed well and was capable of capturing the day-to-day variability of the ET at both sites. PAMII successfully captured the increase (decrease) in accumulated growing season ET for the wet (dry) growing seasons at the short-grass prairie site. Moreover, the optimal minimum reference stomatal resistance term was significantly lower for the barley crop (50 s m^{-1}) than the corresponding value for the short-grass prairie (80 s m^{-1}). Of note is that at the grassland site the optimal stomatal resistance term varied markedly depending on the growing conditions. For example, the optimal value

[2] This is a copy of a paper published by Brimelow et al. (2010b) in the Canadian Water Resources Journal. Reproduced here with permission.

for the wet year was 60 s m^{-1} compared to 90 s m^{-1} for the dry year. That is, no single value worked best for all years, and our findings caution against using a single value for the reference minimum stomatal resistance.

In summary, PAMII captured the salient features of the ET variability at both sites and for contrasting conditions. However, our research has identified several areas where future versions of the PAMII model might be improved.

4.1 Introduction

The grassland eco-climate region of the Canadian Prairies covers an estimated 480 000 km^2. Annual field crops (wheat, canola and barley) cover about 60% of this area, with spring wheat alone accounting for about 50% of the cropped area (Hanesiak et al. 2009. Eighty percent of the significant (≥10 mm) summer rain events over the Canadian Prairies include thunderstorms (Raddatz and Hanesiak 2008). The amount of water vapour available to feed warm season rain events is governed by the advection of water vapour into a region (e.g., Brimelow and Reuter 2005) and surface evapotranspiration (ET) (e.g., Brubaker et al. 1993; Trenberth 1999). Under quiescent atmospheric conditions the daily contribution of ET to moisture in the convective boundary layer (CBL), primarily through transpiration from the vegetation, can exceed that added through advection (Raddatz 2005). Using a crop model, Raddatz (1998) showed that crop phenology on the Prairies exerts an important control on the seasonal pattern and inter-annual variability of regional moisture fluxes.

Given that precipitation tends to be highly variable in both space and time, it is expected that the root-zone soil moisture content across the agriculture zone of the

Prairies will be heterogeneous at any given time. An important consequence of variability in root-zone soil moisture content is the formation of attendant gradients in ET. Spatial discontinuities in ET can generate or enhance mesoscale circulations (Chang and Wetzel 1991; Clark and Arritt 1995), and can play a key role in determining where and when thunderstorms will develop (Pielke 2001; Hanesiak et al. 2004).

Several researchers have underscored the importance of changes in boundary-layer moisture as small as 1 g kg^{-1} on the occurrence and strength of any deep, moist convection that may develop (e.g., Crook 1996). In terms of the convective available energy, Crook (1996) showed that a change in surface mixing ratio of only 1 g kg^{-1} is equivalent to increasing the surface air temperature by 2.5 ºC. Hanesiak et al. (2004) showed that convection initiation typically occurred along the sharp moisture gradients (on the moist side of the boundary) during quiescent synoptic forcing days in the agricultural zone of the Canadian Prairies, highlighting the importance of the gradients in ET and PBL mixing ratios. Additionally, studies have linked local ET influences to tornadic storms on the Canadian Prairies (Raddatz and Cummine 2003), and in the United States (e.g., Kellenbenz et al. 2007).

The absence of a high spatial resolution in-situ soil moisture monitoring network on the Canadian Prairies means that one has to rely on alternative methods for estimating soil moisture and ET. The intent is to utilize the Raddatz crop phenology model (described in section 4.2.1) to map the continually evolving regional spatial distribution of soil moisture and ET in response to atmospheric drivers. Before doing so, however, we need to validate the model's skill at predicting evapotranspiration.

In a recent paper, Brimelow et al. (2010a) determined the skill of the prairie

agrometeorological model (PAMII) when simulating root-zone soil moisture at three grassland sites in Alberta, Canada. They also quantified the sensitivity of modelled root-zone soil moisture and evapotranspiration to uncertainties arising from the specified soil water retention properties. Brimelow et al. (2010a) found that PAMII showed significant skill in simulating the evolution of root-zone soil moisture content during the growing season, and that PAMII also captured the salient features of the soil moisture content at each site. Specifically, correlation coefficients between simulated and observed root-zone soil moisture content were between 0.65 and 0.90, while the mean absolute errors were typically less than 10% of the mean soil moisture content. In light of these findings we are confident that PAMII can be used successfully as a diagnostic tool to track the evolution of root-zone soil moisture content. In this paper, the focus is to establish the ability of PAMII to reproduce daily evapotranspiration above native grassland and a barley field in southern Alberta, in light of the importance of evapotranspiration on regional weather and hydrometeorology. In addition, at the grassland site, the model's performance was validated for contrasting growing seasons.

4.2 Methodology

4.2.1 The prairie agrometeorological model

The second generation prairie agrometeorological model (PAMII; Raddatz 1993) simulates the evolution of soil moisture content and vegetation using a daily time step. Unlike other models which are commonly used to model ET on the Canadian Prairies (e.g., Monteith 1965; Granger and Gray 1989; Akinremi et al. 1996), PAMII model does not explicitly take into account the surface energy balance. Evapotranspiration in PAMII

is governed by photoperiod, vapour pressure deficit, leaf fraction, aerodynamic resistance and canopy resistance (r_s). The magnitude of r_s is inversely proportional to the relative plant available moisture present in the root zone, and the fractional leaf area.

Input data for the model consist of observed daily observations of minimum and maximum temperature and rainfall. In addition to observed precipitation and minimum and maximum temperatures, PAMII also requires the vapour deficit and a profile of temperature, humidity and winds in the PBL. To this end, prognostic soundings from the regional version of the Canadian Global Environmental Multi-scale (GEM; Côté et al. 1998) model were used. Specifically, 0-hour soundings from the daily 1200 UTC and 0000 UTC model runs were used as input for PAMII.

The model does not allow for the interception of precipitation by the canopy, or the re-evaporation of intercepted moisture. The surface temperature of the leaves is assumed to be the same as that of the ambient air. Transpiration is proportional to the difference between the vapour density of the air and the saturation vapour density in the leaves' stomata. A reference value for the minimum canopy stomatal resistance (r_ref) is specified, and at the time of this study, both the crop and pasture versions of PAMII used r_ref = 80 s m^{-1}.

The surface characteristics are described in terms of the terrain height, roughness length, soil class, crop stage, root- and top-zone moisture levels. Green up for pasture/grasses is assumed to occur at the first occurrence of five consecutive days having a mean temperature greater than 5 °C, while dormancy occurs following the first day with a minimum temperature of -5 °C (Raddatz 2005). For perennial grasses, the maximum rooting depth is held constant at 110 cm.

For crops, the phenological stage is determined by the planting date, accumulated heat and photoperiod. Specifically, the model uses bio-meteorological time (BMT; Robertson 1968) to estimate the crop stage and leaf fraction. The root depth increases with time from 10 cm at time of sowing to a maximum depth of 120 cm. The increase in root depth is a function of BMT. The evolution of the canopy is modelled in terms of the fractional leaf area, which is zero at planting and increases to 100% at the heading stage, followed by a decline (Raddatz 1993).

Eleven soil types from the USDA soil triangle can are discerned; values of wilting point, field capacity, saturation level and available water content are specified for each soil class in look-up tables. The same soil type is specified for both the top zone (top 10 cm) and root plus sub zones (120 cm). The subzone shrinks as the root zone grows. The bulk soil moisture in the root/subzone and top zone are tracked separately. Moisture in the top zone is depleted by both transpiration and by evaporation; in the root-zone by transpiration and by deep drainage from the subzone. Allowance is made for the capillary action or wicking of moisture from the relatively moist root-zone when the surface is dry. Rainfall less than 25.4 mm (1 inch) infiltrates into the soil until field capacity is achieved, while rain in excess of 25.4 mm is partitioned between infiltration and run-off depending on the soil moisture in the top 10 cm, even when there is available capacity. Infiltration of rainfall into the root zone is not permitted when the top zone is saturated.

The bulk soil moisture content in the root zone provides little insight concerning whether or not the plants' moisture requirements are being adequately satisfied. For this purpose, it is convenient to quantify the moisture in the root zone in terms of the relative

plant available water content (PAW). Relative PAW is equal to $[(\theta - \theta_{pwp})/(\theta_{fc} - \theta_{pwp})]$ where θ is the observed volumetric water content (VWC) in the root zone, θ_{pwp} is the VWC at the permanent wilting point and θ_{fc} is the VWC at field capacity.

4.2.2 Lethbridge validation site

4.2.2.1 Site description

Validation data for the pasture version of PAMII were from an Ameriflux site (49.71 N, 112.94 W, 951 m) located west of the city of Lethbridge in Alberta, Canada. The site is located in a large field (64 ha) of moist-mixed grassland Prairie which has not been grazed for over 20 years (Flanagan et al. 2002). Vegetation at the site is dominated by C3 grasses (Carlson 2000). Specifically, the dominant native grass species are wheat grasses (*Agropyron dasystachyum* and *Agropyron smithii*) and June grasses (*Koeleria cristata*). Also present are American vetch (*Vicia Americana*), spear grass (*Stipa comata*) and pasture sage (*Artemesia frigidia*). The site is also extensively populated by introduced goat's beard (*Tragopogon dubius*).

Measurements of canopy height and green leaf area index (using a LI-3100) were routinely made throughout the growing season. Grasses at the site are characterized by a low canopy height — between 2001 and 2006 the mean maximum canopy height was near 33 cm, although there is significant inter-annual variability (range 18.5 cm to 39 cm). Wever et al. (2002) noted that there is abundant dead plant material on the ground (dead LAI ~1.2). Between 1998 and 2006 the green leaf area index (LAI) was typically between 0.5 m^2 $m^{-2}$and 1.0 m^2 m^{-2} (mean 0.83 m^2 m^{-2}), and only exceeded 1 m^2 m^{-2} in 2002 and 2005.

Table 4.1: Soil classification and water retention characteristics for validation sites located at Lethbridge and WNC.

Location	Soil Class	Wilting Point (m^{-3} m^{-3})	Field Capacity (m^{-3} m^{-3})	Saturation (m^{-3} m^{-3})
Lethbridge	Clay Loam	0.204	0.339	0.469
WNC	Clay Loam	0.230	0.346	0.515

The soils at the site are Orthic Dark-Brown Chernozem (Li et al. 2004), and classified as clay loam using the USDA soil triangle. The soil texture data, as well as the organic content, down to a depth of 25 cm, were estimated from field samples. Properties of the soil column between 25 cm and 120 cm were extracted from Agricultural Region of Alberta Soil Inventory Database. Table 4.1 lists the volumetric water content at field capacity (FC), permanent wilting point (PWP), and saturation point that were calculated from layer-weighted soil texture and organic matter content in the top 1 m using the pedotransfer function of Saxton and Rawls (2006).

The climate is semi-arid with a mean annual precipitation observed between 1971 and 2000 at Lethbridge airport (located 13 km southeast of the study site) of 386 mm (Environment Canada). The wettest months are May and June which together account for almost 55% of the annual precipitation. Mean monthly temperatures range between -7 8 ºC in January and 18.0 ºC in July; the mean annual temperature is 5.7 ºC. Summers can be hot with maximum temperatures frequently approaching 35 ºC. The mean relative humidity at 3 pm LT (Local Time) is near 40% between May and August. Winds are predominantly from the west, and the area is frequently affected by Chinook winds. Consequently, the mean annual wind speed at the site is relatively high at 5 m s^{-1}.

4.2.2.2 Observed weather conditions May through August

To test the ability of PAMII to discriminate between significantly different growing conditions, we selected three contrasting years from the available data (1998–2006). Specifically, 1999 was cooler (-1 ºC) and drier (72% of average rainfall) compared to climatological mean conditions between May - August (1971 and 2000). In 2000, the area experienced a severe drought (33% of average rainfall) with above normal temperatures, especially in July and August (+2 ºC to +3 ºC). In 2004, temperatures were near normal but below normal in May and June (-1.5 ºC). Overall the precipitation was above normal (112%).

4.2.2.3 Flux data

An eddy covariance (EC) system was used to measure the fluxes of water vapour, CO_2 and sensible heat on a continuous basis. Li et al. (2004), Wever et al. (2002) and Flanagan et al. (2002) have provided detailed information on the eddy covariance system as well as the techniques used to process the EC data. Consequently, here we will only provide a short summary of the system and the data processing techniques. Table 4.2 lists the primary sensors at the Lethbridge site. Fluxes of water vapour and sensible heat were computed using the University of Edinburgh EdiSol software (Moncrieff et al. 1997). Precipitation was recorded in 15-min intervals, while all other data were recorded as 30-min averages. Transfer functions were used to correct for a high frequency component of the flux that was missing from the measurements (Moncrieff et al. 1997).

Table 4.2: Summary of sensors used for surface weather observations and eddy covariance measurements at the validation sites.

	Lethbridge	West Nose Creek
3D winds	Ultrasonic anemometer (Solent 1012) on a 6 m tower	Ultrasonic anemometer (CSAT3) on a 2.5 m tower
Water Vapour Concentration	Closed path, infrared gas analyzer (LI-6262)	Krypton hygrometer (KH2O) at 2.5 m
PAR	Quantum Sensor (LI-190SA) mounted on a 3 m tower.	Not measured
Radiation	Net radiometer (REBS Q*7.1) on a 3 m tower	Four-component radiometer (CNR1)
Temperature and RH	Shielded HMP45C at 2 m	Shielded HMP45 at 2 m
Ground heat flux	HFT3.1 buried 2 cm below the surface	HFT3.0 buried 3 cm below the surface
Precipitation	Tipping bucket rain gauge (TE525) at 1 m	Tipping bucket rain gauge at 1 m

Flanagan et al. (2002) found that there was excellent agreement between the available energy (difference between the net radiation (R_n) and the ground heat flux (G)) and the sum of the latent (LE) and sensible heat (H) fluxes. Specifically, the correlation coefficients for 1998, 1999 and 2000 were at least 0.95, while the slopes of the linear regression were between 0.85 and 0.90 which suggested that there was a tendency to underestimate the sensible and/or latent heat fluxes. For the 260 days in 1999, 2000 and 2004 used to validate the model in this study, the slope of the regression was 0.87, with a correlation coefficient of 0.96.

4.2.3 West Nose Creek (WNC) validation site

4.2.3.1 Site description

The West Nose Creek (WNC) site (51.26 N; 114.17W, 1220 m) is located about 18 km northwest of Calgary International Airport. The site has undulating topography. The eddy covariance system and automatic weather station were installed in a 16-ha barley

field in late June 2005, and data was archived from 1 July onwards. Consequently, the flux data considered here apply to a mature barley canopy.

The mean annual precipitation observed between 1971 and 2000 at Calgary International airport was 413 mm (Environment Canada). The wettest months are June and July which together account for 35% of the annual precipitation. Mean monthly temperatures range between -8.9 ºC in January and 16.2 ºC in July, with a mean annual temperature of 4.1 ºC. The mean relative humidity at 3 pm LT is near 45% between May and August. Winds are predominantly from the west; Chinook winds are frequently observed. The mean annual wind speed at the site is relatively high at 4 m s^{-1}.

The dominant soil of the WNC site is Orthic Black Chernozem of the Antler Series and is classified as clay loam. Water retention characteristics were determined for soil samples taken from 30, 60, and 100 cm with the pressure extractor method (Dane and Hopmans 2002). Table 4.1 lists the water retention characteristics specified for the model runs.

4.2.3.2 Observed weather conditions May through August 2005

With the exception of May and July, the growing season at the WNC site was unusually wet and cool. Specifically the rainfall in June was three times the 1971–2000 average and the mean maximum temperature was 3.0 ºC below average. In August, rainfall was 165% of average, with a mean maximum temperature 2.3 ºC below average. In May and July, Calgary only received about 30% of the mean monthly rainfall; the mean maximum temperature anomalies in May and July were +1.4 ºC and +0.3 ºC, respectively. Consequently, the crop experienced a marked reduction in soil moisture between early July and early August.

4.2.3.3 Flux data

Basic meteorological data were collected at an automatic weather station, which included air temperature, relative humidity, wind speed, and precipitation by a tipping bucket rain gauge.

The eddy-covariance system (Campbell Scientific, CSAT3 and KH20), four-component radiometer (Kipp & Zonen, CNR1), and heat flux plate (Campbell Scientific, HFT3) were installed in the barley field at the WNC site in 2005. The heat flux plate was calibrated by comparing the sensor output with the ground heat flux calculated by the combination method (Sauer 2002) using the soil temperature data measured by a 1.5-m deep thermocouple string. For the 22 days used to validate the model, the slope of the regression was 0.79, with a correlation coefficient of 0.73. The average closure rate was 0.78 which is similar to the closure rate reported by Su et al. (2005) for EC measurements made over a soybean crop. Hayashi et al. (2010) estimated the uncertainty associated with calculating daytime ET estimates, using the EC system at Spy Hill farm, located 10 km south of the WNC site, to be 10-15%. Mo et al. (2008) report that the overall accuracy of eddy covariance fluxes is between 10 and 20% (e.g., Santaren et al. 2007). In this study, the uncertainties of the adjusted observed latent heat fluxes are set as 12.5% of their daily average values.

4.3 Model runs

4.3.1 Input data

ET estimates from PAMII are sensitive to various parameters, such as stomatal resistance, aerodynamic resistance and the vapour density gradient. Scrutiny of the input

data showed that the forecasts of surface temperature and RH from the regional GEM model could be out by up to 7 ºC and 25%, respectively. Because of their high altitude, both WNC and Lethbridge sites are close to the 850-mb level, and consequently temperatures at 850 mb are highly correlated with the surface temperatures. The aerodynamic resistance term in PAMII includes a stability adjustment term, which is a function of the lapse rate in the PBL. While the forecast temperature at 850-mb is adjusted by PAMII so that the potential temperature at 850 mb is approximately the same as that at the surface and the top of the PBL, if the temperature at 850 mb is inconsistent with the observed surface temperature, it is not always possible to adjust the temperature at 850 mb adequately, and spurious lapse rates can result. These spurious lapse rates will in turn result in unrepresentative aerodynamic resistance values which can degrade the ET estimates. Also, if there are gross errors in the surface RH predicted by the GEM model, this will result in unrealistic vapour density gradients, which can also degrade the ET forecast.

Given that the objective of this paper is to validate the ET estimates from PAMII and not the accuracy of the input data, we adjusted the forecast 850-mb temperatures (when necessary) at WNC and Lethbridge to be consistent with the observed maximum surface temperatures, and also adjusted the forecast surface RH at 0000 UTC to be within 2% of the observed minimum surface RH values. In this way we minimized contributions of input data to errors in the predicted ET.

4.3.2 Lethbridge simulations

The grassland/pasture version of PAMII was used for the simulations. For each of the study years, the initial soil root-zone soil moisture (quantified in terms of PAW) was

varied over a range of 10% (increments of 5%), with the control run using that initial value which produced best ET estimates for the growing season.

An extensive literature review of 30 research papers and meta analyses (e.g., Kelliher et al. 1995; Schulze et al. 1994) found that the 95% confidence interval for the mean minimum stomatal resistance term (81 s m^{-1}) for grasses was between 62 and 101 s m^{-1}. Based on these data, the r_ref term in our simulations was varied between 60 s $m^{-1}$and 100 s m^{-1} (in increments of 10 s m^{-1}). Varying the initial soil moisture and r_ref terms resulted in a total of 15 model runs for each growing season. The standard deviation of the ET from all 15 model runs was calculated for each day. This permitted us to obtain an idea of the uncertainty of modelled ET and PAW associated with inaccuracies of the reference stomatal resistance term and the initial soil moisture content. The model simulation was started on 1 April each year.

4.3.3 WNC simulations

The wheat version of PAMII was used for the simulations. While the phenology of wheat and barley are not exactly the same (barley tends to mature earlier than wheat), here we assume that the wheat version of the model is applicable to most cereal crops. The initial soil root-zone soil moisture at the WNC site was varied between 90% and 100%. This range of initial PAW produced soil moisture values which agreed very well with the in-situ moisture measurements on 1 July. A literature review of 52 papers and meta analyses (e.g., Kelliher et al. 1995; Schulze et al. 1994) found that the 95% confidence interval for the mean (49 s m^{-1}) minimum stomatal resistance term for crops was between 43 and 54 s m^{-1}. Based on these data, and the control value used in PAMII (80 s m^{-1}), r_ref was varied between 40 s $m^{-1}$and 80 s m^{-1}. The model simulation was

started on 1 May, and the planting date (obtained from the farmer) was set at 14 May 2005.

4.3.4 Validation: Data and methodology

Eddy covariance data were used to calculate ET only on days when all of the following criteria were met:

- Daytime precipitation ≤ 0.2 mm
- No more than one missing 30-min reading for any of the variables
- No negative sensible heat fluxes during times of high solar radiation
- An energy closure of at least 0.70

After applying the above criteria, 22 (31%) of the 70 days for which data were available at the WNC site were used to validate the model. Of the 46 days not analyzed (67% of total), 27 (59%) were excluded because of missing or faulty data or precipitation, 5 (11%) because of negative sensible heat fluxes, and 14 (30%) of the days failed to meet the energy closure limit of 0.70. At the Lethbridge site a total of 260 days (70% of maximum) were available to validate PAMII. A total of 95 (87%) of the 109 days not analyzed were excluded because of missing data and/or precipitation, 10 (9%) days because of energy closure problems and 4 (4%) days because of negative sensible heat fluxes. The above stringent criteria used to ensure that the validation data set was as accurate as possible.

PAMII simulates the expected ET for the daytime only (i.e., sunrise to sunset). How exactly one defines the daytime period for the purpose of calculating the Bowen ratio varies in the literature. Twine et al. (2000) suggest using only those flux data collected for times when the net incoming radiation (R_n) is greater than 50 W m^{-2}. Others suggest

using fluxes collected when R_n is greater than zero (e.g., Blanken et al. 1997), or arbitrary times such as between 9:00 and 17:00 LT (e.g., Scanlon and Sahu 2008). Sensitivity tests using different thresholds for R_n indicated that the measured daytime ET values were typically within 5% (<0.2 mm) of each other. In order to minimize closure problems that can occur when the available energy is low, data were only used for those times of day when R_n was at least 50 W m^{-2} (Twine et al. 2000). At the WNC site we also accounted for the heat storage in the upper 3 cm of the soil (using the method of Oncley et al. 2007), and this generally increased the daytime energy budget closure by 1% to 3%. We did not take into account energy stored in the plant canopy, because for short vegetation (as studied here) the canopy storage is typically less than 2% of R_n (e.g., Oncley et al. 2007).

For both systems, the daytime Bowen ratio measured by the eddy-covariance system was used to adjust the sensible and latent heat fluxes to force energy balance closure (Twine et al. 2000). Daily evapotranspiration was then calculated using the adjusted mean daytime latent heat flux. Comparison with daily ET estimates derived using the methodology of Hayashi et al. (2010) suggest that our ET estimates probably represent the high end of the expected range. Specifically, Hayashi et al. (2010) used three methods for estimating daily ET. The first estimate (deemed to be the lower bound) was calculated without forcing energy closure (i.e., unadjusted latent heart flux). The second estimate (deemed to be the upper bound) was calculated by adjusting the H and LE fluxes to force closure (while maintaining the Bowen Ratio) using mean values of R_n, G , H and LE for the 24-hr period. The third estimate of daily ET was a simple arithmetic mean of the two. To facilitate direct comparison, we estimated the daily ET by calculating the sum of our daytime values (forcing closure when R_n >50 Wm^{-2}) plus ET calculated (using

the unadjusted LE fluxes) for when R_n <50 Wm^{-2}. We then compared the data for 17 days for which we could calculate the daily ET estimate using the aforementioned methods. Careful comparison between the daytime ET estimates using our methodology and that of Hayashi et al. (2010) suggest that, on average, our daytime ET estimates may be 5% to 7% too high. This equates to about 0.2mm to 0.3 mm of ET per day.

The following verification parameters were used to quantify the performance of the model's daily evapotranspiration predictions: Mean error, mean absolute error (MAE), root-mean square error (RMSE), square of the Pearson product-moment correlation coefficient (R^2), and the Index of agreement (IA). The index of agreement is calculated as follows:

$$\boldsymbol{IA} = 1.0 - \left[\frac{\sum_{i=1}^{N} \left(\boldsymbol{O}_i - \boldsymbol{M}_i \right)^2}{\sum_{i=1}^{N} \left[\left| \boldsymbol{O}_i - \overline{\boldsymbol{O}} \right| + \left| \boldsymbol{M}_i - \overline{\boldsymbol{O}} \right| \right]^2} \right] \tag{4.1}$$

where M and O are the modelled and observed data points, and $\overline{O}$ is the mean of the observed series. R^2 explains the percentage of the total variation in the observations that is explained by the model. Legates and McCabe (1999) suggested that the IA is superior to the correlation coefficient for the purpose of evaluating modelled soil moisture data. IA ranges from 0 to 1, with 1 indicating perfect skill.

4.4 Verification statistics

4.4.1 Lethbridge

4.4.1.1 1999

Fig. 4.1a shows the accumulated rainfall and accumulated modelled ET for the Lethbridge site in 1999; a cool growing season with below average precipitation. For this growing season the accumulated ET exceeded the accumulated precipitation by about 35 mm (~18%). However, Fig. 4.1a shows that most of this deficit was predicted to occur late in the season after the grasses had already senesced, so it is expected that the grasses did not experience significant moisture stress when they were experiencing active growth. Table 4.3 contains a summary of the validation statistics. For the 73 days considered in 1999, the modelled mean daily ET was almost identical to the observed value from the EC system.

Table 4.3: Validation statistics for modelled ET at Lethbridge in 1999. Statistics were calculated for a total of 73 days between 1 May and 31 August. Model runs were made using an initial plant-available water content in the root zone of 30%. Abbreviations are for mean error (ME), mean absolute error (MAE), root-mean square error (RMSE), square of the Pearson product-moment correlation coefficient (R^2), and the index of agreement (IA). R_ref is the reference stomatal resistance.

	r_ref = 60	**r_ref = 70**	**r_ref = 80**	**r_ref = 90**	**r_ref = 100**
ME	0.04	0.05	0.05	0.04	0.03
MAE	0.45	0.45	0.46	0.48	0.49
RMSE	0.56	0.55	0.56	0.58	0.59
R^2	0.58	0.55	0.51	0.47	0.42
IA	0.86	0.85	0.84	0.81	0.80

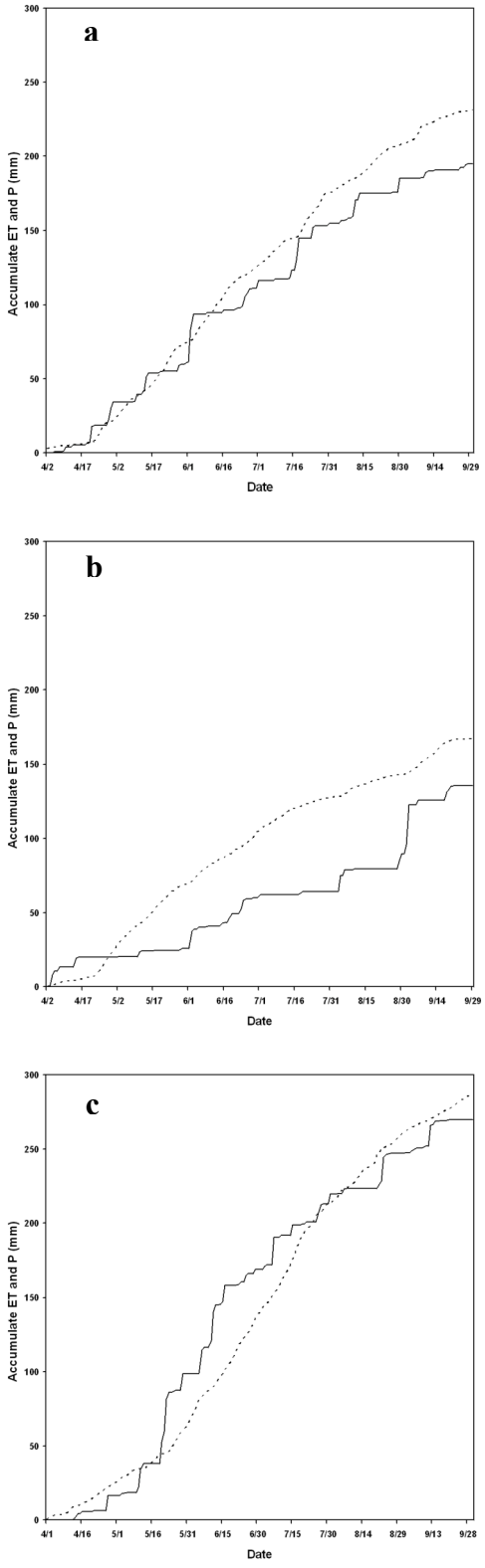

Figure 4.1: Accumulated precipitation (solid line) versus modelled accumulated ET (dashed line) by PAMII at Lethbridge for (a) 1999; (b) 2000; and (c) 2004.

The closest agreement was obtained using a stomatal resistance of 60 s m^{-1}, which resulted in a MAE of 0.45 mm (relative error of 27%), a R^2 of 0.58 and an IA of 0.86. Modelled ET calculated using an r_ref of 100 s m^{-1} performed worst of all cases considered.

The total accumulated ET of 123 mm shown in Fig. 4.2a was in excellent agreement with the observed accumulated ET (120.0 mm), and well within the uncertainty of the ET estimates from the EC system. The range of modelled ET did not vary significantly for increasing r_ref, however, the distribution of the modelled ET was different. Specifically, higher (lower) r_ref resulted in lower (higher) ET earlier (later) in the season.

4.4.1.2 2000

Fig. 4.1b shows the accumulated rainfall and accumulated modelled ET for the Lethbridge site in 2000; a drought year. For this growing season the accumulated ET exceeded the accumulated precipitation by about 53 mm (~60%). A heavy rainfall event of 26 mm in early September reduced the moisture deficit, but not before the vegetation had experienced prolonged and significant moisture stress. Table 4.4 summarizes the validation statistics.

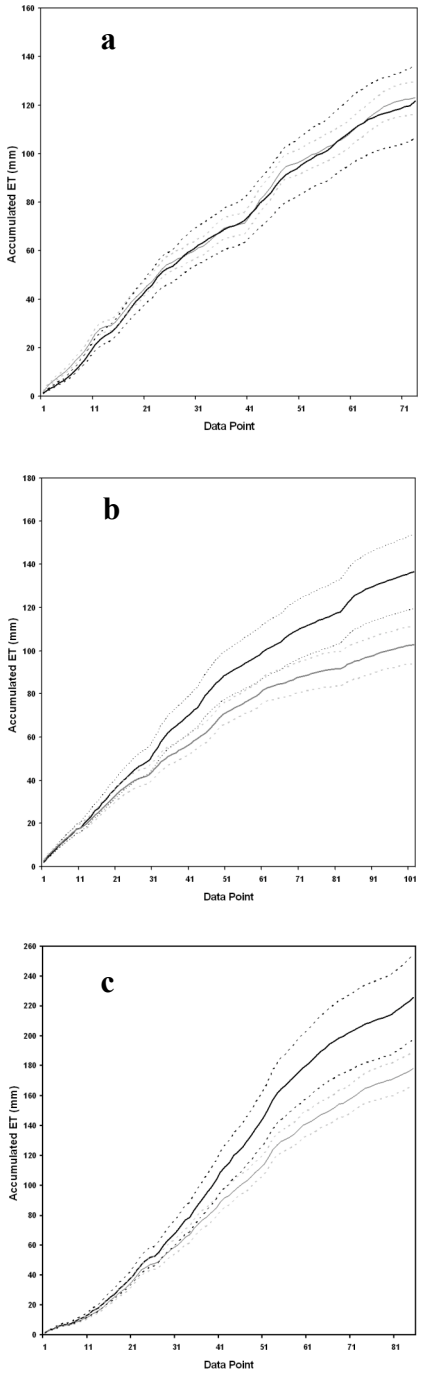

Figure 4.2: Accumulated observed ET (dark line) versus accumulated forecast ET (grey line) for (a) 1999, (b) 2000 and (c) 2004 at Lethbridge. The dashed grey lines represent the forecast uncertainty in accumulated ET obtained by calculating the standard deviation of 15 modelled daily ET values. The standard deviation was obtained by varying the r_ref between 80 and 100 s m^{-1} and using three different initial soil moisture values. Dashed black lines represent the uncertainty of the observed ET calculated using ±12.5% of the daily ET estimated from the eddy covariance data.

For the 102 days considered, the closest agreement with observed data was obtained using a stomatal resistance of 90 s m^{-1}, which resulted in a MAE of 0.39 mm (relative error of 29%), a R^2 of 0.60 and an IA of 0.82.

Modelled ET derived using an r_ref of 60 s m^{-1} performed worst of all cases considered. Fig. 4.2b shows that the total accumulated ET of 103 mm was markedly lower than the observed accumulated ET (136.5 mm). This is reflected by the mean negative bias of 0.33 mm d^{-1}. Once again, the range of modelled ET did not vary significantly for increasing r_ref, however, the distribution of the modelled ET was different, with higher r_ref resulting in lower (higher) ET in the very early part of the season, and lower r_ref resulting in higher ET from June onwards. Modelled ET derived using a r_ref of 60 s m^{-1} performed the worst of all cases considered.

Table 4.4: Validation statistics for modelled ET at Lethbridge in 2000. Statistics were calculated for a total of 102 days between 1 May and 31 August. Model runs were made using an initial plant-available water content in the root zone of 45%. The abbreviations are defined in Table 4.3.

	r_ref = 60	**r_ref = 70**	**r_ref = 80**	**r_ref = 90**	**r_ref = 100**
ME	-0.38	-0.36	-0.34	-0.33	-0.32
MAE	0.48	0.44	0.39	0.39	0.37
RMSE	0.58	0.55	0.53	0.51	0.51
R^2	0.59	0.61	0.61	0.60	0.59
IA	0.79	0.81	0.82	0.82	0.81

4.4.1.3 2004

Fig. 4.1c shows the accumulated rainfall and accumulated modelled ET for the Lethbridge site in 2004, a cool growing season with above average precipitation. In 2004 the accumulated ET and accumulated precipitation were almost the same (~6%).

However, Fig. 4.1c shows that between mid May and mid July the precipitation exceeded the ET, reflecting the very moist conditions observed earlier in the growing season.

Table 4.5: Validation statistics for modelled ET at Lethbridge in 2004. Statistics were calculated for a total of 85 days between 1 May and 31 August. Model runs were made using an initial plant-available water content in the root zone of 25%. The abbreviations are defined in Table 4.3.

	r_ref = 60	**r_ref = 70**	**r_ref = 80**	**r_ref = 90**	**r_ref = 100**
ME	-0.53	-0.54	-0.56	-0.58	-0.60
MAE	0.66	0.64	0.65	0.68	0.73
RMSE	0.85	0.83	0.85	0.87	0.91
R^2	0.71	0.73	0.74	0.72	0.70
IA	0.86	0.86	0.85	0.84	0.82

Table 4.5 summarises the validation statistics for 2004. For the 85 days considered in 2004, the closest agreement was calculated using a stomatal resistance of 70 s m^{-1}, which resulted in a MAE of 0.64 mm (relative error of 24%), a R^2 of 0.73 and an IA of 0.86. Modelled ET obtained using an r_ref of 100 s m^{-1} performed worst of all cases considered. In contrast to 2000, the optimal r_ref value in 2004 (a wet year) was on the low end of the range tested. The total accumulated ET of 175 mm shown in Fig. 4.2c was markedly lower than the observed accumulated ET (225.4 mm). This is reflected by the mean negative bias of ~0.55 mm d^{-1}. Once again, the range of modelled ET did not vary significantly for increasing r_ref, however, the distribution of the modelled ET was different. Specifically, higher r_ref resulted in lower ET for the first half of the season, and lower r_ref resulted in higher ET for the second half of the growing season.

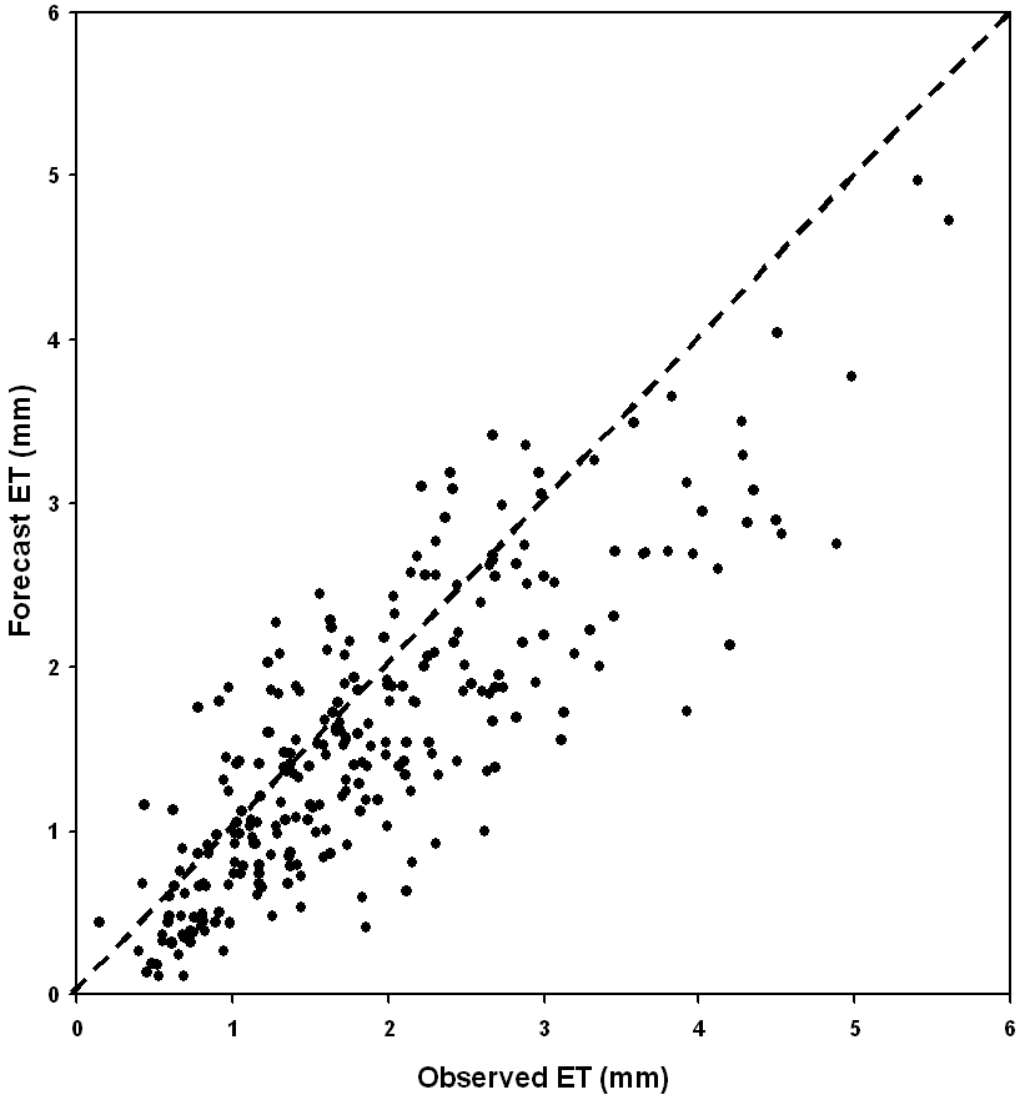

Figure 4.3: Scatter plot for forecast versus observed ET for Lethbridge for 260 days in 1999, 2000 and 2004. Dashed line represents a one-to-one relationship.

4.4.1.4 All data combined

Table 4.6 summarizes the validation statistics for all 260 days in the dataset. There was little to choose between the different model runs. The closest agreement between modelled and observed values was derived using a stomatal resistance of 70 and 80 s m^{-1}, which resulted in a MAE of 0.50 mm (relative error of 27%), a R^2 of 0.70 (Fig. 4.3) and

an IA of 0.88. Modelled ET derived using an r_ref of 100 s m^{-1} performed worst of all cases considered. The total accumulated ET of 403 mm was 16% lower than the observed accumulated ET (483 mm). This is reflected by the mean negative bias of approximately 0.30 mm d^{-1}.

Table 4.6: Validation statistics for modelled ET at Lethbridge for 260 days between 1 May and 31 August in 1999, 2000 and 2004. The abbreviations are defined in Table 4.3.

	r_ref = 60	r_ref = 70	r_ref = 80	r_ref = 90	r_ref = 100
ME	-0.32	-0.31	-0.31	-0.31	-0.32
MAE	0.53	0.51	0.50	0.51	0.53
RMSE	0.67	0.65	0.64	0.66	0.68
R^2	0.69	0.70	0.70	0.68	0.66
IA	0.89	0.89	0.88	0.87	0.86

4.4.2 WNC site

Fig. 4.4 shows the daily rainfall and modelled accumulated ET for the WNC site in 2005. For this growing season the accumulated precipitation exceeded the modelled ET by a significant amount, which would suggest that moisture stress was not an issue. However, July 2005 was a dry month with only 50% of the mean rainfall being recorded. Consequently, the modelled soil moisture data indicate that the relative plant available soil moisture in the root zone dropped below 50% between mid July and mid August which suggests that the plants were probably experiencing moderate moisture stress. Also evident from Fig. 4.4 is that daily ET in May was low, increasing in June, with the greatest increase in accumulated ET occurring during the first half of July, after which the rate of accumulated ET slowly decreased, and almost reached a plateau in late September. This plateau in September is to be expected because the crop would have

been harvested in late August. According to the biometeorological time, the maximum leaf fraction in the model was predicted to occur between 15 July and 22 July 2005, after which it declined steadily. By 7 September 2005, the leaf fraction was predicted to be only 0.6.

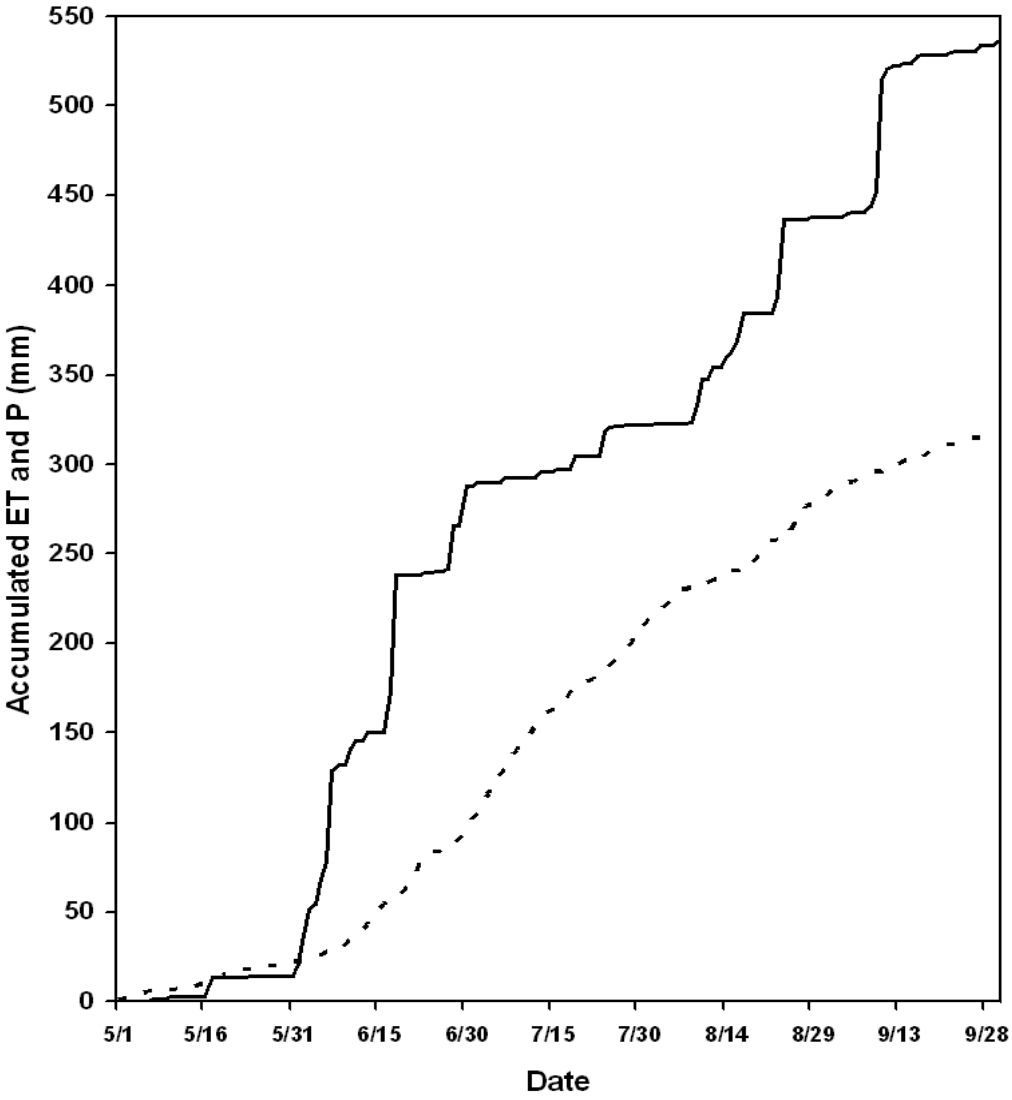

Figure 4.4: Accumulated precipitation (solid line) versus predicted accumulated ET (dashed line) by PAMII at WNC in 2005.

Table 4.7 contains the validation statistics for the simulated ET over the barley crop in 2005. For the range of minimum stomatal resistance values and initial soil moisture contents considered, there was a clear tendency for the model to underestimate the daily ET. Specifically mean errors ranged from -0.4 mm d^{-1} (r_ref = 40 s m^{-1}) to -1.3 mm d^{-1} (r_ref = 80 s m^{-1}). Although the lowest mean errors were obtained for a minimum stomatal resistance reference term of 40 s m^{-1}, the R^2 values associated with these modelled data were the lowest of all the model runs. The mean absolute errors and root-mean square errors were lowest for r_ref in mid-range. The model explained between 42% and 52% of the observed variance in ET, with R^2 values increasing for increasing values of r_ref. However, because of the small number of data points, one should not give too much weight to the R^2 values reported here. Overall, the best validation statistics were obtained for values of r_ref of 50 s m^{-1}.

Table 4.7: Validation statistics for predicted ET at WNC for 22 days between 1 July and 7 September 2005.

	r_ref = 40	**r_ref = 50**	**r_ref = 60**	**r_ref = 70**	**r_ref = 80**
ME	-0.40	-0.68	-0.91	-1.11	-1.29
MAE	1.08	0.98	1.04	1.16	1.30
RMSE	1.27	1.19	1.23	1.32	1.44
R^2	0.42	0.46	0.48	0.50	0.52
IA	0.65	0.66	0.64	0.60	0.56

Figure 4.5 shows the accumulated ET for the 22 days considered here. The curves of integrated ET start to diverge markedly after data point nine (i.e., from 27 July onwards). This also coincides with the marked dry-down period (relative PAW <40%), and suggests that the moisture stress term in the model may be too aggressive. Another factor in the model's underestimation of ET beyond 27 July could be that the modelled leaf fraction

was predicted to be declining steadily which would have also contributed to increasing canopy resistance, because the canopy resistance is inversely proportional to the leaf fraction. On the other hand, field observations made by Shen et al. (2002) found that the leaf resistance of wheat showed a clear seasonal trend, with higher values of stomatal resistance observed at the pre-jointing stage (leaves are not fully extended) and after the milking stage (most of the leaves have become senescent).

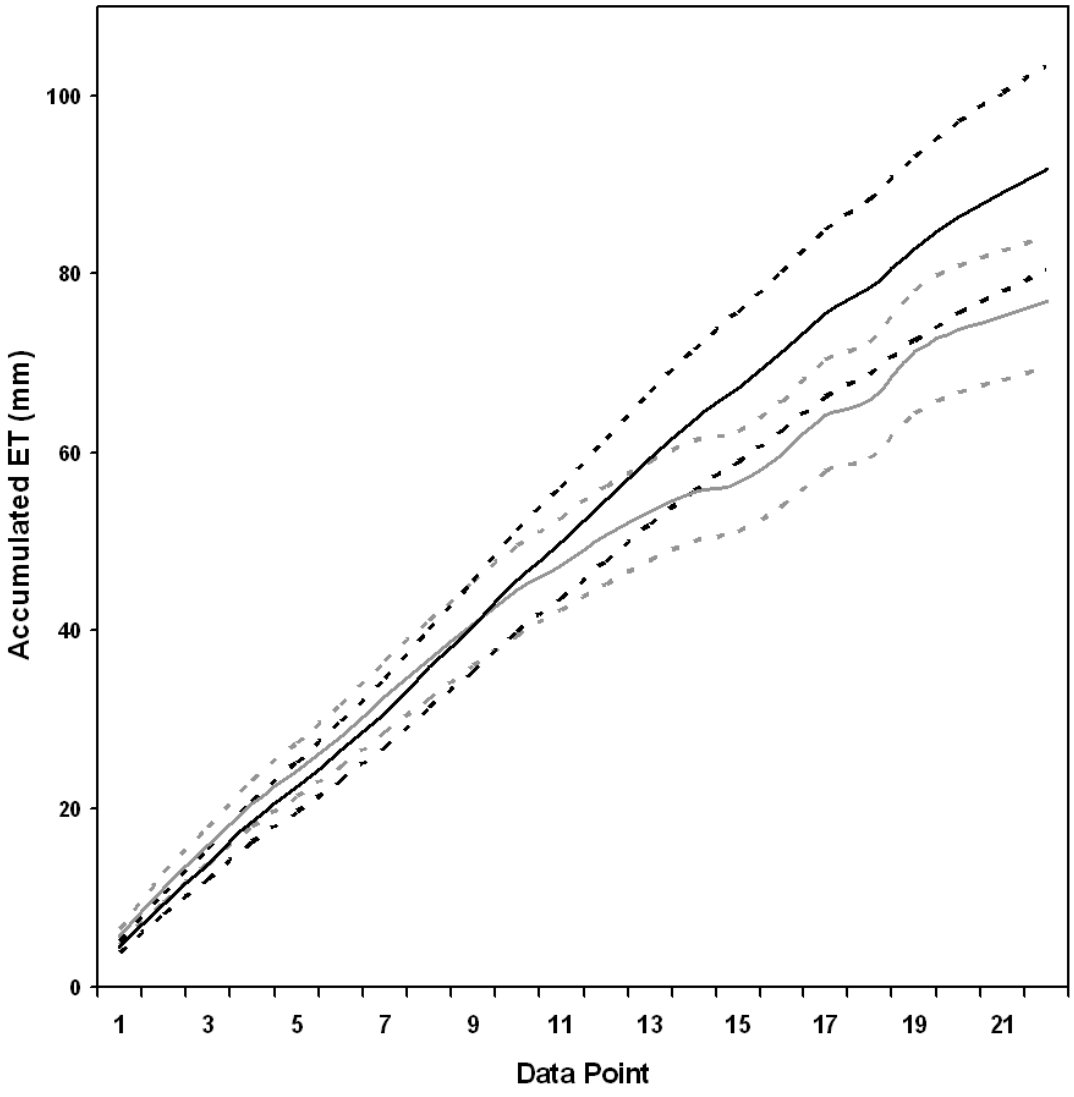

Figure 4.5: Same as Fig 4.2, except for WNC in 2005.

After allowing for uncertainty associated with the modelled and observed daily ET values, the lower bound of ET from EC data and the upper bound of accumulated ET predicted for the modelled data were comparable. The uncertainty (standard deviation) associated with the modelled ET (from all 15 runs) varied between 2 and 15 % of the means daily values, with a mean uncertainty of approximately 10%. Varying the initial PAW between 90% and 100% had virtually no impact on the modelled ET between 1 July and 7 September, with the only slight differences (<0.1 mm d^{-1}) being observed in the first 30 days of the simulation (i.e., May).

4.5 Discussion

Because so few days were available for analysis at the barley site, it is not feasible to try and determine the cause of the systematic negative bias there. Such an analysis was, however, possible for Lethbridge. Before discussing the negative bias in more detail, some background information on the use of minimum stomatal resistance in modelling transpiration is discussed.

4.5.1 Minimum stomatal resistance and transpiration

Stomatal resistance is a critical variable for the prediction of transpiration. Consequently, modelling stomatal resistance has been the focus of research for over 30 years. The response of plants' stomata to environmental and physiological factors is extremely complex and not completely understood (Vitale et al. 2007). It is, however, known that stomatal resistance varies with leaf irradiance, leaf temperature, atmospheric water vapour pressure deficit (VPD) and CO_2 concentration (e.g., Cowan 1977).

Many land-surface schemes used in operational numerical weather prediction (NWP)

models use a Jarvis-type (Jarvis 1976) multiplicative model to simulate stomatal resistance. A critical component of this empirical model is the minimum stomatal resistance (to be consistent with PAMII we will refer to this as r_ref). Körner (1994) defined r_ref as the seasonal minimum leaf resistance achieved in the field for unstressed, well-illuminated leaves which are fully developed but not senescent. In the Jarvis-type models, r_ref is increased in accordance with certain environmental stressors (which are assumed to be multiplicative), such as decreased solar irradiance, high VPD, soil moisture stress and thermal stress.

It has been shown by Niyogi and Raman (1997) and Niyogi et al. (1998) that when using a Jarvis-type canopy resistance scheme, r_ref is a key vegetation parameter in controlling the modelled latent heat fluxes, and thus a critical component of the surface energy budget. Additionally, correctly specifying the r_ref term is important, because errors in r_ref can affect surface hydrology and simulations of boundary layer processes (Alapaty et al. 1997; Cooter and Schwede 2000). Unfortunately, specifying the appropriate value of r_ref (even for a specific plant species) remains elusive. For example, Boone et al. (1999) and Niyogi et al. (1998) note that while most of the parameters critical to calculating surface fluxes (e.g., albedo, surface roughness length) in the interactions between soil-biosphere-atmosphere land surface (ISBA) scheme can be obtained from measurements to within a reasonable accuracy, the same does not apply to r_ref.

Consequently, while the Jarvis approach of calculating stomatal resistance generally works fairly well, it does require considerable calibration, especially of the r_ref term (e.g., Niyogi et al. 2009). In theory r_ref should be unique for a given plant species;

however, it has been shown to vary considerably in time and space in the field, even when measured using a porometer. For example, Wang et al. (2009a) noted that *"because of the complex structure of canopies, heterogeneity of leaf physiological features, and spatial variations in canopy microclimate, g [stomatal conductance] varies significantly among plant leaves, which makes it difficult to accurately derive the canopy values from the leaf-level measurements."* Additionally, Alfieri et al. (2008a) conclude that the variability in r_ref observed in their study arises because of the empirical nature of the Jarvis scheme, and the fact that the Jarvis scheme does not take into account plant physiology. Specifically, they note that the value of r_ref is affected by nutrient content, plant phenology et cetera — factors which are not typically considered in the definition of r_ref.

4.5.2 Possible causes for negative systematic bias of daytime ET at Lethbridge

A striking observation for the model validation at the grassland site is that no single value of r_ref worked for all years. This corroborates the findings of Armstrong et al. (2008) who noted that the most suited r_ref was specific to the schemes being used to calculate ET, and that the optimal value of r_ref is likely specific to the growth phase of the vegetation. Armstrong et al. suggest using approaches that allow for r_ref to vary through the season according to the phenological stage. Similarly, Alfieri et al. (2008a) noted site-to-site and temporal variability in r_ref and suggested incorporating a time-varying r_ref term that takes into account vegetation phenology. Additionally, Wever et al. (2002) found that the fitting coefficient used to calculate optimal r_ref for the Lethbridge grassland site differed significantly for the three years considered in their study (1998, 1999 and 2000). They concluded that in order to accurately reproduce the

surface resistance term for ET calculations one needs to use different coefficients for each year.

In order to try and separate out whether or not the systematic negative bias at the grassland site could be attributed to one or more environmental parameters, we grouped errors according to decreasing values (in classes) of wind speed, net radiation, minimum relative humidity and modelled PAW. Of these variables, only minimum relative humidity and PAW showed marked difference in the relative errors calculated for the observed upper and lower bounds of the variables in question. Specifically, for 40 days when RH_min was 40% or more there was a tendency for the model to underestimate the daily ET, with mean error of -0.7 mm d^{-1} (~37% of observed mean class ET of 1.95 mm d^{-1}). In contrast, for the 58 days when RH_min was 20% or less, then mean error was only +0.06 mm (4% of the observed mean class value of 1.48 mm d^{-1}).

There also appeared to be a connection between model performance and the plant-available moisture in the root zone. Specifically, when the modelled PAW was greater than 40% the modelled error was -0.7 mm d^{-1} (relative error of 21% compared to the mean class ET of 3.26 mm). In contrast when the PAW was less than 20%, then the mean error was -0.2 mm (14% of mean class ET of 1.27 mm). These data suggest that the stomatal resistance may be too high on occasions when the PAW is greater than 40%. Currently the canopy resistance term is inversely proportional to the root-zone relative PAW, so that when the PAW is 50% the reference canopy resistance is doubled.

There was also a tendency for PAMII to underestimate the ET on days following heavy rainfall events (i.e., when the previous day had 10 mm or more), or on days following overnight precipitation. Specifically, about 55% of days when model

significantly underestimated daytime ET (relative errors >25%) in 1999, 2000 and 2004 followed either a day with heavy rain, or followed overnight precipitation. Additionally, for the nine days when ET estimates were available following heavy precipitation, the relative errors of the modelled ET were strongly negative (-30 to -45% of the observed ET). Of the nine days considered, there was only one day when the predicted ET was slightly higher than the observed value. The tendency to underestimate ET following heavy rainfall events, or on days following overnight precipitation, could be attributed to the fact that PAMII does not allow for the re-evaporation of precipitation intercepted by the canopy, and perhaps because PAMII cuts off infiltration to the root-zone when the shallow top zone becomes saturated.

4.5.3 PAMII performance and improvements

Table 4.8 compares the performance of PAMII in this study with the performance of similar models around the world. The statistics in Table 4.8 clearly suggest that the skill of PAMII in simulating daily ET is comparable to a wide range of models of varying complexity. This is especially true for the grassland site. Typical root-mean-square errors scored by other models range between 0.4 and 1.2 mm d^{-1}, with R^2 values ranging between 0.63 and 0.89.

In view of the limitations of the empirical Jarvis model, researchers have developed a new generation of physiology-based models for the purpose of modelling transpiration based on leaf photosynthesis. The most popular examples are the Ball-Berry model (Ball et al. 1987), and a similar model of Leuning et al. (1995). These models have the advantage of allowing one to model ET according to different photosynthetic pathways, and they do not require the specification of r_ref. Rather stomatal resistance is directly

linked to plant physiology activities controlling photosynthesis. As a result, the physiological models require virtually no calibration.

Table 4.8: Summary of performance statistics calculated for different schemes used to predict daily ET over crops and grasslands.

Reference	Model	MAE	RMSE	R^2	Comments
This study	PAMII	0.88 (22.5%)	0.95 mm/day	0.67	Barley
	PAMII	0.50 (27%)	0.43 mm/day	0.70	Grassland
Jamieson et al. (1995	Six crop models	7.5-36%	-	-	Wheat
Armstrong et al. (2008)	Penman-Monteith	-	0.54 mm/day	0.66	C3 grasses
Arora (2003)	CLASS-Jarvis	-	0.6 mm/day	0.63	Wheat
	C-CLASS	-	0.4 mm/day	0.83	
Gustafsson et al. (2004)	TESSEL	-	0.50 mm/day	0.76	Crop
	COUP	-	0.55 mm/day	0.63	Crop
Wang et al. (2005)	BIOME-BGC	-	-	0.77-0.82	Corn and wheat
Seen et al. (1997)		-	0.83 mm/day	-	Grassland
Casanova and Judge (2008)	DSSAT	1.36 mm	1.04 mm/day	-	Corn
Su et al. (2005)	SEBS	0.53- 1.07 mm (11-26%)	0.69-1.21 mm/day	0.82-0.89	Corn and Soybean
Kothavala et al. (2005)			0.7-1.1 mm/day	0.76-0.78	Millet, wheat, maize and soybean

They do, however, require a suite of parameters that are typically not routinely available in current NWP models. That said, recently, several land surface schemes used in NWP models have been successfully modified to use a photosynthetically based method for calculating ET and other processes related to the canopy. Prominent

examples include GEM of Niyogi et al. (2009), EALCO by Wang et al. (2002) and C-CLASS by Kothavala et al. (2005). Regarding the present study, it is important to keep in mind that PAMII uses a simplified version of the Jarvis-type canopy resistance scheme, because the canopy resistance module does not account for the effects of photosynthetically active radiation (PAR), VPD and thermal stress on the canopy resistance. Because PAMII does not require radiation data, it cannot allow for the impact of PAR on stomatal resistance, but it can be modified to take into account the impacts of VPD and thermal stress. Consequently, we believe that future versions of PAMII would benefit from incorporating the following improvements:

1) Incorporate a more sophisticated canopy resistance module.
2) Use a logistic soil moisture stress function in the canopy resistance module.
3) Use different values of r_ref when calculating the morning and afternoon ET.
4) Do not force the root-zone soil moisture back to field capacity in one time step (one day), when the root-zone soil moisture exceeds the field capacity.
5) Allow the interception of precipitation by the canopy, and its re-evaporation.
6) Modify the infiltration scheme to be less restrictive following the saturation of the model's top zone after heavy precipitation.

4.6 Conclusion

Field crops (wheat, canola and barley) cover about 60% of the grassland eco-climate zone of the Canadian Prairies, with spring wheat alone accounting for about 50% of the cropped area (Hanesiak et al. 2009). Given the importance of evapotranspiration (ET) from crops and grasslands for convective processes and the overall water budget of the Canadian Prairies, a part of Canada that is far removed from oceanic moisture sources, it

is crucially important that we can accurately simulate the intra- and inter-seasonal variability in ET.

Here we examined the ability of the second generation prairie agrometeorological model (PAMII) to reproduce evapotranspiration above native grassland and a barley field over southern Alberta. In addition, at the grassland site, the model's performance was validated for contrasting growing seasons. The models' performance was validated against daily estimates of observed ET made using flux data from eddy covariance systems at each site. In an attempt to quantify the uncertainty of the modelled ET, 15 model runs were made by varying the initial root-zone soil moisture, and the reference minimal stomatal resistance term.

Validation statistics show that PAMII was skilful at simulating both the magnitude and evolution of ET over both the barley crop and native grassland. For the range of initial soil moisture and r_ref terms used in this study, the uncertainty of the daily ET estimates are typically less than ±10% of the modelled values. At the barley site, the model explained about 50% of the observed variance in ET for the 22 days considered here. PAMII displayed a systematic negative bias of between -0.7 mm d^{-1} and -1.3 mm d^{-1} (17%–24% relative error) over the cereal crop depending on the value used for r_ref. Mean absolute and RMSE errors were near 1.0 mm d^{-1}. The skill statistics apply only to a barley crop for the second half of the growing season. PAMII showed skill at modelling the day-to-day and inter-seasonal variability in ET at the grassland site. Specifically, the model explained 70% of the variance in observed ET. Mean absolute errors and mean RMSE errors were less than 1.0 mm d^{-1}. The systematic negative bias of approximately -0.30 mm d^{-1}over the grassland represents a relative mean error of 16%.

Based on optimization of the model runs for each site, new reference values for minimum stomatal resistance for grassland (rs_min = 80 s m^{-1}) and cereal crops (rs_min = 50 s m^{-1}) are proposed for PAMII. However, it is important to keep in mind that, as has been noted in several other studies, the r_ref term is site-specific and shows intra- and inter-annual variability. Detailed analysis of the error statistics suggests that improvements to the modelled ET might be attained by allowing for the interception of precipitation and its re-evaporation, by adjusting the infiltration scheme, by modifying the soil moisture stress function to be less aggressive when the plant available water is greater than 50%, and by using a more sophisticated canopy resistance module that takes into account the impacts of VPD and which uses a logistic type curve for modelling the response of the canopy resistance to soil moisture stress.

Several researchers have underscored the importance of changes in boundary-layer moisture as small as 1 g kg^{-1} on the potential and strength of any deep, moist convection that may develop (e.g., Crook 1996). Thus, if we are to gain insight into the linkages between soil moisture, ET and deep, moist convection, it is essential that both the temporal and spatial evolution of boundary layer moisture be predicted as accurately as possible (i.e., errors < 1 g kg^{-1}). In this paper we have shown that the mean absolute error in daily ET predicted by PAMII is <1 mm (equivalent to <1 g kg^{-1} for a 1-km deep boundary layer) at both the grassland and barley sites. Therefore, we suggest that PAMII is a suitable tool for further exploring the linkages between root-zone soil moisture, ET and convective storm activity. Future research will focus on examining these linkages in more detail.

CHAPTER 5

5. PAMII AS A DROUGHT-TRACKING TOOL

This chapter will appear in a Drought Research Initiative professional document edited by Stewart and Lawford (2011). The purpose of this chapter is to demonstrate the utility of PAMII as a drought tracking tool on the Canadian Prairies.

In the absence of a high spatial and temporal resolution soil moisture monitoring network on the Prairies, one has to rely on alternative methods for tracking soil moisture and evapotranspiration. One approach to address this issue is to use numerical land surface models driven using in-situ observations of precipitation and temperature. In previous chapters, Brimelow et al. (2010a,b) compared the performance of PAMII with the skill scores of similar models from around the world and determined that the skill of PAMII is comparable and even superior to a wide range of models of varying complexity when predicting soil moisture and ET. Thus, is has been demonstrated that PAMII can be used with confidence to track the evolution of root-zone soil moisture and evapotranspiration.

To demonstrate the utility of PAMII as a drought tracking tool, we generated maps of mean monthly root-zone plant available moisture (RZPAW) for the Canadian Prairies for each day during the growing season from 1999 to 2005. The model was run at stations across the Prairies for which observed precipitation data and temperature data

were available, in addition to daily soundings from the regional version of the Canadian GEM model (Côté et al. 1998).

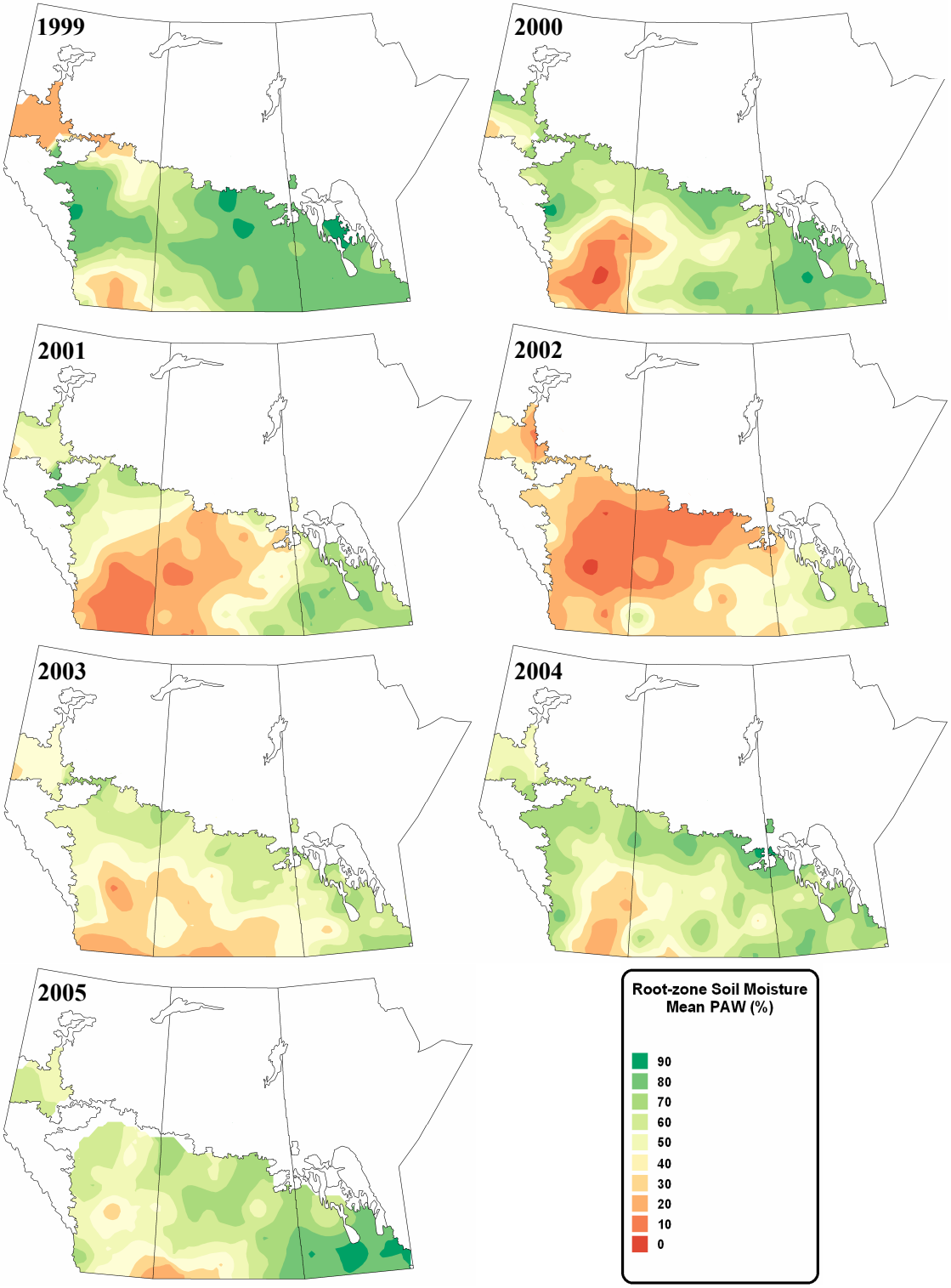

Figure 5.1: Mean modelled July root-zone relative plant available water content (RZPAW) from PAMII for 1999 through 2005.

Rainfall data were quality controlled to remove spurious or missing data points. The number of stations at which PAMII was run varied from year-to-year; the number of stations used varied between 85 and 115 depending on the year. The daily RZPAW data were used to generate monthly mean values, these data were then interpolated onto a uniform grid using a Kriging scheme and contoured (e.g., see Fig. 5.1).

Figure 5.1 shows the modelled mean relative root-zone plant available moisture content (RZPAW) for each July between 1999 and 2005. One can see the areas of drought (orange hues) emerging over southern Alberta in 2000. The drought region then expanded northward and eastward into Saskatchewan by July 2001. In July 2002, the area in agricultural drought covered most of Alberta and Saskatchewan, with the driest conditions observed over central Saskatchewan and central Alberta.

Conditions improved in central Alberta and Saskatchewan by July 2003, but southern Saskatchewan and southern Alberta were still experiencing relatively dry root-zone soil moisture conditions. By July 2004, the soil moisture situation improved over all areas, with the exception of southeastern Alberta. In July 2005, most areas on the Canadian Prairies were once again experiencing favourable root-zone soil moisture conditions.

A limitation of calculating the monthly mean RZPAW (Fig. 5.1) is that this metric does not explain how conditions depart from the long-term mean. In order to create anomaly maps, however, we must have a long-term database. Even then, such anomaly maps do not necessarily provide insight as to the cumulative impact of soil moisture stress on vegetation. Lab and field work has shown that incipient moisture stress for most plants begins when RZPAW approaches 50% (e.g., Shen et al. 2002).

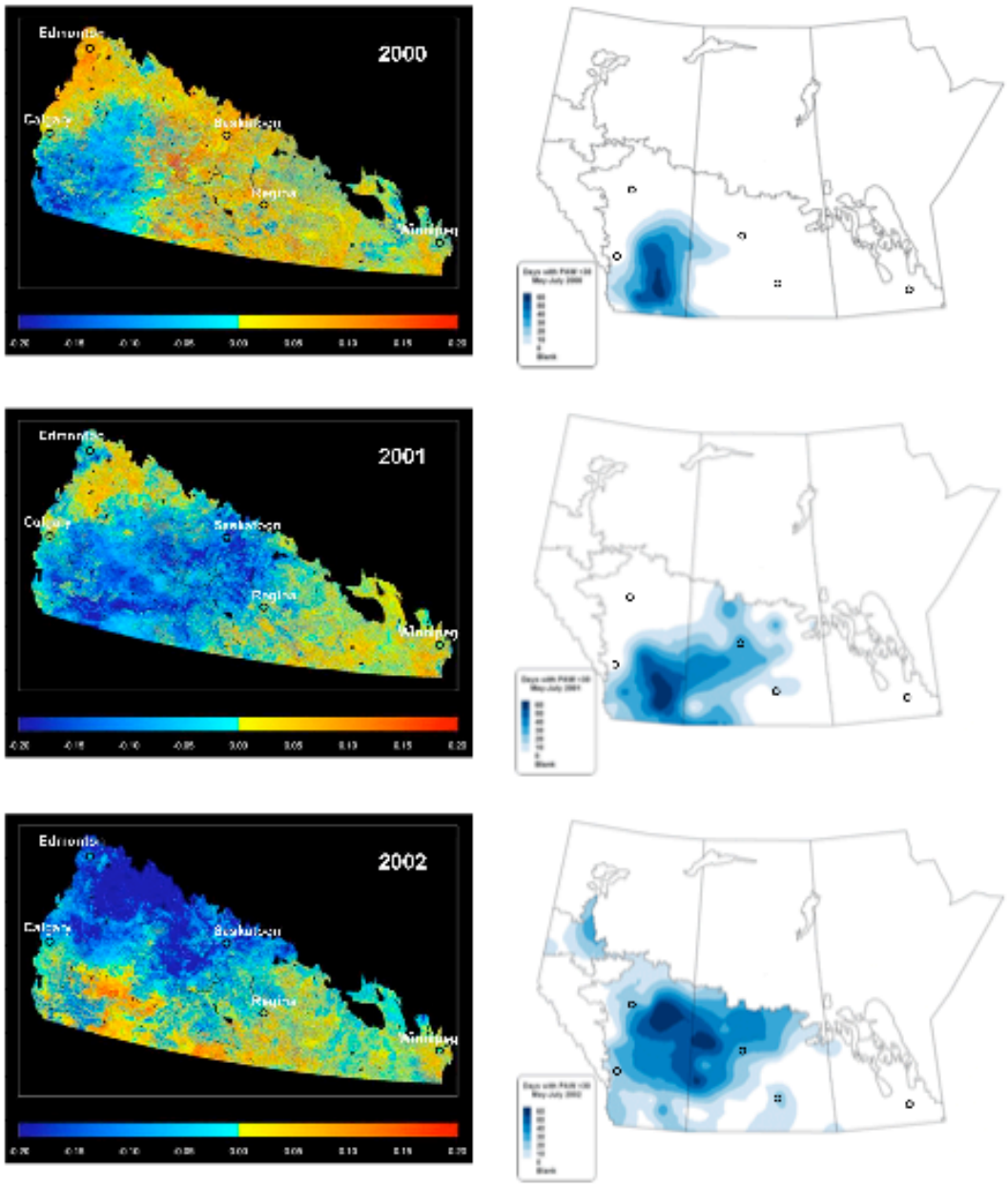

Figure 5.2. Left panel, NDVI anomaly maps for 11-20 July 2000, 2001 and 2002 (courtesy Luo et al. 2008), NDVI anomalies are with respect to the 2000–2008 means. Right panel, total number of days with RZPAW<30% calculated by PAMII between 1 May and 31 July for 2000, 2001 and 2002. Open circles represent locations of major urban centres.

Notable loss of photosynthetic activity (Vico and Porporato 2008), increases in abscisic acid levels (Schurr et al. 1992), and reduction in biomass growth (Mitchell et al. 2001) occur once the RZPAW declines below 30%. Thus, calculating the accumulated number of days during the growing season for which the RZPAW is <30% might be a useful metric for identifying the intensity and extent of agricultural drought.

Normalized Difference Vegetation Index (NDVI) maps are a useful diagnostic tool for tracking drought (e.g., Ji and Peters 2003) and for providing yield forecasts (e.g., Reichert and Caissy 2002). Figure 5.2 compares the NDVI anomalies (for July 11 to 20, 2001–2003) for the Canadian Prairies (Luo et al. 2008) with the (much lower resolution) maps of total number of days with RZPAW <30% between May 1 and July 31, 2000–2003. It is evident from Fig. 5.2 that those areas with a high frequency of severe moisture stress days correspond very closely with those areas shown by the NDVI anomaly maps which have much less dense (i.e., stressed) vegetation than normal.

One limitation of NDVI data is that it typically takes vegetation two to four weeks to respond to anomalies in soil moisture (Adgegoke and Carleton 2002). Thus, the advantage of calculating the accumulated number of days for which RZPAW is <30% is that attention is drawn to those areas in which vegetation is likely to experience significant moisture stress in the coming two to four weeks. Such maps, if made available in real-time, would be of much use for stakeholders and decision-makers as they prepare and make decisions in times of drought. Furthermore, they would complement the information on ET and soil moisture that could be provided by the PAMII model.

CHAPTER 6

6. ON THE SURFACE-CONVECTION FEEDBACK DURING DROUGHT PERIODS ON THE CANADIAN PRAIRIES

[3]**Abstract**

Linkages between the terrestrial ecosystem and precipitation play a critical role in regulating regional weather and climate. These linkages can manifest themselves as positive or negative feedback loops, which may either favour or inhibit the triggering and intensity of thunderstorms. While the Canadian Prairie terrestrial system has been identified as having the potential to exert a detectable influence on convective precipitation during the warm season, little work has been done in this area using in-situ observations.

We present findings from a novel study designed to explore linkages between the Normalized Difference Vegetation Index (NDVI) and lightning duration (DUR) from the Canadian lightning detection network for 38 Census Agriculture Regions (CARs) on the Canadian Prairies. Statistics Canada divides the Prairie agricultural zone into CARs (polygons of varying size and shape) for the purpose of calculating agricultural statistics. Here DUR is used as a proxy for thunderstorm activity. Statistical analyses were undertaken for 38 CARs for summers (JJA) between 1999 and 2008. Specifically, correlation coefficients were calculated between pairs of standardized anomalies of DUR

[3] This chapter is a copy of a paper by Brimelow et al. (2011) that appeared in the journal of Earth Interactions. Reproduced here with permission.

and NDVI by season and by month. Correlations were also made for CARs grouped by size and/or by magnitude of the NDVI anomalies.

The main findings are: (1) JJA lightning activity is overwhelmingly below average within larger dry areas (i.e., areas with below average NDVI); that is, the linkages between NDVI and DUR increased significantly as both the area and magnitude of the dry anomaly increased. (2) In contrast, CARs having above average NDVI did not consistently experience above average lightning activity, regardless of the CAR size; (3) The lower threshold for the length scale of the dry anomalies required to affect the boundary layer sufficiently to reduce lightning activity was found to be approximately 150 km (~18 000 km^2); (4) our analysis suggests that the surface-convection feedback appears to be a real phenomenon, in which drought tends to perpetuate drought with respect to convective storms and associated rainfall, within the limits found in (1) and (3).

6.1 Introduction

Modelling studies have suggested that changes in moisture and energy fluxes associated with soil moisture and vegetation anomalies can contribute to the persistence of wet or dry conditions long after the precipitation anomaly that created them has passed, thereby perpetuating soil moisture anomalies and drought (e.g., Dirmeyer 1994; Beljaars et al. 1996; Schubert et al. 2004).

The size and duration of anomalies of soil moisture in space and time are an important aspect in land-atmosphere interactions. At scales of a few kilometres, advection and turbulence mix out surface-induced variability in the convective boundary layer (CBL; Raupach and Finnigan 1995), so discontinuities must be long-lived and cover a sufficiently large area before they can begin to significantly influence the

evolution of the CBL (Avissar and Chen 1993; Lynn et al. 1995, 1998) and attendant thunderstorm activity. Oglesby et al. (2002) conducted modelling studies over the Mississippi basin and found that the magnitude of the soil moisture anomaly must be much larger than typical inter-annual variability in order for the anomalies to exert a strong influence on the atmosphere. Fennessy and Shukla (1999) used model simulations to investigate the impact of soil moisture on precipitation. They found that the strength of the terrestrial-atmosphere linkage was governed by the magnitude of the soil moisture anomaly, soil wetness persistence, solar forcing, accessibility to other moisture sources, and large-scale dynamics.

Several theoretical studies have used scaling techniques to identify length scales at which heterogeneities are capable of affecting the convective boundary layer (e.g., Raupach and Finnigan 1995; Mahrt 2000). Depending on conditions, the critical length scale can vary between 50 km and 130 km. Few observational studies have investigated links between the size of surface anomalies and convection. Taylor et al. (2003, 2005) studied the link between soil moisture variability (inferred from thermal infrared satellite data) and antecedent rainfall over the Sahel region in Africa. They noted that soil moisture variations on the order of several hundred kilometres could generate low-level circulations, which in turn modulated the presence of thunderstorm activity. Desai et al. (2006) found that CBL depth responded to 50–100 km scale variations in surface energy flux over the southern Great Plains of the US, with decreased influence of soil moisture on CBL depth at scales smaller than 100 km.

Vegetation is known to interact with the overlying atmosphere by influencing surface energy and hydrological budgets (e.g., Kaufmann et al. 2003; Siqueira et al. 2009). By

transporting moisture from the root zone to the CBL, vegetation is a primary pathway for coupling the surface and the atmosphere (e.g., Tsvetsinskaya et al. 2001). Consequently, changes in phenology can have a marked effect on the partitioning of incoming solar radiation (e.g., Liu et al. 2006; Notaro et al. 2006) and on modulating fluxes of mass and momentum (Dominguez and Kumar 2008). Thus, the coupling between the terrestrial surface and overlying atmosphere is strongest during the warm season (Koster et al. 2004; Seneviratne et al. 2006).

As noted by Siqueira et al. (2009), the linkages between soil moisture, vegetation and convection has received much attention (e.g., Koster and Suarez 2004; Kim and Wang 2007) but remains a vexing research problem. The strength of the land–atmosphere interaction is difficult to quantify, but modelling studies (Koster et al. 2004 2006) have identified certain terrestrial "hot spots" where linkages between the land surface and atmosphere are strong. The Great Plains of N. America, including southern portions of the Canadian Prairies, is one such "hot spot". Dirmeyer et al. (2009) conducted an integrated analysis for quantifying land-atmosphere interactions, which was not based on climate model output. Specifically, they used observations of precipitation, re-analysis data (NCEP-DOE) of atmospheric variables, and soil moisture from the Global Soil Wetness Project. Their work identified the Great Plains and southern Canadian Prairies as hot spots for feedbacks in JJA. Hanesiak et al. (2009) determined that knowledge of root-zone soil moisture at the beginning of summer can provide some indication as to the severity of the upcoming storm season on the Canadian Prairies. While the Canadian Prairie ecosystem has been identified as having the potential to exert

a detectable influence on convective precipitation in the summer, little work has been undertaken on this topic.

Linkages between the terrestrial surface and the atmosphere can result in positive or negative feedback loops, which may either favour or inhibit the triggering and intensity of deep, moist convection (e.g., Findell and Eltahir 2003a,b). The amount of moisture in the CBL has important consequences concerning the initiation and intensity of thunderstorms (Segal et al. 1995). Johns et al. (2000) concluded that evapotranspiration (ET) played a significant role in conditioning the pre-storm boundary layer structure for violent tornadoes over the north-central US. Raddatz and Cummine (2003) investigated whether there was a link between crop phenology on the Canadian Prairies and the seasonal pattern of tornadoes. They concluded that the timing of the peak number of tornado days was found to change in step with the time of the maximum specific humidity and maturation of wheat.

Thunderstorms form an important part of the Canadian Prairie hydrological cycle. Statistics from Environment Canada indicate that up to 50% of the annual precipitation on the Canadian Prairies falls during the summer months. Also, an analysis of sounding data from central Alberta by Reuter and Aktary (1995) found that 95% of the summer precipitation occurred on days when the potential for convective instability was present. The Canadian Prairies grassland eco-climate region covers an estimated 480 000 km^2. Annual field crops (wheat, canola and barley) cover about 60% of this area, with wheat accounting for about 50% of the cropped area (e.g., Hanesiak et al. 2009). Raddatz and Hanesiak (2008) investigated almost 1000 significant summertime rain events (≥10 mm in 24 h) on the Canadian Prairies between 2000 and 2004. They found that 79% of the

significant rain events were solely or partially convective (i.e., lightning was recorded by the Canadian Lightning Detection Network at some time during the accumulation period), while lightning was not recorded for the remaining 21%.

Most studies investigating linkages or feedbacks between the land surface, atmosphere and precipitation have had to rely on modelled data. This is because precipitation and soil moisture are typically not adequately resolved at the spatial and temporal scales of summertime precipitation events. One dataset which has received virtually no attention in terms of elucidating land-atmosphere influences on convection is lightning flash data. These data are available at a higher spatial and temporal resolution than are the processes driving convection. Further, by combining lightning flash data with high spatial resolution (and real-time) estimates of Normalized Difference Vegetation Index (NDVI), one could, for the first time, explore land-atmosphere linkages without having to rely on output data form numerical models.

In this paper, the focus is on how land-atmosphere processes over the Canadian Prairies can condition the CBL so as to inhibit or facilitate thunderstorm activity. Specifically, we address the following questions: 1) Is there a link between NDVI and lightning activity on the Canadian Prairies?; 2) What are the required thresholds in terms of both the size and magnitude of the NDVI anomaly to affect lightning activity?; and 3) What is the relationship between NDVI and plant-available root-zone soil moisture in association with (1) and (2)?

To address (1) and (2) we use lightning flash data and NDVI data for a 10-year period spanning 1999–2008 for 38 Census Agricultural Regions (CARs) on the Canadian Prairies (Fig. 6.1). Between 2000 and 2003, the Canadian Prairie region experienced one

of the most severe droughts on record (e.g., Liu et al. 2004). The 1999–2008 period provides a unique opportunity to explore linkages between terrestrial land surface and thunderstorm activity during drought, normal and pluvial conditions. Question (3) is addressed using in-situ root-zone plant-available moisture observations in Alberta and simulated root-zone soil moisture together with NDVI data.

6.2. Data and methodology

6.2.1 Census agriculture regions (CARs)

Statistics Canada divides the agricultural zone on the Canadian Prairies into 43 CARs for the purpose of disseminating agricultural statistics. The CARs are random polygons with areas ranging between 5 000 km^2 (equivalent radius of ~40 km) to over 30 000 km^2 (equivalent radius of ~100 km). In this study, 38 CARs for which reliable NDVI data were available were used —some CARs spanning the Red River Valley in Manitoba were excluded because of frequent flooding that contaminated the NDVI data. Of the 38 CARs considered, 11 were located in Alberta, 20 in Saskatchewan and 7 in Manitoba, see Fig. 6.1.

6.2.2 Cloud-to-ground lightning data

The Canadian Lightning Detection Network (CLDN) continuously records all lightning with peak current greater than 5 kA (3 kA after 2005) detected in North America north of 35°N east of 100°W and north of 40°N west of 100°W (Burrows et al. 2002). We used only cloud-to-ground (CG) lightning flashes in the present study. Detection efficiency of CG flashes for the CLDN over the Prairie agricultural zone is >90%, while the median stroke location accuracy is 500 m or better (Cummins et al. 1999).

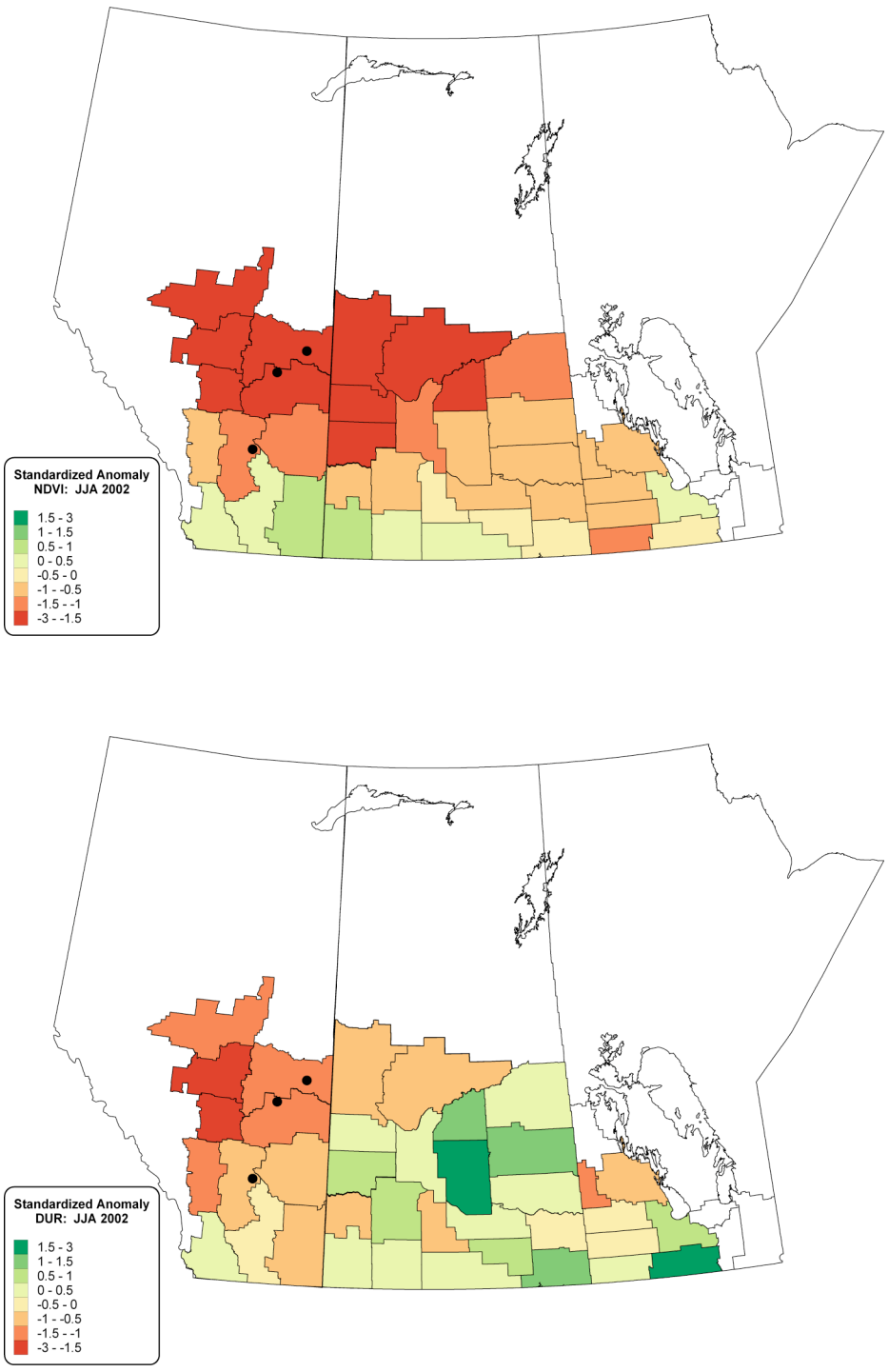

Figure 6.1: Standardized anomalies in of NDVI (top) and DUR (bottom) for JJA 2002. Irregular polygons represent the 38 Census Agricultural Regions (CARs) considered here. Black dots represent the locations of the three DroughtNet sites discussed in section 6.2.4.

To quantify the thunderstorm activity we used the lightning duration (DUR) within each CAR. The lightning duration is defined as the length of time (in hours) between 9:30 local solar time and 19:30 local solar time where flashes occurred "continuously". That is, no more than 10 minutes was allowed to separate a flash and the next flash in a given series of flashes. If more than 10 minute separated two flashes, then the time series was discontinued and a new time series was started when the next flash was recorded. Isolated or "singleton" flashes that occurred more than 10 minutes between different series were allocated a duration of one minute. We used the 09:30 – 19:30 window to avoid issues with time zones, and to focus on surface-based thunderstorms (rooted in the convective boundary layer) which typically develop in response to daytime heating, rather than nocturnal thunderstorms which tend to be elevated. The lightning duration does not consider the location of the flashes, only when they occurred. The length of the series for each solar day in each CAR were summed to calculate monthly and seasonal totals. These data were used to calculate standardized anomalies (see equation 1 in section 6.2.5).

Another metric that was considered for the purpose of quantifying the overall level of lightning activity was lightning flash density (LFD). However, LFD can be skewed by a few storms having a high flash rate over an area. Some preliminary statistics indicated that correlations between DUR and NDVI were higher than between LFD and NDVI. Consequently, in this study, we will focussed on the lightning duration.

6.2.3 Normalized Difference Vegetation Index (NDVI)

Weekly NDVI data valid for each CAR during the growing season were downloaded from the Canadian Crop Condition Assessment Program (CCAP) site

(www.26statcan.ca/ccap), which is operated by Statistics Canada. A land use mask is applied, in which a pixel is classified as crop/pasture if at least 50% of that pixel is crop/pasture. Here, NDVI data for only those pixels classified as crops or pasture are included in the calculation of NDVI for each CAR. However, it is possible that pixels which are classified as crop/pasture, but which may have 40% forest cover. Sensitivity tests (not shown) indicate that applying the mask is expected to have very little impact on the results, probably because most of the CARs are dominated by crops and/or pasture.

Statistics Canada uses data from National Oceanic and Atmospheric Administration satellites carrying the Advanced Very High Resolution Radiometer (AVHRR). A composite of AVHRR images covering a seven-day period removes most or all cloud effects (Reichiert and Caissy 2002). To further minimize errors that may have been introduced by clouds, a constant threshold cloud mask based on the channel 1 composite is generated (Reichiert and Caissy 2002). The cloud mask is applied to the NDVI composite, thereby ensuring that only cloud-free pixels are included when computing the NDVI statistics (Reichiert and Caissy 2002). Because the NDVI data used by CCAP is required to be available near real-time, full post processing of the data is not undertaken. However, corrections are made to remove much of the atmospheric contamination, and to minimize other effects (such as view angle and solar angle). We used the NDVI data as is from the CCAP web site.

6.2.4 Root-zone soil moisture

We also explore the relationship between the root-zone relative plant available water content (RZPAW) and the NDVI. Two sources of RZPAW are used: 1) in-situ measurements from the Alberta Drought Monitoring Network (DroughtNet) (Fig. 6.1),

and 2) modelled root-zone soil moisture from the Second Generation Prairie Agrometeorological Model (PAMII; Raddatz 1993). The drought monitoring network has been established over cropped land throughout Alberta starting in 2002. Hourly measurements of volumetric soil moisture content (θ; in %) are made using calibrated ThetaProbe^{TM} sensors (type ML2X). Measurements at DroughtNet sites are made every hour at four depths (5 cm, 20 cm, 50 cm and 100 cm). Details concerning the DroughtNet sites and the PAMII model can be found in Brimelow et al. (2010a). Data for the DroughtNet sites were provided by Alberta's Department of Agriculture and Rural Development (pers. comm. Ralph Wright).

For the purpose of comparing in-situ soil moisture measurements at the DroughtNet sites with the concomitant NDVI, we used NDVI data provided by CCAP at the township scale. That is, NDVI data are aggregated into 10 km by 10 km squares. NDVI data for the township in which each DroughtNet site is located were then used to calculate weekly-standardized NDVI anomalies. The three sites were Vermilion (53.34º N; 110.88º W, 620 m), Killam (52.85º N; 111.87º W, 692 m) and Hussar (51.19º N; 112.50º W, 971 m). The same approach used by Brimelow et al. (2010a) was used to determine the permanent wilting point (PWP; θ_{pwp}) and field capacity (FC; θ_{fc}) at each site. Specifically, the PWP was estimated by selecting the mean lowest daily mean θ observed at a 20-cm depth between 15 May and 30 September for the entire record; this typically spanned a seven-year period. The FC was approximated by identifying the mean θ at 20 cm, 72 hrs following the time of maximum soil moisture content associated with a heavy precipitation event (> 10 mm).

To determine whether or not the plants' moisture requirements are being adequately

satisfied, it is convenient to quantify the moisture in the root zone in terms of the relative plant available water capacity (e.g., Anderson et al. 2000). The relative plant available water content (or PAW) is equal to $[(\theta - \theta_{pwp})/(\theta_{fc} - \theta_{pwp})]$. RZPAW was calculated by using hourly θ data at each level were used to calculate daily means, which were then used to calculate the daily root-zone soil moisture content between the surface and 100 cm. The equivalent soil moisture contents (in mm) for all the layers in the root zone were then integrated to obtain a bulk soil moisture amount and the RZPAW was calculated using the water retention properties determined for each site.

Given that a Prairie-wide soil moisture monitoring network is not in place, it is necessary to use model data to investigate the relationship between RZPAW and NDVI over several years and over a large area. PAMII was used to simulate the evolution of the root-zone soil moisture content and RZPAW during July and August for 1999—2005 for each CAR. The model was driven using *observed* rainfall, minimum and maximum temperatures from each site, and prognostic profiles of temperature, moisture and winds from the regional version of the Canadian Global Environmental Multiscale (GEM; Côté et al. 1998) model. The surface dew-point depression from the GEM model was used to calculate the near-surface vapour density required for the calculation of transpiration from the canopy. Daily RZPAW data were aggregated into monthly means for July and August. This period was selected because it is when the modelled root-zone extends to near 100 cm, and also includes the time when the crops are maturing and sensitive to water deficits (Mkhabela et al. 2010).

6.2.5 Calculation of standardized anomalies and correlations

All monthly and seasonal NDVI and DUR data were standardized using the methodology employed by Koster and Suarez (2004). Specifically, the monthly (June, July and August) and seasonal (June through August) standardized anomalies were calculated as follows,

$$\Delta X_j = \frac{X_j - \overline{X_j}}{\sigma_j} \qquad (5.1)$$

where X_j is the value of NDVI (or DUR) for a given month j (or a particular summer [JJA]), $\overline{X_j}$ is the mean value of X over the 10 years, and sigma is the standard deviation for month j over the 10 years.

The weekly NDVI data were used to calculate the monthly and seasonal means. The start and end dates for the season and monthly data varied slightly from year to year, with start dates ranging between 3 and 9 June, and end dates between 1 and 7 September. However, this factor was not expected to significantly affect the seasonal NDVI anomalies, because there was typically very little change in NDVI values during these times.

The association between NDVI and DUR was quantified using the coefficient of determination (R^2) between pairs of standardized anomalies of lightning duration (ΔDUR) and NDVI (ΔNDVI) for individual months and also by season (JJA) for a 10-yr period spanning 1999 through 2008. The statistical significance of the correlations was quantified using p-values of 1% ($\alpha = 0.01$) and 5% ($\alpha = 0.05$). A maximum sample size of 380 pairs (38 CARs x 10 years) was available for analysis. Here a CAR season refers to one JJA period for one CAR. Correlation analysis was also undertaken using classes of

CARs ranked by size. It is important to keep in mind that the R^2 values do not speak to causality between ΔNDVI and ΔDUR.

6.3. Linkages between NDVI and DUR

In this section we focus on how the areal extent of the NDVI anomaly, as well as the magnitude of the NDVI anomaly, are related to JJA lightning duration on the Canadian Prairies. Before doing so, we will investigate the relationship between RZPAW and NDVI.

6.3.1 Relationship between RZPAW and NDVI anomalies

The relationship between RZPAW and NDVI anomalies was investigated using two independent data sets consisting of in-situ soil moisture observations and simulated soil moisture from the PAMII model.

6.3.1.1 Observed RZPAW and NDVI

Weekly mean RZPAW values were calculated for 2003 using in-situ soil moisture measurements for three DroughtNet sites in Alberta. The 2003 growing season was selected because it was a season in which two of the three DroughtNet sites with reliable data experienced a significant dry down which resulted in stressed vegetation (as shown by NDVI data). Standardized NDVI anomalies were calculated for the township in which each of the three DroughtNet Sites are located for each week from early June through the end of August, using a baseline period of 1999–2008. Daily measurements of RZPAW from in-situ observations were amalgamated into weekly means; the dates used to calculate the mean weekly RZPAW were those that coincided with the weekly observations for which NDVI data were available.

To investigate the response of NDVI to changes in 0-100 cm RZPAW, box plots were generated for several classes of RZPAW. For example, RZPAW < 40%, RZPAW between 40% and 60%, and RZPAW > 60%; RZPAW < 50%, RZPAW between 50% and 70%, and RZPAW > 70%, and RZPAW < 35%, RZPAW between 35% and 55%, RZPAW >55%. Here we only show the data for those RZPAW classes that showed the greatest degree of separation in the ΔNDVI data. Figure 6.2 shows that there was a clear response of ΔNDVI to RZPAW at the three DroughtNet sites in the summer of 2003, with NDVI declining systematically as RZPAW decreased. Two-sample student-t tests found that the mean ΔNDVI observed for RZPAW less than 35% and the mean ΔNDVI observed for RZPAW between 35% and 55% were statistically different at the 95% confidence level. Similarly, the mean ΔNDVI observed for RZPAW greater than 55% and the mean ΔNDVI observed for RZPAW between 35% and 55% were statistically different at the 95% confidence level.

The inter-quartile range for the ΔNDVI values observed for RZPAW less than 35% (N = 8) was between -1.37 and -0.47 (median of -0.77), with the 95% confidence level for the mean between -1.27 and -0.50. That is, when RZPAW was less than 35%, ΔNDVI values were typically below -0.5 (i.e., the vegetation was stressed and less dense than normal). Apart from two outliers (both from Vermilion), the ΔNDVI data for the intermediate range of RZPAW between 35% and 55% (N = 17) were fairly tightly clustered. The inter-quartile range for these data was between -0.42 and +0.08 (median of -0.13), with the 95% confidence level for the mean between -0.57 and +0.05. That is, this range of RZPAW seemed to be associated with incipient moisture stress.

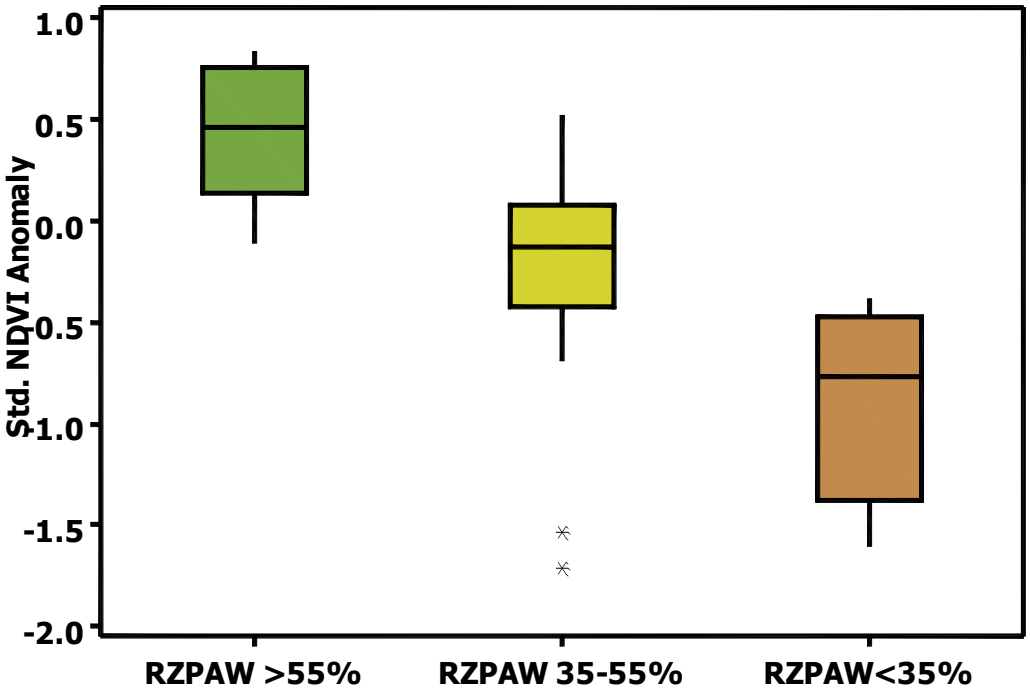

Figure 6.2: Box plot of weekly ΔNDVI (standardized NDVI anomaly) for three classes of 0–100 cm mean weekly root-zone soil moisture (RZPAW) observed between 1 June and 31 August 2003. NDVI data are for the township in which each of the three DroughtNet sites are located. See section 6.3.1.1 for more details. The shaded are represents the inter-quartile range, while the horizontal line in the shaded area represents the median. Asterisks represent outliers, and whiskers represent the highest data value within the upper limit (Q3 + 1.5(Q3-Q1)), where Q1 and Q3 represent the lower and upper quartile values, respectively.

For RZPAW greater than 55% (N = 14) the ΔNDVI values were almost exclusively positive, with an inter-quartile range between +0.14 and +0.75 (median of +0.45), and with the 95% confidence level for the mean between +0.27 and +0.63. Thus, for RZPAW greater than 55%, vegetation was typically at near normal to above-normal density.

Lagged correlations were calculated between the weekly observed RZPAW and ΔNDVI data for lags from 0–4 weeks and for 0–100 cm and 0–50 cm RZPAW. Here, only results for 0–100 cm are discussed, as RZPAW in this layer had higher correlations than did the 0–50 cm layer. The data in Fig. 6.3 suggest that, for all the sites, the R^2 between ΔNDVI and RZPAW increased when ΔNDVI lagged RZPAW by one to two weeks. Between 50% and 90% of the variance in NDVI could be explained by RZPAW depending on the time lags were used.

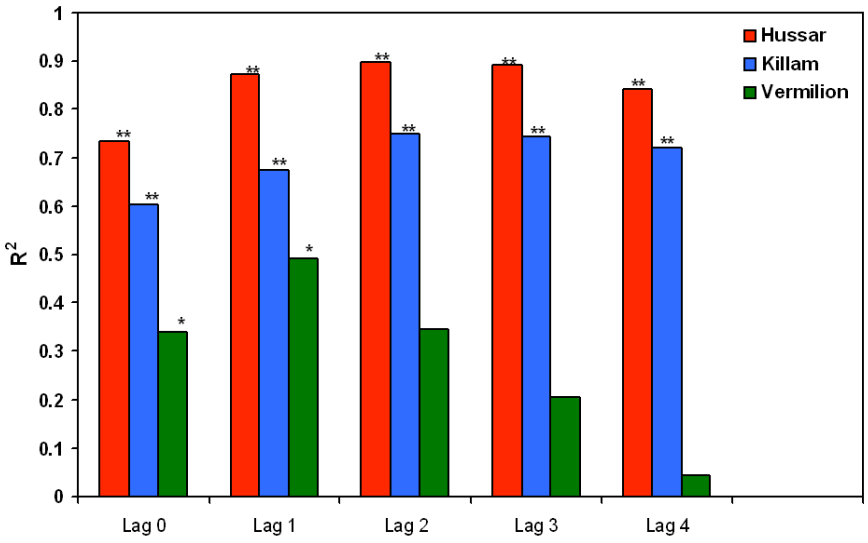

Figure 6.3: R^2 for weekly observed 0-100 cm root-zone plant-available moisture content (RZPAW) versus weekly standardized NDVI anomalies (ΔNDVI) between 1 June and 31 August 2003 for three sites in Alberta. NDVI data were calculated for the township (10 by 10 km square) in which the DroughtNet sites are located. Bars with single asterisk have coefficients of determination which are statistically significant at the 95% level of confidence, while those with two asterisks are statistically significant at the 99% level of confidence.

A caveat concerning the increase in R^2 when calculating lagged correlations — on account of the small sample sizes the increases in R^2 were not found to be statistically

significant after applying a Fisher Z-transform to the correlation coefficients ($r = [R^2]^{0.5}$). The R^2 values reported here are much higher than those found in the literature between RZPAW and NDVI (e.g., Adegoke and Carleton 2002; Wang et al. 2007). A likely reason for the higher R^2 values at Hussar and Killam is possibly because autocorrelation tests showed a statistically significant autocorrelation at a lag of one week in both the RZPAW and NDVI data. At Vermilion there was an autocorrelation for a one-week lag in the NDVI data. Thus the autocorrelation evident in our data is probably attributable to the fact that we are dealing with only one summer's data and when a sustained dry-down period was observed. Had data been used for multiple seasons having more variable conditions then we expect that the R^2 values would be more in line with values from similar studies.

6.3.1.2 Simulated RZPAW and NDVI

The soil moisture data in section 6.3.1.1 are only valid for one season and for three sites, and one could argue that they may not be representative of the Prairies. To address this, we used the PAMII model (run for sites located within the CARs) to quantify the variation of root-zone soil moisture over CARs between 1999 and 2005. PAMII has been shown to reasonably simulate root-zone soil moisture over the cropped grassland of the Prairies. Specifically, Brimelow et al. (2010a) validated the PAMII model against in-situ soil moisture data from DroughtNet sites, and showed that the modelled RZPAW values were typically within 10% of the observations.

The mean monthly RZPAW values for stations located all but three CARs (over far southern Alberta) were calculated. Soil moisture values for CARs over far southern Alberta were not included because RZPAW routinely drops below 30% in July and

August at those sites, and we wished to focus on the response of NDVI to RZPAW in those CARs that typically did not experience very low RZPAW (i.e., < 30%). Depending on the year, simulated RZPAW data were available for between 85 and 115 sites across the Canadian Prairies. To increase the likelihood that point values of RZPAW from PAMII were representative of conditions over large CARs, we only considered those Julys and Augusts that had uniform NDVI anomalies across the CARs (see section 6.3.3). Some CARs had up to four sites with simulated RZPAW, but had drastically different RZPAW because of localized effects. If the simulated mean monthly RZPAW differed by more than 20% between sites, then those data were not included in the analysis. Daily simulated RZPAW data from all sites present in a CAR were then aggregated and then used to calculate the monthly mean RZPAW for July and August, respectively.

The inter-quartile range of ΔNDVI for those CARs experiencing uniformly above-average NDVI in July and August (N = 68) was between +0.9 and +1.4 (median +1.1), with only one of the 68 CARs having a mean ΔNDVI < +0.5 (i.e., +0.44). The inter-quartile range for those CARs experiencing uniformly below-average NDVI (N = 48) was between -1.0 and -1.9 (median -1.5), with only one of the 68 CARs having a mean ΔNDVI > -0.5 (i.e., -0.41).

Figure 6.4 shows the modelled RZPAW for CARs having contrasting vegetation health. The inter-quartile range for the RZPAW values observed in CARs experiencing below-average NDVI (N = 48) was between 19.8% and 37.0% (median of 26%), with the 95% confidence level for the mean between 25.3% and 32.5%. That is, when ΔNDVI < -0.5, RZPAW values were typically below 40%. In contrast, the inter-quartile range for the RZPAW values observed for CARs experiencing uniform above-average NDVI (N =

68) was between 57.7% and 77.9% (median of 65%), with the 95% confidence level for the mean between 62.5% and 69.7%. That is, when ΔNDVI >+0.5, RZPAW values were typically above 55%. The mean simulated RZPAW for CARs experiencing below-average NDVI in July and August and the mean RZPAW modelled for CARs experiencing above-average NDVI were statistically different at the 99% level.

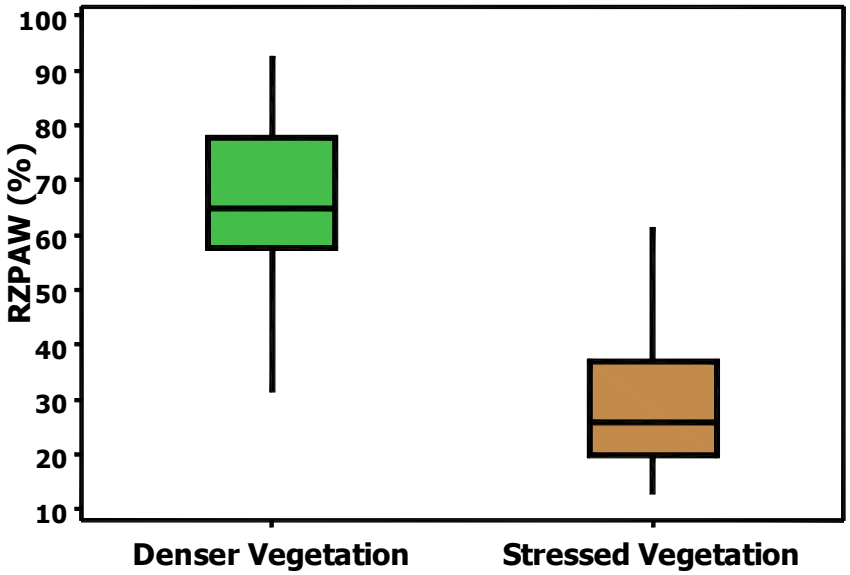

Figure 6.4: Box plot for modelled mean monthly root-zone RZPAW and concomitant ΔNDVI for those CARs experiencing uniformly above-average NDVI for all Julys and Augusts between 1999 and 2008. Here "denser vegetation" refers to ΔNDVI values greater than +0.5, and "stressed vegetation" to ΔNDVI values greater less than -0.5.

These results are consistent with those from the comparison between ΔNDVI and 0-100 cm RZPAW at the three Droughtnet sites. With both datasets suggesting that stressed vegetation (ΔNDVI < -0.5) is typically associated with RZPAW < 40%, while denser than average vegetation (ΔNDVI > +0.5) is typically associated with RZPAW > 55%.

6.3.2 Effect of CAR size

The effect of CAR size on the association between ΔNDVI and ΔDUR was investigated by dividing the CARs into quartiles, and then calculating R^2 between seasonal ΔNDVI and ΔDUR for each quartile. CARs having both positive and negative summer ΔNDVI were considered. Results are displayed in Table 6.1.

For all CARs, the R^2 for JJA between 1999 and 2008 is 5.6% (p-value =0.000). When one ranks the CARs by size, however, a systematic increase in R^2 with increasing CAR size becomes evident. Specifically, R^2 increases from only 0.025 (p-value = 0.135) for the lowest quartile class, to almost 0.13 (p-value = 0.001) for the top quartile class. Table 6.1 shows that R^2 becomes statistically significant at the 99% level of confidence when the class average equivalent radii approach 80 km, with the highest correlations obtained for those classes having mean equivalent radii greater than about 80 km. These data suggest that the size of the CAR is important in governing the strength of the relationship between NDVI and DUR, and that if the area is too small (equivalent radius less than about 75 km) the relationship breaks down.

6.3.3 Effect of both CAR size and magnitude of the NDVI anomaly

In the previous section, all CARs, regardless of the magnitude of ΔNDVI, were included in the analysis. We purport that the relationship between NDVI and DUR should increase as the magnitude of ΔNDVI increases. To this end, we calculated correlation statistics for CAR seasons grouped according to the magnitude of ΔNDVI for all CARs (regardless of size), for subsets of CARs having an equivalent radius in the top 50%, or lower 50%, and finally for those CARs having an equivalent radius of at least 75 km. The results are summarized in Fig. 6.5.

Table 6.1: Coefficient of determination between ΔNDVI and ΔDUR for JJA between 1999 and 2008 for various classes of CARs. L25= lower quartile (lower 25%) of CARs ranked by area; IQ1 = lower inter-quartile range (25–50%); IQ2 = upper inter-quartile range (50–75%), T25 = upper quartile (top 25%) of CARs ranked by area; T50 = Top 50% of CARs ranked by area; B50 = Bottom 50% of CARs ranked by area; R_eq represents the mean equivalent radius of each class. Req_75 represents those CARs having equivalent radii of at least 75 km. Sample sizes are shown in parentheses.

	All (N =380)	**L25 (N =90)**	**IQ1 (N =100)**	**IQ2 (N=100)**	**T25 (N= 90)**	**T50 (N =190)**	**B50 (N = 190)**	**Req_75 (N = 120)**
R^2	0.056**	0.025	0.014	0.098	0.129**	0.112**	0.019	0.112**
R_eq (km)	69.5	53.8	63.1	72.7	88.6	79.7	58.7	85.6

** Coefficient of determination significant at the 99% level of confidence

* Coefficient of determination significant at the 95% level of confidence

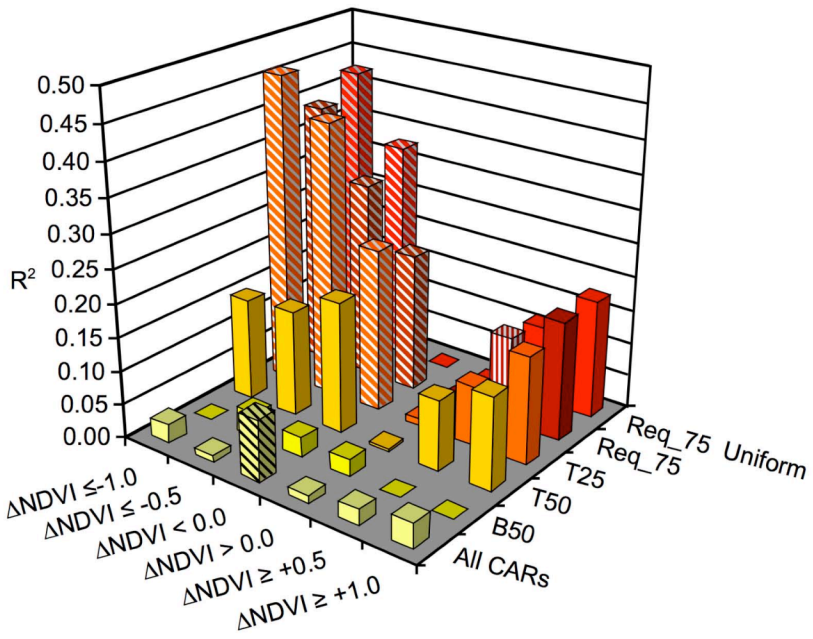

Figure 6.5: Coefficient of determination between ΔNDVI and ΔDUR for JJA between 1999 and 2008 for various classes of ΔNDVI and CAR area. CAR size classes (B50, T50 etc.) have the same meaning as in Table 6.1; "Req_75 Uniform" refers to those CARs having equivalent radii of at least 75 km and uniform standardized NDVI anomalies in space and time (see section 6.3.4 for details). Bars with diagonal hatching have coefficients of determination which are statistically significant at the 99% level of confidence, while those vertical hatching are statistically significant at the 95% level of confidence.

The thresholds for NDVI anomalies were based on observations from the literature and on the nature of the data, and to ensure that the sample sizes were of sufficient number as to calculate reliable statistics. Philippon et al. (2007) defined areas experiencing low (high) photosynthetic activity as those regions where the standardized NDVI anomalies were -0.5 (+0.5). Similarly, we use thresholds of 0, ±0.5 and ±1.0 for the standardized NDVI anomalies.

Figure 6.5 clearly shows that both the size of the CAR class as well as the magnitude of the anomaly have important implications for the association between NDVI and DUR. Specifically, the values of R^2 and their statistical significance rise with increasing mean class radius and also as the magnitude of ΔNDVI increases. The highest correlations (statistically significant at the 99% level of confidence) are only observed for those CARs having both *large* equivalent radii (top quartile and Req_75 km classes) and *significant negative* ΔNDVI (< -0.5). In contrast, even large CAR classes having significant positive ΔNDVI have much lower R^2 values than do those classes having negative ΔNDVI, and are only statistically significant (95% confidence level) for anomalies > +0.5 for the Req_75 class.

The marked increase in R^2 evident for large CAR classes having significant negative ΔNDVI (i.e., severely stressed vegetation) suggests that a positive feedback mechanism may be operating over the course of the boreal summer over drought-affected regions, with drought conditions leading to less lightning activity. The very weak relationship between even large CAR classes having strong positive ΔNDVI and concomitant ΔDUR suggests that dense vegetation is not a necessary, nor a sufficient, condition for above-average lightning duration. We will discuss why this might be in section 6.4.

6.3.4 Effects of spatial and temporal homogeneity of NDVI anomalies

To determine the effect of the uniformity and persistence of the NDVI anomalies on the relationship between NDVI and DUR, we identified those CARs that had uniform NDVI anomalies in both space and time. This was achieved in three steps. First, all CARs having JJA NDVI anomalies of at least ± 0.5 were identified in accordance with findings of Philippon et al. (2007) discussed in section 6.3.3. Second, weekly NDVI

anomaly data was inspected to determine whether or not nine consecutive weeks in JJA were present with positive or negative anomalies. This criterion was adopted to identify CARs having persistent NDVI anomalies that lasted the majority of the growing season; Fennessy and Shukla (1999) noted that initial soil moisture anomalies persisted between 60–90 days after 1 June over most of the regions considered in their study. Increasing the threshold required for consecutive number of weeks significantly reduced the sample size, so 70% was found to yield a decent sample size while still identifying CARs which had NDVI departures for most of the JJA period. Third, weekly NDVI maps (with data aggregated into 10 by 10 km squares) were visually inspected to determine whether or not the NDVI anomaly, for those weeks identified in step 2, was uniform across the CAR in question.

Applying these criteria reduced the number of CAR seasons available for analysis from 380 to 130. Most of the 130 CAR seasons had uniformly positive ΔNDVI (91), with only 31 CAR seasons having uniformly negative ΔNDVI. All of the CAR seasons with uniformly negative ΔNDVI occurred between 2000 and 2004 which coincided with the drought period. Results for only two size classes— "Req_75" and "All CARs"— are shown in Fig. 6.6.

While applying the uniformity criteria to all CARs (regardless of area) did increase the values of R^2 between seasonal (JJA) ΔNDVI and concomitant ΔDUR somewhat, the values remained well below statistically significant levels. Applying the condition of uniformity for the Req_75 class did slightly increase the R^2, as did increasing the magnitude of the negative anomaly. In contrast, correlations for positive ΔNDVI versus ΔDUR were not statistically significant at a 95% confidence level, and applying the

condition of uniformity had no significant impact on the R^2 values, even for large CARs having uniformly positive ΔNDVI > +1.0. These statistics suggest that patch size and the magnitude of the negative anomaly are probably more important for the association between ΔNDVI and ΔDUR than is the uniformity of the anomaly.

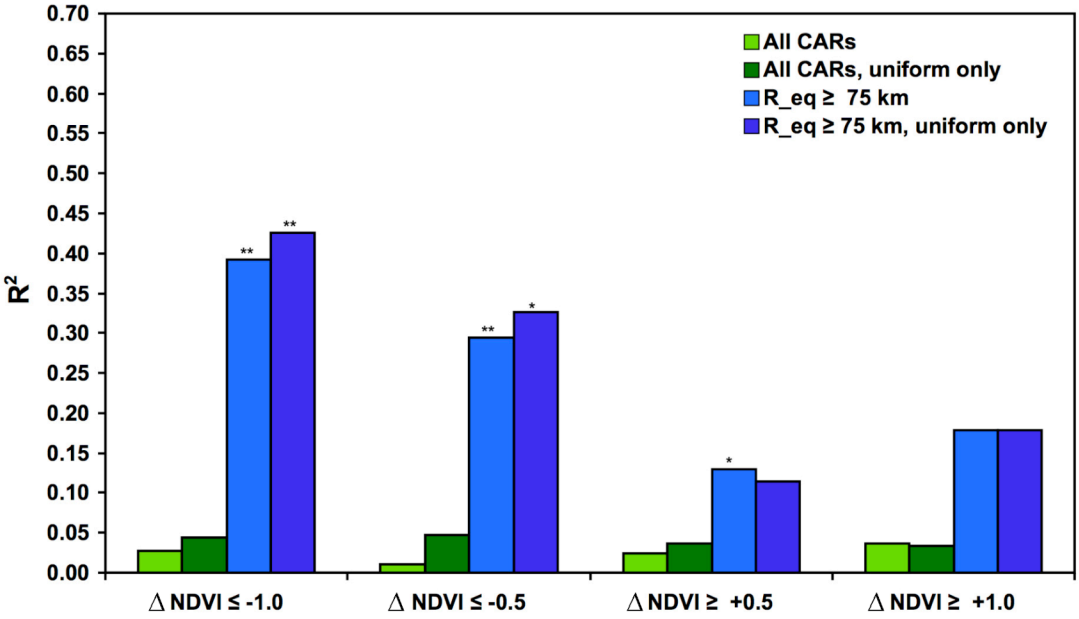

Figure 6.6: Coefficients of determination (R^2) between JJA ΔNDVI and ΔDUR between 1999 and 2008. Bars with single asterisk have coefficients of determination which are statistically significant at the 95% level of confidence, while those with two asterisks are statistically significant at the 99% level of confidence. "All CARs" includes CARs having both uniform and non-uniform spatial and temporal NDVI anomalies, while "uniform" CARs have spatial and temporal NDVI anomalies (see text for details).

Another means of interpreting the data is to calculate the percentage of JJA seasons having above (or below) average ΔDUR for CARs having positive or negative ΔNDVI for JJA. Figure 6.7 shows that almost 80% of those CAR seasons (for all sizes) with uniformly strongly negative ΔNDVI (≤ -1.0) experienced below-average lightning

duration, compared to only about 60% for CARs having non-uniform ΔNDVI. The percentage of CARs with negative ΔDUR also increased as CAR size increased and, to a lesser extent, as the magnitude of the negative ΔNDVI increased.

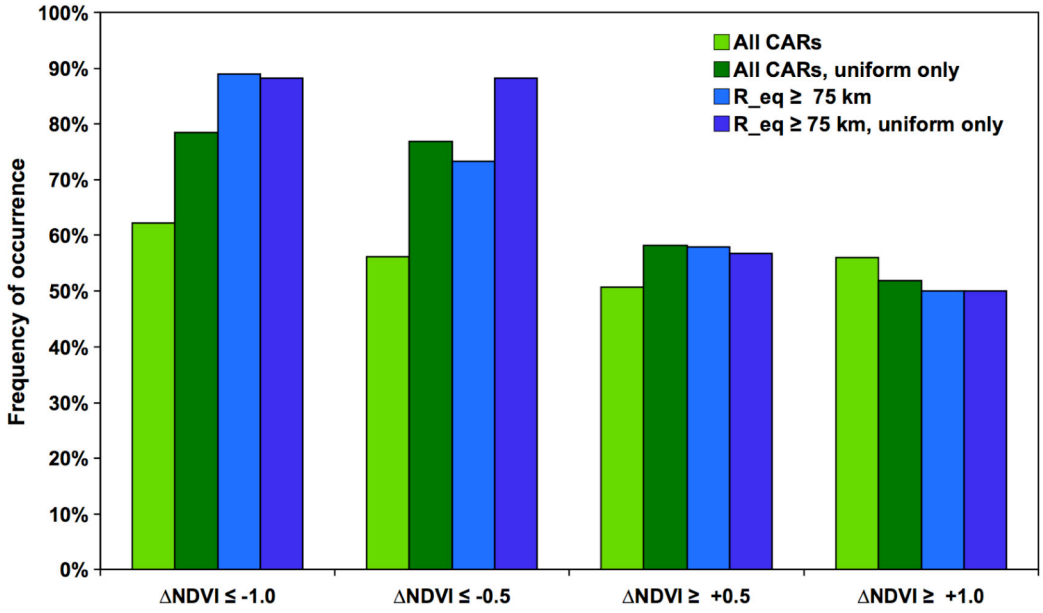

Figure 6.7: Percentage of JJA seasons having positive (or negative) ΔDUR for CARs having positive (or negative) ΔNDVI between 1999 and 2008. For example, for CARs having equivalent radii of at least 75 km, almost 90% of the CAR seasons (JJA) having ΔNDVI ≤ -1.0 had ΔDUR < 0.0. Alternatively, for CARs having equivalent radii of at least 75 km, only about 10% of the CAR seasons (JJA) having ΔNDVI ≤ -1.0 had ΔDUR > 0.0.

Specifically, almost 90% of those CAR seasons with ΔNDVI of -0.5 or lower had below-average ΔDUR. The gap between the percentage of below-average ΔDUR for all CARs having below average ΔNDVI and for the Req_75 class decreased when the uniformity criterion was applied, especially for CAR seasons with negative ΔNDVI. This suggests that applying the uniformity criterion for CAR seasons having negative ΔNDVI

reduces the importance of the anomalys' area in modulating the relationship between ΔNDVI and ΔDUR. As found in section 6.3.3, Fig. 6.7 shows that no clear trend is evident in ΔDUR in CARs having positive ΔNDVI, even for large CARs having spatially and temporally consistent positive ΔNDVI. For all CAR seasons with positive ΔNDVI, just over 50% of concomitant seasons have positive ΔDUR, regardless of the magnitude of the positive ΔNDVI. That is, the odds of a CAR season having above- or below-average DUR are about the same, regardless of the magnitude or uniformity of the positive NDVI anomaly.

6.3.5 Linkages between late June NDVI on July DUR

In this section we investigated whether or not the state of the land surface in late June, as quantified by ΔNDVI, had any bearing on lightning duration in July. The start date of weeks used to calculate ΔNDVI varied between 23 June and 29 June, with end dates between 28 June and 4 July. The correlation coefficients were calculated for CARs of varying size and of varying magnitude of ΔNDVI.

Figure 6.8 shows that for CAR seasons having negative ΔNDVI, R^2 increases as ΔNDVI becomes more negative and as the CAR size increases. For large CARs (T25) having June ΔNDVI < -0.5, almost 50% of the variance in July lightning duration is explained by late June ΔNDVI (p-value = 0.01). The association between late June ΔNDVI and July ΔDUR is weakest for the smallest 50% of CARs (B50). Thus, if the vegetation in late June is severely stressed over a large area, the concomitant July lightning duration is very likely to also be below average.

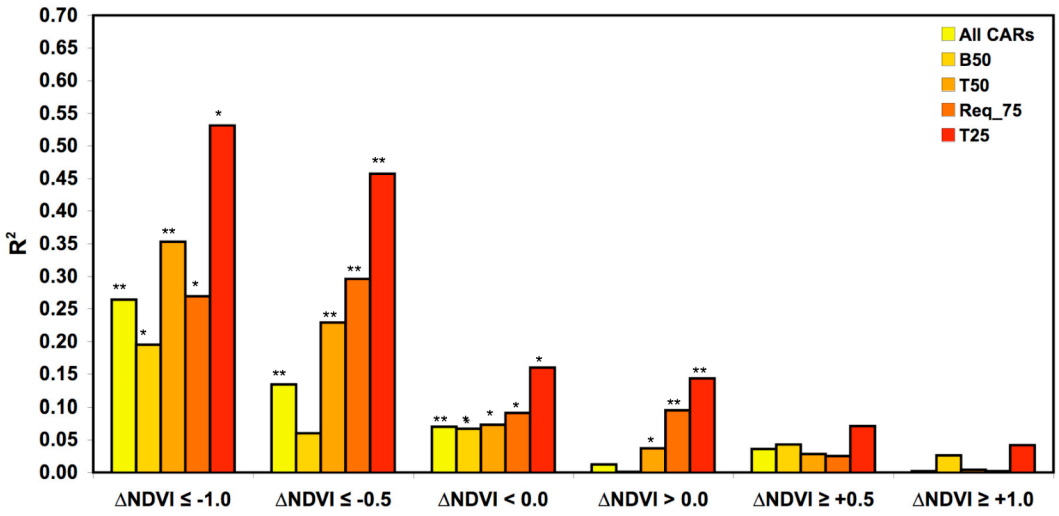

Figure 6.8: Late June ΔNDVI versus July ΔDUR between 1999 and 2008. Bars with single asterisk have coefficients of determination which are statistically significant at the 95% level of confidence, while those with two asterisks are statistically significant at the 99% level of confidence. CAR size classes (B50, T50 etc.) have the same meaning as in Table 6.1

In contrast, the magnitude of a positive ΔNDVI in late June explains very little about July ΔDUR. Additionally, the values of R^2 decrease as the magnitude of the positive June ΔNDVI increases. The R^2 between June NDVI and July ΔDUR for Req_75 and T25 are statistically significant at the 95% confidence level, but only when one considers all CAR seasons having above-average late June ΔNDVI. These statistics suggest that lush vegetation in late June does not necessarily translate into positive ΔDUR in July.

6.3.6 Linkages between late June NDVI and early August NDVI

In this section we investigated whether NDVI anomalies in late June persist into early August. July is the most active month for thunderstorms on the Canadian Prairie (Burrows et al. 2002), so anomalies in early August ΔNDVI should arise primarily in

response to the amount of convective precipitation in July. Also, in section 6.3.4 it was found that negative ΔNDVI in late June were typically associated with below -average ΔDUR in July. Is this reflected in early August ΔNDVI, or is it masked by non-convective synoptic-scale precipitation events? The weeks used to calculate ΔNDVI for June were the same as in section 6.3.4; the dates for early August ΔNDVI varied between 30 July and 4 August, and 4 August and 10 August. The correlation coefficients were again calculated for CARs of varying size and of varying magnitudes of ΔNDVI.

Figure 6.9 shows that R^2 between late June ΔNDVI and early August ΔNDVI is only 0.11 (p-value = 0.01) for all CARs having ΔNDVI < 0.0. However, as was the case for the association between late June ΔNDVI and July ΔDUR, the R^2 between late June ΔNDVI and early August ΔNDVI increased as the size of the CARs and the magnitude of the negative ΔNDVI increased. Specifically, for the T25 group, over 60% of the variance in early August ΔNDVI can be explained by late June ΔNDVI for seasons with late June ΔNDVI < -0.5 (and < -1.0). The weakest association was found for the smallest 50% of CARs. With the exception of the B50 class, all R^2 are significant at the 99% level of confidence for late June ΔNDVI < -0.5 (and < -1.0).

When grouped by positive June ΔNDVI, the R^2 between late June ΔNDVI and early August ΔNDVI are much lower for all size classes and anomaly classes than for positive late June ΔNDVI and early August ΔNDVI. For large CARs (T25), up to 35% of the variability in early August ΔNDVI can be explained by June ΔNDVI for seasons with late June ΔNDVI > +0.0 (and > +0.5). Interestingly, the weakest association between late June ΔNDVI and early August ΔNDVI was found for seasons when ΔNDVI > +1.0. This is essentially the opposite of what was observed for negative late June ΔNDVI and early

August ΔNDVI. Reasons for this counterintuitive result are not clear. These data suggest that it is more likely that CARs with stressed vegetation in late June are much less likely to transition to lush vegetation by early August, especially for large CARs. However, more data are required to generalize this statement. Nonetheless, these data support the hypothesis that a positive feedback mechanism may be present between negative NDVI and reduced DUR during drought years.

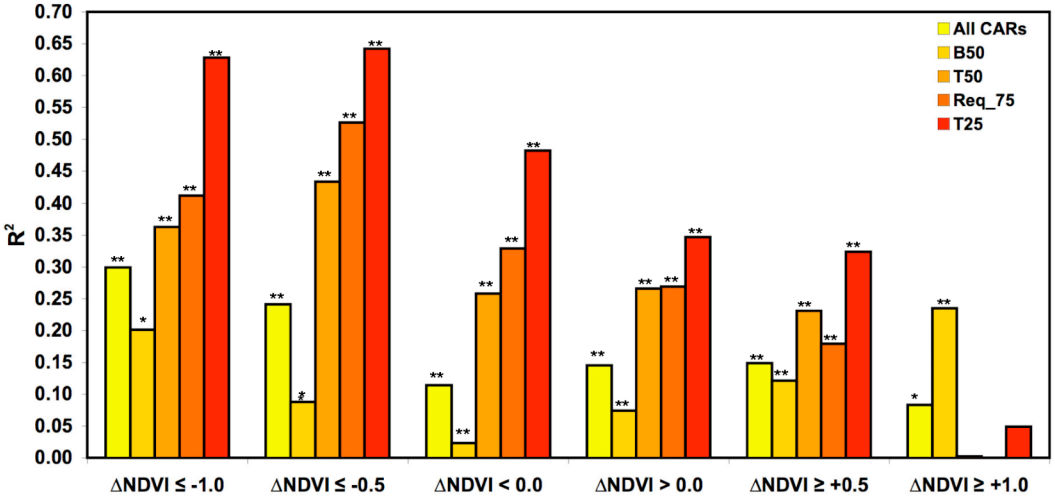

Figure 6.9: Late June ΔNDVI versus early August ΔNDVI between 1999 and 2008. Bars with single asterisk have coefficients of determination that are statistically significant at the 95% level of confidence, while those with two asterisks are statistically significant at the 99% level of confidence.

6.4 Discussion

6.4.1 Impact of magnitude and extent of NDVI anomalies on DUR

We expect that the association between anomalies at the terrestrial surface and attendant lightning activity will strengthen as the size of the anomaly increases, and also as the magnitude of the anomaly increases. Our data indicate that the relationship

between ΔNDVI and ΔDUR becomes statistically significant at the 99% level of confidence when the class average equivalent radii approach 80 km, and that the highest R^2 obtained for those CARs having both large equivalent radii (top quartile and Req_75 classes) and significant negative ΔNDVI (< -0.5). Thus, CAR area is critical in governing the strength of the relationship between NDVI and DUR, and that if the area is too small (R_eq less than about 75 km) the relationship breaks down.

The critical anomaly size identified here is consistent with estimates of critical patch size determined from both modelling studies and theoretical values. For example, Raupach and Finnigan (1995) used scaling techniques to identify length scales at which heterogeneities at the surface affect the convective boundary layer (CBL). They estimate the appropriate critical length scale to be the product of the mean horizontal wind speed in the CBL (U) and the entrainment time scale (T; time required for renewal of CBL by entrainment from the free atmosphere). For quiescent conditions in the CBL (U~ 3 m s^{-1} or ~10 km hr^{-1}) and an entrainment time scale of about 12 hours, the corresponding length scale is (L) 130 km (radius of 65 km). If U increases to 5 m s^{-1}, then L increases to just over 200 km. Consider two adjacent patches having contrasting soil moisture anomalies. At length scales greater than the aforementioned thresholds for L, the low-level air cannot move between the patches in the time it takes the CBL to develop—so the CBLs over the patches become "energetically independent" (Raupach and Finnigan (1995). As noted earlier, Desai et al. (2006) analyzed satellite-derived surface soil moisture data and measurements from aircraft and found that over the southern Great Plains of the US, CBL depth responded to 50–100 km scale variations in surface energy flux over the southern Great Plains of the US, with decreased influence of soil moisture

on CBL depth at scales smaller than 100 km. These data all suggest that the minimum equivalent radii of 70–80 km in this study perhaps represent the high end of the range at which NDVI anomalies become sufficiently large as to affect thunderstorm activity.

6.4.2 Asymmetric relationship between NDVI and DUR

An intriguing finding is the asymmetric relationship between NDVI and DUR. Specifically, the relationship between positive ΔNDVI and ΔDUR is very weak, even for large CAR classes having strong positive ΔNDVI. Realization of thunderstorms requires three criteria to be satisfied: instability, low-level moisture and a trigger. For drought conditions (ΔNDVI < -1.0) the resultant reduction of moisture into the CBL from evapotranspiration reduces the amount of moisture available for thunderstorms (e.g., Jamieson et al. 1995). That is, a necessary criterion for convection (low-level moisture) has been weakened, which may explain the close relationship between those CAR seasons having ΔNDVI < -1.0 and attendant ΔDUR. Of course, the lack of low-level moisture does not always preclude thunderstorm activity, but it has a notable impact as shown in our analysis. The opposite is not necessarily true for CAR seasons having positive ΔNDVI. We purport that a possible reason for this asymmetric relationship is that the presence of abundant CBL moisture (years with NDVI > +1.0) from vegetation transpiring freely under ideal soil moisture conditions, is a necessary but not sufficient condition for thunderstorms. One reason for this could be that the higher soil moisture may result in a cooler and more stable CBL, which may lead to reduced convection (e.g., Cook et al. 2006), or other processes that inhibit convection are at play (e.g., lack of a trigger or strong capping lid).

This hypothesis is illustrated by events in 2005, a pluvial summer on the Canadian

Prairies during which all CARs had above average JJA ΔNDVI. However, despite the dense vegetation in 2005, 10 of the 12 CARs with ΔNDVI ≥ +1.0 had ΔDUR < 0.0. In contrast, only six CAR seasons between 1999 and 2008 had ΔNDVI ≤ -1.0 but ΔDUR > 0.0, and of these, only two had R_eq of at least 75 km. North American Regional Reanalysis (NARR; Mesinger et al. 2006) anomaly data indicate that the summer of 2005 was predominantly cool and wet over the Canadian Prairies. NARR data also show that conditions were typically not favourable for thunderstorms on account of the abnormally high convective inhibition and below-average Convective Available Potential Energy (CAPE), especially over Alberta and western Saskatchewan. In contrast, CAPE values were above average over southern Manitoba. Enhanced ascent at 500 hPa was present over most of the Prairies. Thus most of the rainfall, especially west of Manitoba, which led to positive ΔNDVI in JJA of 2005 was likely associated with synoptic-scale baroclinic systems. This is supported by lightning duration data, with notable positive ΔDUR (> +0.5) observed over only seven of the 38 CARs (< 20%) in 2005. Six of these were located near the Saskatchewan-Manitoba border where NARR data suggest conditions were more favourable for thunderstorms. These observations are consistent with those made by Raddatz (2005), who noted that between 1997 and 2003 the critical ingredients required for the realization of convection (such as lift and CAPE) were less prevalent over drought CARs than pluvial CARs.

6.4.3 Relationship between NDVI and RZPAW

Values of R^2 calculated here between NDVI and RZPAW (0.50–0.90) are much higher than those found in the literature. For example, Adegoke and Carleton (2002) calculated lagged R^2 between root-zone soil moisture and NDVI of between 0.18 and

0.23. Wang et al. (2007) calculated R^2 values of 0.21 and 0.30 between detrended root-zone soil moisture and NDVI at three sites in New Mexico, Arizona and Texas. As discussed in section 6.3.1.1, the high values of R^2 between NDVI and RZPAW appear to be in part attributable to autocorrelation, so this caveat should be exercised before drawing definitive conclusions concerning the lags. The dataset considered here is small (i.e., only one season), and more data is required to make specific deductions concerning the optimal lag between RZPAW and NDVI at these sites, for example.

With that said, the analysis here does show that NDVI is responding to changes in the RZPAW. The data also suggest that the response in NDVI may be strongest for lags between one to three weeks, with two weeks favoured for the finer textured clay loam soils (e.g., Hussar), and one week lag favoured for the coarser sandy loam soils (e.g., Vermilion). The suggestion of a lagged response of NDVI to RZPAW is consistent with similar research. For example, Adegoke and Carleton (2002) found the highest R^2 when NDVI lagged root-zone soil moisture by two weeks. By comparison, Wang et al. (2003b) found that the response time of grasses and crops in Kansas to heavy precipitation events was 8–26 days, with the most common delay 11–24 days (about 1–3 weeks).

Both observed and modelled datasets suggest that stressed vegetation (ΔNDVI < -0.5) is typically associated with RZPAW < 40%. These findings are in good agreement with data from controlled lab and field experiments, which have shown that incipient moisture stress for most plants starts when the RZPAW approaches 50% (e.g., Shen et al. 2002). Controlled lab and field experiments show that notable losses of photosynthetic activity (Vico and Porporato 2008), increases in abscisic acid levels (Schurr et al. 1992)

and reductions in biomass growth (Mitchell et al. 2001) occur once the RZPAW declines below 30%.

6.5 Conclusions

Thunderstorms form a critical part of the Canadian Prairie hydrological cycle, with up to 50% of the annual precipitation sourced from summertime convective rainfall. While the Canadian Prairie terrestrial system has been identified as having the potential to exert a detectable influence on convective precipitation in the summer, relatively little work has been dedicated to the impacts of land-atmosphere feedbacks on thunderstorm activity on the Canadian Prairies.

We introduced a novel approach of using lightning flash data with high spatial resolution (and real-time) estimates of NDVI to investigate linkages between vegetation density and concomitant and antecedent thunderstorm activity. The degree of association between NDVI and DUR was quantified using the coefficient of determination between pairs of standardized anomalies of lightning duration (ΔDUR) and NDVI (ΔNDVI) for individual summer months and also by season (JJA) for a 10-yr period spanning 1999 through 2008. Anomalies were calculated for 38 Census Agricultural Regions (CARs) on the Canadian Prairies. Linkages between RZPAW and NDVI were investigated using in-situ root-zone plant available moisture observations in Alberta and model-simulated root-zone plant-available soil moisture (RZPAW) together with NDVI data. Primary research findings are:

- The size of the CAR is important in governing the strength of the relationship between NDVI and DUR. If the area of the anomaly is too small (area less than 18 000 km^2, or

equivalent radius less than about 75 km), the relationship breaks down. Additionally, the relationship strengthens as the magnitude of the anomaly increases, and is especially strong when negative anomalies are larger than typical inter-annual variability ($\Delta NDVI \leq -1.0$).

- An asymmetric relationship exists between $\Delta NDVI$ and ΔDUR. Specifically, a positive feedback mechanism is evident over the course of the summer over drought-affected regions, with drought conditions leading to less thunderstorm activity. In contrast, a very weak relationship was found in pluvial regions, even over large CARs having strongly positive $\Delta NDVI$. This suggests that positive $\Delta NDVI$ alone are not a necessary, nor a sufficient, condition for above-average lightning duration.
- If the vegetation in late June is severely stressed over a large CAR, the concomitant July lightning duration will likely be below average. In contrast, lush vegetation in late June does not necessarily translate into positive ΔDUR in July. However, analysis over more years is needed to generalize this statement.
- CARs with stressed vegetation in late June are much less likely to transition to lush vegetation by early August, especially for large CARs. These data support the hypothesis that a positive feedback mechanism is present between NDVI and DUR during drought years (2000–2003).
- Both observed and modelled soil moisture datasets suggest that stressed vegetation ($\Delta NDVI < -0.5$) is typically associated with RZPAW < 40%.

The findings presented here (i.e., patch size and anomaly magnitude) are consistent with and corroborate both theoretical studies and modelling work. Future work will

focus on how land-atmosphere processes (e.g., NDVI anomalies) over the Canadian Prairies can condition the CBL layer so as to inhibit or facilitate thunderstorm activity, while also considering the role of synoptic-scale forcing on modulating summer thunderstorm activity.

CHAPTER 7

7. IMPACTS OF LAND-ATMOSPHERE FEEDBACKS ON DEEP, MOIST CONVECTION ON THE CANADIAN PRAIRIES

[4]Abstract

The purpose of this study was to focus on how anomalies in the Normalized Difference Vegetation Index (NDVI; a proxy for soil moisture) over the Canadian Prairies can condition the convective boundary layer (CBL) so as to inhibit or facilitate thunderstorm activity, while also considering the role of synoptic-scale forcing (both surface and upper-air) on modulating summer thunderstorm activity. Our study focused on a census agricultural region (CAR) over central Alberta for which we had observed lightning data (proxy for deep, moist convection), NDVI data, and in-situ sounding data (to quantify impacts of vegetation vigour on the CBL characteristics) for 11 summers from 1999 to 2009. Our data suggest that storms over the study area are more likely to develop and are longer lived (or widespread) when they develop in an environment in which the surface and upper-air synoptic-scale forcing are synchronized. On days when a surface or upper-air feature is present, storms are more likely to be triggered when NDVI is much above average, compared to when NDVI is much-below average. Additionally, we found the response of thunderstorm duration to NDVI anomalies to be asymmetric. That is, the response of lightning duration to anomalies in NDVI is most noticeable when NDVI is below average, but not necessarily when NDVI is above average. We propose a conceptual model, based almost entirely on observations, which integrates all of the above findings to describe how a reduction in vegetation vigour — in response to soil moisture deficits — modulates the partitioning of available energy into sensible and latent heat fluxes at the surface, thereby modulating lifting condensation level heights, which in turn affect lightning activity.

---

[4] This is a copy of a paper that is in review at Earth Interactions at the time of thesis submission. Authors are Brimelow, Hanesiak and Burrows.

7.1. Introduction

Recently, Brimelow et al. (2011) presented findings from a novel study designed to explore linkages between the Normalized Difference Vegetation Index (NDVI) and lightning duration (DUR) from the Canadian lightning detection network for 38 Census Agriculture Regions (CARs) on the Canadian Prairies. Brimelow et al. (2011) found a strong coupling between NDVI and DUR was evident during the summer months over drought-affected regions on the Canadian Prairies, with drought conditions associated with less lightning activity. They also noted that the strength of the relationship between NDVI and DUR increased significantly as both the area and magnitude of the dry anomaly increased. In contrast, they noted a very weak relationship between NDVI and DUR over those CARs experiencing pluvial conditions. They concluded that these observations suggest that dense vegetation alone is not a sufficient condition for above-average lightning duration.

Modelling studies have suggested that changes in low-level moisture and energy fluxes associated with soil moisture and vegetation anomalies can perpetuate drought conditions (e.g., Dirmeyer 1994; Beljaars et al. 1996). Vegetation is known as an important pathway for coupling the surface and the atmosphere. As a result, changes in vegetation vigour can have a marked impact on the partitioning of incoming solar radiation (e.g., Liu et al. 2006) and on modulating surface fluxes (e.g., Dominguez and Kumar 2008), which can in turn affect thunderstorm activity (e.g., Toumi and Qie 2004; Taylor et al. 2009). Consequently, coupling between the land surface and overlying atmosphere is strongest during the warm season (Koster et al. 2004). The strength of the land–atmosphere interaction, or coupling, is difficult to quantify. For example, Dirmeyer

(2006) suggested that soil moisture is "strongly" modulated by antecedent precipitation, that soil moisture in turn exerts a "moderate" influence on evapotranspiration (ET), but that the impact of ET on precipitation is "tenuous". Modelling studies (Koster et al. 2004, 2006) have identified "hot spots" where coupling between the land surface and atmosphere is marked. The Great Plains of North America, including southern portions of the Canadian Prairies, is one such "hot spot". Dirmeyer et al. (2009) conducted an integrated analysis for quantifying land-atmosphere interactions that was not based on numerical models and this too identified the Great Plains and southern Canadian Prairies as hot spots for land-atmosphere coupling in the summer (JJA).

Using observed surface temperature and moisture, soil moisture and precipitation data, Findell and Eltahir (1999) did not find a positive correlation between the surface moist static energy (MSE) and rainfall over Illinois. There was, however, a significant negative correlation between the soil moisture (top 10 cm) and the lifting condensation level (LCL), and between the LCL and the rainfall. Alfieri et al. (2008b) investigated the relationship between warm season soil moisture and subsequent precipitation in the USA Midwest from 1971 to 2003. They identified convective precipitation days using convective available potential energy (CAPE) calculated from observed soundings. Next, they correlated convective rainfall incidence against soil moisture (top 50 cm), with precipitation lagging soil moisture by one day. They concluded that the possibility of a positive feedback between soil moisture and convective precipitation exists, but that soil moisture alone cannot unambiguously isolate the signal.

Recently, satellite-derived vegetation indices and soil moisture data have been used to try to determine the effects of changes in vegetation vigour during the warm season on

the boundary layer and subsequent precipitation. However, the results have not been conclusive. Notaro et al. (2006) used photosynthetically active radiation (PAR) data derived from satellite data to examine the interaction between vegetation and precipitation over the USA between 1982 and 2000. They noted that the impacts of PAR on precipitation were complex and weaker than the feedback for temperature. For example, the correlation for PAR leading precipitation was negative over the northern Great Plains in JJA, but positive in fall and spring. Liu et al. (2006) conducted a similar study to that of Notaro et al. (2006), but for all global ice-free landmasses. Specifically, they investigated feedbacks between PAR, observed surface temperature and precipitation. They were unable to identify a significant correlation over North America when PAR led precipitation. In fact, for JJA over the Canadian Prairies, they identified a negative correlation when PAR led precipitation by one month, suggesting a negative feedback between precipitation and PAR there.

Wang et al. (2006) applied Granger causality tests to observed gridded temperature, precipitation and NDVI from 1982–2000 over the northern grasslands of the USA. They found a significant causal relationship between NDVI early in the season and precipitation and temperature later in the season (July onwards). They purport that initially enhanced vegetation may deplete soil moisture faster, thereby leading to drier and warmer anomalies later in the season. Kim and Wang (2007) investigated the soil-moisture-vegetation-precipitation feedback over the Mississippi River Basin using ensemble simulations from the coupled Community Atmosphere Model-Community Land Model. They focused on the impact of vegetation feedbacks arising from initial soil

moisture anomalies through the entire soil column, and found that in JJA, initial wet soil moisture anomalies increased precipitation through increased ET.

One possibility for these conflicting results is that many of them were based primarily on numerical modelling output. For example, Hohenegger et al. (2009) found that the sign of the soil-moisture precipitation feedback in model simulations over Europe depended on the horizontal grid spacing and cloud convection schemes used in their model. Kim and Wang (2007) found that initial dry soil moisture anomalies did not show a significant impact on precipitation and vegetation, but conclude that this was because of the dry bias in the model they used. Additionally, studies examining feedbacks between soil moisture and vegetation anomalies and precipitation often do not discern between convective and stratiform precipitation.

Before proceeding further, we provide a brief review of the conceptual models used to describe the physical mechanisms whereby anomalies in the underlying soil moisture and vegetation can affect subsequent deep, moist convection. Most of the conceptual models have their origins in modelling studies (e.g., Trier et al. 2004; Findell and Eltahir 2003a,b; Pal and Eltahir 2001; Schär et al. 1999). Additionally, theoretical and modelling studies have shown that the amount of moisture in the convective boundary layer (CBL) has important consequences for the initiation and intensity of thunderstorms (Segal et al. 1995; Crook 1996; Yamada 2008).

Given that convection is an important component of the hydrological cycle on the Canadian Prairies (Raddatz and Hanesiak 2008), the purpose of this study was to focus on how anomalies in NDVI (a proxy for soil moisture) over the Prairies can condition the CBL so as to inhibit or facilitate thunderstorm activity, while also considering the role of

synoptic-scale forcing on modulating summer thunderstorm activity. Our study focused on a census agricultural region over central Alberta (CAR11) for which we had observed lightning data, NDVI data, and in-situ sounding data for 11 summers (1 June through 31 August) from 1999 to 2009. In this paper, we were interested in examining the relative importance of the forcing mechanisms for deep-convection in conjunction with the NDVI anomalies. In order to identify whether anomalies in underlying vegetation had any impact on lightning duration for similar synoptic-scale forcing conditions, we adopted an ingredients-based approach to identify the three criteria required for thunderstorm formation, namely: (1) low level moisture, (2) instability, and (3) trigger or lift mechanism. To address our main goal, we used lightning data as a proxy for deep-convection, NDVI data as a measure of vegetative vigour, synoptic-scale upper air and surface data to assess (2) and (3), and operational rawinsonde soundings for (1) and (2). Our focus was on a region surrounding Stony Plain in central Alberta (see Fig. 7.1) due to the availability of observed soundings and because it is located within a land-atmosphere feedback "hot spot".

The paper is structured as follows. In section 7.2, the various datasets and our methodology are described. In section 7.3, the relative roles of surface and upper-air forcing and NDVI on lightning duration are explored. Section 7.4 focuses on the relationships between observed sounding parameters and NDVI, and how these are related to lightning duration. In section 7.5, we present a conceptual model which integrates our findings concerning the linkages between NDVI and CBL characteristics, synoptic-scale forcing and lightning duration. The paper concludes with a summary of our primary findings.

7.2. Data and methodology

7.2.1 Study area

Statistics Canada divides the agricultural zone on the Canadian Prairies into census agricultural regions (CARs) for the purpose of calculating agricultural statistics. Here we will consider relationships between vegetation vigour, synoptic-scale forcing and lightning duration over CAR11 located in central Alberta (see Fig. 7.1). CAR11 has an area of about 16 500 km^2 (equivalent radius of ~72 km) and is located in the parkland eco-climatic zone, which marks the transition zone between the Boreal forest and the prairie grasslands. Western portions of the CAR are located about 100 km NE of the Rockies, with the centroid located about 200 km NE of the Rockies. Terrain heights range from 650 m (ASL) in the northeast to 950 m in the southwest. About 60–65% of CAR11 is dedicated to agriculture (crops and pasture), with pockets of Aspen groves, especially in the far west, north and east. Crops are predominantly cereal crops. Planting dates vary from year to year and range from early May to the end of May, depending on soil moisture and temperature conditions, with crops typically maturing in mid August (e.g., Mkhabela et al. 2010). NDVI data between 1987 and 2009 show NDVI values over CAR11 peaking in the week of 19–25 July, with a rapid decline after mid August.

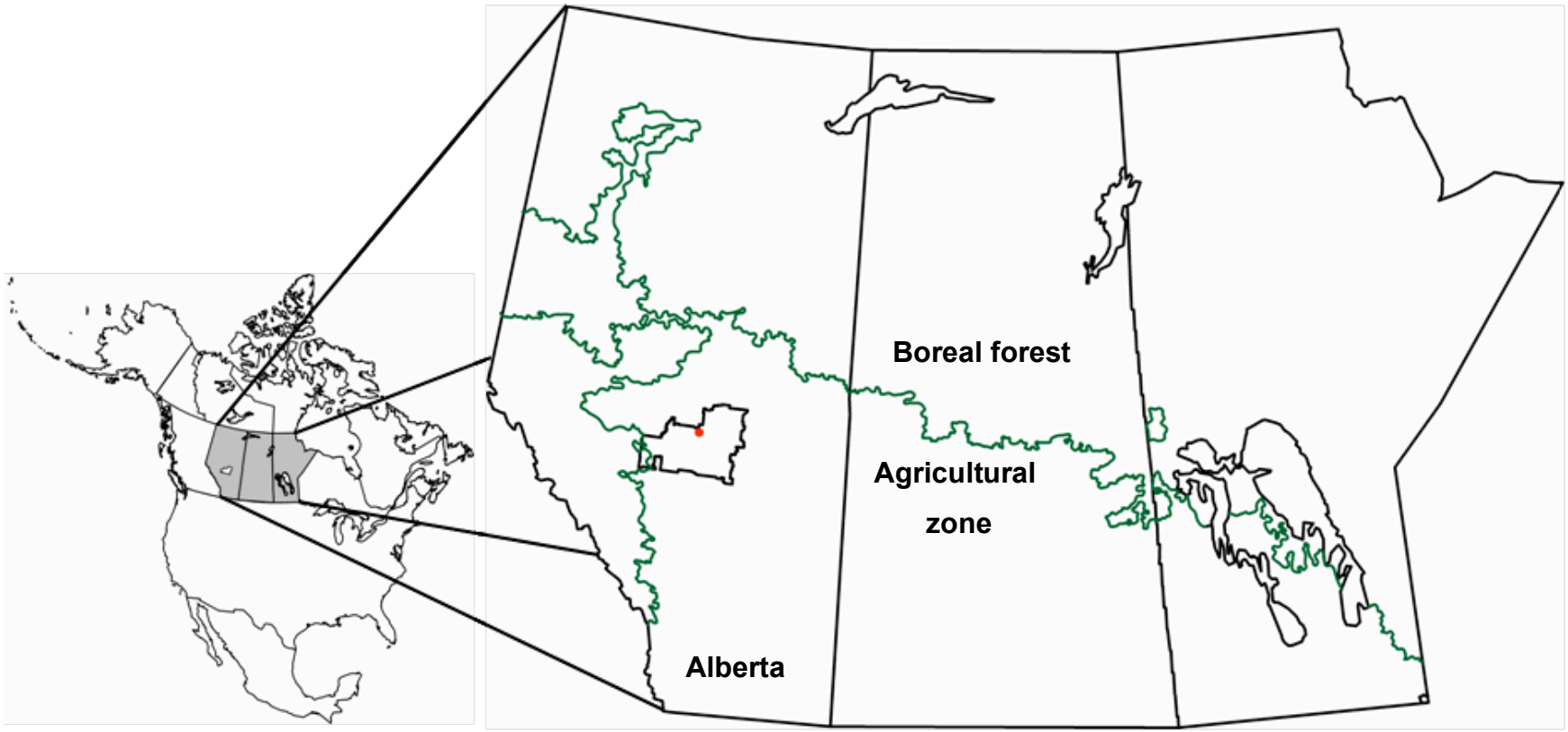

Figure 7.1: Map of the study area. The polygon over central Alberta is CAR11, which is inside the agricultural area (indicated by the green border). The red dot represents the location of the Stony Plain upper-air site.

7.2.2 Cloud-to-ground lightning data

We used cloud-to-ground (CG) lightning flash data from the Canadian Lightning Detection Network (CLDN) in this study as a proxy for thunderstorm occurrence and longevity over the study area. Detection efficiency of CG flashes for the CLDN over the Prairie agricultural zone is >90%, while the median stroke location accuracy is 500 m or better (Cummins et al. 1999).

To quantify the thunderstorm activity, we used the lightning duration within CAR11. The lightning duration is defined as the length of time (in hours) between 9:30 local solar time (LST) and 19:30 LST where flashes occurred "continuously"; during the summer months in central Alberta, LST typically precedes Mountain Time (MT) by about 90 minutes. No more than 10 minutes was allowed to separate a flash and the next flash in a given series of flashes. If more than 10 minutes separated two flashes, then the time series was discontinued and a new time series was started when the next flash was recorded. The reader is referred to Brimelow et al. (2011) for details concerning the CLDN data and calculation of DUR.

We used the 09:30–19:30 LST time window to focus on surface-based thunderstorms (rooted in the convective boundary layer) that typically develop in response to daytime heating, rather than nocturnal thunderstorms that tend to be elevated. According to Burrows and Kochtubajda (2010), from 1999 to 2008, CG lightning within a 50 km radius of Edmonton International airport was a minimum between 06:00 and 10:00 (MT; UTC -6 hrs), with the peak time for lightning activity occurring between 16:00 and 22:00 MT. From 1999 to 2008, about 60% of all lightning strikes over CAR11 in JJA were observed between 09:30 and 19:30 MT.

7.2.3 Normalized Difference Vegetation Index (NDVI)

We used NDVI as a measure of vegetation vigour and a proxy for root-zone soil moisture content. Vegetation is known as an important pathway for coupling the surface and the atmosphere, and vegetation health affects the partitioning of available energy and moisture flux into the CBL. The latent heat flux of moisture is an important source of moisture in the CBL, with transpiration from a dense and unstressed canopy under favourable conditions capable of increasing the mixing ratio of the CBL by 4–8 g kg^{-1} per day (Raddatz 1993; Segal et al. 1995).

NDVI is the normalized difference between the near-infrared and visible red reflectance, and responds to changes in both the chlorophyll content and the intracellular spaces in the spongy mesophyll of plant leaves (Gu et al. 2007). Higher NDVI values reflect greater vigour and photosynthetic capacity of the canopy, whereas lower NDVI values are indicative of vegetative stress resulting in chlorophyll reductions and changes in the leaves' internal structure due to wilting (Gu et al. 2007). NDVI is a commonly used satellite-derived index for monitoring vegetation vigour and tracking drought (e.g., Ji and Peters 2003); the reader is referred to Tucker (1979) for more information about NDVI.

Weekly NDVI data valid for CAR11 during the growing season were downloaded from the Canadian Crop Condition Assessment Program (CCAP) site (www.26statcan.ca/ccap), which is operated by Statistics Canada. In brief, a land use mask is applied, in which a pixel is classified as crop/pasture if at least 50% of that pixel is crop/pasture. Here, NDVI data for only those pixels classified as crop/pasture are included in the calculation of NDVI for each CAR. However, it is possible that some

pixels which are classified as crop/pasture could have 40% forest cover. Statistics Canada uses data from the National Oceanic and Atmospheric Administration satellites carrying the Advanced Very High Resolution Radiometer (AVHRR). A composite of AVHRR images covering a seven-day period removes most or all cloud effects (Reichiert and Caissy 2002). Corrections are also made to remove much of the atmospheric contamination, and to minimize other effects (such as view angle and solar angle).

7.2.4 Atmospheric sounding data

Sounding data are very useful for quantifying and describing two of the criteria required for thunderstorms: the presence of instability and low-level moisture. Additionally, the sounding data can be used to quantify the effects, if any, of changes in vegetation vigour on the structure and characteristics of the convective boundary layer (e.g., Desai et al. 2006).

For this purpose, we examined 00 UTC weather balloon data from the sounding site at Stony Plain (53.53° N; 114.10° W) from 1 June to 31 August for 1999 to 2009 (see Fig. 1). During this period, over 1000 soundings were released from Stony Plain. Before the soundings could be used to calculate sounding parameters, each sounding was visually inspected to determine whether errors or missing data were present, and whether the sounding had been contaminated by rain. This resulted in 81 soundings being excluded from our analysis. Soundings released in precipitation (i.e., saturated profile) accounted for the vast majority of contaminated soundings. Only 81 (less than 9%) soundings were released on the 365 days when lightning was observed over CAR11, for the 33 summer months from 1999 to 2009, were excluded from the data analysis. Consequently, we are confident that the soundings captured the mean conditions

observed during each of the 33 summer months. Because the sounding data are from a specific point in time they may not always be representative of pre-storm conditions over the entire CAR for the 09:30–19:30 time period. CAR11 has an equivalent radius of just over 70 km, which lies well within the range criteria for proximity soundings typically applied in the literature (e.g., Potvin et al. 2010). The temporal criteria for proximity soundings cited in Potvin et al. range from ±30 minutes from the sounding time to 6 hrs before and 3 hrs following the sounding time.

A commercial software package called RAOB (RAwinsonde OBservation Program) was used to batch process the sounding data. These data were then aggregated into monthly and seasonal means for the purpose of calculating standardized anomalies (see section 7.2.6). RAOB was also used to generate composite soundings (i.e., mean profiles) for each of the 33 months.

7.2.5 NARR data

While the sounding data were useful for quantifying thermodynamic and moisture profiles, they did not offer insight into the vertical motion and moisture advection occurring over CAR11. Here we considered the 500-mb vertical pressure velocity (omega or ω_{500}) and the 0–30 mb above-ground moisture flux divergence (MCON) from the North American Regional Reanalysis (NARR; Mesinger et al. 2006). The vertical velocity data were used to quantify the degree of synoptic-scale ascent (or descent) that favours (or inhibits) deep convection. The MCON was used to quantify how much near-surface moisture was being introduced into (or removed from) the study area. NARR data were available on a 0.33 by 0.33 degree grid. The daily mean, area-averaged 500-

mb omega and MCON data were calculated by averaging the 3-hrly values (for 25 NARR grid points located over CAR11) between 18 UTC and 03 UTC.

7.2.6 Calculation of standardized anomalies and correlations

All monthly and seasonal NDVI, DUR and sounding data were standardized using the methodology employed by Koster and Suarez (2004) and Brimelow et al. (2011). Specifically, the monthly (June, July and August) and seasonal (June through August) standardized anomalies were calculated as follows,

$$\Delta X_j = \frac{X_j - \overline{X_j}}{\sigma_j} \tag{7.1}$$

where X_j is the value of NDVI (or DUR or sounding parameter) for a given month j (or a particular summer [JJA]), $\overline{X_j}$ is the mean value of X over the 11 years, and sigma is the standard deviation for month j over the 11 years. The weekly NDVI data were used to calculate the monthly and seasonal means. The start and end dates for the seasonal and monthly data varied slightly from year to year, with start dates ranging from 3 to 9 June, and end dates from 1 to 7 September. However, this factor was not expected to significantly affect the seasonal NDVI anomalies, because there was typically very little change in NDVI values during these times.

The association between NDVI and DUR was quantified using the coefficient of determination (R^2) between pairs of standardized anomalies of lightning duration (ΔDUR), NDVI (ΔNDVI), and 500-mb omega ($\Delta\omega_{500}$) and all sounding-derived parameters for individual months and also by season (JJA) for a 11-yr period spanning 1999 through 2009. The statistical significance of the correlations was quantified using p-values between 1% and 10%. It is important to keep in mind that the R^2 values do not speak to causality between selected variables. However, as noted by Seneviratne et al.

(2010) *"while correlations cannot demonstrate links of causality, they can nonetheless be used as indirect estimates of coupling for relationships for which causality has been established."*

7.2.7 Surface data and upper-air classification

In this section we use both subjective and objective analyses to quantify the surface and upper-air synoptic-scale circulation patterns (i.e. surface and upper-air forcing) over CAR11 for 22 summer months having contrasting NDVI and/or DUR. By "contrasting" we mean months having standardized NDVI and DUR anomalies of at least ± 0.5. The rationale for identifying this sub-sample was to closer examine the role of NDVI and synoptic-scale forcing in modulating DUR.

Although vertical ascent in the mid-troposphere is not necessarily directly responsible for triggering or perpetuating storms per se, the relationship between synoptic-scale ascent and thunderstorm activity in the mid latitudes is well established, and this must be accounted for in the analysis. Doswell (1987), Moller (2001), and Schumann and Roebber (2010) note that synoptic-scale disturbances act to destabilize the atmosphere and weaken the capping lid through slow ascent, which favours the formation of widespread convection. Synoptic-scale systems have long been recognized as modulating thunderstorm activity over central and southern Alberta (e.g., Longley and Thompson 1965; Strong 1986; Smith and Yau 1993a,b).

Given the oftentimes rapid evolution of the upper-air field and the paucity of upper-air analyses (i.e., only available at 12 UTC and 00 UTC), we objectively quantified whether or not the synoptic-scale upper-air environment was favourable for thunderstorm activity by calculating the mean, area-averaged 500-mb daily omega from the NARR as

described in section 7.2.5. We applied a threshold of -1.0 μbar s^{-1} to identify days with organized and persistent ascent. This value is lower than that cited in the literature. For example, Wang et al. (2009b) used a threshold of -2 μbar s^{-1} for 600-mb velocity to track mid-tropospheric perturbations. Stensrud and Fritsch (1993) considered events associated with ascent of greater than -1 μbar s^{-1} to be "weakly forced". The difference in thresholds between this study and others is not surprising given that the value used here represents the mean of 25 grid points over a period of nine hours, whereas others have typically discussed instantaneous values at point locations.

Raddatz and Hanesiak (2008) investigated almost 1000 significant summer rainfall events (≥10 mm in 24 hours) on the Canadian Prairies from 2000 to 2004. They found that surface features play an important role in initiating and organizing thunderstorms in this region. In this study, we adopted a similar method to that of Raddatz and Hanesiak (2008) to identify surface features—a manual analysis of surface maps for each day. Specifically, 3-hrly maps between 18 UTC and 03 UTC of mass divergence, equivalent potential temperature (θ_e), streamlines and surface pressure were generated using the Plymouth State University Weather Centre interactive plotting tool. The maps were generated using all available surface observations, and then subjectively examined to identify robust surface features (e.g., fronts and troughs).

The surface and upper-air data described above were then combined on each day and classified into the following six classes using the decision tree shown in Fig. 7.2: High pressure or ridge; Surface forcing only; Upper-air forcing only; Surface or upper-air forcing; Surface and upper-air forcing, and Mesoscale.

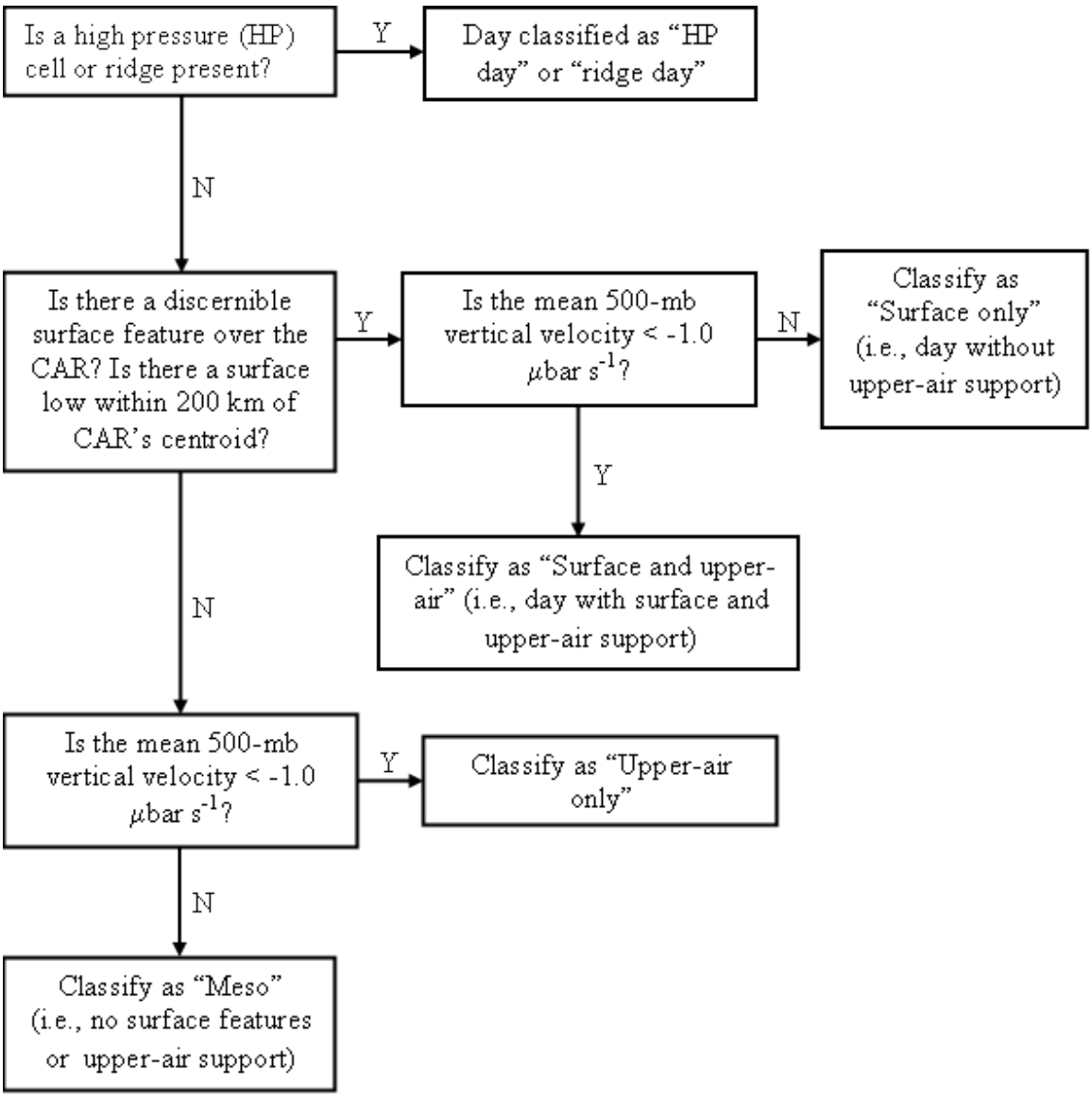

Figure 7.2: Decision tree used to classify the surface and upper-air pattern on each day. See text for details.

The mesoscale classification is defined as a day with no discernible surface features and with mean 500-mb ascent greater than -1.0 μbar s^{-1}. With the exception of surface lows and highs (the centres of which had to occur within 200 km of CAR11—see

Raddatz and Hanesiak (2008)), all other features had to have moved across or been situated over CAR11 at some point between 18 UTC and 03 UTC.

7.3 Response of lightning activity to synoptic-scale forcing

Recently, Brimelow et al. (2011) suggested that a positive feedback mechanism was evident during the summer months over drought-affected regions on the Canadian Prairies, with drought conditions leading to less lightning activity. They also noted that the relationship between NDVI and DUR increased significantly as both the area and magnitude of the dry anomaly increased. For CAR11 for the 33 summers months from 1999 through 2009, a statistically significant relationship was found between NDVI and DUR ($R^2 = 0.14$, $p = 0.03$). This R^2, albeit statistically significant, is relatively low, which suggests that other factors are at play in modulating DUR. Before discussing the role of vegetation vigour in modulating lightning activity over CAR11, we will first explore the relationship between synoptic-scale forcing (e.g., mean daily and monthly 500-mb vertical motion) and lightning activity over the study area.

7.3.1 Relationship between 500-mb ascent and DUR

As a first step towards elucidating the relationship between mean daily 500-mb vertical motion (ω_{500}) over CAR11 and the concomitant DUR, we examined the relationship between ω_{500} and DUR by partitioning the velocity for all days into two groups: $\omega_{500} < 0.0$ μbar s^{-1} (mean ascent) and $\omega_{500} > 0.0$ μbar s^{-1} (mean descent). Fifty percent of the days with mean ascent over CAR11 produced lightning. In contrast, only 23% of the days with mean descent over CAR11 produced lightning. Further partitioning of the lightning data according to ω_{500} revealed that 62% of days with marked upper-air

ascent (ω_{500} < -1.0 μbar s^{-1}) produced thunderstorms over CAR11, while 32% of days with intermediate vertical motion (-1.0 μbar s^{-1} < ω_{500} < +1.0 μbar s^{-1}) produced lightning. In contrast, only 16% with marked descent (ω_{500} > +1.0 μbar s^{-1}) produced lightning. Thus, a systematic increase in the likelihood of thunderstorms is evident as vertical ascent increases.

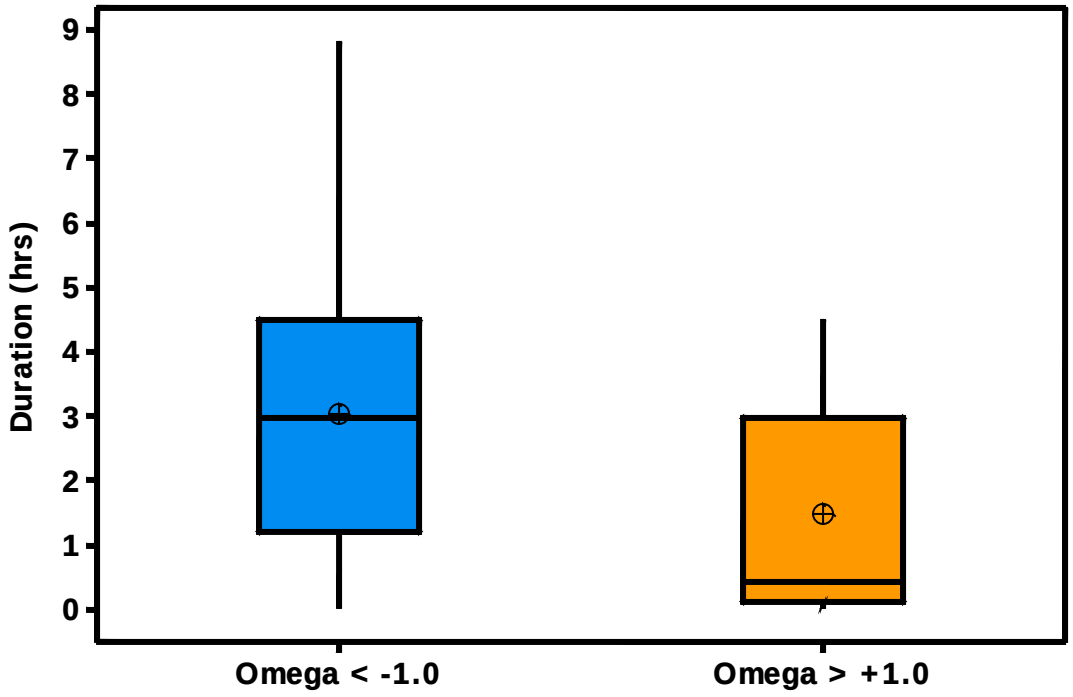

Figure 7.3: Duration over CAR11 for days with contrasting mean area-averaged ω_{500} (Omega) and when thunderstorms were observed. Cross hairs represent the mean.

Figure 7.3 shows the lightning duration over CAR11 for thunderstorm days having contrasting ω_{500}. Thunderstorm days occurring when there was marked mid-level ascent over CAR11 tended to be associated with more lightning activity (mean DUR of 3.0 hrs, with 95% confidence interval (CI) for the mean between 2.7 hrs and 3.4 hrs) than on days when storms developed when there was marked mid-level descent (mean DUR of 1.5 hrs,

with 95% CI for the mean between 0.7 hrs to 2.2 hrs). The mean DUR values for these two contrasting ω_{500} classes are different at the 99% confidence level. These data suggest that storms are longer-lived and/or more organized when they develop in an environment with favourable synoptic-scale conditions.

The R^2 between monthly ΔDUR and $\Delta\omega_{500}$ for 33 summer months was 0.187 ($p = 0.012$). The relationship was especially marked in July ($R^2 = 0.44$, $p = 0.03$) and June ($R^2 = 0.30$, $p = 0.08$), but virtually non-existent in August ($R^2 = 0.01$, $p = 0.806$). Hence, ω_{500} does explain a significant amount of variance of DUR for the 33 summer months considered, and especially in June and July combined ($R^2 = 0.37$, $p = 0.003$, $N = 22$).

7.3.2 Relationship between both surface and upper-air forcing and DUR

In section 7.3.1 we considered only mid-level vertical motion. As discussed earlier, however, surface features play an important role in triggering and organizing thunderstorms (e.g., Raddatz and Hanesiak 2008). Consequently, in order to further explore the relationship between DUR and synoptic-scale forcing, we studied the linkages between monthly DUR anomalies associated with the six forcing classes for the subset of 22 months referred to in section 7.2.7. The months included in this subset, and data for each month, are listed in Table 7.1.

Three metrics were then calculated for each forcing class and for both NDVI groups. The first metric is the mean DUR calculated for all days in the group, including days with no lightning.

Table 7.1: Summary of 22 summer months between 1999 and 2009 with contrasting ΔNDVI and/or ΔDUR. "Contrasting" means months having standardized NDVI and DUR anomalies of at least ± 0.5 (with weekly standardized NDVI anomalies for at least 15 days exceeding ± 0.5). Other standardized monthly anomalies are for: ω_{500} = NARR 500-mb vertical velocity; MCON = NARR 0-30 mb above-ground moisture flux convergence, LCL = Height of the LCL from Stony Plain soundings, MH = Mixing height from soundings, r_{50} = Mean mixing ratio in lowest 50-mb above ground from soundings, and $\Gamma_{850\text{-}700}$ = Lapse rate between 850 mb and 700 mb. See text for more details. Here negative standardized anomalies for ω_{500}, MCON and $\Gamma_{850\text{-}700}$ represent above-average ascent, stronger than average moisture flux divergence and a stronger lapse rate between 850 mb and 700 mb, respectively.

Month	ΔNDVI	ΔDUR	Δ ω_{500}	ΔMCON	ΔLCL	ΔMH	Δ r_{50}	Δ$\Gamma_{850\text{-}700}$
June 2001	-0.92	+0.83	+0.53	+1.18	-0.77	-0.86	+0.02	+0.40
June 2002	-1.64	-0.91	+0.89	+0.08	+1.41	+1.85	-0.46	-1.40
June 2004	-0.18	-1.29	+0.43	+0.02	+0.29	-0.36	-0.24	+0.17
June 2005	+1.55	+0.81	-0.77	-0.12	-1.63	-1.03	+1.35	+1.53
June 2006	+0.90	-1.48	+1.17	-0.70	+0.32	+0.66	+0.96	-0.10
June 2007	+0.88	+1.46	-0.20	+2.05	-1.11	-0.80	+1.30	+1.18
June 2008	+0.54	+0.97	-2.30	-1.71	-0.30	+0.53	+0.40	0.00
June 2009	-1.39	-0.24	-0.17	-0.73	+1.64	+0.89	-1.93	-1.23
July 2000	+0.22	+1.91	-1.12	-0.28	-1.39	-1.15	+0.92	+0.94
July 2001	-0.16	+0.96	-2.12	+0.16	-0.51	-0.41	-0.14	+0.96
July 2002	-2.22	-1.13	+1.37	+1.34	+2.01	+1.54	-0.81	-1.89
July 2005	+1.35	-0.05	+0.84	-0.87	-0.46	-1.01	-0.50	-0.30
July 2007	+0.97	-1.02	+1.08	-0.23	+0.02	-0.32	+1.79	+0.29
July 2008	+0.74	+0.87	-0.06	-1.34	-0.29	+0.06	-0.36	-0.31

Table 7.1 continued

July 2009	-1.18	-1.35	-0.46	-0.34	-0.04	+0.06	-0.42	+0.68
August 1999	+1.35	+2.81	-0.24	+0.71	-0.31	-1.13	+1.79	+0.40
August 2001	+0.96	-0.64	+1.04	-1.26	+0.53	-1.35	+0.68	-1.30
August 2003	-1.52	-0.29	+0.84	+2.47	+1.13	+0.04	+0.59	+0.27
August 2005	+1.47	-0.48	+0.12	-0.39	+0.06	+0.22	-0.90	+0.16
August 2007	+0.58	-0.04	-1.60	-0.61	-1.89	-1.02	+0.31	+1.36
August 2008	-0.35	-0.81	-0.34	+0.34	+0.28	+0.85	+0.34	-0.10
August 2009	-1.25	-0.18	+0.17	-0.98	+0.52	0.00	-1.07	+0.39

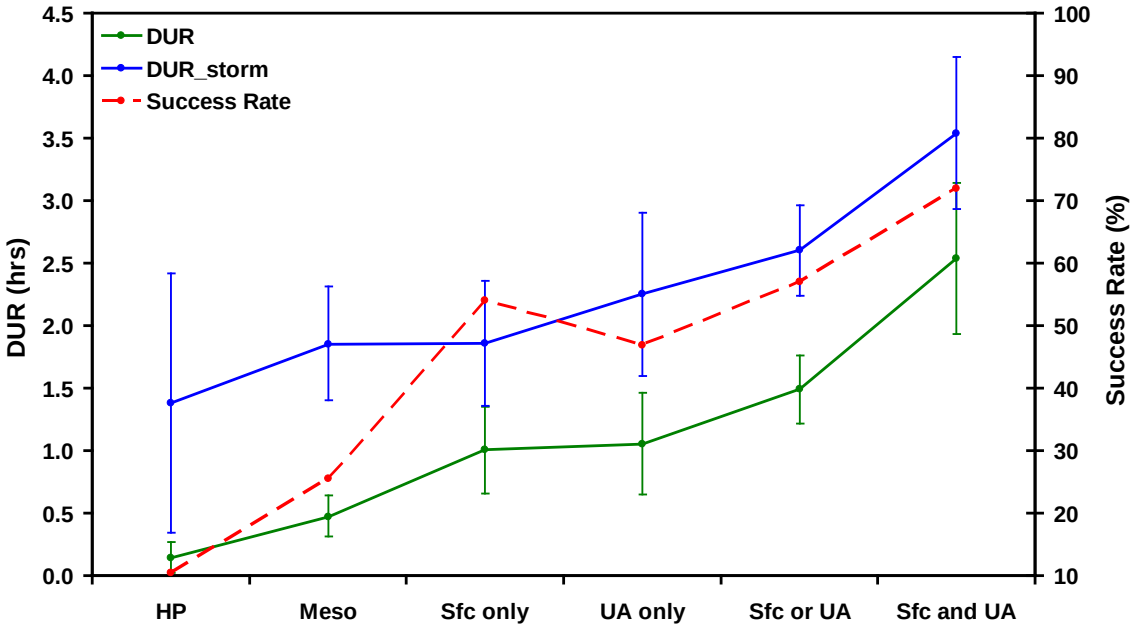

Figure 7.4: DUR (solid green), success rate (dashed red) and DUR on storm days (solid blue) for various forcing classes identified using the decision tree in Fig. 7.2. Error bars for the DUR data represent the 95% confidence interval of the class mean.

The second metric is the "success rate", which refers to the percentage of days in a given class that produced lightning over CAR11. The third metric is the mean DUR for only those days in each class that produced lightning.

Figure 7.4 shows the lowest mean DUR was observed for days in the "HP" class, with the longest mean duration observed for days in the "Surface and upper-air" class. That is, the most lightning was typically observed on days when a discernible surface feature was evident in tandem with mid-tropospheric ascent. Two-sample t-tests indicated that the difference in mean DUR between adjacent classes was statistically

significant (90% confidence level), but not between the "Surface only" and "Upper-air only" classes.

A similar pattern is evident for the mean DUR on storm days, with DUR increasing from 1.4 hrs for the "HP" class to 3.5 hrs for the "Surface and upper-air" class. Unlike the mean DUR for all days, the differences in mean DUR between adjacent classes for storm days were not statistically significant at the 90% confidence level, with one exception: between the "Surface or upper-air" and "Surface and upper-air" classes. The difference in DUR for storm days was also statistically significant between "Surface and upper-air" and "Upper-air only" classes (99% confidence level). The difference in mean DUR on storm days between "Meso" and "HP", "Upper-air only" and "Surface only", and "Upper-air or surface" and "Upper-air only" classes were statistically different at only the 80% level of confidence. The smaller sample sizes in each class for storm days (i.e., days with lightning) made distinguishing between class means difficult.

Figure 7.4 also shows that the success rate increases as one progresses from "HP" class (about 10%) to "Surface and upper-air" class (72%). Proportion tests between adjacent classes determined that, with one exception, the differences in success rate were statistically significant at least at the 90% confidence level. There is little difference in DUR between the "surface only" and "upper-air only" classes. Days classified as "Surface only" did have a higher success rate than days classified as "Upper-air only", but this difference was only statistically significant at the 80% confidence level. These results suggest that surface features are more likely to initiate and perpetuate storms than upper-air features alone, and that surface and upper-air features acting in concert are especially effective at initiating and organizing thunderstorms.

7.3.3 Isolating the impact of NDVI on DUR

In previous sections, we demonstrated that synoptic-scale forcing notably affects lightning activity over CAR11. Given the importance of forcing, any potential signal from NDVI could be swamped by strong synoptic forcing. Consequently, extracting a signal from the contribution (if any) of vegetation vigour to DUR is difficult.

To address this we looked at the surface and upper-air forcing for the subset of 22 months with contrasting DUR and NDVI. Specifically, we considered the response of DUR on days with similar synoptic forcing, but occurring during weeks with contrasting NDVI conditions ($+0.5 \leq NDVI \leq -0.5$). For example, all days classified as "mesoscale" were cross-referenced with the weekly NDVI anomalies for CAR11. If a day was classified as "mesoscale" and occurred during a week when NDVI was ≤ -0.5, it was grouped into the much below average class (MBA). Similarly, those days classified as "mesoscale" which were observed during weeks when NDVI was $\geq +0.5$ were added to the much above average class (MAA; Table 7.2).

Table 7.2: Lightning metrics by forcing class for contrasting NDVI conditions. MAA refers to MAA NDVI ($\Delta NDVI > +0.5$), and MBA refers to MBA NDVI ($\Delta NDVI < -0.5$). N refers to sample sizes for each class.

JJA	MBA N	MAA N	Mean DUR (all days)		Success rate (%)		Mean DUR (storm days)	
			MBA	MAA	MBA	MAA	MBA	MAA
High/Ridge	50	74	0.09	0.18	0.14	0.08	0.64	2.24
Mesoscale	82	106	0.32	0.59	0.24	0.26	1.31	2.24
Surface only	33	41	0.94	1.06	0.55	0.54	1.77	1.97
Upper-air only	25	39	0.94	1.13	0.52	0.44	1.80	2.59
Surface or upper-air	82	116	1.34	1.60	0.57	0.57	2.33	2.79
Surface and upper-air	24	36	2.30	2.70	0.67	0.75	3.14	3.60

In this way, the effect of synoptic forcing was minimized thereby allowing us to focus on the response, if any, of the lightning to changes in antecedent vegetation vigour. Two-sample t-tests and 2-sample proportion tests were used to determine whether differences between the lightning metrics for the same classes (but contrasting NDVI) were statistically significant.

As was observed in section 7.3.2, a systematic increase in mean DUR, success rate and mean DUR on storm days is seen as the forcing becomes more organized (Table 7.2). This was true regardless of the vegetation vigour. Statistical tests found that the differences for mean DUR for contrasting vegetation vigour were statistically different for days classified as "Mesoscale" ($p = 0.042$ or >95% confidence) and as "Surface or upper-air" ($p = 0.171$ or >80% confidence). The differences were more marked when considering the mean DUR on storm days only, with statistically significant differences obtained for the "Mesoscale" class ($p = 0.018$ or >95% confidence), "Upper-air only" ($p = 0.107$) and "Surface or upper-air" ($p = 0.110$, almost 90% confidence). The success rate when NDVI was much above average was higher than when NDVI was much below average for only the "Mesoscale" and "Surface or upper-air " classes, with the difference being statistically different for only the "Surface or upper-air" class.

This analysis suggests that longer DUR can be expected when storms develop on days when NDVI is much above average than on days having similar synoptic-scale forcing, but with much below NDVI. Also, the data suggest that on days when a surface or upper-air feature is present, storms are more likely to be triggered and longer-lived when NDVI over CAR11 is much above average, compared to when NDVI is much below average.

7.3.4 Overview of impact on forcing and NDVI on DUR

The interplay between mid-tropospheric synoptic-scale ascent and NDVI anomalies on DUR over CAR11 for 33 summer months from 1999 through 2009 can be visualized using a surface map as shown in Fig. 7.5.

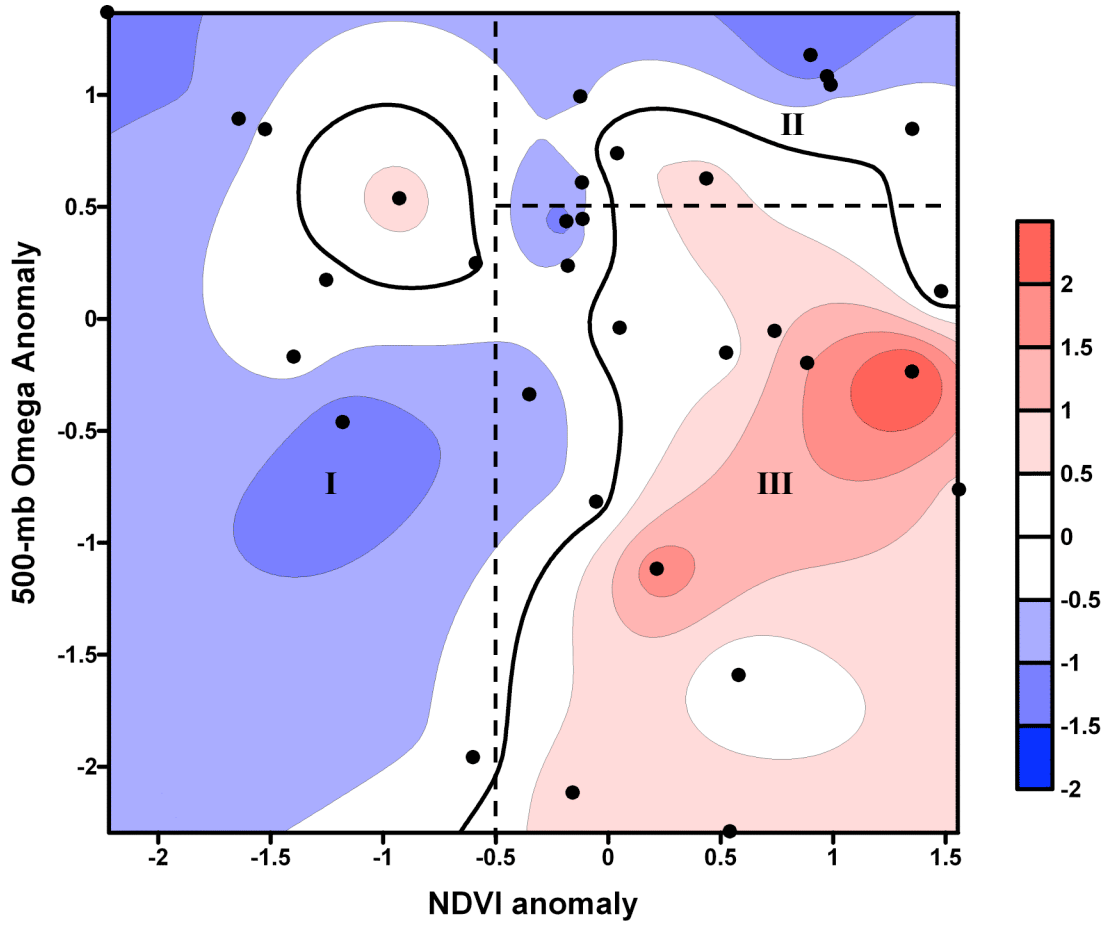

Figure 7.5: Monthly ΔDUR (shading) as a function of ΔNDVI and $\Delta\omega_{500}$ (standardized monthly 500-mb omega anomalies). Black dots represent individual data points for each of the 33 summer months. Dashed lines delineate the three zones discussed in the text. Data were interpolated using a Kriging scheme.

Several features are evident, in particular, the parameter space may be roughly divided into three zones as indicated by the dashed lines:

- **Zone I:** Below-average ΔDUR (< -0.5) is typically observed when ΔNDVI < -0.5, even when the mid-tropospheric ascent is above average (< 0.0).
- **Zone II:** If the forcing is relatively weak (> +0.5), then ΔDUR is unlikely to be below average even if ΔNDVI is much above average (> +1.0).
- **Zone III:** If ΔNDVI is above average and vertical motion is favourable ($\Delta\omega_{500}$ < +0.5), then ΔDUR is highly likely to be above average.

The positive slope of the +0.5 ΔDUR contour suggests that the ascent required to produce above-average DUR increases as NDVI decreases. But we do not have sufficient data to support that hypothesis, because even considering data for all summer months available we were unable to sample the entire NDVI-Omega-DUR parameter space. A couple of months in Fig. 7.5 are clearly outliers, and inspection of data from Table 7.1 sheds some light as to why this might be. It should be noted that for the 33 months considered here, MCON was poorly correlated with DUR and with low-level moisture, and barely statistically significantly correlated with monthly NDVI. Nevertheless, MCON does explain some of the discrepancies. For example, June 2001 had near normal ascent at 500 mb and below-average NDVI, yet DUR was much above average. This may, in part, have been attributed to the strong moisture flux *convergence*, which despite the stressed vegetation, led to near-normal low-level mixing ratios. The combination of resultant lower cloud base heights, and near-normal ascent, may explain the above-average DUR.

7.4. Relationship between sounding data, NDVI and DUR

In this section, we explore relationships between monthly standardized anomalies of sounding parameters derived from 00 UTC Stony Plain soundings and the concomitant standardized anomalies of NDVI and DUR over CAR11. We will focus on eight sounding-derived variables that are significantly correlated with *both* NDVI and DUR. The rationale being to investigate the mechanisms by which anomalies in NDVI could affect the sounding structure in the low levels, which could, in turn, affect thunderstorm activity.

Of the parameters summarized in Table 7.3, three (Td_{850}, r_{50}, T_{dsfc}) represent low-level moisture, two ($\Gamma_{850\text{-}700}$ and MH) represent low-level lapse rates, two (LCL and CCL) represent the integrated affects of low-level moisture and temperature, and one (T_{con}) represents the affects of low-level moisture and low-level lapse rates. Table 7.3 indicates that for all Junes, Julys and Augusts combined, the strongest relationships were between ΔLCL (and ΔMH) and both ΔNDVI and ΔDUR. The weakest relationships, although still statistically significant, were for ΔTd_{850} and ΔT_{con} and ΔNDVI and ΔDUR. When the relationships for individual months are examined (Table 7.4), August showed no statistically significant correlations between most sounding parameters and ΔNDVI. Only the low-level moisture variables (Td_{850}, r_{50} and Td_{sfc}) were positively correlated with ΔDUR at statistically significant levels in August.

Table 7.3: Comparison of R^2 between standardized anomalies of selected sounding variables (from 00 UTC WSE soundings) and standardized anomalies of NDVI and DUR over CAR 11 in Alberta for different subsets of data. JJ refers to all Junes and Julys combined; JA is all Julys and Augusts combined; J, J, A is all Junes, Julys and Augusts (33 months) combined; and JJA is July through August for each of the 11 years. R^2 values with one asterisk are significant at the 90% level of confidence, those with two asterisks are significant at the 95% level, and those with three are significant at the 99% level. CCL = Convective Condensation Height; LCL = Lifted Condensation Level; MH =Mixing Height; Td_{sfc} = Surface dew-point, Td_{850}= Dew-point at 850 mb; T_convect = Convective temperature; r_{50}= Mean mixing ratio at 50 mb above ground level; $\Gamma_{850\text{-}700}$ = Lapse rate between 850 mb and 500 mb.

	JJ	**N=22**	**J,J,A**	**N=33**	**JA**	**N=22**	**JJA**	**N=11**
Sounding variable	**ΔNDVI**	**ΔDUR**	**ΔNDVI**	**ΔDUR**	**ΔNDVI**	**ΔDUR**	**ΔNDVI**	**ΔDUR**
ΔCCL (m)	0.453^{***}	0.446^{***}	0.314^{***}	0.204^{***}	0.216^{**}	0.133^{*}	0.550^{***}	0.380^{**}
ΔLCL (m)	0.438^{***}	0.476^{***}	0.319^{***}	0.314^{***}	0.218^{**}	0.237^{**}	0.563^{***}	0.524^{**}
ΔMH (m)	0.338^{***}	0.379^{***}	0.286^{***}	0.321^{***}	0.256^{**}	0.254^{**}	0.371^{**}	0.591^{***}
ΔTd_{sfc} (°C)	0.357^{***}	0.070	0.296^{***}	0.137^{**}	0.169^{*}	0.144	0.422^{**}	0.153
ΔTd_{850} (°C)	0.160^{*}	0.025	0.092^{*}	0.089^{*}	0.005	0.081	0.130	0.000
Δr_{50} (g kg^{-1})	0.254^{**}	0.043	0.200^{***}	0.120^{**}	0.085	0.129^{*}	0.211	0.037
$\Delta T_{convect}$ (°C)	0.124	0.354^{***}	0.088^{*}	0.103^{*}	0.068	0.033	0.322^{*}	0.472^{*}
$\Delta\Gamma_{850\text{-}700}$ (°C km^{-1})	0.297^{***}	0.278^{**}	0.144^{**}	0.213^{***}	0.042	0.162^{*}	0.046	0.028

Table 7.4: Same as Table 7.3, except for individual months.

	June		July		August	
Sounding variable	**ΔNDVI**	**ΔDUR**	**ΔNDVI**	**ΔDUR**	**ΔNDVI**	**ΔDUR**
ΔCCL (m)	0.563***	0.390**	0.355*	0.506**	0.112	0.000
ΔLCL (m)	0.579***	0.499**	0.318*	0.454**	0.137	0.090
ΔMH (m)	0.350*	0.476**	0.325*	0.293*	0.194	0.218
ΔTd_{sfc} (°C)	0.655***	0.123	0.148	0.031	0.191	0.341*
ΔTd_{850} (°C)	0.587***	0.107	0.003	0.000	0.012	0.340*
Δr_{50} (g kg^{-1})	0.577***	0.103	0.061	0.009	0.113	0.389**
$\Delta T_{convect}$ (°C)	0.136	0.361	0.113	0.347*	0.034	0.051
$\Delta\Gamma_{850\text{-}700}$ (°C km^{-1})	0.528**	0.334*	0.133	0.226	0.002	0.109

Figure 7.6 shows the relationship between ΔNDVI and ΔLCL, and between ΔLCL and ΔDUR for 33 summer months at Stony Plain. ΔLCL and ΔNDVI were negatively correlated, with LCL heights decreasing as NDVI increased. The relationship between ΔLCL and ΔDUR was also negative, with DUR increasing as the LCL heights decreased. This is consistent with the findings made by Peppler and Lamb (1993), who found that area-averaged rainfall and LCL heights calculated from Stony Plain sounding data were negatively correlated for May through August for the three years considered in their study.

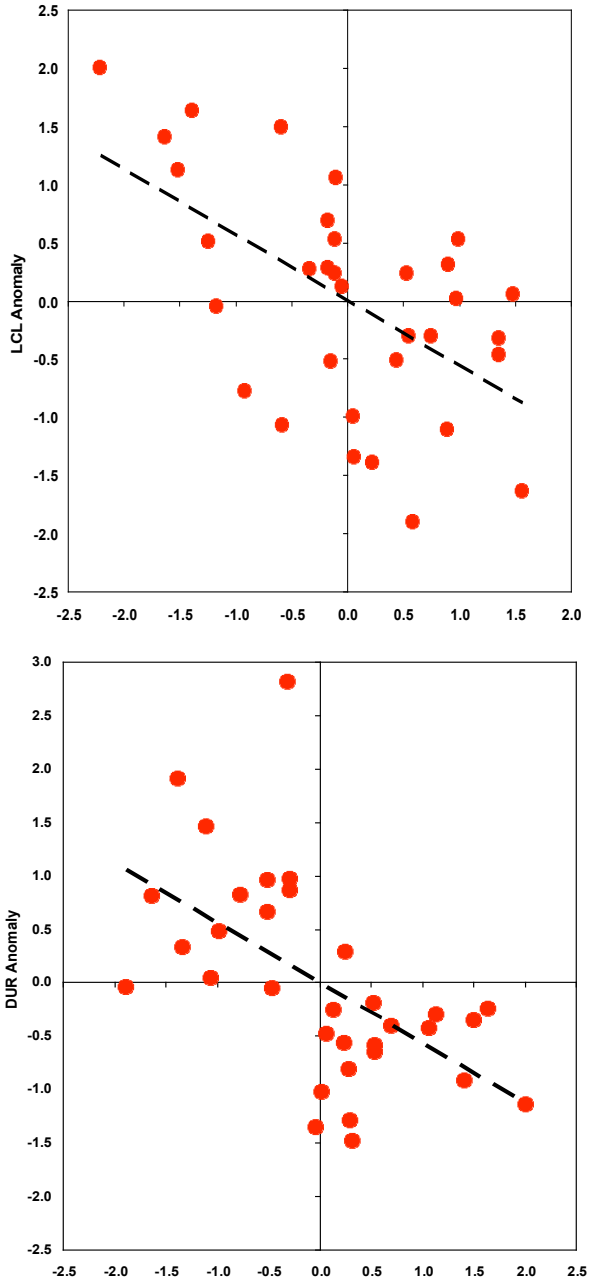

Figure 7.6: Scatter plots of ΔNDVI versus ΔLCL, and between ΔLCL and DUR for 33 summer months from 1999 to 2009 over CAR11.

The above relationship between ΔNDVI and ΔLCL is intuitive, because ΔNDVI is also positively correlated with low-level moisture (Table 7.5). This suggests that the

increase in LCL heights with decreasing vegetation vigour is occurring primarily in response to a decrease in low-level moisture, which is in turn related to decreased ET from drier soils and sparser vegetation.

Table 7.5: Sign of correlation between monthly standardized anomalies of sounding variables and ΔNDVI and ΔDUR for 33 summer months from 1999 to 2009 over CAR11.

Sounding variable	versus ΔNDVI	versus ΔDUR
ΔCCL (m)	Negative	Negative
ΔLCL (m)	Negative	Negative
ΔMH (m)	Negative	Negative
ΔTd_{sfc} (°C)	Positive	Positive
ΔTd_{850} (°C)	Positive	Positive
$\Delta T_{convect}$ (°C)	Negative	Negative
Δr_{50} (g kg^{-1})	Positive	Positive
$\Delta\Gamma_{850\text{-}700}$ (°C km^{-1})	Positive	Positive

This is supported by the statistically significant relationship between ΔNDVI over CAR11 and standardized anomalies of monthly accumulated ET at Edmonton International airport (~30 km southeast of Stony Plain) from 1999 to 2005. Monthly ET totals were calculated from daily output from the Second Generation Prairie Agrometeorological Model (PAMII; see Raddatz 1993). Brimelow et al. 2010a,b validated PAMII against in-situ observations and found it successfully captured the inter- and intra-annual variability in soil moisture and ET. For the period 1999 through 2005, the R^2 between ΔNDVI and ΔET was 0.334 ($p = 0.006$, $N = 21$), which indicates that ΔNDVI and ΔET are closely related. A statistically significant correlation ($R^2 = 0.58$; $p = 0.000$) was also found between ΔNDVI and ΔET for summers between 1999 and 2004

using data for 12 CARs having equivalent radii of 75 km or more (data provided by Rick Raddatz).

All three low-level moisture variables are positively correlated with ΔNDVI, which is consistent with the relationship between NDVI and ET discussed above. Namely, decreased vegetation vigour is associated with lower ET (i.e., latent heat flux) into the CBL. The moisture variables are in turn all positively correlated with ΔDUR, with lower low-level moisture typically associated with decreased thunderstorm activity (i.e., DUR). This is expected given that low-level moisture is a necessary condition for thunderstorms.

The relationship between ΔMH and ΔNDVI is negative, suggesting that as vegetation vigour decreases, MH increases (i.e., deeper CBL). MH is also negatively correlated with DUR (not shown), suggesting that a deeper CBL over this region is typically unfavourable for thunderstorm activity. MH is positively correlated with low-level moisture parameters, which suggests that low vegetation vigour results in a deeper, drier CBL on account of a higher sensible heat flux. The relationships between ΔNDVI and both ΔCCL height and T_{con} are also negative. This reflects the higher T_{con} and increasing CCL height with decreasing vegetation vigour. These particular changes in T_{con} and CCL height are likely being modulated by decreases in low-level moisture associated with reduced vegetation vigour and concomitant ET. CCL height and T_{con} are also both negatively correlated with DUR. Specifically, as T_{con} increases, DUR typically decreases. This is not surprising as higher convective temperatures make it increasingly unlikely that solar heating alone will provide sufficient lift to initiate storms.

$\Gamma_{850\text{-}700}$ is positively correlated with both ΔNDVI and ΔDUR, with $\Gamma_{850\text{-}700}$ increasing as vegetation vigour decreases. This is consistent with a deeper and warmer CBL

observed on account of increased sensible heat flux associated with below-average NDVI. The positive correlation between lapse rate and DUR suggests that, in this region, as the 850-700 mb lapse rate increases, DUR decreases. While weaker lapse rates being associated with greater DUR may seem counterintuitive, this may suggest that, on average over CAR11 a shallower (but moister) CBL is more likely to support thunderstorms than is a deeper, drier CBL.

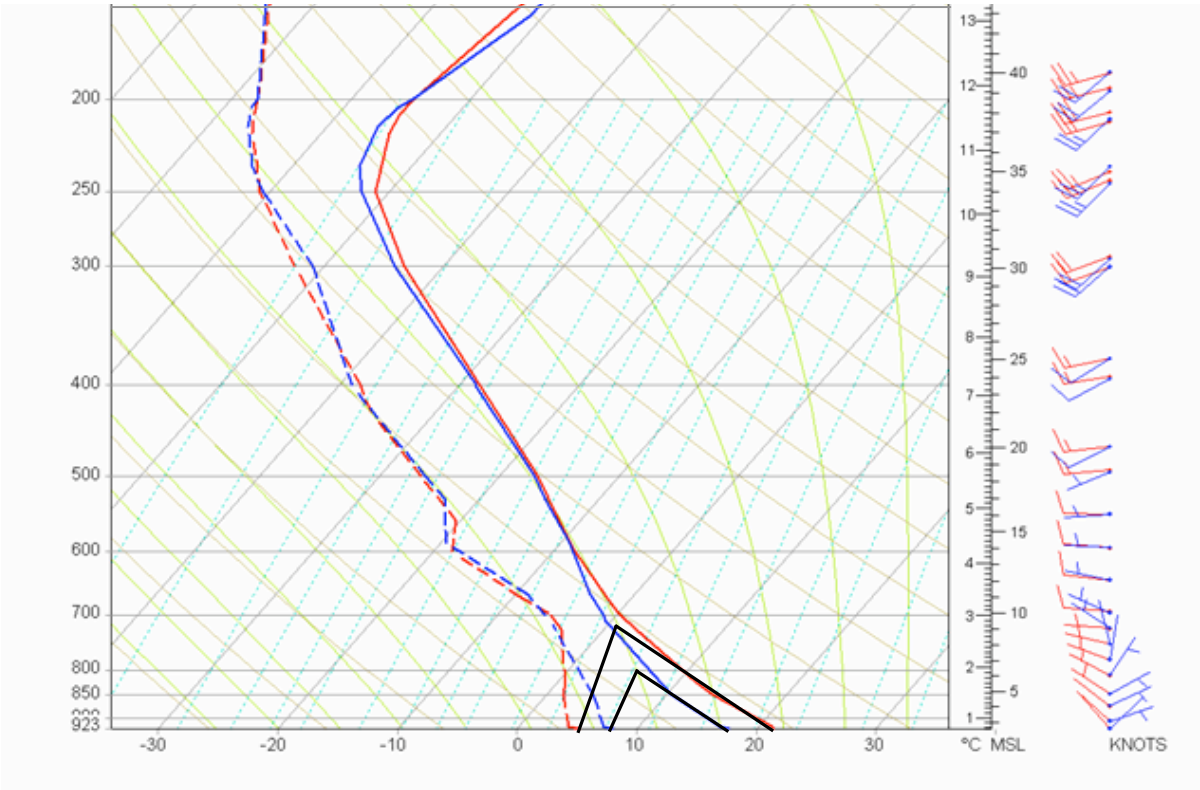

Figure 7.7: Composite soundings for Stony Plain in June 2002 (red lines), when CAR11 was experiencing drought conditions, and in June 2005 (blue lines), when CAR11 was experiencing pluvial conditions.

The composite sounding in Fig. 7.7 for two contrasting June months demonstrates the above relationships. In 2002, drought conditions were present over CAR11 (ΔNDVI = -1.6), with much below-average lightning duration (ΔDUR = -0.9). In 2005, pluvial conditions were observed over (NDVI = +1.6), with much above-average duration (ΔDUR = +0.8). The LCL height for the 2002 composite sounding was much higher at 2783 m above ground level (at 2 °C), compared to 1974 m (at 6 °C) in 2005. The mean mixing ratio in the lowest 50 mb in 2002 was 5.5 g kg^{-1}, compared to 6.6 g kg^{-1} in 2005. The mean root-zone soil moisture in June 2005 (as predicted by the PAMII model) for Edmonton International was 71%, with a predicted accumulated monthly ET of 54 mm. In contrast, in June 2002, the mean root-zone soil moisture was 32%, with a predicted accumulated monthly ET of 41 mm (about 25% less than in 2005).

Figure 7.7 shows that mean low-level winds in 2005 were upslope, while in 2002 mean winds were alongslope (i.e., northwesterly). It is known that upslope winds in this region typically result in the pooling of moisture along the foothills (e.g., Strong 1986); so it is possible that (in contrast to 2002) the upslope flow in 2005 was partly responsible for increasing the depth of moisture in the CBL over CAR11. However, the monthly means of 0-30 mb (above ground) moisture flux convergence (from NARR) over CAR11 from Table 7.1 for June 2002 and for June 2005 were very similar at -1.49E10^{-08} s^{-1} and -1.81E10^{-08} s^{-1}, respectively. So the NARR data indicate that moisture flux *divergence* of similar magnitude was present over CAR11 for both months. Another clue that differences in CBL moisture in Fig. 7.7 were not primarily the result of advection is that the moisture traces only diverge within the CBL (below about 800 mb), with the greatest differences being observed at the surface.

Hence, moisture advection was unlikely the primary reason for the differences in low-level moisture. Rather, NDVI data and ET data (from PAMII) suggest that reduced latent heat flux (and higher sensible heat flux) on account of the low soil moisture and stressed vegetation were largely responsible for the deeper, warmer and drier boundary layer in 2002. All things being equal (e.g., similar synoptic-scale forcing), the drier and warmer CBL in June 2002 would have limited thunderstorm activity compared to June 2005. In fact, considering days with "Surface or upper-air forcing", the mean daily DUR for storm days in June 2002 was 2.1 hrs compared to 2.8 hrs in 2005. The success rate in 2005 was 73% compared to 60% in 2002.

Brimelow et al. (2011) indicated an asymmetric relationship between ΔNDVI and ΔDUR for CARs on the Canadian Prairies, with positive ΔNDVI not a sufficient condition for above-average lightning duration. Our results here corroborate this, with months with below-average NDVI typically associated with below-average DUR, while the opposite was not necessarily true when NDVI was above average. Specifically, R^2 between ΔNDVI and ΔDUR for months having much below-average NDVI was 0.306 ($p = 0.12$, $N = 9$), while R^2 between ΔNDVI and ΔDUR for months having much above-average NDVI was 0.001 ($p = 0.77$, $N = 12$).

To investigate the nature of the asymmetric response of DUR to NDVI, sounding parameters to contrasting vegetation vigour were calculated R^2 between standardized anomalies of selected sounding variables (from 00 UTC Stony Plain soundings) and standardized anomalies of NDVI and DUR over CAR 11 for months having contrasting NDVI.

Table 7.6: Comparison of R^2 between standardized anomalies of selected sounding variables and standardized anomalies of NDVI and DUR over CAR 11 in Alberta for months having below average NDVI (ΔNDVI < 0.0) and above average NDVI (ΔNDVI > 0.0). Asterisks have the same meanings as in Table 7.3.

	ΔNDVI < 0.0 (N=17)		**ΔNDVI > 0.0 (N=16)**	
Sounding Parameter	**NDVI**	**DUR**	**NDVI**	**DUR**
ΔCCL (m)	0.390***	0.190*	0.090	0.044
ΔLCL (m)	0.250**	0.230*	0.077	0.174*
ΔMH (m)	0.018	0.210*	0.003	0.219*
ΔTd_{sfc} (°C)	0.176*	0.115	0.008	0.013
ΔT_{sfc} (°C)	0.105	0.214*	0.040	0.037
ΔTd_{850} (°C)	0.110	0.001	0.027	0.052
Δr_{50} (g kg^{-1})	0.057	0.010	0.001	0.038
$\Delta T_{convect}$ (°C)	0.193*	0.158	0.036	0.026
$\Delta\Gamma_{850\text{-}700}$ (°C km^{-1})	0.047	0.128	0.066	0.135

Table 7.6 summarizes the correlations for months ranked by ΔNDVI grouped according to whether NDVI was greater or less than 0.0; this threshold was applied to increase the sample size. For below-average ΔNDVI, both ΔCCL and ΔLCL were correlated with ΔNDVI and ΔDUR at the 90% confidence level, while ΔTd_{sfc} was correlated with ΔNDVI at the 90% confidence level, but was not so with ΔDUR. ΔT_{con} was statistically significantly correlated with ΔNDVI, and with ΔDUR at marginally statistically significant levels (p = 0.115). In contrast, when NDVI was above average, only ΔLCL and ΔMH were correlated with DUR at the 90% confidence level. Clearly the coupling between the surface condition, sounding parameters and lightning activity is not robust when NDVI is above average.

7.4.2 Regression models

4.2 Regression models

Here we investigate the impact of using different combinations of selected sounding parameters and mid-tropospheric ascent on the variance explained in DUR. The coefficients of determination for multiple linear regression models for all 33 months are shown in Table 7.7. Results are also shown for the subset of 22 months to assess the impact of including information about the surface synoptic-scale forcing. Because ΔLCL and $\Delta\Gamma_{850\text{-}700,}$ ΔLCL and ΔMH, and ΔMH and $\Delta\Gamma_{850\text{-}700}$ were strongly correlated, regression models were run using only one of the variables from each pair to avoid introducing redundancy. The R^2 between the number of days per month with surface or upper-air forcing (∑SUA) and ω_{500} (< -1 μbars^{-1}) was 0.64.

Table 7.7: Coefficients of determination (R^2) for various multiple linear regression models. When more than one predictor was used, the adjusted R^2 (R^2_{adj}) is provided. "Plus" symbols indicate which variables (i.e., predictors) were used in the correlation. The bottom half of the table indicates which variables were used for the subset of 22 months.

ΔNDVI	$\Delta\omega_{500}$	$\Delta\Gamma_{850\text{-}700}$	ΔLCL	∑SUA	R^2 versus ΔDUR (33 months)	R^2 versus ΔDUR (22 months)
+					0.142 (0.031)	0.133 (0.095)
	+				0.186 (0.012)	0.269 (0.013)
		+			0.212 (0.007)	0.202 (0.036)
			+		0.314 (0.001)	0.317 (0.006)
+	+				0.249 (0.005)	0.272(0.019)
	+		+		0.343 (0.001)	0.314 (0.011)
+		+			0.211 (0.011)	0.159 (0.074)
	+	+			0.261 (0.004)	0.240 (0.029)
				+	N/A	0.361 (0.003)
+				+	N/A	0.396 (0.003)
			+	+	N/A	0.394 (0.006)
		+		+	N/A	0.307 (0.012)

NDVI was not correlated with ω_{500} or $\sum$SUA. ΔLCL (which implicitly includes the impact of low-level moisture) and $\Delta\omega_{500}$ together explain most of the variance in DUR, which underscores the importance of synoptic-lift and moisture for thunderstorm activity. The variance in ΔDUR explained using ΔNDVI and $\Delta\omega_{500}$ is virtually the same as that explained using $\Delta Td_{\_sfc}$ and $\Delta\omega_{500}$ or Δr_{50} and $\Delta\omega_{500}$. These results suggest that NDVI is a suitable proxy for low-level moisture. The relationships between sounding variables and DUR for the subset of 22 months were very similar to those for all 33 months. The most noticeable difference is that including information about the surface features ($\sum$SUA) increases the variance in DUR explained over using 500-mb ascent alone. Using ΔMH and $\sum$SUA explains the most variance in ΔDUR.

7.5. Conceptual model and discussion

The relationships between synoptic-scale forcing, NDVI, CBL characteristics and DUR discussed in previous sections can be summarized in the conceptual model shown in Fig. 7.8. In our conceptual model, we assume that large-scale forcing initially results in a significant precipitation deficit that in turn results in stressed vegetation and reduced vegetation vigour. Liu et al. (2004) studied the moisture transport and upper-air circulation patterns for the 2000–2001 drought over the Canadian Prairies. They noted that during summer drought, moisture transport from the Gulf of Mexico was reduced on account of a persistent upper-air blocking, and that attendant large-scale subsidence lowered precipitation. Several studies have demonstrated that NDVI responds to changes in root-zone soil moisture (e.g., Adegoke and Carleton 2002), and that soil moisture responds to precipitation anomalies (e.g., Dirmeyer 2006).

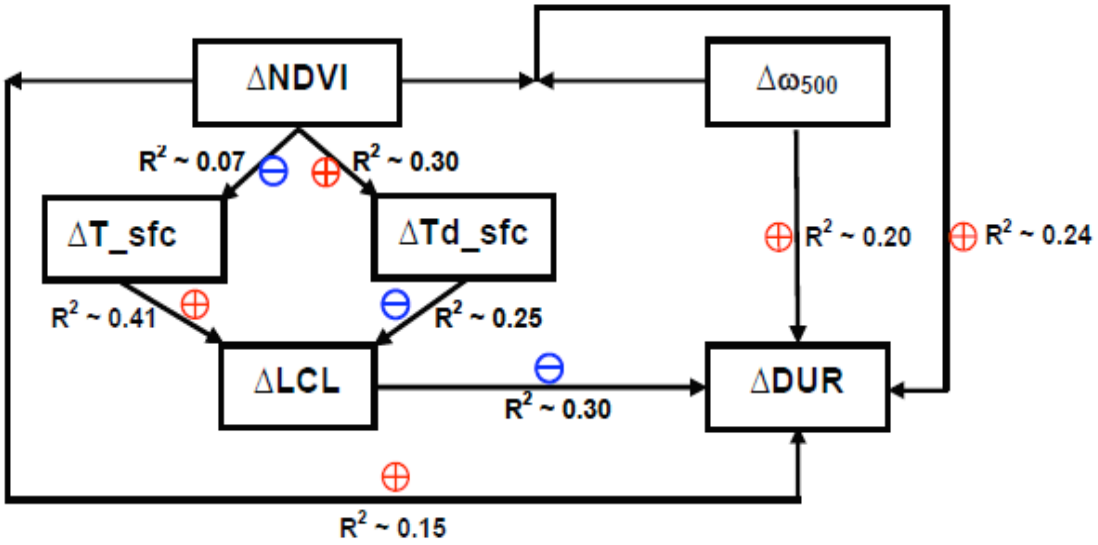

Figure 7.8: Conceptual model describing the relationships between NDVI, synoptic-scale forcing, CBL characteristics and DUR over CAR11. Red cross-hair symbols represent a positive correlation, and blue cross-hair symbols represent a negative correlation.

Studies have shown that changes in vegetation (i.e., NDVI) in response to soil moisture anomalies can have a marked effect on the partitioning of available energy (e.g., Liu et al. 2006), which in turn affects the structure (and moisture content) of the CBL (e.g., Basara and Crawford 2000; Taylor et al. 2009).

As shown in Fig. 7.8, our analysis of sounding, NDVI and soil-moisture data indicates that a reduction in vegetation vigour — in response to soil moisture deficits — modulates the partitioning of available energy into sensible and latent heat fluxes at the surface. Under such conditions, the latent heat flux is reduced while the sensible heat flux is increased, thereby causing higher surface temperatures and lower moisture in the CBL. These factors combined then result in a warmer, drier and deeper CBL, with steeper low-level lapse rates. Additionally, the higher temperatures and lower near-surface moisture increase the height of the LCL. This acts to lower moist static energy,

lower the in-cloud liquid water content of clouds, and also potentially increases the evaporation of any precipitation below cloud base (e.g., Yamada 2008). Together, these factors ultimately result in a positive feedback between vegetation vigour and DUR. We have demonstrated that ΔNDVI is positively correlated with low-level moisture, which suggests that the increase in LCL heights with decreasing vegetation vigour is occurring primarily in response to a decrease in low-level moisture, which is in turn related to decreased evapotranspiration from drier soils and sparser vegetation. It should be noted that the CCL heights were also strongly correlated with both NDVI and DUR — that is, the CCL strongly reflected changes in vegetation vigour and explained a significant amount of variation in DUR. For this reason, the CCL height could potentially be substituted for LCL heights in the conceptual model. In the end we decided upon LCL because it had a higher correlation with DUR than did CCL, and because the LCL takes into account the impact of both low-level moisture and temperature on cloud-base height.

Our conceptual model also includes the important contribution of synoptic-scale forcing to thunderstorm activity in this region. In fact, the NDVI-DUR coupling is probably of secondary importance to synoptic-scale forcing, at least for this region. As illustrated by the analysis for a subset of 22 months (section 7.4.2), including information about surface features in addition to mid-tropospheric ascent significantly increases the variance of DUR explained.

Our conceptual model is consistent with previous research that demonstrated that the amount and depth of moisture in the boundary layer is critical in determining the amount of convective instability and the intensity of storms. Theoretical analysis and simulations by Crook (1996) demonstrated that small changes in low-level mixing ratio (as small as 1

g kg^{-1}) can have significant effects on the initiation and intensity of thunderstorms. Siqueira et al. (2009) explored links between soil moisture dynamics and convection triggers over a pine plantation in the southeastern USA. They found that the boundary layer grew more quickly under water-stressed conditions than when soil moisture was plentiful. However, the rapid growth of the CBL did not translate into triggering of convection because the height of the LCL also increased rapidly under water-stressed conditions, thereby preventing parcels from reaching the LCL. Siqueira et al. (2009) also determined that the advection of low-level moisture from external sources had to be present to initiate convection above dry soils. Additionally, cloud model simulations of convection over the Tibetan plateau by Yamada (2008) found that the higher cloud base height for drier soil conditions produced a lower rain rate at the surface, because of increased evaporation of precipitation within the deeper and drier sub-cloud layer. Matyas and Carleton (2010) investigated the relationship between convection intensity (quantified by reflectivity data from radar) and soil moisture over the Corn Belt in the USA. They found that for climate divisions located over the eastern Corn Belt, a positive correlation existed between the intensity of convection and soil moisture conditions on days with weak or weak-to-moderate forcing. Juang et al. (2007) examined the impact of contrasting soil moisture content and low-level RH on warm season convective precipitation events over the southeastern USA. Their analysis indicated convective precipitation over moist soils was typically greater in intensity, and led to higher precipitation accumulation, than for convective events occurring over dry soil conditions. Garrity et al. (2010) used the NCEP/NCAR Reanalysis data to study the impact of extreme wet and dry regions over the western USA on atmospheric moisture profiles.

They found that vertical impact of drought and wet surface conditions is primarily limited to the lower troposphere (below 700 mb), with less low-level moisture for drought conditions, and suggested that this indicates a potential influence of thunderstorms in modulating drought.

Our observations over central Alberta corroborate findings made in studies using models and reanalysis data. Specifically, that NDVI appears to be modulating DUR by altering the moisture content of the CBL and in turn the LCL height. Betts (2004), Betts and Viterbo (2005) found a strong link between a soil moisture index (equivalent to plant available water (PAW)) and the height of the LCL in the ECMWF reanalysis data (ERA40). Betts (2007) examined ERA40 data over sub-basins of the Mississippi for the warm seasons from 1983 to 2001 and found that increased ET increased low-level relative humidity, which in turn lowered the LCL. Betts (2007) also found that LCL decreased as soil moisture and precipitation increased, and that precipitation in both the ERA40 and National Climate Data Center datasets increased with a lowering of the LCL. Jiang et al. (2009) found a similar relationship between daily mean LCL, soil moisture and subsequent precipitation in both the Weather Research and Forecasting model and the NARR data.

7.5.1 Comparison with other conceptual models

It is worth noting that our conceptual model is based largely on observations, unlike other conceptual models proposed for land-atmosphere feedbacks that are typically based on numerical modelling studies (e.g., Kim and Wang 2007; Lawrence and Slingo 2005; Trier et al. 2004; Pal and Elatir 2001; Schär et al. 1999). With that said, the in-situ observational datasets used in this study corroborate the conceptual models based on

numerical model simulations. Our conceptual model lends support to the so-called *"indirect soil moisture-precipitation feedback"* mechanism postulated by Schär et al. (1999), which describes how changes in soil moisture affect precipitation by influencing CBL characteristics and instability.

Our results are also consistent with those of Raddatz (2005), who found that for CARs on the Canadian Prairies from 1997 to 2003, dry and wet conditions were perpetuated over CARs through moisture and energy feedbacks between the surface and atmosphere. Raddatz (2005) suggested that the critical ingredients required for the realization of convection (such as lift) were less prevalent over drought areas than over pluvial areas.

Our findings are, however, not consistent with those of Myoung and Nielsen-Gammon (2010a), who used NCEP-NCAR reanalysis from 1948–2003 to investigate mechanisms controlling the variability of convective precipitation around the globe. They found that the magnitude of convective inhibition (CIN) is negatively correlated with precipitation over the continents in July, including over the Canadian Prairies (see their Fig. 6c). Myoung and Nielsen-Gammon (2010b) used NCEP-NCAR reanalysis data and observed precipitation data (NCDC) over Texas to examine the relationship between soil moisture and precipitation there from 1948 through 2003. They found that reduced precipitation decreases the soil moisture, which increases the surface temperature and lowers the dew-point, which together with warmer temperatures at 700 mb, increased CIN. They noted that an increase in CIN inhibits convection, even if precipitable water and CAPE are favourable. They concluded that the CIN mechanism is the primary factor maintaining drought conditions in the study area. In contrast, in our study we found no

relationship between DUR and CIN or between NDVI and CIN. Rather, as described above, the link between soil moisture and convection appears to be manifested through the LCL height.

7.5.2 Asymmetry and seasonality of feedback

Brimelow et al. (2011) found an asymmetry between NDVI and DUR for 38 CARs across the Prairies, with much above-average NDVI not a sufficient condition for above-average lightning duration. In this study, we too found an asymmetry of the coupling between NDVI and DUR over CAR11. Specifically, the coupling between NDVI and DUR is strong when vegetation is stressed or less vigorous, with much below-average NDVI typically associated with higher LCL heights and below average DUR. However, the opposite is not necessarily true when NDVI is much above average.

We purport that this asymmetry is attributable to the fact that if low-level moisture drops below a critical point, because of reduced transpiration on account of dry soils, then regardless of the amount of instability and lift, convection is unlikely. In contrast, increasing low-level moisture beyond a critical value means that moisture is no longer the limiting condition for thunderstorm formation; lift and instability then are. This hypothesis is supported by observational studies that shown the relationship between soil moisture stress and canopy resistance is asymmetrical and can be described by a logistic regression model (e.g., Anderson et al. 2007). In particular, observations find that there is little impact on canopy resistance (i.e., transpiration) for root-zone plant available water content as low as 50%, but a rapid increase in canopy resistance and photosynthetic activity is observed below that point (e.g., Schulze 1986; Mitchell et al. 2001).

While the asymmetric relationship between NDVI (or soil moisture) and precipitation has been identified in several numerical modelling studies, our research is (to the best of our knowledge) the first to confirm the existence of this asymmetric feedback using observations. Pal and Eltahir (2001) conducted simulations for the US Midwest for two contrasting warm seasons and found that the soil-moisture–precipitation feedback was stronger during the drought years. Similarly, simulations by Oglesby et al. (2002) found that soil moisture deficits had a more marked impact on subsequent precipitation than did wet soil moisture conditions. Hohenhegger et al. (2009) conducted modelling studies over the Alpine region in Europe and they too found an asymmetric response in precipitation to soil moisture, with precipitation more sensitive to dry soil moisture anomalies than to wet anomalies.

7.6 Conclusions

This study focuses on how anomalies in soil moisture and vegetation (e.g., NDVI anomalies) over the Canadian Prairies can condition the CBL layer so as to inhibit or facilitate thunderstorm activity, while also considering the role of synoptic-scale forcing on modulating summer thunderstorm activity. Our study focused on a census agricultural region over central Alberta (CAR11) for which we had observed lightning data, NDVI data, and in-situ sounding data for 11 summers (1 June through 31 August; 1999–2009). We used lightning duration as a proxy for thunderstorm occurrence and persistence (longevity).

To identify whether vegetation anomalies had any impact on lightning duration over CAR11 for similar synoptic-scale forcing conditions, we adopted an ingredients-based

approach to identify the three criteria required for thunderstorm formation: instability, low-level moisture and a trigger mechanism. Sounding data from Stony Plain were examined for the purpose of quantifying and describing the presence of instability and low-level moisture, and to quantify the impacts of changes in vegetation vigour on the structure of the boundary layer. We used both subjective (surface analysis) and objective analyses (NARR 500-mb omega) to quantify the surface and upper-air synoptic-scale forcing (i.e., trigger) each day for 22 summer months having contrasting NDVI and/or DUR. Our primary findings may be summarized as follows:

- Storms over CAR11 are longer-lived when they develop in an environment with favourable synoptic-scale conditions. Also, the amount of variance in monthly DUR explained increases significantly when incorporating information on surface features and upper-air lift, rather than using mid-tropospheric ascent alone.
- Surface and upper-air features (especially when working in concert) are important for thunderstorm occurrence and longevity over CAR11, with the longest DUR and highest success rate observed on days when surface forcing and upper-air forcing were synchronized.
- Longer DUR can be expected over CAR11 when storms develop over areas with high vegetation vigour, regardless of the degree of synoptic-scale forcing. Additionally, on days when a surface or upper-air feature is present, storms are more likely to be triggered when the NDVI over CAR11 is much above average, compared to when NDVI is much-below average.
- Below-average ΔDUR was typically observed when ΔNDVI < -0.5, even when the mid-tropospheric ascent was above average ($\Delta\omega_{500} < 0.0$). If the ascent was relatively

weak ($\Delta\omega_{500}$> +0.5), then ΔDUR was unlikely to be below average even if ΔNDVI was much above average (ΔNDVI > +1.0). If ΔNDVI was above average and vertical motion was favourable ($\Delta\omega_{500}$ < +0.5), then ΔDUR was highly likely to be above average.

- High coefficients of determination between selected sounding parameters (e.g., LCL height, lowest 50-mb mixing ratio) and ΔNDVI suggest that the vegetation is affecting the sounding structure in the low levels and boundary-layer evolution, which in turn is affecting DUR.
- We find a robust, consistent and coherent picture when comparing sounding data, underlying vegetation condition (NDVI) and concomitant thunderstorm activity (DUR).
- Our analysis of the sounding data in concert with the NDVI and DUR data suggests that the coupling between the vegetation and lower atmosphere over CAR11 is asymmetric. That is, the response of DUR to anomalies in NDVI is most noticeable for dry conditions (lower vegetation vigour), but not necessarily discernible when NDVI is above average.

We propose a conceptual model which describes how a reduction of vegetation vigour — in response to soil moisture deficits — modulates the partitioning of available energy into sensible and latent heat fluxes at the surface. We also demonstrated that ΔNDVI is positively correlated with low-level moisture, which suggests that the increase in LCL heights associated with decreasing vegetation vigour is occurring primarily in response to a decrease in low-level moisture, which is in turn related to decreased ET from drier soils and sparser vegetation. Our proposed conceptual model, is consistent

with similar conceptual models, but is unique in that it is the first framework based almost entirely on observational data (rather than results from numerical modelling experiments or reanalysis data) to describe the coupling between vegetation, boundary layer characteristics, synoptic-scale forcing and lightning activity. Importantly, our findings lend strong support to the hypotheses that the coupling between vegetation vigour and antecedent lightning duration appears to be manifested through LCL heights, and that the response of thunderstorm duration to NDVI anomalies is asymmetric.

CHAPTER 8

8. CONCLUSIONS

Vegetation and soil states are known to regulate the structure of the boundary layer by modulating fluxes of mass, heat and momentum (Dominguez and Kumar 2008). Consequently, linkages between the terrestrial ecosystem (i.e., vegetation and soil) and precipitation play a critical role in regulating regional weather and climate, especially during the warm season. Land-atmosphere linkages have thus been the focus of much research over the years (e.g., Pan et al. 1996; Entekhabi et al. 1996; Seneviratne et al. 2010). These linkages can manifest themselves as positive or negative feedback loops, which may either favour or inhibit the triggering (and intensity) of deep, moist convection (e.g., Findell and Eltahir 2003a,b). Further, Guo et al. (2006) noted that deep convection is likely a key component for linking the surface and overlying atmosphere, because it is very sensitive to variations in moist static energy in the convective boundary layer (CBL). The primary goal of this thesis was to explore how land-atmosphere processes over the Canadian Prairies can condition the CBL to favour or inhibit deep, moist convection during the summer.

While much insight into the underlying processes and mechanisms within the soil-vegetation-atmosphere matrix has been gained in recent decades, attempts to assign causality between anomalies in the terrestrial surface and convection have remained problematic. The reasons for this are: 1) there are several thermodynamic and hydrometeorological processes taking place simultaneously in a highly non-linear system

(Bosilovich and Schubert 2001; Dirmeyer 2006); additionally, 2) the signal has to be discernable from the background noise (Wang et al. 2006). These factors perhaps explain why there is often conflicting evidence from both modelling and observational studies as to the signs of the feedbacks between soil moisture and precipitation, soil moisture and vegetation, and vegetation and precipitation.

Koster et al. (2002) postulated that the strength of the coupling between the land and the atmosphere controls the degree to which soil moisture anomalies affect the overlying atmosphere and, ultimately, the generation of precipitation. Since then, several independent studies (using combinations of model output, reanalysis products and observations) have identified the Great Plains of N. America as a global hot spot for land-atmosphere coupling during the warm season (Koster et al. 2004, 2006; Dirmeyer 2006). Additionally, research has identified the Canadian Prairie ecosystem as having the potential to exert a detectable influence on convective precipitation in the warm season, yet only some pioneering studies have been undertaken on this topic, and there is uncertainty regarding the nature of the mechanisms involved, and under which conditions they are important. Fortunately, there are also new datasets continually coming online that could be useful in elucidating the workings of linkages and feedbacks between the surface and atmosphere.

In this thesis we adopted a paper format. The first two papers dealt with the validation of soil moisture and ET estimates from the Second Generation Prairie Agrometeorological Model (PAMII). The final two papers explored linkages between the terrestrial surface and thunderstorm activity on the Canadian Prairies using satellite-derived Normalized Difference Vegetation Index (NDVI), observed lightning, observed

sounding and model data (from the North American Regional Reanalysis and PAMII). This thesis has undertaken a thorough validation of simulations of root-zone soil moisture and evapotranspiration (ET) from PAMII using in-situ measurements and observations on the Canadian Prairies. This research has demonstrated that PAMII is a reliable tool for exploring linkages between soil moisture, ET and atmosphere.

The first paper, Chapter 3, Brimelow et al. (2010a), validated PAMII against in-situ soil moisture observations from three sites (having contrasting soil texture) on the Canadian Prairies in 2004 and 2005. They also quantified the sensitivity of modelled root-zone soil moisture and ET to uncertainties arising from the specified soil hydraulic properties. Additionally, PAMII showed skill in simulating the evolution of root-zone soil moisture content during the growing season and also captured the salient features of the soil moisture content at each study site.

The coefficient of determination (R^2) between simulated and observed root-zone soil moisture content was between 0.65 and 0.90, while the mean absolute errors were typically less than 10% of the mean soil moisture content. Simulated root-zone plant available moisture content (RZPAW) values were typically within 10% of the observations. They noted, however, that correct modelling of soil moisture content is contingent on accurately specifying the site-specific soil hydraulic properties (e.g., permanent wilting point and field capacity). By adopting a novel approach of using an ensemble of multiple pedotransfer functions (PTFs), they demonstrated that there is merit in using the multi-model PTF ensemble to quantify the uncertainty in simulating soil moisture associated with errors in the soil texture and associated soil hydraulic properties.

In the second paper, Chapter 4, Brimelow et al. (2010b), the simulated daytime ET estimates from PAMII were validated using daytime ET estimates from eddy covariance systems at West Nose Creek (a barley field located northwest of Calgary, Alberta) and a Fluxnet site (short-grass Prairie located west of Lethbridge, Alberta). The model's performance was validated for contrasting growing seasons at the grassland site. At the barley site, the model explained about 50% of the observed variance in ET for the 22 days considered. PAMII displayed a systematic negative bias of between -0.7 mm d^{-1} and -1.3 mm d^{-1} (17% to 24% relative error) over the cereal crop, depending on the reference value specified for the minimum stomatal resistance (rs_min). Mean absolute and root mean square errors (RMSE) were near 1.0 mm d^{-1}.

PAMII showed skill at modelling the day-to-day and inter-seasonal variability in ET at the short-grass Prairie site. Specifically, the model explained 70% of the variance in observed ET. Mean absolute errors and mean RMSE errors were less than 1.0 mm d^{-1}. PAMII successfully captured the increase (decrease) in accumulated growing season ET for the wet (dry) growing seasons at the Prairie site. Based on optimization of the model runs for each site, new reference values for minimum stomatal resistance for grassland (rs_min = 80 s m^{-1}) and cereal crops (rs_min = 50 s m^{-1}) were proposed for PAMII. Brimelow et al. (2010b) noted that no single value of minimum reference stomatal resistance worked best for all years at the grassland site and proposed several improvements to the canopy resistance module and water stress function in PAMII, for example. This thesis has also identified possible areas where PAMII can be improved, and these should be implemented and tested. An independent validation of soil moisture simulations from PAMII for spring wheat sites in Saskatchewan and Manitoba was

published after Brimelow et al. (2010a,b) by Gervais et al. (2010). Gervais et al. noted similar issues with the PAMII model as were noted by Brimelow et al. (2010b). In particular Gervais et al. showed that PAMII soil moisture simulations could be improved by using a more realistic canopy resistance function and by allowing infiltration (during heavy rainfall events) to continue regardless of the top-zone's water content.

The potential for using PAMII as a drought tracking tool was briefly explored in Chapter 5. Specifically, a comparison between the integrated number of days with RZPAW < 30% from PAMII and the concomittant NDVI from 1999 to 2005 was made. This prelimniary analysis suggested that the integrated number of days to date with RZPAW is <30% shows promise for highlighting those areas where vegetation is likely to experience significant moisture stress in the coming two to four weeks. The potential to track agricultural drought using this approach needs to be further explored and quantified.

As alluded to earlier, while the Canadian Prairie terrestrial system has been identified as having the potential to exert a detectable influence on convective precipitation in the summer, relatively little work has been dedicated to studying the impacts of land-atmosphere feedbacks on thunderstorm activity on the Canadian Prairies. The final two research papers were aimed at addressing this gap in our knowledge, while also elucidating the mechanisms at work.

One might ask why model output data from the PAMII model were not used more extensively in the third and fourth papers (Chapters 6 and 7). The primary reason for this is that NDVI is a reliable and quantitative descriptor of vegetation vigour, and is available at a much higher spatial resolution than is model output. Additionally,

preliminary investigations have revealed that for census agricultural regions (CARs) on the Canadian Prairies area-averaged ET anomalies (from PAMII) and NDVI anomalies for JJA were highly correlated (R^2 near 0.60) from 1999 to 2004, which suggests that NDVI is a good proxy for ET. Also, the model output were only available form 1999–2005, which would have greatly reduced the size of the datasets. Finally, as was shown in Chapters 3 and 4, the model does have bias issues and we wished to avoid introducing unknown factors into our analysis.

In the third paper, Chapter 6, Brimelow et al. (2011), we presented findings from a novel study designed to explore linkages between the Normalized Difference Vegetation Index (NDVI), and lightning duration (DUR) from the Canadian lightning detection network for 38 CARs (polygons of varying size and shape) on the Canadian Prairies. DUR was used as a proxy for thunderstorm activity. Statistical analyses were undertaken for 38 CARs for 10 summers (JJA) between 1999 and 2008. Specifically, correlation coefficients were calculated between pairs of standardized anomalies of DUR and NDVI by season and by month. Correlations were also made for CARs grouped by size and/or by magnitude of the NDVI anomalies.

The main findings were that: (1) JJA lightning activity was overwhelmingly below average within larger dry areas (i.e., areas with below average NDVI); that is, the correlation between NDVI and DUR increased significantly as both the area and magnitude of the dry anomaly increased; (2) The relationship between DUR and NDVI was asymmetric, that is CARs having above average NDVI did not consistently experience above average lightning activity, regardless of the CAR size. This suggests that positive NDVI anomalies alone are not a necessary, nor a sufficient, condition for

above-average DUR; (3) The lower threshold for the length scale of the dry anomalies required to affect the boundary layer sufficiently to reduce lightning activity was found to be approximately 150 km (~18 000 km^2); (4) CARs with stressed vegetation in late June were much less likely to transition to lush vegetation by early August, especially for large CARs; (5) our analysis suggests that the surface-convection feedback appears to be a real phenomenon, in which drought tends to perpetuate drought with respect to convective storms and associated rainfall, within the limits found in (1) and (3). These findings (based on observations) concerning the role of patch size and anomaly magnitude, and the asymmetric nature of the feedback were consistent with and corroborate both theoretical studies and modelling work.

In the final paper, Chapter 7, the mechanisms responsible for the linkages and asymmetric nature of the feedback identified in Brimelow et al. (2011) were examined more closely. Specifically, the purpose was to focus on how surface anomalies (i.e., NDVI anomalies) over the Canadian Prairies can condition the CBL layer so as to inhibit or facilitate thunderstorm activity, while also considering the role of synoptic-scale forcing on modulating summer thunderstorm activity. The study focused on a census agricultural region (CAR 11) over central Alberta for which we had observed lightning data, NDVI data, and in-situ sounding data for 11 summers between 1999 and 2009. As before, lightning duration (DUR) was used as a proxy for thunderstorm occurrence and longevity. We used both subjective (surface analysis maps) and objective analyses (North American Regional Reanalysis 500-mb vertical motion data over CAR11) to quantify the surface and upper-air synoptic-scale circulation patterns over CAR11 between 18 UTC and 03 UTC each day for a sub-set of 22 summer months having

contrasting NDVI and/or DUR. We then considered the response of DUR on days with similar synoptic forcing, but occurring during weeks with contrasting NDVI conditions. This way, the impact of synoptic forcing was removed, thereby allowing us to focus on the response, if any, of the lightning to changes in vegetation vigour.

Our data suggest that storms over CAR11 are more likely to develop and are more widespread when they develop in an environment in which the surface and upper-air synoptic-scale forcing are synchronized. Also, the variance in monthly DUR explained increases significantly when incorporating information about surface features and mid-tropospheric ascent, rather than information on surface features or ascent alone. Additionally, on days when a notable surface or upper-air feature is present, storms are more likely to be triggered when NDVI over CAR11 is much above average, compared to when NDVI is much-below average. For the subset of 22 summer months, about 13% of the variance in lightning duration is explained by the NDVI alone, compared to 27% of the variance in lightning duration explained by 500-mb vertical motion alone. In comparison, the totals of days per month with surface or upper-air forcing explained about 36% of the variance in lightning duration. Thus, incorporating information of surface and upper-air forcing in addition to the NDVI increased the variance in lightning duration explained to almost 40%. This underscores the importance of surface features in triggering thunderstorms.

As was observed in Brimelow et al. (2011), we also found that the response of thunderstorm duration to NDVI anomalies was asymmetric over central Alberta. That is, the response of DUR to anomalies in NDVI was most noticeable when NDVI is below average, but not necessarily when NDVI was above average. In summary, we found a

robust, consistent and coherent picture when comparing sounding data, underlying vegetation condition (NDVI) and concomitant thunderstorm activity (DUR). We proposed a conceptual model, based almost entirely on observations, which integrates all of the above findings to describe how reduction of vegetation vigour — in response to soil moisture deficits — modulates the partitioning of available energy into sensible and latent heat fluxes at the surface, which modulates LCL heights, which in turn affects lightning duration. We also demonstrated that NDVI is positively correlated with low-level atmospheric moisture, which suggests that the increase in LCL heights with decreasing vegetation vigour is occurring primarily in response to a decrease in low-level moisture, which is in turn related to a decrease in ET from drier soils and sparser vegetation.

The proposed conceptual model is the first framework, describing the coupling between the vegetation, boundary layer characteristics and synoptic-scale forcing and lightning activity, which is based almost exclusively on observations rather than results from numerical modelling experiments or reanalysis data. Importantly, our findings also lend strong support to modelling work that suggest that the coupling between vegetation vigour and antecedent lightning duration appears to be manifested through the LCL heights, and that the response of thunderstorm duration to NDVI anomalies is asymmetric.

In conclusion, our research has verified that (under certain constraints), thunderstorm activity on the Canadian Prairies is modulated to a degree by changes in vegetation vigour arising from changes in soil moisture. The primary factor in regulating convection appears to be synoptic-scale forcing, with linkages between the terrestrial surface and

convection of secondary importance. Additionally, using observations, we have also identified mechanisms by which changes in vegetation vigour affect characteristics of the boundary layer and in turn convective activity.

Future work could extend our methodology of applying lightning, sounding and NDVI data to examine relationships between vegetation and thunderstorms activity to other locations on the Prairies, while also more closely examining the physical mechanisms purported to be responsible for the asymmetric response of DUR to NDVI anomalies. Additionally, further work could be undertaken into identifying why the coupling between the land surface and CBL and in turn lightning activity appears to be strongest during the first half of the growing season (June and July). Our datasets could also be used to validate future modelling studies designed to investigate land-atmosphere feedbacks on the Canadian Prairies. Finally, the PAMII model output could be used in future studies to examine the impact of NDVI anomalies on ET. Given the good correspondence between NDVI and ET referred to earlier, it may be possible to derive an empirical relationship between NDVI anomalies and ET anomalies, thereby providing near real-time high spatial and temporal estimates of ET across the Canadian Prairies. Such a study should probably be undertaken once the suggested improvements to the model have been implemented and tested.

APPENDIX

List of Acronyms

AGCM	Atmospheric General Circulation Model
AVHRR	Advanced Very High Resolution Radiometer
AWC	Available Water Content
BMT	Biometeorological Time
BR	Bowen Ratio
CAPE	Convective Available Potential Energy
CAR	Census Agricultural Region
CBL	Convective Boundary Layer
CCAP	Canadian Crop Condition Assessment Program
CG	Cloud-to-ground lightning flash
CIN	Convective Inhibition
CLASS	Canadian Land Surface Scheme
CLDN	Canadian Lightning Detection Network
DUR	Lighting Duration
EC	Eddy Covariance
ECMWF	European Centre for Medium Range Weather Forecasting
ERA40	Forty-Year European Reanalysis
ET	Evapotranspiration
FC	Field Capacity
GDD	Growing Degree Days
GEM	Global Environmental Multi-scale
GLACE	Global Land-Atmosphere Coupling Experiment
IA	Index of Agreement
ISBA	Interactions Soil-Biosphere-Atmosphere
JJA	June, July and August (Boreal summer)
LAI	Leaf Area Index

LCL	Lifting Condensation Level
LFC	Level of Free Convection
LST	Local Solar Time
LWC	Liquid Water Content
MAE	Mean Absolute Error
MCON	Moisture Flux Divergence
ME	Mean Error
MRB	Mackenzie River Basin
MSE	Moist Static Energy
MT	Mountain Time
MTP	Mid-tropospheric Perturbation
NARR	North American Regional Reanalysis
NCDC	National Climatic Data Center
NCEP	National Centers for Environmental Prediction
NDVI	Normalized Difference Vegetation Index
NWP	Numerical Weather Prediction
PAMII	Second Generation Prairie Agrometeorological Model
PAR	Photosynthetically Active Radiation
PBL	Planetary Boundary Layer
PTF	Pedotransfer Function
PWP	Permanent Wilting Point
RH	Relative Humidity
RMSE	Root-Mean Square Error
RZPAW	Root-zone Plant Available Water
SVAT	Surface-Vegetation-Atmosphere-Transfer
US	United States
USDA	United States Department of Agriculture
UTC	Coordinated Universal Time
VPD	Vapour Pressure Deficit
VWC	Volumetric Water Content
WNC	West Nose Creek

REFERENCES

Adegoke, J.O., and A.M. Carleton, 2002: Relations between soil moisture and satellite vegetation indices in the U.S. corn belt. *J. Hydrometeor.*, **3**, 395-405.

Akinremi, O.O., S.M. McGinn, and A.G. Barr, 1996: Simulation of soil moisture and other components of the hydrological cycle using a water budget approach. *Can. J. Soil Sci.*, **76**, 133-142.

Alapaty, K., J. Pleim, S. Raman, D.S. Niyogi, and D. Byun, 1997: Simulation of atmospheric boundary layer processes using local – and nonlocal-closure schemes. *J. Appl. Meteor.*, **36**, 214–233.

Alfieri, J.G., P.D. Blanken, D.N. Yates, and K. Steffen, 2007: Variability in the environmental factors driving evapotranspiration from a grazed rangeland during severe drought conditions. *J. Hydrometeor.*, **8**, 207-220

Alfieri, J.G., D. Nyogi, P.D. Blanken, F. Chen, M.A. LeMone, K.E. Mitchell, and M.B. Ek, 2008a: Estimation of the minimum canopy resistance for croplands and grasslands using data from the 2002 International H_2O Project. *Mon. Wea. Rev.*, **128**, 4452-4469.

Alfieri, J.G., P. Claps, P. D'Odorico, F. Laio, and T.M. Over, 2008b: An analysis of the soil moisture feedback on convective and stratiform precipitation. *J. Hydrometeor.*, **9**, 280-291.

Anderson, B.T., G. Salvucci, A. Ruane, M. Kanamitsu, and J.O. Roads, 2008: A new metric for estimating the influence of evaporation upon seasonal precipitation rates. *J. Hydrometeor.*, **9**, 576-588.

Anderson, B.T., A.C. Ruane, J.O. Roads, and M. Kanamitsu, 2009: Estimating the influence of evaporation and moisture-flux convergence upon seasonal precipitation rates, Part II: An analysis for North America based upon the NCEP-DOE Reanalysis II model. *J. Hydrometeor.*, **10**, 893-911.

Anderson, M.C., J.C. Norman, T.P. Meyers, and G.R. Diak, 2000: An analytical model for estimating canopy transpiration and carbon assimilation fluxes based on canopy light-use efficiency. *Agric. Forest Met.*, **101**, 265-289.

Anderson, M. C., J. M. Norman, J. R. Mecikalski, J. A. Otkin, and W. P. Kustas, 2007: A five year analysis of MODIS NDVI and NDWI for grassland drought assessment over the central Great Plains of the United States. *Geophys. Res. Lett.*, 34, L06407, doi:10.1029/2006GL029127.

Anthes, R.A., 1984: Enhancement of convective precipitation by mesoscale variations in vegetative covering in semiarid regions. *J. Clim. Appl. Meteor.*, **23**, 541-554.

Armstrong, R.N. Pomeroy, and L.W. Martz, 2008: Evaluation of three evaporation estimation methods in a Canadian prairie landscape. *Hydrol. Process.*, doi: 10.1002/hyp.7054.

Arora, V., 2003: Simulating energy and carbon fluxes over winter wheat using coupled land surface and terrestrial ecosystem models. *Agric. Forest Met.*, **118**, 21–47.

Atlas, R., N. Wolfson, and J. Terry, 1993: The effect of SST and soil-moisture anomalies on GLA model simulations of the 1988 U.S. summer drought. *J. Climate,* **6**, 2034–2048.

Avissar, R. and F. Chen, 1993: Development and analysis of prognostic equations for mesoscale kinetic energy and mesoscale (subgrid scale) fluxes for large-scale atmospheric models. *J. Atmos. Sci.*, **50**, 3751-3774.

Avissar, R., and Y. Liu, 1996: Three-dimensional numerical study of shallow convective clouds and precipitation induced by land surface forcing. *J. Geophys. Res.*, **101**, 7499-7518.

Avissar, R., and T. Schmidt, 1998: An evaluation of the scale at which ground-surface heat flux patchiness affects the convective boundary layer using large-eddy simulations. *J. Atmos. Sci.*, **55**, 2666-2689.

Baidya R, S., and R. Avissar, 2002: Impact of land use/land cover change on regional hydrometeorology in Amazonia. *J. Geophys. Res.,* **107**, D20, DOI 10.1029/2000JD000266.

Ball, J.T., I.E. Woodrow, and J.A. Berry, 1987: A model predicting stomatal conductance and its contribution to the control of photosynthesis under different environmental conditions. In: Biggins, J. (Ed.), Progress in Photosynthesis Research, vol. 4. Martinus Nijhoff Publishers, Netherlands, pp. 221–224.

Basara, J. B., and T. M. Crawford, 2000: Improved installation procedures for deep layer soil moisture measurements. *J. Atmos. Oceanic Technol*., **17**, 879– 884.

Batjes, N.H., 1996: Development of a world data set of soil water retention properties using pedotransfer rules. *Geoderma*, **71**, 31-52.

Beljaars, A. C. M., P. Viterbo, M. J. Miller, and A. K. Betts, 1996: The anomalous rainfall over the United States during July 1993: Sensitivity to land surface parameterization and soil moisture anomalies. *Mon. Wea. Rev.,* **124,** 362–383.

Bernadet, L.R., L. D. Grasso, J. E. Nachamkin, C. A. Finley, and W. R. Cotton, 2000: Simulating convective events using a high-resolution mesoscale model. *J. Geophys. Res.,* **105,** 14 963–14 982.

Betts, A. K., and J. Ball, 1995: The FIFE surface diurnal cycle climate. *J. Geophys. Res.,* **100**, 25,679–25,693.

Betts, R.A., J.H. Ball, A.C.M. Beljaars, M.J. Miller, and P. Viterbo, 1996: The land-surface- atmosphere interaction: A review based on observational and global modelling perspectives. *J. Geophys. Res.,* **101**, 7209-7225.

Betts, A.K., 2004: Understanding hydrometeorology using global models. *Bull. Amer. Meteor. Soc.*, **85**, 1673–1688.

Betts, A. K. and P. Viterbo, 2005: Land surface, boundary layer, and cloud field coupling over the southwestern Amazon in ERA 40. *J. Geophys. Res.*, **110**, D14108, doi:10.1029/2004JD005702.

Betts, A. K., 2007: Coupling of water vapor convergence, clouds, precipitation, and land surface processes. *J. Geophys. Res.*, **112**, D10108, doi:10.1029/2006JD008191.

Blanken, P.D., T.A. Black, P.C. Yang, H.H. Neumann, Z. Nesic, R. Staebler, G. den Hartog, M.D. Novak, and X. Lee, 1997: Energy balance and canopy conductance of a boreal aspen forest: Partitioning overstory and understory components. *J. Geophys. Res.*, **102**, 28,915-28,927.

Blöschl, G., and M. Sivapalan, 1995: Scale issues in hydrological modeling: A review. *Hydrol. Process.*, **9**, 251-290.

Blyth, E.M., A.J. Dolman, and J. Noilhan, 1994: The effect of forest on mesoscale rainfall: an example from HAPEX-MOBILHY. *J. Appl. Meteor.,* 33, 445–454.

Bonan, G. B., K. W. Oleson, M. Vertenstein, S. Levis, Z. Zeng, Y. Dai, R. E. Dickinson, and Z. L. Yang, 2002: The land surface climatology of the Community Land Model coupled to the NCAR Community Climate Model. *J. Climate,* **15,** 3123–3149.

Boone, A., J-C. Calvet, and J .Noilhan, 1999. Inclusion of a third soil layer in a land surface scheme using the force-restore method. *J. Appl. Meteor.*, **38**, 1611-1630.

Bosilovich, M. G., and S. D. Schubert, 2002: Water vapor tracers as diagnostics of the regional hydrologic cycle. *J. Hydrometeor.,* **3,** 149– 165.

Bosilovich, M. G., and J.-D Chern, 2006: Simulation of water sources and precipitation recycling for the MacKenzie, Mississippi, and Amazon River basins. *J. Hydrometeor.,* **7***,* 312-329.

Bougeault, P., B. Bret, P. Lacarrère, and J. Noilhan, 1991: An experiment with an advanced surface parameterization in a mesobeta-scale model. Part II: The 16 June 1986 simulation. *Mon. Wea. Rev*., **119**, 2374–2392.

Bouma, J., and H.A.J. van Lanen, 1987. Transfer functions and threshold values: from soil characteristics to land qualities, In: Beek, K., Burrough, P.A., and McCormack, D.D. (Editors), Proc. Workshop by ISSS/SSSA on Quantified Land Evaluation Procedures, 1TC publication No. 6, Enschede, The Netherlands, pp. 106-111.

Bounoua, L., G.J. Collatz, S.O. Los, P.J. Sellers, D.A. Dazlich, C.J. Tucker, and D.A. Randall, 2000: Sensitivity of climate to changes in NDVI. *J. Climate,* **13,** 2277–2292.

Braun, F.J., and G. Schädler, 2005: Comparison of soil hydraulic parameterizations for mesoscale meteorological models. *J. Appl. Meteor.*, **44**, 1116-1132.

Brimelow, J.C., and G.W. Reuter, 2005: On the transport of Gulf of Mexico moisture to the southern Mackenzie River basin during extreme summertime rainfall events. *J. Hydrometeor*., **6**, 423–440.

Brimelow, J.C., J.M. Hanesiak, and R.L Raddatz, 2010a: Validation of soil moisture simulations produced by the Canadian prairie agrometeorological model, and an examination of their sensitivity to uncertainties in soil hydraulic parameters. *Agric. Forest Met*., **150**, 100-114.

Brimelow, J.C., J.M. Hanesiak, R.L. Raddatz, and M. Hayashi, 2010b: Validation of ET estimates from the Canadian Prairie Agrometeorological Model for contrasting vegetation types and growing seasons**.** *Can. Water Res. J.***, 35,** 209-230.

Brimelow, J.C., J.M. Hanesiak, and W.R. Burrows, 2011: On the surface-convection feedback during drought periods on the Canadian Prairies. *Earth Interactions*, in press.

Brooks, R.H., and A.T. Corey, 1964: Hydraulic properties of porous media. Colorado State Univ. Hydrol. Paper No. 3, 27 pp.

Bruand, A., D. Baize, and M. Hardy, 1994: Prediction of water retention properties of clayey soils: Validity of relationships using a single soil characteristic. *Soil Use Management*, **10**, 99–103.

Brubaker, K.L., D. Entekhabi, and P.S. Eagleson, 1993: Estimation of continental precipitation recycling. *J. Climate*, **6**, 1077-1089.

Brubaker, K.L., P.A. Dirmeyer, A. Sudradjat, B.S. Levy, and F. Bernal, 2001: A 36-yr climatological description of the evaporative sources of warm-season precipitation in the Mississippi River basin. *J. Hydrometeor.,* **2,** 537–557.

Budyko, M.I., 1974: *Climate and Life*, 508 pp., Academic Press, New York.

Burrows, W.R., P. King, P.J. Lewis, B. Kochtubajda, B. Snyder, and V. Turcotte, 2002: Lightning occurrence patterns over Canada and adjacent United States from lightning detection network observations. *Atmos.-Ocean*, **40**, 59-81.

Burrows, W.R., and B. Kochtubajda, 2010: A decade of cloud-to-ground lightning in Canada: 1999-2008. Part 1: Flash density and occurrence. *Atmos.-Ocean*, **48**, 177-194

Calvet, J., S.R. Santos-Alvalá, G. Jaubert, C. Delire, C. Nobre, I. Wright, and J. Noilhan, 1997: Mapping surface parameters for mesoscale modeling in forested and deforested southwestern Amazonia. *Bull. Amer. Meteor. Soc.*, **78**, 413-423.

Campbell, G.S., 1974: A simple method for determining unsaturated conductivity from moisture retention data. *Soil Sci.*, **117**, 311-314.

Campbell, G.S., and J.M. Norman, 1988. *An Introduction to Environmental Biophysics*. Springer-Vedrlag, 285 pp.

Carleton, A.M., D. Jelinski, D. Travis, D. Arnold, R Brinegar, and D. Easterling, 1994: Climate-scale vegetation—cloud interactions during drought using satellite data. *Intl. J. Clim.*, **14**, 593-623.

Carleton, A.M., D.J. Travis, J.O. Adegoke, D.L. Arnold, and S. Curran, 2008: synoptic circulation and land surface influences on convection in the Midwest U.S. "Corn Belt" during the summers of 1999 and 2000. Part II: Role of vegetation boundaries. *J. Climate*, **21**, 3617-3641.

Carlson, P.J., 2000: Seasonal and inter-annual variation in carbon dioxide exchange and carbon balance in a mixed grassland. M.Sc. Thesis, University of Lethbridge, Lethbridge, Alta.

Carsel, R.F., and R.S. Parrish, 1988: Developing joint probability distributions of soil water retention characteristics. *Water Resour. Res.*, **24**, 755-769.

Casanova, J.J., and J. Judge, 2008: Estimation of energy and moisture fluxes for dynamic vegetation using coupled SVAT and crop-growth models. *Water Resour. Res.*, **44**, doi: 10.1029/2007WR006503.

Chahine, M. T., 1992: The hydrologic cycle and its influence on climate. *Nature,* **359,** 373-380.

Challinor, A.J., and T.R. Wheeler, 2008. Use of a crop model ensemble to quantify CO2 stimulation of water-stressed and well-watered crops. *Agric. Forest Met.*, **148**, 1062-1077.

Chang, J.-T., and P.J. Wetzel, 1991: Effects of spatial variations of soil moisture and vegetation on the evolution of a prestorm environment: A case study. *Mon. Wea. Rev.,* **119,** 1368-1390.

Chen, F., and R. Avissar, 1994: The impact of land-surface wetness heterogeneity on mesoscale heat fluxes. *J. Appl. Meteor.*, **33**, 1323-1340.

Chen, B., J.M. Chen, G. Mo, C.-W Yuen, H. Margolis, K. Higuchi, and D. Chan, 2007: Modeling and scaling coupled energy, water, and carbon fluxes based on remote sensing: An application to Canada's landmass. *J. Hydrometeor.*, **8**, 123-143.

Cheng, W.Y.Y., and W.R. Cotton, 2004: Sensitivity of a cloud-resolving simulation of the genesis of a mesoscale convective system to horizontal heterogeneities in soil moisture initialization. *J. Hydrometeor.*, **5**, 934-958.

Clapp, R.B., and G.M. Hornberger, 1978: Empirical equations for some soil hydraulic properties. *Water Resour. Res.*, **14**, 601-604.

Clark, C.A., and R.W. Arritt, 1995: Numerical simulations of the effect of soil moisture and vegetation cover on the development of deep convection. *J. Appl. Meteor.*, **34**, 2029-2045.

Colby, F. P., Jr., 1984: Convective inhibition as a predictor of convection during AVE-SESAME II. *Mon. Wea. Rev.,* **112,** 2239-2119.

Collins, D., and R. Avissar, 1994: An evaluation with the Fourier amplitude sensitivity test (FAST) of which land-surface parameters are of greatest importance for atmospheric modelling. *J. Climate,* **7,** 681-703.

Cook, B. I., G. B. Bonan, and S. Levis, 2006: Soil moisture feedbacks to precipitation in Southern Africa. *J. Climate*, **19,** 4198-4206.

Cooter E., and D. Schwede, 2000: Sensitivity of the National Oceanic and Atmospheric Administration multilayer model to instrument error and parameterization uncertainty. *J. Geophys. Res.*, **105**, 6695-6704.

Cosby, B.J., G.M. Hornberger, R.B. Clapp, and T.R. Ginn, 1984: A statistical exploration of the relationships of soil moisture characteristics to the physical properties of soils. *Water Resour. Res.*, **20**, 682-690.

Côté, J., S. Gravel, A. Méthot, A. Patoine, M. Roch, and A. Staniforth, 1998: The operational CMC/MRB global environmental multiscale (GEM) model: Part I – Design considerations and formulation. *Mon. Wea. Rev.*, **126**, 1373-1395.

Cowan, I. R., 1977: Stomatal behaviour and environment. Evolutionary patterns and processes in ferns. R. D. Preston and H. W. Woolhouse, Vol. 4, Advances in Botanical Research, Academic Press, 117-228.

Crawford, T.M., D.J. Stesnrud, T.N. Carlson, and W.J. Capehart, 2000: Using a soil hydrology model to obtain regionally averaged soil moisture values. *J. Hydrometeor.*, **1**, 353-363.

Cresswell, H.P., Y. Coquet, A. Bruand, and N.J. McKenzie, 2006: The transferability of Australian pedotransfer functions for predicting water retention characteristics of French soils. *Soil Use Management*, **22**, 62-70.

Crook, A., 1996: Sensitivity of moist convection forced by boundary layer processes to low-level thermodynamic fields. *Mon. Wea. Rev.,* **124,** 1767-1785.

Cummins, K.L., R.B. Pyle, and G. Fournier, 1999: An integrated North American lightning detection network. In: Proc. 11th Intl. Conf. On Atmospheric Electricity, NASA, 7–11 June 1999, Guntersville AL, pp. 218-221.

Cutrim, E., D.W. Martin, and R.M. Rabin, 1995: Enhancement of cumulus clouds over deforested lands in Amazonia. *Bull. Amer. Meteor. Soc.,* **76**, 1801-1805.

D'Odorico, P., and A. Porporato, 2004: Preferential states in soil moisture and climate dynamics. *Proc. Nat. Aca. Sci.*, **101** (24), 8848-8851.

Da Silva, A., and B.D. Kay, 1997: Estimating the least limiting water range of soils from properties and management. *Soil Sci. Soc. Am. J.*, **61**, 877-883.

Dalu, G. A., and R. A. Pielke, 1993: Vertical heat fluxes generated by mesoscale atmospheric flow induced by thermal inhomogeneities in the PBL. *J. Atmos. Sci.,* **50,** 919-926.

Dane, J.H. and J.W Hopmans, 2002: Pressure plate extractor. In: J.H. Dane and G.C. Topp (Editors), Methods of Soil Analysis, Part 4. Physical Methods. Soil Science Society of America Book Series 5, Madison, Wisconsin. pp. 688-690.

De Lannoy, G.J.M., N.E.C. Verhoest, P.R. Houser, T.J. Gish, and M. Van Meirvenne, 2006: Spatial and temporal characteristics of soil moisture in an intensively monitored agricultural field (OPE3). *J. Hydrol.*, **331**, 719-730.

Del Sole, T., M. Zhao, and P. Dirmeyer, 2009: A new method for exploring coupled land-atmosphere dynamics. *J. Hydrometeor.*, **10**, 1040-1050.

Desai A.R., K.J. Davis, C.J. Senff, S. Ismail, E.V. Browell, D.R. Stauffer, and B.P. Reen, 2006: A case study on the effects of heterogeneous soil moisture on mesoscale boundary-layer structure in the Southern Great Plains, U.S.A. Part I: simple prognostic model. *Boundary-Layer Meteor.*, **119**, 195-238

Dirmeyer, P. A., 1994: Vegetation stress as a feedback mechanism in midlatitude drought. *J. Climate,* **7,** 1463-1483.

Dirmeyer, P. A., and K. L. Brubaker, 1999: Contrasting evaporative moisture sources during the drought of 1988 and the flood of 1993. *J. Geophys. Res.,* **104,** 19 383-19 397.

Dirmeyer, P.A., 2000: Using a global soil wetness dataset to improve seasonal climate simulation. *J. Climate*, **13**, 2900-2922.

Dirmeyer, P.A., 2006: The hydrologic feedback pathway for land-climate coupling. *J. Hydrometeor.*, **7**, 857-867.

Dirmeyer, P.A., R.D. Koster, and Z.C. Guo, 2006: Do global models properly represent the feedback between land and atmosphere? *J. Hydrometeor.,* **7**, 1177-1198.

Dirmeyer, P.A., and K.L., Brubaker, 2007: Characterization of the global hydrologic cycle from a back-trajectory analysis of atmospheric water vapor. *J. Hydrometeor.*, **8,** 20-37.

Dirmeyer, P.A., C.A. Schloser, and K.L. Brubaker, 2009: Precipitation, recycling, and land memory: An integrated analysis. *J. Hydrometeor.*, **10**, 278-288.

Dominguez, F., P. Kumar, X. Liang, M. Ting, 2006: Impact of atmospheric Moisture storage on precipitation recycling. *J. Climate*, **19**, 1513-1530.Dominguez, F., and P. Kumar, 2008: Precipitation variability and ecoclimatological stability—A study using NARR data. Part I: Central U.S. Ecoregion. *J. Climate*, **21**, 5165-5186.

Dong, J., W. Ni-Meister, and P.R. Houser, 2007: Impacts of vegetation and cold season processes on soil moisture and climate relationships over Eurasia. *J. Geophys. Res*., **112,** 1-11.

Doran, J.C., W.J. Shaw, and J.M. Hubbe, 1995: Boundary layer characteristics over areas of inhomogeneous surface fluxes. *J. Appl. Meteor*., **34**, 559-571.

Doswell, C.A., 1987: The distinction between large-scale and mesoscale contribution to severe convection: A case study example. *Wea. Forecasting*, **2**, 3-16.

Doswell, C.A., and L.F. Bosart, 2001: Extratropical synoptic-scale processes and severe convection. *Meteorological Monographs*, **28**, 27-69.

Douville, H., 2003: Assessing the influence of soil moisture on seasonal climate variability in AGCMs. *J. Hydrometeor.,* **4**, 1044-1066.

Dunne, K., and C.J. Willmott, 1996: Global distribution of plant-extractable water capacity of soil. *Int. J. Clim.*, **16**, 841-859.

Eltahir, E.A.B., and R.L. Bras, 1994: Precipitation recycling in the Amazon basin. *Q. J. R. Meteor. Soc.,* **120,** 861-880.

Eltahir, E.A.B., and R.L. Bras, 1996: Precipitation recycling. *Rev. Geophys.,* **34,** 367-378.

Entekhabi, D., I. Rodriguez-Iturbe, and F. Castelli, 1996: Mutual interaction of soil moisture state and atmospheric processes. *J. Hydrol.,* **184,** 3-17.

Entekhabi D., Coauthors, 1999: An agenda for land surface hydrology research and a call for the second international hydrology decade. *Bull. Amer. Meteor. Soc.*, **80**, 2043-2058.

Federer, C.A., C. Vorosmarty, and B. Fekete, 2003: Sensitivity of annual evapotranspiration to soil and rot properties in two models of contrasting complexity. *J. Hydrometeor.*, **4**, 1276-1290.

Fennessy, M.J., and J. Shukla, 1999: Impact of initial soil wetness on seasonal atmospheric prediction. *J. Climate*, **12**, 3167-3180.

Findell, K.L., and E.A.B. Eltahir, 1997: An analysis of the soil moisture–rainfall feedback, based on direct observations from Illinois. *Water Resour. Res.,* **33,** 725-735.

Findell, K.L., and E.A.B. Eltahir, 1999: Analysis of the pathways relating soil moisture and subsequent rainfall in Illinois. *J. Geophys. Res.,* **104**, 31,565-31,574.

Findell, K.L., and E.A.B. Eltahir, 2003a: Atmospheric controls on soil moisture–boundary layer interactions. Part I: Framework development. *J. Hydrometeor.,* **4,** 552-569.

Findell, K.L., and E.A.B. Eltahir, 2003b: Atmospheric controls on soil moisture–boundary layer interactions. Part II: Feedbacks within the continental United States. *J. Hydrometeor.,* **4,** 570-583.

Fischer, M.L., D.P. Billesbach, J.A. Berry, W.J. Riley, and M.S. Torn, 2007: Spatiotemporal variations in growing season exchanges of CO_2, H_2O, and sensible heat in agricultural fields of the southern Great Plains. *Earth Interactions*, **11**, 1-17.

Flanagan L.B., L.A. Wever, and P.J. Carlson, 2002: Seasonal and interannual variation in carbon dioxide exchange and carbon balance in a northern temperate grassland. *Global Change Biol.*, **8**, 599-615.

Garrison, M.V., W.D. Batchelora, R.S. Kanwara, and J.T. Ritchie, 1999: Evaluation of the CERES-Maize water and nitrogen balances under tile-drained conditions. *Agric. Sys.*, **62**, 189-200.

Garrity C.M., R.S. Cerveney, and E.A Wentz, 2010: Vertical moisture profile characteristics of severe surface drought and surface wetness in the western United States: 1973 – 2002. *Int. J. Clim.,* **30**, 894–900.

Georgescu, M., C.P. Weaver, R. Avissar, R.L.Walko, and G. Miguez-Macho, 2003: Sensitivity of model-simulated summertime precipitation over the Mississippi River basin to the spatial distribution of initial soil moisture. *J. Geophys. Res.,* **108,** 8855, doi:10.1029/2002JD003107.

Gervais, M., P. Bullock, P. Mkhabela, M. Finlay, and R. Raddatz, 2010: Improvements to the accuracy of modelled soil water content from the Second Generation Prairie Agrometeorological Model. *Can. J. Soil Sci.,* **90**, 527-542.

Gijsman, A.J., S.S Jagtap, and J.W. Jones, 2003: Wading through a swamp of complete confusion: How to choose a method for estimating soil water retention parameters for crop models. *Eur. J. Agron.*, **18**, 77-106.

Giorgi, F., L. O. Mearns, C. Shields, and L. Mayer, 1996: A regional model study of the importance of local versus remote controls of the 1988 drought and 1993 flood over the central United States. *J. Climate,* **9,** 1150-1162.

Granger, R.J., and D.M Gray, 1989: Evaporation from natural nonsaturated surfaces. *J. Hydrol.*, **111**, 21-29

Gu, L., T. Meyers, S.G. Pallardy, P.J. Hanson, B. Yang, M. Heuer, K.P. Hosman, J. S. Riggs, D. Sluss, and S.D. Wullschleger, 2006: Direct and indirect effects of atmospheric conditions and soil moisture on surface energy partitioning revealed by a prolonged drought at a temperate forest site. *J. Geophys. Res.*, **111**, D16102, doi:10.1029/2006JD007161.

Gu, Y., J. F. Brown, J. P. Verdin, and B. Wardlow, 2007: A five year analysis of MODIS NDVI and NDWI for grassland drought assessment over the central Great Plains of the United States. *Geophys. Res. Lett.*, **34**, L06407, doi:10.1029/2006GL029127.

Guber, A.K., Y.A. Pachepsky, M.Th. van Genuchten, W.J. Rawls, J. Simunek, D. Jacques, T.J. Nicholson, and R.E. Cady, 2006: Field-scale soil water flow

simulations using ensembles of pedotransfer function for soil water retention. *Vadose Zone* J., **5**, 234-247.

Guillevic, P., R.D. Koster, M.J. Suarez, L. Bounoua, G.J Collatz, and S.P.Mahanama, 2002: Influence of the interannual variability of vegetation on the surface energy balance—a global sensitivity study. *J. Hydrometeor.*, **3**, 617-629.

Guo, Z., and the GLACE Team, 2006: GLACE: The Global Land-Atmosphere Coupling Experiment. 2. Analysis. *J. Hydrometeor.,* **7**, 611-625.

Guo, Z., P.A. Dirmeyer, X. Gao, and M. Zhao, 2007: Improving the quality of simulated soil moisture with a multi-model ensemble approach. *Q.J.R. Meteor. Soc.*, **133**, 731-747.

Gustafsson, D., E. Lewan, and P. Jansson, 2004: Modeling water and heat balance of the boreal landscape—comparison of forest and arable land in Scandinavia. *J. Appl. Meteor.*, **43**, 1750-1767.

Gutmann, E.D., and E.E. Small, 2005. The effect of soil hydraulic properties vs. soil texture in land surface models. *Geophys. Res. Lett.*, **32**, L02402, doi:10.1029/2004GL021843.

Hall, D.G., M.J. Reeve, A.J. Thomasson, and V.F. Wright, 1977: Water retention, porosity and density of field soils. Soil Survey of England and Wales. Harpenden, Technical Monograph No. 9, 75 pp.

Hamill, T.M., J.S. Whitaker, and X. Wei, 2004: Ensemble re-forecasting: Improving medium-range forecast skill using retrospective forecasts. *Mon. Weather Rev.*, **132**, 1434-1447.

Hanesiak, J.M., R.L. Raddatz, and S. Lobban, 2004: Local initiation of deep convection on the Canadian Prairie Provinces. *Bound.-Layer Meteor.*, **110**, 455-470.

Hanesiak J.M., R.L. Raddatz, and A. Tat, 2009: Initial soil moisture as a predictor of subsequent severe summer weather in the cropped grassland of the Canadian Prairie provinces. *Int. J. Clim.*, **29**, 899-909.

Hao, Y., and Coauthors, 2007: Seasonal and interannual variation in water vapor and energy exchange over a typical steppe in Inner Mongolia, China. *Agric. Forest Met.*, **146**, 57-69

Hayashi, M., J. Jackson, and L. Xu, 2010: Application of the Versatile Soil Moisture Budget model to estimate evaporation from prairie grassland. *Can. Water Res. J.*, **35**, 187-208.

Heuvelink, G.B.M., and R. Webster, 2001: Modelling soil variation: past, present, and future. *Geoderma*, **100**, 269-301.

Hochheim, K.P., T. Hirose, J. Bennett, P.R. Bullock, R.L. Raddatz, G.F. Fedosejevs, and P.M. Teillet, 2002: Improved crop specific projections from the integration of in situ and remote sensing data in an agrometeorological model. *Geoscience and Remote Sensing Symposium*, 4, 2391-2393.

Hohenegger, C., P. Brockhaus, C.S. Bretherton, and C. Schär, 2009: The soil moisture–precipitation feedback in simulations with explicit and parameterized convection. *J. Climate*, **22**, 5003-5020.

Holt, T.R., D. Niyogi, F. Chen, K. Manning, M. A. LeMone, and A. Qureshi, 2006: Effect of land atmosphere interactions on the IHOP 24–25 May 2002 convection case. *Mon. Wea. Rev.,* **134**, 113-133.

Holton, J.R., 1979: *An introduction to dynamic meteorology.* International Geophysics series, volume 23, Academic Press, 391 pp.

Hong, S.-Y., and E. Kalnay, 2000: Role of sea surface temperature and soil moisture feedback in the 1998 Oklahoma–Texas drought. *Nature,* **408,** 842-844.

Huang, J., H.M. van den Dool, and K.P. Georgakakos, 1996: Analysis of model-calculated soil moisture over the United States (1931-1993) and applications to long-range temperature forecasts. *J. Climate*, **9**, 1350-1362.

Islam K., A. McBratney, and B. Singh, 2005: Rapid estimation of soil variability from the convex hull biplot area of topsoil ultra-violet, visible and near-infrared diffuse reflectance spectra. *Geoderma*, **128**, 249-257.

James, K.A., D.J. Stensrud, and N. Yussouf, 2009: Value of real-time vegetation fraction to forecasts of severe convection in high-resolution models. *Wea. Forecasting*, **24**, 187-210.

Jamieson, P.D., G.S. Francis, D.R. Wilson, and R.J. Martin, 1995: Effects of water deficits on evapotranspiration from barley. *Agric. Forest Met*., **76**, 41-58.

Jarvis, P.G., 1976: The interpretation of the variations in leaf water potential and stomatal conductance found in canopies in the field. *Philosophical Transactions of the Royal Society of London Series B,* **273**, 593-610.

Ji, L., and A. Peters, 2003: Assessing vegetation response to drought in thenorthern Great Plains using vegetation and drought indices. *Remote Sens. Environ.*, **87**, 85-98.

Jiang, X., G-Y. Niu, and Z-L. Yang, 2009: Impacts of vegetation and groundwater dynamics on warm season precipitation over the central United States. *J. Geophys. Res.*, **114**, D06109, doi:10.1029/2008JD010756.

Johns, R.H., C. Broyles, D. Eastlack, H. Guerrero, and K. Harding, 2000: The role of synoptic patterns and moisture distribution in determining the location of strong and violent tornado episodes in the north-central United States. *20th Conf. Severe Local. Storms*. Amer. Meteor. Soc, MA, 489-492.

Jones, A.R., and N.A. Brunsell, 2009: Energy balance partitioning and net radiation controls on soil moisture-precipitation feedbacks. *Earth Interactions,* **13**, 1-25.

Juang, J.-Y., A. Porporato, P.C. Stoy, M.S. Siqueira, A.C. Oishi, M. Detto, H.-S. Kim, and G.G. Katul, 2007: Hydrologic and atmospheric controls on initiation of convective precipitation events. *Water Resourc. Res.*, **43,** doi:10.1029 2006WR004954.

Juskiw, P.E., Y.-W Jame, and L. Kryzanowski, 2001: Phenological development of spring barley in a short season growing area. *Agron. J.*, **93**, 370-379.

Kaufmann, R.K., and D.I. Stern, R.B. Myneri, C.J. Tucker, D. Slayback, N.V. Shabanov, and J. Pinzon, 2003: The effect of vegetation on surfactemperature: A statistical analysis of NDVI and climate data. *Geophys. Res. Lett.,* **30,** 2147, doi:10.1029/ 2003GL018251.

Kellenbenz D.J., T.J. Grafenauer, and J.M. Davies, 2007: The North Dakota tornadic supercells of 18 July 2004: issues concerning high LCL heights and evapotranspiration. *Wea.Forecasting*, **22**, 1200-1213.

Kelliher F.M., R. Leuning, M.R. Raupach, and E.D. Schulze, 1995: Maximum stomatal conductances for evaporation from global vegetation types. *Agric. Forest Met.*, **73**, 1-16.

Kern, J.S., 1995: Evaluation of soil water retention models based on basic soil physical properties. *Soil Sci. Soc. Am. J.*, **59**, 1134-1141.

Kersebaum, K.C., A. Wurbs, R. de Jong, C.A Campbell, J. Yang, and R.P. Zentner, 2008: Long-term simulation of soil-crop interactions in semiarid southwestern Saskatchewan, Canada. *Eur. J. Agron.*, **29**, 1-12.

Kim, Y., and G. Wang, 2005: Modeling seasonal vegetation variation and its validation against Moderate Resolution Imaging Spectroradiometer (MODIS) observations over North America. *J. Geophys. Res.*, **110**, D04106, doi:10.1029/2004JD005436.

Kim, Y., and G. Wang, 2007: Impact of vegetation feedback on the response of precipitation to antecedent soil moisture anomalies over North America. *J. Hydrometeor.*, **8**, 534-550.

Kochendorfer, J.P., and J.A. Ramírez, 2005: The impact of land–atmosphere interactions on the temporal variability of soil moisture at the regional scale. *J. Hydrometeor.*, **6**, 53-67.

Körner, Ch., 1994: Leaf diffusive conductances in the major vegetation types of the globe. In: Schulze, E.-D., Caldwell, M.M. (Eds.), Ecophysiology of Photosynthesis. Springer, New York, pp. 463-490.

Koster, R., and Coauthors, 1986: Global sources of local precipitation as determined by the NASA/GISS GCM. *Geophys. Res. Lett.,* **13,** 121-124.

Koster, R.D., and M. J. Suarez, 2001: Soil moisture memory in climate models. *J. Hydrometeor.,* **2,** 558-570.

Koster R. D., P. A. Dirmeyer, A. N. Hahmann, R. Ijpelaar, L. Tyahla, P. Cox, and M. J. Suarez, 2002: Comparing the degree of land-atmosphere interaction in four atmospheric general circulation models. *J. Hydrometeor.*, **7**, 590-610.

Koster, R.D., M. J. Suarez, R. W. Higgins, and H. M. Van den Dool, 2003: Observational evidence that soil moisture variations affect precipitation. *Geophys. Res. Lett.,* **30,** 1241, doi:10.1029/2002GL016571.

Koster, R. D., and M. J. Suarez, 2004: Suggestions in the observational record of land-atmosphere feedback operating at seasonal time scales. *J. Hydrometeor.*, **5**, 567-572.

Koster, R.D., P. A. Dirmeyer, and Z. Guo, and the GLACE team, 2004: Regions of strong coupling between soil moisture and precipitation. *Science,* **305,** 1138-1140.

Koster, R.D., and Coauthors, 2006: GLACE: The Global Land-Atmosphere Coupling Experiment. Part I: Overview. *J. Hydrometeor.,* **7,** 590-610.

Koster, R.D., S. Schubert and M.J. Suarez, 2009: Analyzing the concurrence of meteorological droughts and warm periods, with implications for the determination of evaporative regime. *J. Climate.,* **22**, 3331-3341.

Kothavala, Z., M.A. Arain, T.A. Black, and D. Verseghy, 2005: The simulation of energy, water vapor and carbon dioxide fluxes over common crops by the Canadian Land Surface Scheme (CLASS). *Agric. Forest Met.*, **133**, 89-108.

Kunkel, K.E., 1990: Operational soil moisture estimation for the midwestern United States. *J. Appl. Meteor.*, **29**, 1158-1166.

Kurita, N., and H. Yamada, 2008: The role of moisture recycling evaluated using stable isotope data from the middle of the Tibetan plateau during the monsoon season. *J. Hydrometeor.*, **9**, 760-775.

Lakhtakia, M.N., and T.T. Warner, 1987: A real-data numerical study of the development of precipitation along the edge of an elevated mixed layer. *Mon. Wea. Rev.,* **115,** 156-168.

Large, E.G., 1954. Growth stages in cereals: Illustration of the Feeke's scale. *Pl. Path.*, **3**: 128-129.

Lawrence, D.M., and J.M. Slingo, 2005: Weak land-atmosphere coupling strength in HadAM3: Moisture variability. *J. Hydrometeor.*, **6**, 670-680.

Legates, D.R., and G.J. McCabe Jr., 1999: Evaluating the use of "goodness-of-fit" measures in hydrologic and hydroclimate model validation. *Water Resour. Res.*, **35**, 233-241.

Lenhardt, R.J., 1984: Effects of clay-water interactions on water retention in porous media. PhD Thesis. 145 pp. Oregon State University, Corvallis, OR, USA.

Leuning, R., F. Kelliher, D. De Pury, E. Schulze, 1995: Leaf nitrogen, photosynthesis, conductance and transpiration: scaling from leaves to canopies. *Plant, Cell, Environ.,* **18**, 1183-1200.

Li, T., R.E. Grant, and L.B. Flanagan, 2004: Climate impact on net ecosystem productivity of a semi-arid natural grassland: modeling and measurement. *Agric. Forest Met.,* **126**, 99-116.

Liang, X., D.P. Lettenmaier, E.F. Wood, and S.J. Burges, 1994: A simple hydrologically based model of land surface water and energy fluxes for general circulation models. *J. Geophys. Res.*, **99**, 14 415-14 428.

Liu, J, R.E. Stewart, and K.K. Szeto, 2004: Moisture transport and other hydrometeorological features associated with the severe 2000/01 drought over the western and central Canadian Prairies. *J. Climate*, **17**, 305-319.

Liu, Z., M. Notaro, J. Kutzbach, and N. Liu, 2006: Assessing global vegetation-climate feedbacks from observations. *J. Climate*, **19**, 787-814.

Longley, R.W., and C.E. Thompson, 1965: A study of causes of hail. *J. Appl. Meteor.*, **4**, 69-82.

Luo, Y., A. P. Trishchenko, and K.V.Khlopenkov, 2008: Developing clear-sky, cloud and cloud shadow mask for producing clear-sky composites at 250-meter spatial resolution for the seven MODIS land bands over Canada and North America. *Remote Sens. Environ.*, **112**, 4167-4185.

Lynn, B.H., D. Rind, and R. Avissar, 1995: The importance of mesoscale circulations generated by subgrid-scale landscape-heterogeneities in general circulation models. *J. Climate,* **8**, 191-205.

Lynn, B.H., W.-K. Tao, and P.J. Wetzel, 1998: A study of landscape-generated deep moist convection. *Mon. Wea. Rev.*, **126**, 828-942.

Ma, L., G. Hoogenboom, L.R. Ahuja, D.C. Nielsen, and J.C. Ascough II, 2005: Development and evaluation of the RZWQM-CROPGRO hybrid model for soybean production. *Agron. J.*, **97**, 1172-1182.

Magnani, F., S. Leonardi, R. Tognetti, J. Grace, and M. Borghetti, 1998: Modelling the surface conductance of a broad-leaf canopy: effects of partial decoupling from the atmosphere. *Plant, Cell, Environ.*, **21**, 867-879.

Mahfouf, J.-F., E. Richard, and P. Mascart, 1987: The influence of soil and vegetation on the development of mesoscale circulations. *J. Clim. Appl. Meteor.*, **26**, 1483-1495.

Mahrt, L., J.S. Sun, D. Vickers, J.I. MacPherson, J.R. Pederson, and R.L. Desjardins, 1994: Observations of fluxes and inland breezes over a heterogeneous surface. *J. Atmos. Sci*., 51, 2484-2499.

Mahrt, L., 2000: Surface heterogeneity and vertical structure of the boundary layer. *Boundary-Layer Meteor.*, **96**, 33-62.

Margulis, S.A., D. Entekhabi, and D. McLaughlin, 2006: Spatiotemporal disaggregation of remotely sensed precipitation for ensemble hydrologic modeling and data assimilation. *J. Hydrometeor.*, **7**, 511-533.

Matsui, T., V. Lakshmi, and E.E. Small, 2005: The effects of satellite derived vegetation cover variability on simulated land-atmosphere interactions in the NAMS. *J. Clim*ate, **18**, 21-40.

Matthews, E., 1983: Global vegetation and land use: New high-resolution data bases for climate studies. *J. Clim. Appl. Meteor.,* **22**, 474-487.

Matyas, C.J., and A.M. Carleton, 2010: Surface radar-derived convective rainfall associations with Midwest US land surface conditions in summer seasons 1999 and 2000. *Theor. Appl. Climatol.*, **99**, 315-330

Mayr, T., and N.J. Jarvis, 1999: Pedotransfer functions to estimate soil water retention parameters for a modified Brooks-Corey type model. *Geoderma*, **91**, 1-9.

McBratney, A.B., and J.J. DeGruijter, 1992: A continuum approach to soil classification by modified fuzzy k means with extra grades. *J. Soil Sci*., **34**, 137-162.

McBratney, A.B., B. Minasny, S.R. Cattle, and R.W. Vervoort, 2002: From pedotransfer functions to soil inference systems. *Geoderma*, **109**, 41-73.

McCaul, E.W., and C. Cohen, 2002: The impact on simulated storm structure and intensity of variations in the mixed layer and moist layer depths. *Mon. Wea. Rev.,* **130**, 1722-1748

McNaughton K.G., and P.G. Jarvis, 1983: Predicting the effects of vegetation changes on transpiration and evaporation. In *Water Deficits and Plant Growth* (ed. T.T. Kozlowskii), pp. 1-47. Academic Press, New York.

McPherson, R. A., D.J. Stensrud, and K.C. Crawford, 2004: The impact of Oklahoma's winter wheat belt on the mesoscale environment. *Mon. Wea. Rev.,* **132,** 405-421.

McPherson, R.A., and D.J. Stensrud, 2005: Influences of a winter wheat belt on the Eevolution of the boundary layer. *Mon. Wea. Rev*., **133**, 2178-2199.

Meng, L., and S.M. Quiring, 2008: A comparison of soil moisture models using soil climate analysis network observations. *J. Hydrometeor.*, **9**, 641-659

Mengelkamp, H.T., and co-authors, 2006: Evaporation over a heterogeneous land surface. *Bull. Amer. Met. Soc*., **87**, 775-786.

Mesinger, F., G. Dimego, E. Kalnay, K. Mitchell, P.C. Shafran, W. Ebisuzaki, D. Jović, J. Woollen, E. Rogers, E.H. Berbery, M.B. Ek, Y. Fan, R. Grumbine, W. Higgins, H. Li, Y. Lin, G. Manikin, D. Parrish, and W. Shi, 2006: North American Regional Reanalysis. *Bull. Amer. Meteor. Soc.*, **87**, 343-360.

Minasny, B., A.B. McBratney, and K.L. Bristow, 1999: Comparison of different approaches to the development of pedotransfer functions for water-retention curves. *Geoderma*, **93**, 225-253.

Mirschel, W., K.O Wenkel, and R. Koitzsch, 1995: Simulation of soil water and evapotranspiration using the model BOWET and data sets from Krummbach and Eisenbach, two research catchments in North Germany. *Ecological Modelling*, **81**, 53-69.

Mitchell, R.A.C, V.J. Mitchell, and D.W. Lowler, 2001: Response of wheat canopy and water gas-exchange to soil water content under ambient and elevated CO_2. *Global Change Biol.*, **7**, 599-611.

Mkhabela, M.; P. Bullock, M. Gervais, G. Finlay, and H. Sapirstein, 2010: Assessing indicators of agricultural drought impacts on spring wheat yield and quality on the Canadian prairies. *Agric. Forest Met*., **150**, 399-410.

Mo, X., J.M. Chen, W. Ju, and T.A. Black, 2008: Optimization of ecosystem model parameters through assimilating eddy covariance flux data with an ensemble Kalman filter. *Ecological Modelling*, **217**, 157-173.

Mohanty, B.P., and J. Zhu, 2007: Effective hydraulic parameters in horizontally and vertically heterogeneous soils for steady-state land-atmosphere interaction. *J. Hydrometeor.*, **8**, 715-729.

Moller, A.R., 2001: Severe local storms forecasting. *Meteorological Monographs*, **28**, 433-480.

Moncrieff, J.B., J.M. Massheder, A. Verhoef and co-authors, 1997: A system to measure surface fluxes of energy, momentum and carbon dioxide. *J. Hydrol.*, 188–189:589–611.

Monteith, J.L., 1965: Evaporation and environment. In: G.E. Fogg (Editor), The state and movement of water in living organisms. Sympos. Soc. Exper. Biol., Vol. 19, Academic Press, pp. 205-234

Mueller, C.K., J.W. Wilson, and N. A. Crook, 1993: The utility of sounding and mesonet data to nowcast thunderstorm initiation. *Wea. Forecasting*, **8**, 132-146.

Myoung, B., and J.W. Nielsen-Gammon, 2010a: Sensitivity of monthly convective precipitation to environmental conditions. *J. Climate*, **23**, 166-188.

Myoung, B., and J.W. Nielsen-Gammon, 2010b: The convective instability pathway to warm season drought in Texas. Part I: The role of convective inhibition and its modulation by soil moisture. *J. Climate*, **23**, 4461-4473.

Nachamkin, J. E., and W. R. Cotton, 2000: Interactions between a developing mesoscale convective system and its environment. Part II: Numerical simulation. *Mon. Wea. Rev.,* **128**, 1225-1244.

Namais, J., 1991: Spring and summer 1988 drought over the contiguous United States – causes and prediction. *J. Climate*, **4**, 54-65.

Negri, A. J., R.F. Adler, L. Xu, and J. Surratt, 2004: The impact of Amazonian deforestation on dry season rainfall. *J. Climate,* **17**, 1306-1319.

Nemes, A., W.J. Rawls, and Y.A. Pachepsky, 2006: Use of the nearest neighbour approach to estimate soil hydraulic properties. *Soil Sci. Soc. Am. J.*, **70**, 327-336.

Nielsen, D.R., J.W. Biggar, and K.T. Erh, 1973: Spatial variability of field-measured soil water properties. *Hilgardia*, **42**, 215-260.

Niyogi, D., and S. Raman, 1997: Comparison of stomatal resistance simulated by four different schemes using FIFE observations. *J. Appl. Meteor.*, **36**, 903-917.

Niyogi, D., S. Raman, and K. Alapaty, 1998: Comparison of four different stomatal resistance schemes using FIFE observations, part 2: analysis of terrestrial biospheric-atmospheric interactions. *J. Appl. Meteor.,* **37**, 1301-1320.

Niyogi, D., K. Alapaty, S. Raman, and F. Chen, 2009: Development and evaluation of a coupled photosynthetic-based gas exchange evapotranspiration model (GEM) for mesoscale weather forecasting applications. *J. Appl. Meteor. Clim.,* **48**, 349-368.

Notaro, M., Z. Liu, and J.W. Williams, 2006: Observed vegetation climate feedbacks in the United States. *J. Climate,* **19**, 763-786.

Numaguti, A., 1999: Origin and recycling processes of precipitating water over the Eurasian continent: Experiments using an atmospheric general circulation model. *J. Geophys. Res*, **104**, 1957-1972.

Oglesby, R. J., 1991: Springtime soil moisture variability and North American drought as simulated by the NCAR Community Climate Model I. *J. Climate,* **4**, 890-897.

Oglesby, R.J., S. Marshall, J.O. Roads, and F.R. Robertson, 2001: Diagnosing warm season precipitation over the GCIP region from a GCM and reanalysis. *J. Geophys. Res.*, **D4**, 3357-3370.

Oglesby, R.J., S. Marshall, D.J. Erickson III, J.O. Roads, and F.R. Robertson, 2002: Thresholds in atmosphere–soil moisture interactions: Results from climate model studies. *J. Geophys. Res.,* **107,** 4224, doi:10.1029/2001JD001045.

O'Neal, M., 1996: Interactions between land cover and convective cloud cover over midwestern North America detected from GOES satellite data. *Int. J. Remote Sens.,* **17,** 1149-1181.

Oke, T. R., 1987: *Boundary Layer Climates*. Methuen, 435 pp.

Oncley, S.P. and co-authors, 2007: The Energy Balance Experiment EBEX-2000. Part I: overview and energy balance. *Boundary-Layer Meteor.*, **123**, 1-28.

Ookouchi, Y., M. Segal, R.C. Kessler, and R.A. Pielke, 1984: Evaluation of soil moisture effects on the generation and modification of mesoscale circulations. *Mon. Wea. Rev.*, **112**, 2281-2292.

Oosterveld, M., and C. Chang, 1980: Empirical relations between laboratory determinations of soil texture and moisture characteristic. *Can. Agric. Eng.*, **22**, 149-151.

Pal, J.S., and E.A.B. Eltahir, 2001: Pathways relating soil moisture conditions to future summer rainfall within a model of the land-atmosphere system. *J. Climate*, **14**, 1227-1242.

Pan, Z., E. Takle, M. Segal, and R. Turner, 1996: Influences of model parameterization schemes on the response of rainfall to soil moisture in the central United States. *Mon. Wea. Rev.*, **124**, 1786-1802.

Peppler, R.A., and P.J. Lamb, 1989: Tropospheric static stability and central North American growing season rainfall. *Mon. Wea. Rev.*, **117**, 1156-1180.

Petersen, G.W., R.L. Cunningham, and R.P. Matelski, 1968. Moisture characteristics of Pennsylvania soils: I. Moisture retention as related to texture. *Soil Sci. Soc. Am. Proc.*, **32**, 271-275.

Philippon, N., L. Jarlan, N. Martiny, P. Camberlin, and E. Mougin, 2007: Characterization of the intraseasonal variability of west African vegetation between 1982 and 2002 by mean of NOAA AVHRR NDVI data. *J. Climate*, **20**, 1202-1218.

Pielke, R.A., Sr., 1984: Mesoscale meteorological modeling. Academic Press, New York, N.Y., 612 pp.

Pielke, R.A., Sr. and M. Segal, 1986: Mesoscale circulations forced by differential terrain heating. Mesoscale Meteorology and Forecasting, P. Ray, Ed., AMS, Chapter 22, 516-548.

Pielke, R.A., Sr., 2001: Influence of the spatial distribution of vegetation and soils on the prediction of cumulus convective rainfall. *Rev. Geophys*., **39**, 151-177.

Potvin, C.K., K.L. Elmore, and S.J. Weiss, 2010: Assessing the impacts of proximity sounding criteria on the climatology of significant tornado environments. *Wea. Forecasting*, **25**, 921-930.

Rabin, R.M., 1977: The surface energy budget of a summer convective period. M.S. thesis, Dept. of Atmospheric and Oceanic Sciences, McGill University. 125 pp.

Rabin, R.M., S. Stadler, P.J. Wetzel, D.J. Stensrud, and M. Gregory, 1990: Observed effects of landscape variability on convective clouds. *Bull. Amer. Meteor. Soc.,* **71**, 272-280.

Raddatz, R.L., 1993: Prairie agroclimate boundary-layer model: A simulation of the atmosphere/crop-soil interface. *Atmos.-Ocean*., **4**, 399-419.

Raddatz, R.L., C.F. Shaykewich, and P.R. Bullock, 1994: Prairie crop yield estimates from modelled phenological development and water-use. *Can. J. Plant Sci.*, **74**, 429-436.

Raddatz, R.L., 1998: Anthropogenic vegetation transformation and the potential for deep convection on the Canadian prairies. *Can. J. Soil Sci.*, **78**, 657-666.

Raddatz, R.L., 2000: Summer rainfall recycling for an agricultural region of the Canadian prairies. *Can. J. Soil Sci.*, **80**, 367-373.

Raddatz, R.L. and J.D. Cummine, 2003: Inter-annual variability of moisture flux from the prairie agro-ecosystem: impact of crop phenology on the seasonal pattern of tornado days. *Boundary-Layer Meteor.,* **106**, 283-295.

Raddatz, R.L., 2005: Moisture recycling on the Canadian Prairies for summer droughts and pluvials from 1997 to 2003. *Agric. Forest Met.*, **131**, 13-26.

Raddatz, R.L., 2007: Evidence for the influence of agriculture on weather and climate through the transformation and management of vegetation: Illustrated by examples from the Canadian Prairies. *Agric. Forest. Met.*, **142**, 196-202.

Raddatz, R.L., and J.M. Hanesiak, 2008: Significant summer rainfall in the Canadian Prairie Provinces: modes and mechanisms 2000-2004. *Int. J. Clim.*, **28**, 1607-1613.

Raupach, R. R., and J.J. Finnigan, 1995: Scale issues in boundary-layer meteorology: surface energy balances in heterogeneous terrain. *Hydro. Proc.*, **9**, 589-612.

Rawls, W.J., and D.L. Brakensiek, 1982. Estimating soil water retention from soil properties. *J. Irrig. Drain. Div. Amer. Soc. Civ. Eng.*, **108**, 166-171.

Rawls, W.J., D.L Brakensiek, and K.E. Saxton, 1982: Estimation of soil water properties. *Transactions of the ASAE*, **25**, 1316-1328.

Reichert G.C., and D. Caissy, 2002: A reliable Crop Condition Assessment Program (CCAP) incorporating NOAA AVHRR data, a geographic information system and the Internet. *ESRI User Conference*, San Diego, California.

Reuter, G.W., and N. Aktary, 1995: Convective and symmetric instabilities and their effects on precipitation: Seasonal variations in central Alberta during 1990 and 1991. *Mon. Wea. Rev*., **123**, 153-162.

Reynolds, C.A., T.J. Jackson, and W.J. Rawls, 2000: Estimating soil water-holding capacities by linking the Food and Agriculture Organization soil map of the world with global pedon databases and continuous pedotransfer functions. *Water Resour. Res.*, **36**, 3653-3662.

Ritchie, J.T., and S. Otter, 1985: Description and performance of CERES-Wheat: A user-oriented wheat yield model. ARS Wheat Yield Project*,* USDA Rep. ARS-38, 159-175.

Robertson, G.W., 1968: A biometeorological time scale for a cereal crop involving day and night temperatures and photoperiod. *Int. J. Biometeor*., **12**, 191-223.

Robinson, J.M., and K.G. Hubbard, 1990: Soil water assessment model for several crops in the high plains. *Agron. J.*, **82**, 1141-1148.

Robock, A., K.Y. Vinnikov, G. Srinivasan, J.K. Entin, S.E. Hollinger, N.A. Speranskaya, S. Liu, and A. Namkhai, 2000: The global soil moisture data bank. *Bull. Amer. Meteor. Soc*., **81**, 1281-1300.

Rowntree, P. R., and J. A. Bolton, 1983: Simulations of the atmospheric response to soil moisture anomalies over Europe. *Q. J. R. Meteor. Soc.*, **109,** 501-526.

Salvucci, G. D., J.A. Saleem, and R. Kaufmann, 2002: Investigating soil moisture feedbacks on precipitation with tests of Granger causality. *Adv. Water Res.,* **25**, 1305-1312.

Santanello, J. A., M.A. Friedl, and M. Ek, 2007: Convective planetary boundary layer interactions with the land surface at diurnal time scales: Diagnostics and feedbacks. *J. Hydrometeor*., **8**, 1082-1097.

Santaren, D., P. Peylin, N. Viovy, and P. Ciais, 2007: Optimizing a process-based ecosystem model with eddy-covariance flux measurements: a pine forest in southern France. *Global Biogeochemistry Cycles,* **21**, GB2013, doi:10.1029/2006GB002834.

Sauer T.J., 2002: Heat flux density. In: J.H. Dane and G.C. Topp (Editors), Methods of Soil Analysis, Part 4. Physical Methods. Soil Science Society of America Book Series 5, Madison, Wisconsin. pp. 1233-1248

Saxton, K.E., W.J. Rawls, J.S. Romberger, and R.I. Papendick, 1986: Estimating generalized soil-water characteristics from texture. *Soil Sci. Soc. Amer. J.*, **50**, 1031-1036.

Saxton, K.E., and W.J. Rawls, 2006: Soil water characteristic estimates by texture and organic matter for hydrologic solutions. *Soil Sci. Soc. of Amer. J.*, **70**, 1569-1578.

Scanlon, T.M., and P. Sahu, 2008: On the correlation structure of water vapor and carbon dioxide in the atmospheric surface layer: A basis for flux partitioning. *Water Resour. Res.,* W10418, doi:10.1029/2008WR006932.

Schaap, M.G.**,** and F.J. Leij, 1998: Using Neural Networks to predict soil water retention and soil hydraulic conductivity. *Soil & Tillage Research*, **47**, 37-42.

Schaap, M.G., A. Nemes, M.Th. Van Genuchten, 2004: Comparison of models for indirect estimation of water retention and available water content in surface soils. *Vadose Zone J.*, **2**, 1455-1463.

Schädler, G., 2007. A comparison of continuous soil moisture simulations using different soil hydraulic parameterizations for a site in Germany. *J. Appl. Meteor. Clim.*, **46**, 1275-1289.

Schär, C., D. Luthi, and U. Beyerle, 1999: The soil-precipitation feedback: A process study with a regional climate model. *J. Climate,* **12,** 722-741.

Schlosser, C.A., and P.C.D. Milly, 2002: A model-based investigation of soil moisture predictability and associated climate predictability. *J. Hydrometeor.,* **3**, 483-501.

Schubert, S.D., M.J. Suarez, P.J. Pegion, R.D. Koster, and J.T. Bacmeister, 2004: Causes of long-term drought in the U.S. Great Plains**.** *J. Climate*., **17**, 485-503.

Schulze, E.D., 1986: Carbon dioxide and water vapor exchange in response to drought in the atmosphere and in the soil. *Ann. Rev. Plant. Physiol.,* **37**, 247-274.

Schulze, E.D., F.M. Kelliher, C. Körner, J. Lloyd, and R. Leuning, 1994: Relationships among maximum stomatal conductance, ecosystem surface conductance, carbon assimilation rate, and plant nitrogen nutrition: A global ecology scaling exercise. *Ann. Rev. Ecol. Syst.,* **25**: 629-660.

Schumann, M.R., and P.J. Roebber, 2010: The influence of upper-tropospheric potential vorticity on convective morphology. *Mon. Wea. Rev.*, **138**, 463-474.

Schurr U., T. Gollan, and E.D. Schulze, 1992: Stomatal response to drying soil in relation to changes in sap composition of Helianthus annuus. II. Stomatal sensitivity to abscisic acid imported from the xylem sap. *Plant, Cell Environ.*, **15**, 561-567.

Seen, D.L., A. Chehbouni, E. Njoku, S. Saatchi, E. Mougin, and B. Monteny, 1997: An approach to couple vegetation functioning and soil-vegetation-atmosphere transfer models for semiarid grasslands during the HAPEX-Sahel experiment. *Agric. Forest Met.,* **83**, 49-74.

Segal, M., R. Avissar, M.C. McCumber, and R.A. Pielke, 1988: Evaluation of vegetation effects on the generation and modification of mesoscale circulations. *J. Atmos. Sci*., **45**, 2268-2292.

Segal, M., and R.W. Arritt, 1992: Non-classical mesoscale circulations caused by surface sensible heat-flux gradients. *Bull. Amer. Meteor. Soc.,* **73**, 1593-1604.

Segal, M., R.W. Arritt, C. Clark, R. Rabin, and J. Brown, 1995: Scaling evaluation of the effect of surface characteristics on potential for deep convection over uniform terrain. *Mon. Wea. Rev.*, **123**, 383-400.

Sellers, P.J., and F.G. Hall, 1992: FIFE in 1992: Results, scientific gains, and future research directions. *J. Geophys. Res.,* **97**, 19 091-19 109.

Seneviratne S.I., and co-authors, 2006: Soil moisture memory in AGCM simulations: Analysis of Global Land–Atmosphere Coupling Experiment (GLACE) Data. *J. Hydrometeor.*, **7**, 1090-1112.

Seneviratne, S.I**.**, T. Corti, E.L. Davin, M. Hirschi, E.B. Jaeger, I. Lehner, B. Orlowsky, and A.J. Teuling, 2010: Investigating soil moisture-climate interactions in a changing climate: A review. *Earth-Science Reviews*, **99**, 125-161.

Shao, Y., and P. Irannejad, 1999: On the choice of soil hydraulic models in land-surface schemes. *Boundary-Layer Meteor.,* **90**, 83-115.

Shaw, W.J., and J.C. Doran, 2001: Observations of systematic boundary layer divergence patterns and their relationship to land use and topography. *J. Climate,* **14**, 1753

Shen, Y., A. Kondoh, C. Tang, Y.Zhang, J. Chen, W. Li, Y. Sakura, C. Liu, T. Tanaka, and J. Shimada, 2002: Measurement and analysis of evapotranspiration and surface conductance of a wheat canopy. *Hydrol. Process.*, **16**, 2173-2187.

Shukla, J., and Y. Mintz, 1982: Influence of land surface evapotranspiration on the Earth's climate. *Science*, **215**, 1498-1501.

Siqueira, M.B., G. Katul, and A. Porporato, 2009: Soil moisture feedbacks on convection triggers: the role of soil-plant hydrodynamics. *J. Hydrometeor.*, **10**, 96-112.

Smith, S.B., and M.K. Yau, 1993a: The causes of severe convective outbreaks in Alberta. Part I: A comparison of a severe outbreak with two nonsevere events. *Mon. Wea. Rev.*, **121**, 1099-1125.

Smith, S.B., and M. K. Yau, 1993b: The causes of severe convective outbreaks in Alberta. Part II: Conceptual model and statistical analysis. *Mon. Wea. Rev.*, **121**, 1126-1133.

Sridhar, V., K.G. Hubbard, J. You, and E.D. Hunt, 2008. Development of the soil moisture index to quantify agricultural drought and its "user friendliness" in severity-area-duration assessment. *J. Hydrometeor.*, **9**, 660-676.

Stensrud, D.J., and J.M. Fritsch, 1993: Mesoscale convective systems in weakly forced large-scale environments. Part I: Observations. *Mon. Wea. Rev.*, **121**, 3326-3344.

Stewart, R.E., and R.L. Lawford, Eds., 2011. *The 1999–2005 Canadian prairies Drought: Science, impacts, and lessons.* Drought Research Initiative, Winnipeg, Canada.

Stohl, A., and P. James, 2005: A Lagrangian analysis of the atmospheric branch of the global water cycle. Part II: Moisture transports between earth's ocean basins and river catchments. *J. Hydrometeor.*, **6**, 961-984.

Strong, G.S., 1986: Synoptic to mesoscale dynamics of severe thunderstorm environments. A diagnostic study with forecasting implications. Ph.D Thesis, Department of Geography. University of Alberta, 345 pp.

Su, H., F. McCabe, and E.F. Wood, 2005: Modeling evapotranspiration during SMACEX: Comparing two approaches for local- and regional-scale prediction. *J. Hydrometeor.*, **6**, 910-922.

Sud, Y. C., D. M. Mocko, K.-M. Lau, and R. Atlas, 2003: Simulating the Midwestern U.S. drought of 1988 with a GCM. *J. Climate,* **16,** 3946-3965.

Szeto, K.K., 2002: Moisture recycling over the Mackenzie Basin. *Atmos-Ocean*, **40**,191-197.

Taylor, C. M., and T. Lebel, 1998: Observational evidence of persistent convective-scale rainfall patterns. *Mon. Wea. Rev.,* **126,** 1597-1607.

Taylor, C.M., R.J. Ellis, D.J. Parker, R.R. Burton, and C.D. Thorncroft, 2003: Linking boundary-layer variability with convection: A case-study from JET2000. *Q. J. R. Meteor. Soc.*, **129**, 2233-2253.

Taylor, C.M., D.J. Parker, C.R. Lloyd, and C.D. Thorncroft, 2005: Observations of synoptic-scale land surface variability and its coupling with the atmosphere. *Q. J. R. Meteor. Soc*. **131**, 913-937.

Taylor, C.M., P.P. Harris, and D.J. Parker, 2009: Impact of soil moisture on the development of a Sahelian mesoscale convective system: A case-study from the AMMA special observing period. *Q. J. R. Meteor. Soc*., **136**, 456-470.

Timlin, D.J., Y.A. Pachepsky, B. Acock, and F. Whisler, 1996: Indirect estimation of soil hydraulic properties to predict soybean yield using GLYCIM. *Agric. Syst.*, **52**, 331-353.

Tomasella, J., and M.G. Hodnett, 1998: Estimating soil water retention characteristics from limited data in Brazilian Amazonia. *Soil Sci.*, **163**,190-202.

Toumi, R., and X. Qie, 2004: Seasonal variation of lightning on the Tibetan Plateau: A Spring anomaly? *Geophys. Res. Lett.*, **31**, L04115, doi:10.1029/2003GL018930.

Trenberth, K.E., 1999: Atmospheric moisture recycling: role of advection and local ET. *J. Climate*, **12**, 1368-1381.

Trier, S.B., F. Chen, and K.W. Manning, 2004: A study of convection initiation in a mesoscale model using high-resolution land surface initial conditions. *Mon. Wea. Rev.,* **132**, 2954-2976.

Tsvetsinskaya, E.A., L.O. Mearns, and W.E. Easterling, 2001: Investigating the effect of seasonal plant growth and development in three-dimensional atmospheric simulations. Part II: Atmospheric response to crop growth and development. *J. Climate*, **14**, 711-729.

Tucker, C. J., 1979: Red and photographic infrared linear combinations for monitoring vegetation. *Remote Sens. Environ.*, **8**, 127-150.

Twine T.E., W.P. Kustas, J.M. Norman, D.R. Cook, P.R. Houser, T.P. Meyers, J.H. Prueger, P.J. Starks , and M.L. Wesley, 2000. "Correcting eddy-covariance flux underestimates over a grassland. *Agric. Forest Met.*, **103**, 279-300.

van der Ent, R.J., H.H.G. Savenije, B. Schaefli, and S.C. Steele-Dunne, 2010: Origin and fate of atmospheric moisture over continents. *Water Resour. Res.*, **46**, W09525, doi:10.1029/2010WR009127.

Van der Keur, P., and B.V. Iversen, 2006. Uncertainty in soil physical data at river basin scale – a review. *Hydrol. Earth Syst. Sci.*, **10**, 889-902.

Van Genuchten, M.Th., 1980: Predicting the hydraulic conductivity of unsaturated soils. *Soil Sci. Soc. Am. Proc.*, **44**, 892-898.

Vico, G., and A. Porporato, 2008: Modelling C_3 and C_4 photosynthesis under water-stressed conditions. *Plant Soil*, **313**, 187-203. doi 10.1007/s11104-008-9691-4.

Vidale, P.L., R.A. Pielke, A. Barr, and L.T. Steyaert, 1997: Case study modeling of turbulent and mesoscale fluxes over the BOREAS region. *J. Geophys. Res*., **102**, 29167-29188.

Vitale, M., S. Anselmi, E. Salvatori, and F. Manes, 2007: New approaches to study the relationship between stomatal conductance and environmental factors under Mediterranean climatic conditions. *Atmos. Environ.*, **41**; 5385-5397.

Viterbo, P. and A.K. Betts, 1999: The impact of the ECMWF reanalysis soil water on forecasts of the July 1993 Mississippi flood. *J. Geophys. Res*., **104**, 19361-19366.

Wai, M.M.-K., and E.A. Smith, 1998: Linking boundary layer circulations and surface processes during FIFE 89, part II, Maintenance of secondary circulation. *J. Atmos. Sci.,* **55**, 1260-1276.

Wang, F., C.W Fraisseb, N.R. Kitchen, and K.A Sudduth, 2003a: Site-specific evaluation of the CROPGRO soybean model on Missouri claypan soils. *Agric. Sys.*, **76**, 985-1005.

Wang, J., R.L. Bras, and E.A.B. Eltahir, 2000: The impact of observed deforestation on the mesoscale distribution of rainfall and clouds in Amazonia. *J. Hydrometeor*, **1**, 267–286.

Wang J., P.M. Rich, and K.P. Price, 2003b: Temporal responses of NDVI to precipitation and temperature in the central Great Plains, USA. *Int. J. Remote. Sens.*, **24**, 2345-2364.

Wang, Q., W. Masataka, and Q. Zhu, 2005: Simulation of water and carbon fluxes using BIOME-BGC model over crops in China. *Agric. Forest Met.,* **131**, 209-224.

Wang S., R.F. Grant, D.L. Verseghy, and T.A. Black, 2002: Modelling carbon-coupled energy and water dynamics of a boreal aspen forest in a general circulation model land surface scheme. *Int. J. Clim.*, **22**, 1249-1265.

Wang S., Y. Yang, A.P. Trishchenko, A.G. Barr, T.A. Black, and H. McCaughey, 2009a: Modeling the response of canopy stomatal conductance to humidity. *J. Hydrometeor*., **10**, 521-532.

Wang S.Y., T.C. Chen, and J. Correia, 2009b: Climatology of summer midtropospheric perturbations in the U.S. northern plains. Part I: influence on northwest flow severe weather outbreaks. *Clim. Dyn.*, doi:10.1007/s00382-009-0696-3

Wang,W., B. T. Anderson, N. Phillips, R. K. Kaufmann, C. Potter, and R. B. Myneni, 2006: Feedbacks of vegetation on summertime climate variability over the North American grasslands. Part I: Statistical analysis. *Earth Interactions*, **10**, 1-27.

Wang, X.L., C.-R. João, and X. Zhang, 1996: Intraseasonal oscillations and associated spatial-temporal structure of precipitation over China. *J. Geophys. Res.,* **101**, 19,035-19,042.

Wang X., H. Xie, H. Guan, and X. Zhou, 2007: Different responses of MODIS-derived NDVI to root-zone soil moisture in semi-arid and humid regions. *J. Hydrol.*, **340**, 12-24.

Weaver, C.P., and R. Avissar, 2001: Atmospheric disturbances caused by human modification of the landscape. *Bull. Amer. Meteor. Soc*., **82**, 269-281.

Weaver, C.P., 2004a: Coupling between large-scale atmospheric processes and mesoscale land-atmosphere interactions in the U.S. southern Great Plains during summer. Part I: Case Studies. *J. Hydrometeor.,* **5**, 1223-1246.

Weaver, C.P., 2004b: Coupling between large-scale atmospheric processes and mesoscale land-atmosphere interactions in the U.S. southern Great Plains during summer. Part II: Mean impacts of the mesoscale**.** *J. Hydrometeor.,* **5**, 1247-1258.

Wegehenkel, M., and W. Mirschel, 2006: Crop growth, soil water and nitrogen balance simulation on three experimental field plots using the Opus model—A case study. *Ecological Modelling*, **190**, 116-132.

Wei, J., R.E. Dickinson, and H. Chen, 2008: A negative soil moisture–precipitation relationship and its causes. *J. Hydrometeor.*, **9**, 1364-1376

Wen, L., Z. Wu, G. Lu, C.A. Lin, J. Zhang, and Y. Yang, 2007: Analysis and improvement of runoff generation in the land surface scheme CLASS and comparison with field measurements from China. *J. Hydrol.*, **345**, 1-15.

Wetzel, P.J., and J.-T Chang, 1987: Concerning the relationship between evapotranspiration and soil moisture. *J. Clim. Appl. Meteor.*, **26**, 18-27.

Wetzel, P.J., S. Argentini, and A. Boone, 1996: Role of land surface in controlling daytime cloud amount: Two case studies in the GCIP-SW area. *J. Geophys. Res.,* **101**, 7359-7370.

Wever, L.A., L.B. Flanagan, and P.J. Carlson, 2002: Seasonal and interannual variation in evapotranspiration, energy balance and surface conductance in a northern temperate grassland. *Agric. Forest Met.*, **112**, 31-49.

Williams, R.D., L.R. Ahuja, and J.W. Naney, 1992: Comparison of methods to estimate soil water characteristics from soil texture, bulk density and limited data. *Soil Sci.,* **153**, 172-184.

Wösten, J.H.M., M.H. Bannink, and J. Bouma, 1987. Land evaluation at different scales: You pay for what you get. *Soil Survey of Land Evaluation*, **7**, 13-24

Wösten, J.H.M., Y.A. Pachepsky, and W.J. Rawls, 2001: Pedotransfer functions: Bridging the gap between available basic soil data and missing soil hydraulic characteristics. *J. Hydrol.*, **251**, 123-150.

Xia, Y.Q., and M.A Shao, 2008: Soil water carrying capacity for vegetation: A hydrologic and biogeochemical process model solution. *Ecological modeling*, **214**, 112-124.

Xue, Y., F.J. Zeng, and C.A. Schlosser, 1996. SSiB and its sensitivity tos oil properties-A case study using HAPEX-Mobihly data. *Global Planet. Change*, **13**, 183-194.

Xue, Y., F. De Sales, W. Li, C.R. Mechoso, C. Nobre, and M.H.H.-Juang, 2006: Role of land surface processes in South American monsoon development. *J. Climate*, **19**, 741-762.

Yamada, H., 2008: Numerical simulations of the role of land surface conditions in the evolution and structure of summertime thunderstorms over a flat highland. *Mon. Wea. Rev.*, **136**, 173-188.

Yan, H., and R.A. Anthes, 1987: The effect of latitude on the sea breeze. *Mon. Wea. Rev*., **115**, 936-956.

Zacharias, S., and G. Wessolek, 2007: Excluding organic matter content from pedotransfer predictors of soil water retention. *Soil Sci. Soc. Am. J.*, **71**, 43-50.

Zadoks, J.C., T.T. Chang, and C.F. Konzak, 1974: A decimal code for the growth stages of cereals. *Weed Research*, **14**, 415-421

Zangvil, A., D.H. Portis, and P.J. Lamb, 2004: Investigation of the large-scale atmospheric moisture field over the midwestern United States in relation to summer precipitation. Part II: Recycling of local evapotranspiration and association with soil moisture and crop yields. *J. Climate,* **17,** 3283-3301.

Zeng, N., and J.D. Neelin, 2000: The role of vegetation–climate interaction and inter-annual variability in shaping the African savanna. *J. Climate,* **13**, 2665-2670.

Zhang, Y., T. Kadota, T. Ohata1, and D. Oyunbaata, 2007: Environmental controls on evapotranspiration from sparse grassland in Mongolia. *Hydrol. Process.,* **21**, 2016-2027.

Zhu, J., and P. Mohanty, 2002: Spatial averaging of van Genuchten hydraulic parameters for steady-state flow in heterogeneous soils: A numerical study. *Vadose Zone J.*, **1**, 261-272.